THE UNIVERSITY
of EDINBURGH

THE UNIVERSITY *of* EDINBURGH

ER-Mitochondria interactions and neurodegeneration

Mark Harmon

A thesis submitted for the degree of Doctor of Philosophy

The University of Edinburgh

2018

Abstract

Physical membrane contact sites between the ER and mitochondria play a critical role in regulating a variety of processes including calcium signalling, lipid exchange, controlling mitochondrial dynamics and cell death signalling. These contact sites are formed at specialised regions of membrane, termed mitochondrial associated membranes or MAMs, that are enriched for a group of proteins acting as tethers to hold the ER and mitochondria at appropriate distances from one another. The distance of these junctions is usually defined between 10-30 nm but can vary in response to certain cellular conditions and it is believed that heterogeneity in the distance of the contact sites may be reflective of different protein compositions or activities at these sites. Abnormal alterations to ER-mitochondria contacts are observed in numerous neurodegenerative disorders including Alzheimer's, Parkinson's and amyotrophic lateral sclerosis (ALS) and therefore, it is believed that a dysfunction to the MAMs may be a common pathogenic mechanism underlying neuronal cell death.

Due to the associated dysfunction of organelle contact sites in neurodegenerative disorders, the ability to detect these structures could provide critical information on the pathogenic mechanisms of neuronal cell death. Existing techniques for detecting MAMs have numerous limitations or are restricted to fixed samples. The aim of this thesis was to develop a fluorescent-based method for the visualisation of contact sites that can also be applied to living systems to study organelle contact dynamics. Here, we have generated split fluorescent Venus fragments targeted to the ER and outer mitochondrial membrane respectively, as the basis for our bi-fluorescence complementation (BiFC) system for the detection and quantification of MAMs in living cells. The principle of this technique relies on close spatial proximity of the reporter probes for the restoration of the fluorescent protein and the emission of a detectable signal. Validation of this method highlighted several advantages over existing methods of detecting ER-mitochondria contacts and we were able to report on changes in agreement with previously published, high-resolution electron

microscopy studies. Adaptations to the technique allow for the detection of other organelle contact sites by varying the targeting sequence of the complementary Venus fragments.

As these reporter proteins detect junctions of a maximum distance of around 6-10 nm, we could use the BiFC system to correlate the Venus signal with specific functions of the MAMs to try and elucidate the functional significance of these particularly tight contact sites. Our results suggest that some of these contact sites may represent sites of actively dividing mitochondria. Furthermore, our results indicated that these tight ER-mitochondria contacts are formed on a sub-population of mitochondria of higher than average resting membrane potential and mitochondrial calcium levels, which may indicate differences in the bioenergetic state or the health of mitochondria with tight ER-mitochondria contact sites.

Finally, this technique was used to investigate the role of a MAM-enriched protein, VAPB, of which a proline to serine missense mutation is associated with a dominantly inherited form of ALS termed ALS8. The data shows that expression of the mutant disease-linked $VAPB^{P56S}$ significantly increases the mean number of contact sites per cell whereas altering the levels of wild-type VAPB has no significant effect. This finding suggests that the expression of $VAPB^{P56S}$ induces abnormalities in ER-mitochondria tethering but it is still unclear whether this is through direct binding properties of mutant VAPB or through an indirect secondary mechanism. As the MAMs regulate many of the pathways that are commonly perturbed in neurodegenerative disorders, alterations in ER-mitochondria contact sites may represent a key early pathogenic event in ALS.

Lay Summary

Within a cell there are a number of different structures termed organelles that carry out unique processes that ensure the correct functioning and survival of the cell. These organelles do not function in isolation but are constantly interacting with one another via complex mechanisms to regulate their activity. One of the ways this coordination takes place is by the formation of physical contact sites between closely apposed organelles. These contact sites are formed by the binding of particular proteins on the surface membranes of the respective organelles that tether them at an appropriate distance from one another. One of the best characterised type of contact sites are between organelles known as the endoplasmic reticulum (ER), which is responsible for synthesising proteins, and the mitochondria, involved in energy production and these contacts are formed at specialised regions of membrane termed mitochondrial associated membranes or MAMs.

A disruption to ER-mitochondria contacts has been observed in a number of diseases including Alzheimer's disease, Parkinson's disease and motor neuron disease/amyotrophic lateral sclerosis (ALS). Therefore, it is important for us to be able to detect and visualise these contact sites within cells to try and investigate how changes could be linked to disease progression.

In this thesis, we have developed a technique for the visualisation and quantification of contact sites in living cells based on split fluorescent protein fragments targeted to the ER and mitochondria membranes respectively. The principle behind this technique is that neither protein fragment alone will fluoresce but when brought within close proximity at organelle contact sites, the fluorescent protein will be restored and a signal will be emitted that can be detected by a fluorescent microscope. Validation of this method has highlighted several advantages over existing techniques for investigating ER-mitochondria contacts and through this, we have investigated the role of a motor neuron disease-linked protein called VAPB on contact sites. Our results have demonstrated that the presence of the disease-causing mutant form of VAPB increases the average number of ER-mitochondria

contact sites within a cell, providing supporting evidence that a dysfunction to the MAMs may be playing a role in cell death.

Declaration

I hereby declare that the work presented in this thesis was composed entirely by myself with minor contributions from lab members where clearly indicated in the text. This work has not been submitted for any other degree or professional qualification.

Mark Harmon

Abbreviations list

AAV – Adeno-associated virus

ACBD5 – Acyl-coenzyme A-binding protein 5

AD – Alzheimer's disease

ADP – adenosine di-phosphate

AICD – AβPP intracellular domain

ALS – Amyotrophic lateral sclerosis

AMPA - α-amino-3-hydroxy-5-methyl-4-isoxazolepropionic acid receptor

ANOVA – Analysis of variance

APP – Amyloid precursor protein

ATAD3 – AAA domain-containing protein 3

ATF4 – Activating transcription factor 4

ATF6 – Activating transcription factor 6

Atg – Autophagy related protein

ATP – adenosine tri-phosphate

ATPB – ATP-synthase subunit β

Aβ – Beta-amyloid

BACE1 – β-site APP-cleaving enzyme 1

Bap31 – B-cell receptor-associated protein 31

Bax – Bcl-2 associated X protein

Bcl-2 – B-cell lymphoma 2

BiFC – Bi-fluorescence complementation assay

BSA – Bovine Serum Albumin

b-ZIP – Basic leucine zipper

C9Orf72 – Chromosome 9 open reading frame 72

CAPK – Ceramide associated protein kinases

CAPP – Ceramide associated protein phosphatases

CC – Coiled-coil

CCCP – Carbonyl cyanide m-chlorophenyl hydrazine

CERT – Ceramide transfer protein

CFP – Cyan fluorescent protein

CHO – Chinese hamster ovary

CHOP – CCAAT/enhancer binding protein homologous protein

CNO – Clozapine N-oxide

CNS – Central nervous system

COPII – Coat protein complex II

COX1 – Cyclooxygenase 1

CSF – Cerbrospinal fluid

CT – C-terminus

CW-gSTED – Continuous wave gated stimulated emission depletion microscopy

Cy2/3/5 – Cyanine 2/3/5

DAG – Diacylglycerol

DAPI – 4',6-Diamidino-2-phenylindole

ddFP – Dimerization-dependent fluorescent proteins

DGAT2 – Diacylglycerol acyltransferase 2

DMEM – Dulbecco's Modified Eagle Medium

DMSO – Dimethyl Sulfoxide

DNA – Deoxyribonucleic Acid

Dnm1 – Dynamin-1

DPC – Dodecylphosphocholine

DREADD – Designer Receptor Exclusively Activated by Designer Drugs

Drp1 – Dynamin-related protein 1

ECL – Enhanced Chemiluminescence

EEA1 – Early endosome antigen 1

EGFR – Epidermal growth factor receptor

eIF2α - Eukaryotic initiation factor 2

EM – Electron microscopy

ER – Endoplasmic reticulum

ERES – ER exit sites

ERGIC – ER-Golgi intermediate compartment

ERMES – ER-mitochondria encounter structure

FAPP2 – Glycosylceramide-transfer protein Golgi-associated four-phosphate adaptor protein 2

FBS – Foetal Bovine Serum

FDR – False Discovery Rate

FFAT – Two phenyalanines (FF) within an acid tract

FIP200 – Focal adhesion kinase family interacting protein of 200 kD

Fis1 – Fission homologue 1

FRET – Fluorescence resonance energy transfer

FTD – Frontotemporal lobe dementia

FUS – Fused in Sarcoma

FYCO1 – FYVE and coiled-coil domain containing 1

GABA – Gamma-aminobutyric acid

GFP – Green fluorescent protein

GSK-3β – Glycogen synthase kinase-3β

HEK – Human embryonic kidney

HeLa cells – Henrietta Lacks cells

IMM – inner mitochondrial membrane

IP_3R – Inosital 1,4,5-triphosphate receptor

iPSC – Induced pluripotent stem cell

IRE1 – Inositol requiring 1

JNK1 – c-Jun N-terminal protein kinase 1

LSCM – Laser Scanning Confocal Microscopy

lssDNA – Long single-stranded DNA

MAMs – mitochondrial associated membranes

MCC – Mander's Correlation Coefficient

MCU – Mitochondrial channel uniporter

MEF – Mouse embryonic fibroblast

MERCs – Mitochondria ER contacts

MFN1 – Mitofusin-1

MFN2 – Mitofusin-2

Miro – Mitochondrial Rho GTPase

Mito-RCaMP – Mitochondrially targeted-Red-cyclic adenosine monophosphate

MPT – Mitochondrial permeability transition

MSP – Major sperm protein

mtDNA – Mitochondrial DNA

mTOR – Mammalian target of rapamycin

N2a – Neuro-2a

NA – Numerical Aperture

NIR2 – (Pyk2 N-terminal domain-interacting receptor 2)

NMJ – Neuromuscular junction

NPC1 – Niemann-Pick disease type C1

Npl4 – Nuclear protein localization homolog 4

NSF – N-ethylmalemide sensitive fusion protein

OMM – outer mitochondrial membrane

OPA1 – Optic atrophy protein 1

Orai1 – Calcium-release activated calcium channel protein 1)

ORP1L – OSBP-related protein 1L

ORP5 – Oxysterol-binding protein-related protein 5

OSBP – Oxysterol binding protein

OSH – Oxysterol binding homology

PACS2 – Phosphoacidic cluster sorting protein 2

PALM – Photoactivated localisation microscopy

PBL – Peripheral blood leukocytes

PBS – Phosphate buffered saline

PC – phosphatidylcholine

PCC – Pearson's Correlation Coefficient

PCR – Polymerase chain reaction

PD – Parkinson's disease

PDI – Protein disulphide isomerase

PDZD8 – PDZ-containing 8

PE – phosphatidylethanolamine

PERK – PKR-like ER kinase

PH – Pleckstrin homology

PI3K – Phosphatidylinositol 3-kinase

PI4P – Phosphatidylinositol 4-phosphate

PINK1 – PTEN-induced putative kinase 1

PIP2 – Phosphatidylinositol biphosphate

PKA – Protein kinase A

PM – plasma membrane

PS – phosphatidylserine

PS-1 – Presenilin 1

PS-2 – Presenilin 2

PtdIns3P – Phosphatidylinositol 3-phosphate

PTP1B – Protein tyrosine phosphatase 1 B

PTPIP51 – Protein tyrosine phosphatase interacting protein 51

REEP1 – Receptor expression enhancing protein 1

ROS – Reactive oxygen species

Rpt3 – Regulatory particle triple-ATPase subunit 3

RyR – Ryanodine receptor

S1P – Site-1 protease

S2P – Site-2 protease

sALS – Sporadic amyotrophic lateral sclerosis

SEM – Standard error of the mean

SERCA1 – S1T variant of sarco/endoplasmic reticulum Ca^{2+} ATPase

SETX – Senataxin

Sf-Cherry – Super-folded cherry

SIM – Structured Illumination Microscopy

SNARE – Soluble NSF attachment protein receptor

SOCE – Store operated calcium entry

SOD1 – Superoxide dismutase 1

STAR – Steroidogenic acute regulatory protein

STARD3 – STAR-related lipid transfer domain containing 3

STARD3NL – STARD3 N-terminal like

STED – Stimulated emission depletion

STIM1 – Stromal interacting molecule 1

TDP-43 – TAR DNA-binding protein 43

Tfam – Mitochondrial transcription factor A

TMD – Transmembrane domain

TMX – thioredoxin-related oxidoreductase

TNF – Tumour necrosis factor

TOMM20 – Translocase of outer mitochondrial membrane 20

TORC1 – TOR complex 1

TRAF2 – TNF-receptor-associated factor 2

tRNAIle – Mitochondrial transfer RNA isoleucine

TULIP – Tubular lipid binding

UBQLN2 – Ubiquilin 2

Ufd1 – Ubiquitin fusion degradation 1

ULK – Unc-51-like kinase

UPR – Unfolded protein response

UPS – Ubiquitin-proteasome system

V1 – Venus 1

V2 – Venus 2

VAMP – Vesicle associated membrane protein

VAPA – VAMP-associated protein A

VAPB – VAMP-associated protein B

VCP – Valosin-containing protein

VDAC – Voltage-dependent anion channel

XBP1 – X-box binding protein 1

YFP – Yellow fluorescent protein

YIF1A – Yip1-interacting factor homologue A

Acknowledgements

First and foremost, I would like to express my deepest gratitude to my supervisor Dr. Paul Skehel for his patience, guidance and support throughout the entire process. His help was invaluable in getting me to where I am today.

I would also like to thank Dr. Mandy Jackson who was like a second supervisor to me, always willing to offer her guidance and technical support when needed, and the other members of my thesis committee, Dr. Philip Larkman and Prof. Giles Hardingham for all their help.

To the other members of my lab, Ms. Brenda Murage and Dr. Cornelia Roesl, I am extremely appreciative of the support and friendship you have offered me throughout this experience. I would also like to thank Dr. Philip Hasel for providing several of the reagents used in my work and for his willingness to teach and advise on a number of experimental techniques.

A very special mention to my dear friend Dr. Yvonne Clarkson, you were with me from day one of this experience and were always there for me through all of the high points and low points of the PhD process. I can never thank you enough for all of your help.

I am grateful to the Euan MacDonald Centre for providing the funding to allow me to travel to present and share my work internationally and gain valuable insight from other researches in the field of motor neuron disease research.

Last but not least, a huge thank you to my friends and family for everything they have done for me along the way.

Table of Contents

Chapter 1
Introduction

1.1 Inter-organelle contact sites

Organelles of the cell do not function in isolation but rather, complex, coordinated signalling between the various subcellular compartments plays an essential role in regulating a wide range of physiological processes. An emerging body of evidence has shown that perturbations in the maintenance or structure of these membrane contact sites can result in a dysfunction to a variety of cellular processes and has been highlighted as a potential pathogenic mechanism in diseases such as neurodegenerative disorders (Paillusson et al., 2016).

The ER, a vast network of interconnected, membrane-bound tubules, can be viewed as a central hub for organelle interactions with physical contact sites being observed between the ER membrane and many organelles including mitochondria, the plasma membrane, endosomes, lysosomes, peroxisomes and the Golgi apparatus [As reviewed by (English and Voeltz, 2013)] **(Fig1.1)**. Many of the pathogenic molecular mechanisms associated with neurodegeneration can be attributed to a dysfunction in the cellular processes mediated by organelle contact sites. Different examples of inter-organelle contacts will be discussed in more detail in the following sections.

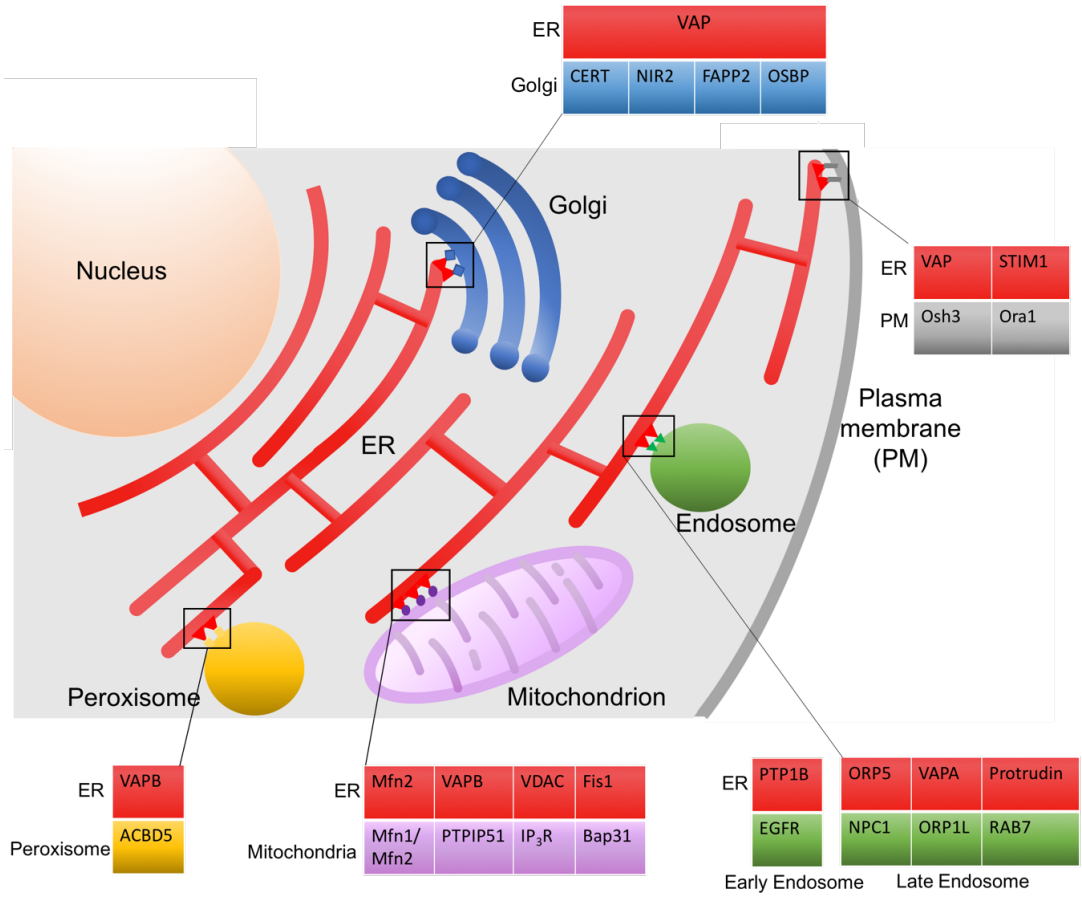

Fig 1.1: Schematic illustration of various inter-organelle contact sites within a cell. The ER forms membrane contact sites with a variety of different organelles within a cell. Coloured boxes indicate some examples of known protein binding pairs mediating physical ER contact sites. Adapted from (Raiborg et al., 2015a).

1.1.1 ER-mitochondria contacts

Mitochondria are highly dynamic organelles, bound by an outer mitochondrial membrane (OMM) and an inner mitochondrial membrane (IMM) with several invaginations called *cristae*, and play a central role in the bioenergetics of a cell through the catabolism of sugars and fatty acids to recycle ADP to ATP. The morphology of the organelle varies between cells, most often being found as an interconnected mitochondrial network. However, structural changes can be induced in response to a number of factors, including the energetic state of the cell, a process

which is regulated by a delicate balance between mitochondrial fission and fusion events (Scorrano, 2013; Youle and van der Bliek, 2012).

Coordinated signalling between the endoplasmic reticulum and mitochondria is vital for a number of physiological processes including lipid biosynthesis and transport, the maintenance of calcium homeostasis, regulating mitochondrial morphology and the execution of cell death pathways (Hayashi et al., 2009; van Vliet et al., 2014; Friedman et al., 2011). Sites of close proximity between these two organelles were first defined by Jean Vance in 1990 as distinct, tightly associated structures that can be purified by cell fractionation (Vance, 1990). Regions of ER membrane in close apposition to the OMM are referred to as mitochondrial associated membranes or MAMs. Ultrastructural studies have revealed that regions of ER membrane in juxtaposition to the mitochondria can vary between discrete points of contact to almost complete circumscription of the outer mitochondrial membrane (Sherrington et al., 1995) (Friedman et al., 2011). These contact points also vary in the distance of the junctions, ranging approximately between 9-16 nm between the mitochondria and smooth ER and 19-30 nm at the rough ER, as quantified by electron microscopy, with approximately 12% of the mitochondrial perimeter being in close proximity to the ER (Csordas et al., 2006). It is believed that the organelles are tethered at an appropriate distance from one another by the formation of protein complexes between the ER and OMM and the recent identification of several proteins who appear to regulate the nature of these contact points has strengthened this observation **(Table 1.1)**.

Although several proteins are found to be enriched in the MAM fraction, it is unclear what signalling mechanisms target the proteins to these specific sub-domains of ER membranes. Palmitoylation is the post-translational addition of fatty acids including palmitic acid and it has been shown that the palmitoylation of calnexin and thioredoxin-related oxidoreductase (TMX), is essential for their localisation to the MAMs ((Lynes et al., 2012). Similarly, a 5-amino acid sequence was identified in the cytosolic domain of diacylglycerol acyltransferase 2 (DGAT2) that is required for the

proteins targeting to ER-mitochondria contact sites (Stone et al., 2009). However, the presence of a MAM-targeting motif has not been identified in other MAM-enriched proteins and so further research on these signalling mechanisms is required.

Table 1.1: Examples of proteins implicated in regulating ER-mitochondria associations, their general function at the MAMs, their localisation site along with the corresponding references.

Protein name (Abbreviation)	Specific Function at the MAMs	Localisation	Reference
Mitofusin 2 (MFN2)	Regulating ER morphology and mitochondrial fusion	ER/OMM	(de Brito and Scorrano, 2008) (Filadi et al., 2015) (Leal et al., 2016) (Cosson et al., 2012)
Phospho-acidic cluster sorting protein 2 (PACS-2)	ER trafficking and homeostasis	ER	(Simmen et al., 2005)
VAMP-associated protein B (VAPB)	Vesicular trafficking and regulating ER morphology	ER	(De Vos et al., 2012) (Stoica et al., 2014)
Protein tyrosine phosphatase interacting protein 51 (PTPIP51)	Apoptosis and the regulation of cell morphology	OMM	(De Vos et al., 2012) (Stoica et al., 2014)
Inositol 1,4,5-triphosphate receptor (IP_3R)	Calcium signalling	ER	(Szabadkai et al., 2006)
Voltage-dependent anion channel (VDAC)	Calcium signalling	OMM	(Szabadkai et al., 2006) (Rapizzi et al., 2002)
B-cell receptor-associated protein 31 (Bap31)	Apoptotic signalling	ER	(Iwasawa et al., 2011)
Fission homologue 1 (Fis1)	Mitochondrial fission and apoptotic signalling	OMM	(Iwasawa et al., 2011)
Mitochondrial Rho GTPase (Miro)	Mitochondrial movement	OMM	(Kornmann et al., 2011) (Yi et al., 2004)
Truncated S1T variant of sarco/endoplasmic reticulum Ca^{2+} ATPase (SERCA1)	Ca^{2+} ATPase	ER	(Chami et al., 2008)
PKR-like ER kinase [PERK]	ER stress	ER	(Harding et al., 1999)
Receptor expression enhancing protein 1 (REEP1)	ER membrane shaping protein	ER	(Lim et al., 2015)
Presenilin 1 (PS-1)	γ-secretase protease complex	Predominantly ER	(Area-Gomez et al., 2012)
Presenilin 2 (PS-2)	γ-secretase protease complex	Predominantly ER	(Area-Gomez et al., 2012) (Zampese et al., 2011)
α-Synuclein	Mitochondrial function	Cytosol/OMM	(Cali et al., 2012)
Parkin	Mitophagy	Cytosol/OMM	(Cali et al., 2013) (Celardo et al., 2016)
PTEN-induced putative kinase 1 (PINK1)	Mitophagy	Cytosol/OMM	(Celardo et al., 2016)
Sigma-1 Receptor	Calcium signalling	ER and nucleus	(Hayashi and Su, 2007) (Bernard-Marissal et al., 2015)
Amyloid Precursor Protein C-terminal fragment (99aa) (C99)	Intermediate fragment in Aβ generation	Predominantly endosomes	(Pera et al., 2017)
PDZ domain containing 8 (PDZD8)	Cytoskeletal organisation	ER	(Hirabayashi et al., 2017)

1.1.2 Functions of MAMs

1.1.2.1 MAMs and lipid biosynthesis and exchange

Maintaining the lipid composition of cellular and organelle membranes is a tightly regulated process and relies on efficient lipid trafficking from the ER membrane where the majority of lipid synthesis occurs. The inner membrane of mitochondria is highly enriched for phosphatidylethanolamine (PE) and a reduction in the PE content is associated with abnormal mitochondrial morphology, oxygen consumption and ATP production (Tasseva et al., 2013). One of the major pathways in which PE is synthesised is in the mitochondria by the decarboxylation of phosphatidylserine (PS) but in order for this to take place, PS must be transported from its site of synthesis in the ER to the inner mitochondrial membrane (Zborowski et al., 1983). The diffusion of lipids through the aqueous environment of the cytosol is an energetically unfavourable process and so the possibility has been raised that non-vesicular trafficking of lipids may take place at the MAMs (Vance, 2014). In support of this, the two proteins that synthesise PS, PS synthase 1 and 2, are highly enriched in the MAMs in comparison to the rest of the ER (Stone and Vance, 2000). An experiment inhibiting PS decarboxylase using hydroxylamine resulted in an increase in the levels of PS in the MAM fraction which stayed constant, in contrast to untreated cells in which the PS pool gradually declined (Shiao et al., 1995). Similarly, depleting ATP levels, which is essential for phospholipid transport, also caused PS to accumulate in the MAM fraction (Shiao et al., 1995). In hepatocytes, newly synthesised PE is transported from the mitochondria back to the ER where it is methylated to form phosphatidylcholine (PC), further supporting a key role of the ER-mitochondria interface in lipid biosynthesis (Voelker, 2005).

Enzymes involved in the synthesis of cholesterol and cholesteryl esters are found to be enriched in the MAMs including 3-hydroxy-3-methylglutaryl-CoA reductase and acyl-CoA acyltransferase which implicates a role of these contact sites in cholesterol synthesis (Rusinol et al., 1994). In comparison to the bulk ER, the MAMs are enriched with cholesterol (Hayashi and Fujimoto, 2010) and depleting the levels of cholesterol increases ER-mitochondria associations (Fujimoto et al., 2012). The transport of

cholesterol from the ER to the mitochondria is essential for steroid and bile acid production and while evidence may suggest that this transfer could occur via the MAMs, a direct role of these contact sites in cholesterol transport has not yet been elucidated. In CHO cells, a reduction in VDAC1 levels decreases cholesterol transfer to the IMM which suggests a role of this protein, that is highly enriched at the MAMs, in cholesterol transport (Kennedy et al., 2012). Similarly, the AAA domain-containing protein 3 (ATAD3) is present at the MAMs and plays a key role in cholesterol transport, indicating a possible role of the contact sites in this process (Issop et al., 2015).

1.1.2.2 MAMs and calcium homeostasis

The endoplasmic reticulum is a major store for calcium ions that play a critical role in a wide host of signalling pathways within the cell and upon the release of calcium ions into the cytoplasm, mitochondria can act as buffers to uptake calcium and maintain appropriate cytosolic ion concentrations (van Vliet et al., 2014). The intake of extra-mitochondrial calcium exerts a strong effect over the phosphorylation states of several metabolic enzymes in the mitochondrial matrix, including pyruvate dehydrogenase and isocitrate dehydrogenase and therefore plays an important role in metabolic regulation (Nicholls and Budd, 2000; Hopper et al., 2006).

This calcium exchange function was attributed to the MAMs upon the discovery that mitochondria are exposed to higher concentrations of Ca^{2+} in comparison to the cytosol, following Ca^{2+} release from the ER (Rizzuto et al., 1998) and that mitochondria in very close proximity to the ER had higher calcium levels than those that were not (Rutter and Rizzuto, 2000). The mitochondrial calcium channel uniporter (MCU) is the protein that allows Ca^{2+} to be transported in to the mitochondrial matrix across the electrochemical gradient (De Stefani et al., 2011). However, an apparent discrepancy exists between the low affinity of MCU for Ca^{2+} and the steep rise in mitochondrial Ca^{2+} following release from the ER. This inconsistency can be explained by the fact that this calcium exchange takes place at tight ER-mitochondria junctions that are enriched for IP_3R (mediating ER calcium release) and voltage-dependent anion channels (VDAC) that allow Ca^{2+} ions to

transverse the OMM (Rapizzi et al., 2002; Szabadkai et al., 2006). The MAMs provide a site where mitochondria can sense microdomains of high cytosolic Ca^{2+} levels following release from IP_3R and rapidly uptake Ca^{2+} within the mitochondrial matrix (Csordas et al., 2010; Rizzuto et al., 2012). The sigma-1 receptor protein that is involved in regulating calcium exchange between the two organelles is also enriched at the MAMs (Hayashi and Su, 2007).

Studies have shown that altering the distance between the ER and mitochondria at the MAMs has an impact on the ability of mitochondria to uptake calcium. Treatment with trypsin or proteinase K loosened ER-mitochondria contacts and disrupted calcium exchange between the organelles without effecting IP_3R-mediated ER calcium release or the actual ability of mitochondria to uptake calcium ions (Csordas et al., 2006). In contrast, transfecting cells with artificial linker proteins consisting of an N-terminus OMM targeting sequence and a C-terminus ER targeting domain tightened the junctions, increasing mitochondrial calcium uptake capacity and making them susceptible to calcium overloading and opening of the MPT to activate apoptosis (Csordas et al., 2006). The influence of MAMs over calcium levels is bi-directional as the association of the ER with the mitochondria can also be regulated by cytosolic calcium levels (Wang et al., 2000; Goetz et al., 2007).

1.1.2.3 MAMs and mitochondrial morphology

In mammalian cells, fission events rely on dynamin-related protein 1 (Drp1) (Dynamin-1/Dnm1 in yeast), a cytoplasmic protein that is capable of self-oligomerising into helices that surround and constrict the mitochondrial membrane for division. The activity of this protein is controlled by calcium-mediated phosphorylation/dephosphorylation of Ser656 by the OMM protein kinase A (PKA) (Dickey and Strack, 2011; Ingerman et al., 2005). Mitochondrial fusion events on the other hand, are regulated by a number of proteins including Mitofusin-1 and 2 (MFN1/MFN2) (Chen et al., 2003). Some of the factors controlling fission and fusion events of the mitochondrial network can also regulate *cristae* morphology which has been shown to alter structurally, depending on the respiratory state of the cell, as revealed by electron tomography studies (Mannella et al., 2001; Pich et al., 2005).

As the IMM possesses the proteins necessary for ATP synthesis, the tight regulation of mitochondrial fission and fusion events has important implications for not only the structure of the mitochondria but for their function in metabolism.

Through fluorescent live-cell imaging of yeast cells, Dnm1 puncta were seen to localise to the points of contact of fluorescently labelled ER and mitochondria in the vast majority of mitochondrial division events (87%), suggesting that these fission events occur predominantly at the MAMs (Friedman et al., 2011). Furthermore, Drp1-dependent mitochondrial division is regulated by fission 1 homologue (Fis1), a protein believed to be involved in ER-mitochondria tethering through the formation of a complex with the integral ER membrane protein B-cell receptor-associated protein 31 (Bap31) (Iwasawa et al., 2011; Ingerman et al., 2005).

Mitofusin-2 (MFN2) is one of the best studied tethers between the mitochondria and ER and plays a role in regulating mitochondrial morphology and directing fusion events. The protein has both an ER and mitochondrial localisation but is enriched 14-fold in the MAM fraction in comparison to the mitochondrial fraction in Percoll-purified subcellular fractions (de Brito and Scorrano, 2008). In order to form ER-mitochondria contacts, MFN2 forms homotypic interactions with other MFN2 proteins or heterotypic fusions with MFN1 that is found only on the outer mitochondrial membrane (de Brito and Scorrano, 2008). While it is generally agreed that altering the levels of MFN2 impacts ER-mitochondria contacts, confounding evidence exists as to what the exact nature of this change is. Some studies have demonstrated an increase in the association of the ER with mitochondria following knock-down of MFN2 expression with a consequent increase in mitochondrial calcium levels (Filadi et al., 2015; Leal et al., 2016; Cosson et al., 2012), while others have observed a reduction in ER-mitochondria associations causing a decrease in mitochondrial calcium uptake and lower levels of phosphotidylserine incorporated into phosphotidylethanolamine (de Brito and Scorrano, 2008).

1.1.2.4 MAMs and cell survival and death

The regulation of mitochondrial calcium levels is intrinsically linked to apoptosis, a mechanism of programmed cell death that activates in response to a variety of initiator stimuli and manifests as characteristic cell morphological changes and the destruction of the cell (Kerr et al., 1972). Upon excessive calcium uptake by the mitochondria, changes are induced to mitochondria membrane potential and the oligomerisation of a protein called BAX (Bcl-2 associated X protein) is promoted (Nicotera and Orrenius, 1998) (Scorrano et al., 2003). This results in the opening of the mitochondrial permeability transition (MPT) pore that allows for the consequent release of pro-apoptotic factors such as cytochrome c into the cytosol, resulting in the death of the cell (Nicotera and Orrenius, 1998). Therefore, a relationship exists between apoptotic cell death and the regulation of the MAMs.

One of the hallmark features of apoptosis is the fragmentation of the mitochondrial network due to the recruitment of Drp1 protein to the outer mitochondrial membrane to induce fission events, a process which takes place specifically at the MAMs (Frank et al., 2001). Furthermore, expression of a dominant-negative form of Drp1 blocks apoptosis and prevents cell death, strengthening the link between Drp1 activity at the MAMs and apoptosis (Frank et al., 2001). Silencing expression of the ER-mitochondria tether protein PACS2 results in the upregulation of pro-apoptotic factors illustrating how disrupting ER-mitochondria associations can lead to a cell death response (Simmen et al., 2005).

Although a role of the MAMs in apoptosis was implicated, the mechanism by which cell death signals were communicated between the two organelles was unclear until the identification of a Fis1-Bap31 complex spanning the ER-mitochondria junction (Iwasawa et al., 2011). Bap31 localises to the ER membrane and forms a protein complex with several known regulators of apoptosis such as B-cell lymphoma 2 (Bcl-2) (Ng et al., 1997). The binding of Bap31 to the outer mitochondrial membrane protein Fis1 not only acts as a tether for ER-mitochondria interactions but generates a platform for pro-caspase 8 recruitment to cleave Bap31 and propagate pro-apoptotic signals (Iwasawa et al., 2011)**(Fig 1.2)**. The cleavage product of Bap31

promotes the emptying of ER calcium stores thereby resulting in an increase in mitochondrial calcium levels to promote MPT pore opening.

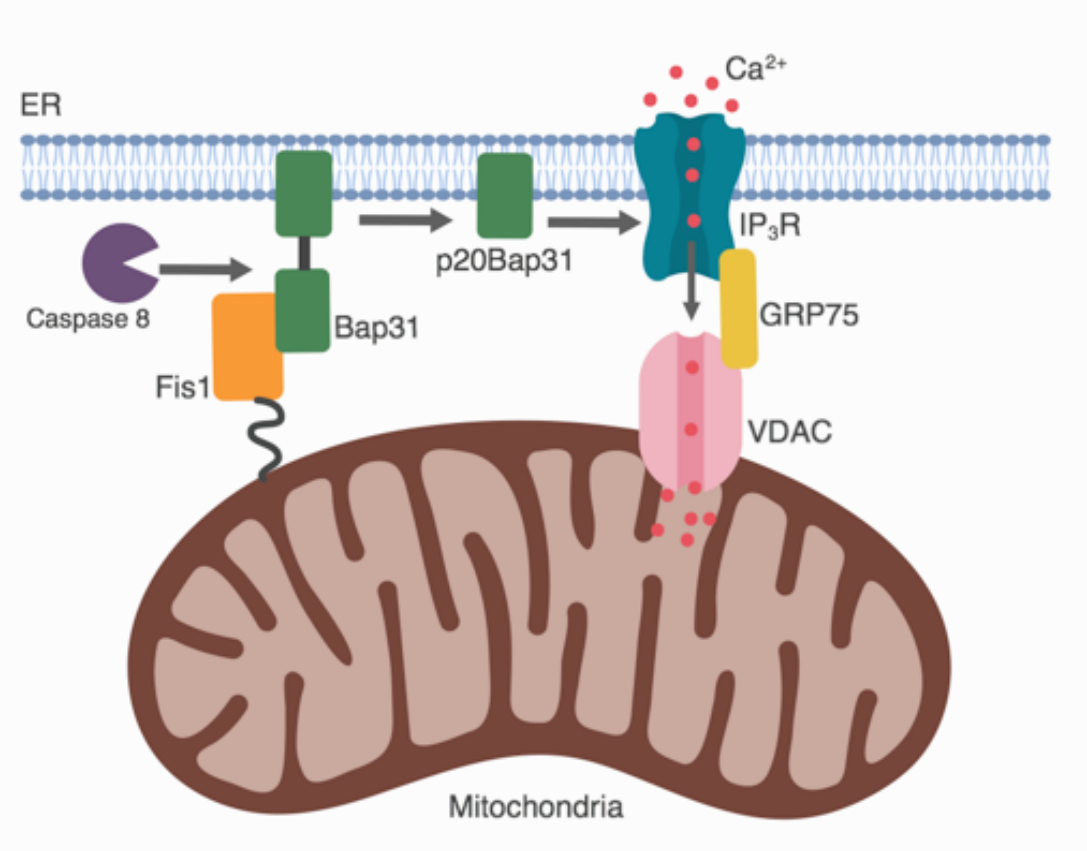

Fig 1.2: Schematic illustration of the Fis1/Bap31 protein complex in promoting ER calcium release. The Fis1/Bap31 protein complex is formed at regions of close apposition between the ER and mitochondria and creates a platform for the recruitment of caspase-8 under cellular stress conditions. Proteolytic activity of caspase-8 generates the p20Bap31 truncation product that induces IP_3R calcium release. Subsequent mitochondrial calcium uptake can trigger the release of pro-apoptotic factors into the cytoplasm. Illustration was produced on BioRender [Available at https://app.biorender.io].

1.1.2.5 MAMs and the initiation of autophagosome formation

Autophagy is one of the main intracellular protein degradation pathways involving the bulk sequestration of cytoplasmic contents in double-membraned vesicles termed autophagosomes and the eventual degradation and recycling of the contents via fusion with late endosomes and lysosomes. The role of autophagy has been

linked to a wide number of physiological process including adaptation to nutrient starvation, the clearance of misfolded proteins or protein aggregates, the aging process, elimination of microorganisms and cell death [For a review see (Mizushima, 2005)]. The process of autophagosome membrane formation is highly conserved between species and involves a family of proteins termed the autophagy related (atg) proteins, identified from yeast genetic screens (Klionsky et al., 2003). Nutrient deprivation is a key inducer of autophagy through the mammalian target of rapamycin (mTOR) signalling pathway in which the TOR complex 1 (TORC1) is a negative regulator of autophagy in both yeast and mammals (Mizushima et al., 2011; Ravikumar et al., 2004).

In mammalian cells, Unc-51-like kinase 1/2 (ULK) (the homologue of yeast Atg1) is a serine/threonine kinase that forms a stable complex and can bind to the phosphatidylinositol 3-kinase (PI3K) complex, which includes Atg14 and Beclin-1 (Hosokawa et al., 2009; Itakura et al., 2008; Mizushima et al., 2011). The ULK1 protein complex is constitutively formed but is deactivated by mTORC1 phosphorylation under nutrient rich conditions (Hosokawa et al., 2009). These complexes then translocate to the autophagosome formation site upon suppression of mTORC1 where PI3K produces phosphatidylinositol 3-phosphate (PI3P), an essential component for autophagosomes formation (Obara et al., 2008; Mizushima et al., 2011; Axe et al., 2008). Atg14 is likely the determinant for the specific localisation of the PI3K complex to the ER membrane as ectopic localisation of Atg14 to the plasma membrane also results in the localisation of Beclin-1 and other proteins of the PI3K complex to be found at this site (Matsunaga et al., 2010). In nutrient-rich conditions, Bcl-2 binds to Beclin-1 to inhibit its autophagic function but under starvation conditions, JNK1 (c-Jun N-terminal protein kinase 1) phosphorylates Bcl-2 to promote its dissociation from Beclin-1 (Wei et al., 2008). Atg12-Atg5-Atg16L form a protein complex conjugation system that forms regardless of nutrient conditions on the outside of the autophagosome membrane during the elongation

process and dissociates once the membrane formation is completed (Mizushima et al., 2001; Mizushima et al., 2011).

Although many of the steps in the autophagosome formation process have been elucidated, controversial evidence exists as to where the source of the membrane comes from, particularly as the majority of proteins involved are cytosolic (Xie and Klionsky, 2007). The endoplasmic reticulum is probably the best candidate for the pre-existing source of membranes for autophagosome formation. Atg14 is essential for the translocation of the PI3K complex to the ER membrane (Matsunaga et al., 2010) and electron microscopy images suggest that the ER membrane may form a template for the elongation of the autophagosome and provide the lipid components necessary for this process (Mizushima et al., 2011; Hayashi-Nishino et al., 2009).

Atg9 is the only known transmembrane Atg protein and while its function is not well understood, it has been seen to shuttle between omegasomes (autophagy-related structures), endosomes and the trans-Golgi network, highlighting these as potential membrane sources (Young et al., 2006; Tooze and Yoshimori, 2010). In further support of this, in yeast cells some of the proteins involved in vesicle exit from the Golgi have also been implicated in the early stages of autophagy (Geng et al., 2010; van der Vaart et al., 2010).

Recently, it has been proposed that the MAMs may be the sites of autophagosome formation. Under starvation conditions, fluorescently-tagged Atg14 and Atg5 relocalised into puncta that appeared at the sites of ER-mitochondria contact (Hamasaki et al., 2013). Furthermore, Percoll centrifugation was used to isolate the MAMs and indicated that Atg14 as well as other components of the PI3K complex shifted to the MAM fraction under starvation conditions (Hamasaki et al., 2013). In starved cells, when the expression of either of two ER-mitochondria protein tethers, PACS-2 or MFN2 was knocked-down *in vitro* to decrease ER-mitochondria associations, it prevented the relocalisation of Atg14 to the MAMs and inhibited

autophagosome formation (Hamasaki et al., 2013). An additional study demonstrated that under starvation conditions, fluorescently labelled phosphotidylserine transferred from the ER to the mitochondria at the MAMs was incorporated in to autophagosomes and knocking-down MFN2 inhibited this process (Hailey et al., 2010).

1.1.2.6 MAMs and ER stress

The endoplasmic reticulum is the primary site where proteins are synthesised, folded and post-translationally modified and as such, this organelle has evolved to be rich in various ER chaperone proteins and enzymes involved with post-translational modifications. The concentration of proteins in the ER lumen is very high and the simultaneous folding of thousands of polypeptides creates a risk of folding errors or protein aggregation (Stevens and Argon, 1999). Protein folding is an energy demanding process with many ER chaperone proteins being sensitive to ER Ca^{2+} levels and requiring ATP (Corbett et al., 1999; Blond-Elguindi et al., 1993). If a cellular state is reached whereby the folding load of the ER lumen exceeds the protein folding capacity of the ER, it is referred to as ER stress. Cells have an adaptive unfolded protein response (UPR) to detect and overcome the presence of ER stress [as reviewed by (Oslowski and Urano, 2011)]. The three ER proteins that sense ER stress are Activating Transcription Factor 6 (ATF6) (Shen et al., 2002), Inositol Requiring 1 (IRE1) (Wang et al., 1998) and PKR-like ER kinase [PERK] (Harding et al., 1999) **(Fig 1.3)**.

IRE1 is a type I ER membrane kinase that senses an accumulation of misfolded or unfolded proteins and autophosphorylates to become activated. Once active, this protein splices XBP1 (X-box binding protein 1) mRNA that then encodes for a transcription factor to upregulate the expression of UPR genes including the ER folding protein disulphide isomerase (PDI) and ATF6 (Lee et al., 2003; Calfon et al., 2002). Additionally, under prolonged periods of ER stress, activated IRE1 can recruit TNF-receptor-associated factor 2 (TRAF2), leading to JNK activation and the promotion of apoptotic signalling (Urano et al., 2000b; Urano et al., 2000a).

PERK is another type I ER membrane kinase that is self-activated by autophosphorylation under ER stress conditions, phosphorylating and activating the α subunit of eukaryotic initiation factor 2 (eIF2α) (Harding et al., 1999). Activated eIF2α inhibits mRNA translation globally in an attempt to alleviate the protein folding load of the ER (Harding et al., 2000b). However, while the translation of most mRNA is repressed, eIF2α activation selectively promotes the translation of Activating Transcription Factor 4 (ATF4) which in turn upregulates the pro-apoptotic protein CHOP (CCAAT/enhancer-binding protein (C/EBP) homologous protein) in periods of prolonged ER stress (Harding et al., 2000a).

ATF6 is a 90 kDa type II integral ER transmembrane protein that undergoes a proteolytic cleavage by Site-1 protease (S1P) and Site-2 protease (S2P) upon the induction of ER stress to generate an activated basic-leucine zipper (b-ZIP) factor that translocates to the nucleus and upregulates genes involved in protein folding and degradation (Ye et al., 2000; Haze et al., 1999).

During the early adaptive stage of ER stress, several studies have shown an associated increase in the number of ER-mitochondria contacts (Chami et al., 2008; Csordas et al., 2006; Bravo et al., 2011). Cells treated with tunicamycin, an inhibitor of N-linked glycosylation, demonstrated a migration of the mitochondrial network towards the nucleus coinciding with increased ER-mitochondria associations, hyperpolarisation of mitochondrial membrane potential and increased ATP production suggesting that increased ER-mitochondria contacts may be a response mechanism to the energy demands of ER stress (Bravo et al., 2011). Under periods of prolonged ER stress, a truncated S1T isoform of the sarco/endoplasmic reticulum Ca^{2+} ATPase (SERCA1) was seen to localise to the MAMs, resulting in increased associations between the two organelles and eventual mitochondrial calcium overload and pro-apoptotic signalling (Chami et al., 2008). The expression of S1T is mediated by ATF4, activated through the PERK-eIF2α signalling pathway during UPR (Chami et al., 2008). PERK also seems to have a direct influence on ER-mitochondria contacts, independent of the UPR, as this protein was found to be enriched in the

MAMs and genetic deletion of PERK in mouse embryonic fibroblasts (MEFs) reduced ER-mitochondria associations (Verfaillie et al., 2012). A direct interaction between PERK and MFN2 at these contact sites has been identified. Knock-down of MFN2 expression was shown to upregulate markers of UPR (Ngoh et al., 2012) although there was defective apoptotic and autophagic responses to ER stress (Munoz et al., 2013). Under basal conditions, MFN2 directly interacts with PERK and negatively regulates it and an ablation of MFN2 expression is linked with enhanced phosphorylation of PERK and increased mitochondrial Ca^{2+} levels (Munoz et al., 2013). In addition to ER-mitochondria contacts, PERK has also recently been implicated in establishing contact sites between the ER and plasma membrane through the interaction with Filamin A (van Vliet et al., 2017).

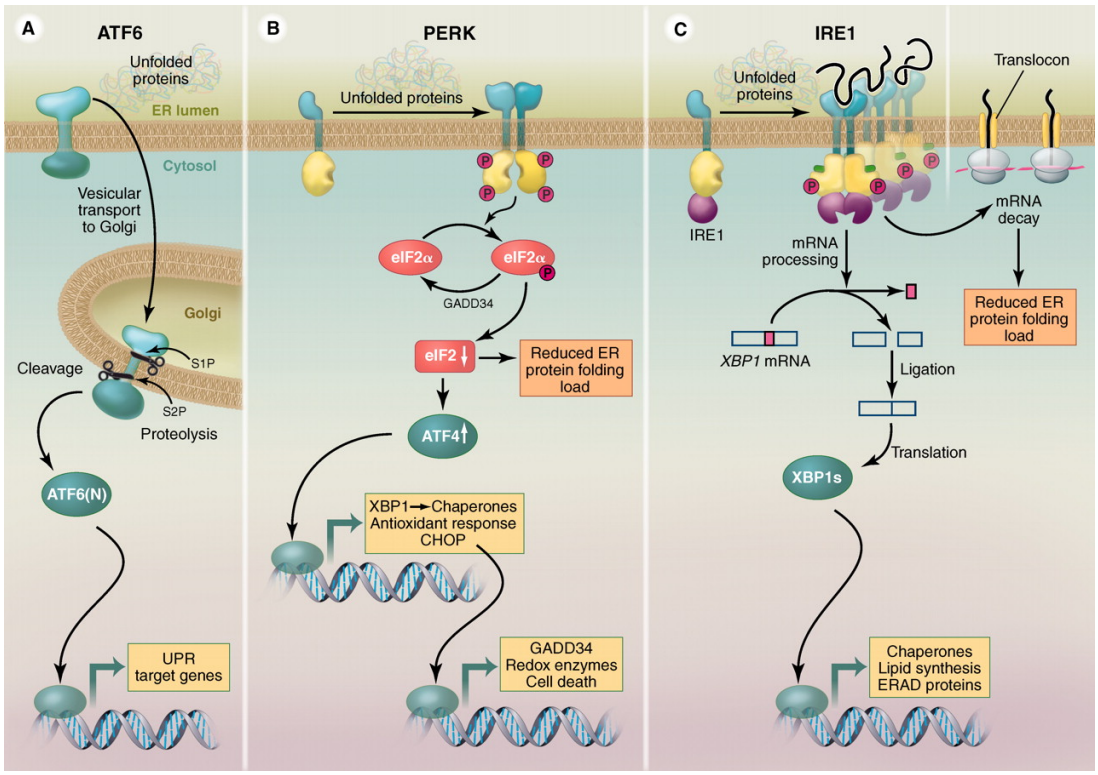

Figure 1.3: Schematic illustration of the unfolded protein response (UPR). The induction of ER stress activates the three main pathways of the UPR; ATF6, PERK and IRE1/XBP1 pathways that work to alleviate protein load, upregulate the expression of UPR target genes involved in protein folding and degradation. In periods of extended ER stress, the PERK pathway can upregulate pro-apoptotic factors. Figure as published in (Walter and Ron, 2011). Reprinted with permission from AAAS.

1.1.2.7 MAMs and mitochondrial/ER movements

The endoplasmic reticulum and mitochondria are highly dynamic organelles that are capable of moving in a bidirectional fashion with the assistance of the motor proteins dynein and kinesin along the microtubule network (Wozniak et al., 2009; Pilling et al., 2006). Live-cell imaging experiments have demonstrated that the ER and mitochondria appear to stay in contact with one another as the organelles move and that the two organelles colocalised over post-translationally acetylated microtubules (Friedman et al., 2010). It has been suggested that this post-translational modification may be a regulatory mechanism ensuring the migration of the organelles along the same microtubule or potentially, the movement of one organelle may be dominant and pull the tethered membrane of the other organelle along with it (Friedman et al., 2010; Rowland and Voeltz, 2012). Controlling ER and mitochondrial movements may be one mechanism by which the formation of contact sites at the MAMs is promoted. In mammalian cells, mitochondrial movements involve the OMM mitochondrial Rho GTPase subfamily Miro 1 and 2 proteins which binds to milton which is in turn bound to kinesin-1 on the microtubules (Glater et al., 2006). Miro proteins localise well to the MAMs (Kornmann et al., 2011) and are sensitive to elevated cytosolic calcium levels, halting mitochondrial mobility in response (Saotome et al., 2008). Stopping mitochondrial movements encourages the formation of close contacts with the ER, enhancing their calcium uptake ability and ATP production when the demand is high (Lee et al., 2016; Saotome et al., 2008; Yi et al., 2004).

1.1.2.8 MAMs and mtDNA replication

In mammalian cells, mitochondrial DNA (mtDNA) is packaged within nucleoids that are evenly distributed throughout the mitochondrial network (**Garrido et al., 2003**). The spatiotemporal regulation of mtDNA replication is functionally linked to mitochondrial fission, that occurs at ER-mitochondria contact sites, as disrupting fission events leads to nucleoid aggregation and mtDNA abnormalities (**Ishihara et al., 2015**; **Itoh et al., 2013**). Accordingly, nucleoids were seen to be spatially linked to ER-mitochondria contact sites in both yeast and mammalian cells (**Murley et al.,**

2013; Lewis et al., 2016). Although there are many physical interaction sites between the ER and mitochondria in a given cell, only a small subset of contact points are associated with mitochondrial division events. Specific fluorescent labelling of a sub-set of nucleoids actively undergoing mtDNA synthesis (approx. 10%) revealed that the majority of mitochondrial fission events occurred within 1 μm of nucleoids engaged in mtDNA synthesis (Lewis et al., 2016). The evidence illustrates that replicating nucleoids mark nascent mitochondrial fission events proximal to sites of close physical apposition of the ER and mitochondria, and precedes the recruitment of Drp1 (Lewis et al., 2016). Disruption of the ER structure reduced the number of replicating nucleoids within the mitochondrial network, and so it is hypothesised that efficient ER-mitochondria contact formation permits mtDNA synthesis, perhaps by creating a platform for the recruitment of proteins and other components involved in mtDNA replication (Lewis et al., 2016).

1.1.2 ER-endosome contacts

As stated, the ER does not only form physical complexes with the mitochondria but with many other organelles including endosomes (Raiborg et al., 2015b). The endocytic pathway involves the uptake and transport of materials by inward budding of the plasma membrane to form early endosomes that sort cargo to their target destinations (Conner and Schmid, 2003). Early endosomes gradually mature into late endosomes that fuse with the lysosome for the degradation of remaining cargo. Fluorescence resonance energy transfer (FRET) studies provided evidence of close physical interaction between endosomes and the ER by quantifying FRET between Cy3-conjugated tyrosine phosphatase PTP1B localised on the ER and a GFP-tagged receptor tyrosine kinase, epidermal growth factor receptor (EGFRs) contained within early endosomes (Haj et al., 2002). This permitted the identification of sites of direct EGFR dephosphorylation by PTP1B and identified these sites as the physical contact points between the ER and endosomes (Haj et al., 2002), an observation that was subsequently confirmed by electron microscopy (Eden et al., 2010). ER-endosome contact sites appear to increase as endosomes mature and it is estimated that 99%

of late endosomes will have a contact site with ER membrane, covering approximately 5% of the endosome surface area (Friedman et al., 2013). Electron microscopy images have defined these contact sites as being between 3-15 nm on average (Alpy et al., 2013). A key regulator of ER-endosome contacts is the integral ER membrane protein VAPA which can bind to the FFAT motifs (two phenylalanines [FF] in an acidic tract) of various endosomal proteins including OSBP (Oxysterol-related binding protein)-related protein 1L (ORP1L) (Rocha et al., 2009), STAR related lipid transfer domain containing 3 (STARD3) and STARD3 N-terminal like (STARD3NL) (Alpy et al., 2013) to hold the organelles in close apposition. FFAT motifs contain the amino acid sequence EFFDAxE and are found within lipid-binding proteins (Loewen et al., 2003). Similar to the function of MAMs, ER-endosome contact sites are involved in cholesterol transfer from late endosomes to the ER through the binding of the ER protein oxysterol-binding protein-related protein 5 (ORP5) with the endosome-membrane associated Niemann-Pick disease type C1 (NPC1) cholesterol transporter (Du et al., 2011).

Further commonalities exist between the functions of ER-endosome contacts and ER-mitochondria contacts. During lysosomal permeabilisation, localised spikes in cytosolic calcium levels induce IP_3R mediated ER calcium release and this coupling is bi-directional as ER calcium release can be accumulated by lysosomes (Lopez-Sanjurjo et al., 2013). Ca^{2+} channel opening generates microdomains of elevated Ca^{2+} concentrations and therefore it is likely that this Ca^{2+} signalling is occurring at sites of close apposition between the ER and lysosomes (Shuai and Parker, 2005; van der Kant and Neefjes, 2014). The biological relevance of this calcium coupling is believed to be in endosomal fusion and maturation as some studies suggest that Ca^{2+} is necessary for early endosomal fusion (Colombo et al., 1997) and for the fusion of late endosomes to the lysosome (Pryor et al., 2000). A role of the ER tubules in defining sites of fission events also seems to be conserved across organelles. Live-cell imaging has revealed the movement of an ER tubule to constrict early endosomes, preceding endosomal budding and fission events (Rowland et al., 2014).

An additional role of ER-endosome contacts is to regulate endosomal motility and position. Protrudin is an ER membrane protein that binds RAB7 and phosphatidylinositol 3-phosphate (ptdIns3P) on the late endosome membrane in order to form a physical inter-organelle link (Raiborg et al., 2015a). Protrudin then binds to the heavy chain of the microtubule motor protein kinesin-1 to facilitate its binding to FYCO1 (FYVE and coiled-coil domain containing 1), guiding the movement of the endosomes to the cell periphery where it can promote the outward growth of neurites (Raiborg et al., 2015a).

1.1.3 ER-plasma membrane contacts (ER-PM)

Numerous proteins have been implicated in forming membrane contact sites between the ER and the plasma membrane (PM), which are believed to play a role in calcium signalling and lipid transfer. Under conditions of reduced ER lumen calcium concentrations, the ER-protein stromal interacting molecule 1 (STIM1) can accumulate at existing ER-PM contact sites while also inducing the formation of new contact sites where it binds to the plasma membrane protein Orai1 (calcium-release activated calcium channel protein 1) (Wu et al., 2006). The binding of STIM1 to Orai1 induces an influx of extracellular calcium ions through the store operated calcium entry (SOCE) system to replenish ER calcium levels and maintain homeostasis [As reviewed by (Lewis, 2007)]. Using single-molecule tracking to analyse diffusion rates of STIM1 and Orai1 illustrated that once bound to one another, their movement is trapped within these junctional complexes which suggests that ER-PM contact sites may represent regions of distinct microenvironments (Henne et al., 2015; Wu et al., 2014). VAPs have also been implicated in regulating ER-PM contacts through their interaction with the FFAT motif of Oxysterol binding homology (OSH) proteins that possess phosphatidylinositol 4-phosphate (PI4P) PH (Pleckstrin homology) binding domains that allow them to interact directly with the PM (Stefan et al., 2011). Through this interaction, ER-PM contact sites are involved in the transfer of sterols, bound to OSH proteins such as Osh3, from the ER to the PM (Stefan et al., 2011; Henne et al., 2015). ER-PM junctions are consistently between 10–25 nm and are formed at regions of ER membrane that lack ribosomes (Henne et al., 2015). As VAP

proteins are relatively shorter than other proteins implicated in mediating ER-PM contacts, it is believed that the recruitment of binding partners via FFAT motifs is essential in order to span the width of the ER-PM junction (Henne et al., 2015).

1.1.4 ER-Golgi contacts

The Golgi apparatus in eukaryotic cells has a characteristic structure composed of membrane-enclosed cisternae arranged in stacks that can be sub-divided into *cis*, medial and *trans* cisternae (Day et al., 2013). ER exit sites (ERES) are believed to be the site of Golgi organelle generation where it receives COPII vesicles containing newly synthesised proteins from the ER (Suda and Nakano, 2012). The Golgi apparatus then plays a critical role in protein modification, as it is enriched for glycosylation and other enzymes, and mediates transport of the proteins to their final destinations [As reviewed by (Stanley, 2011)].

Similar to other inter-organelle contact sites, membrane contact sites between the ER and Golgi apparatus also play a key role in the non-vesicular transport of lipids. Several proteins have been identified that are localised to these junctions including CERT (ceramide transfer protein) (Kawano et al., 2006), the phosphatidylinositol-transfer protein NIR2 (Pyk2 N-terminal domain-interacting receptor 2) that regulates DAG (diacylglycerol) levels in the Golgi (Litvak et al., 2005), the glycosylceramide-transfer protein Golgi-associated four-phosphate adaptor protein 2 (FAPP2) (D'Angelo et al., 2007) and OSBP (Mesmin et al., 2013). All of these proteins possess a PH domain allowing them to bind PI4P on the Golgi and FFAT motifs allowing them to interact with VAP which again highlights the VAP protein family as being a key modulator of organelle contact site formation (Phillips and Voeltz, 2016). Depletion of VAP levels results in the mislocalisation of the previously mentioned lipid transport proteins and a consequent disruption of Golgi structure (Peretti et al., 2008). The regulation of ER-Golgi contact sites and correct maintenance of lipid homeostasis within the Golgi is also critical for the efficient vesicular transport of proteins [as reviews by (McMaster, 2001)].

1.1.5 ER-peroxisome contacts

Peroxisomes are organelles derived from ER membrane that function in the metabolism of lipids and reactive oxygen species (Hoepfner et al., 2005). The function of the peroxisome depends on close spatial proximity to the ER and the formation of a protein complex tethering the two organelles has been identified through the binding of the ER membrane protein VAPB to the peroxisomal membrane protein acyl-coenzyme A-binding domain protein 5 (ACBD5) (Costello et al., 2017). Co-expression of VAPB and ACBD5 increased ER-peroxisome associations and tightened the distance of the junction between these organelles while silencing the expression of either protein reduced contacts (Costello et al., 2017). Peroxisomes lack enzymes necessary for lipid biosynthesis and so an important function of the tight physical association between the ER and peroxisome is the nonvesicular transport of lipids from the ER to rapidly provide the lipids required for peroxisome membrane formation and maintenance (Raychaudhuri and Prinz, 2008).

Due to the wide variety of processes that are regulated by inter-organelle contact sites, it is unsurprising that a perturbation to the correct formation and maintenance of these structures has been implicated in a number of diseases including neurodegenerative disorders. As will be covered in the following sections, some of the main pathways implicated in the neuropathological process of neurodegeneration are linked with organelle membrane contact sites. Using three examples of neurodegenerative disorders, evidence for how a dysfunction to these contact sites could link the molecular mechanisms of neurodegeneration together will be discussed.

1.2 Molecular mechanisms of neurodegeneration

Neurodegeneration is an umbrella term encompassing a group of heterogeneous disorders characterised by the progressive death of specific neuronal subtypes. Common examples of neurodegenerative disorders include Alzheimer's disease

(AD), Parkinson's disease (PD) and amyotrophic lateral sclerosis (ALS). Although these diseases vary greatly in their underlying genetic causes and clinical manifestations, the pathogenic mechanisms of neurodegeneration converge on several, seemingly disparate cellular pathways. The broad range of molecular mechanisms involved in neurodegeneration has presented a significant challenge to therapeutics and therefore it is of particular research interest to elucidate commonalities in the pathogenic mechanisms of neuronal cell death.

1.2.1 Mitochondrial dysfunction and oxidative stress

Due to the high energy demands of neurons, an impairment of mitochondrial function can have devastating consequences to the cell and is observed in a number of neurodegenerative diseases [As reviewed by (Johri and Beal, 2012)]. Perturbations to the mitochondria can result in three main metabolic defects, creating a pathogenic "mitochondrial spiral" in which any one of the functional impairments can induce the other two in a downward spiral towards cell death (Blass, 2000). These main defects are insufficient energy metabolism, dysregulation of calcium homeostasis and oxidative stress (excessive production of oxidants as a by-product of respiration or an impairment to the antioxidant system), all of which can result in a release of pro-apoptotic signals from the mitochondria to induce neuronal degeneration (Blass, 2000). An abundance of evidence exists for the role of mitochondrial dysfunction in neurodegeneration as illustrated in the following three examples.

1.2.1.1 Mitochondrial dysfunction in PD

Parkinson's disease is a neurodegenerative disease arising from the gradual degeneration of dopaminergic neurons of the *substantia nigra pars compacta* and is characterised by the presence of Lewy body protein aggregates containing α-synuclein (Hirsch et al., 1999; Spillantini et al., 1997). Approximately 10% of PD cases arise from autosomal recessive mutations in genes encoding PINK1 (PTEN Putative Kinase 1) and parkin and autosomal-dominant mutations in α-synuclein (Valente et al., 2004; Shimura et al., 2000; Polymeropoulos et al., 1997).

The PD associated PINK1 protein is a mitochondrial serine/threonine kinase involved in the regulation of mitochondrial structure and function and mitophagy, a selective degradative pathway involved with the specific clearance of damaged mitochondria (Rogov et al., 2014; Scarffe et al., 2014). PINK1 accumulates on the surface of depolarised mitochondria where it phosphorylates and recruits ubiquitin and parkin, which in turn causes the ubiquitination and degradation of mitochondrial proteins (Koyano et al., 2014; Yoshii et al., 2011). Due to the role of these proteins in mitochondrial quality control, it is feasible to predict that an impairment to mitophagy may contribute to PD pathogenesis, inefficiently clearing damaged mitochondria that can then induce further damage within the cell.

The PD-associated α-synuclein protein also plays a role in regulating mitochondrial fission/fusion (Kamp et al., 2010; Nakamura et al., 2011). In mutant α-synuclein transgenic mouse models of PD, abnormal morphological changes in the mitochondrial network were observed along with increased reactive oxygen species production and a loss of membrane potential (Martin et al., 2006). Similar mitochondrial defects were observed in cells overexpressing α-synuclein (Shavali et al., 2008; Hsu et al., 2000).

While the evidence shows that mitochondrial defects occur in PD disease progression, it is not entirely certain whether these defects are the cause of neuronal degeneration or arise as a secondary effect of other pathogenic insults. Some evidence for mitochondrial defects being a cause rather than a consequence of dopaminergic neurodegeneration comes from mouse models with a knock-out of the mitochondrial transcription factor A (Tfam), involved with regulating mitochondrial DNA (mtDNA) transcription and copy number (Larsson et al., 1998; Ekstrand et al., 2007). Mitochondrial DNA encodes for 13 key subunits involved in energy metabolism and therefore, defects in the regulation of mtDNA can result in respiratory defects. In agreement with this, mice with a knock-out of Tfam develop severe mitochondrial metabolic defects and a Parkinsonian phenotype in adulthood,

providing strong evidence that mitochondrial defects can be an early primary pathogenic event in neurodegeneration (Ekstrand et al., 2007).

Defects in energy production are not the only evidence for mitochondrial dysfunction in PD and a role of oxidative stress has also been implicated. In the brains of PD patients, lipid peroxidation and cholesterol lipid hydroperoxides are detected at excessive levels in comparison to age-matched controls, a consequence of excessive free radical species production (Dexter et al., 1989). It was suggested that this lipid peroxidation could be due to an impairment of the antioxidant defence system as suggested by the decreased levels of the antioxidant enzyme activity, glutathione peroxidase, resulting in excessive free radical toxicity (Dexter et al., 1989; Johannsen et al., 1991). The combined data suggests that both oxidative and metabolic mitochondrial defects are pathogenic events in PD.

1.2.1.2 Mitochondrial dysfunction in ALS

Amyotrophic lateral sclerosis is a fatal neurodegenerative disease involving degeneration of both the upper and lower motor neurons in the brainstem, ventral horn of the spinal cord and motor cortex. The age of onset and rate of progression of the disease is variable but most commonly occurs in patients over the age of 55, manifesting as symptoms such as muscle atrophy and weakness, spasticity and ultimately death [As reviewed by (Robberecht and Philips, 2013)]. Some ALS cases also present with frontotemporal lobe dementia (FTD) suggesting that ALS pathogenesis is not only restricted to the motor neurons and indeed, C9Orf72 (Chromosome 9 open reading frame 72) expansions, which are the most common cause of familial ALS, are also one of the most common forms of inherited FTD (Renton et al., 2011). Other genetic causes of ALS include the copper/zinc superoxide dismutase (SOD1) (Rosen et al., 1993), alsin (Yang et al., 2001), senataxin (SETX) (Chen et al., 2004), TAR DNA-binding protein 43 (TDP43) (Sreedharan et al., 2008), Fused in Sarcoma (FUS) (Vance et al., 2009), Valosin-containing protein (VCP) (Johnson et al., 2010), VAMP-associated protein B (VAPB) (Nishimura et al., 2004) and sigma-1 receptor protein (Al-Saif et al., 2011).

In human sporadic ALS (SALS) cases, clustering of mitochondria with abnormal morphology has been observed within the intramuscular nerves (Atsumi, 1981). Additionally, in SALS skeletal tissue samples there was a clear decrease in respiratory chain activity (Wiedemann et al., 1998). However, it is not clear whether this is a primary or secondary pathogenic event in ALS pathogenesis. When ALS-linked mutant SOD1 is expressed in primary motor neuronal cultures it causes a depolarisation of mitochondrial membrane potential with a higher level of reactive oxygen species (ROS) produced (Rizzardini et al., 2006). Mutant SOD1 expressing cells had adverse bioenergetics defects and were more sensitive to cell death induced by inhibition of the glycolytic pathway (Menzies et al., 2002).

Furthermore, mutations in two mitochondrial genes, cyclooxygenase 1 (COX1) and mitochondrial transfer RNA isoleucine (tRNAIle), results in the degeneration of motor neurons with a phenotype resembling that of ALS (Comi et al., 1998; Borthwick et al., 2006). This suggests that perturbations to mitochondrial function may be an underlying cause of neuronal degeneration.

1.2.1.3 Mitochondrial dysfunction in AD

Alzheimer's disease (AD) is a neurodegenerative disease characterised by the presence of extracellular plaques predominantly composed of β-amyloid (Aβ), an accumulation of neurofibrillary tangles containing hyperphosphorylated tau protein and progressive neuronal death in the cortex and hippocampus [as reviewed by (Goedert and Spillantini, 2006)]. Most cases of AD are sporadic but approximately 1% of cases arise from an inherited autosomal-dominant mutation in the amyloid-β-precursor protein [*APP*], presenilin-1 *(PSEN1)* or presenilin-2 *(PSEN2)* genes (Goate et al., 1991; Rogaev et al., 1995; Sherrington et al., 1995). Aβ is generated from proteolytic processing of the APP protein into fragments of various lengths, the most common of which are a 40 amino acid length fragment ($A\beta_{40}$) or the more pathogenic 42aa length fragment ($A\beta_{42}$) (Iwatsubo et al., 1994; Kang et al., 1987). This cleavage event is carried out initially by the β-site APP-cleaving enzyme 1 (BACE1/β-secretase) followed by a further cleavage by the γ-secretase complex containing presenilin 1

(PS-1) and presenilin 2 (PS-2) (Wolfe et al., 1999). One proposed model for AD pathogenesis is the amyloid cascade hypothesis, which states that the accumulation of toxic $A\beta_{42}$ into neuritic plaques causes an increase in intracellular calcium levels with a consequent upregulation of tau phosphorylation (Hardy and Higgins, 1992).

In AD pathogenesis, several reports have shown that the presence of pathogenic Aβ species affects mitochondrial integrity, resulting in defects to the respiratory cycle and excessive release of ROS, causing oxidative stress (Pappolla et al., 1998; Bozner et al., 1997; Lustbader et al., 2004). In support of this, lipoperoxidative, glycoxidative and other oxidative markers are readily detectable in the brains of AD patients (Smith et al., 1995). In Tg2576 mouse models of AD, a positive correlation was detected between levels of soluble Aβ and hydrogen peroxide production, providing evidence that Aβ is causing oxidative stress in AD models (Manczak et al., 2006). With respect to the other functions of the mitochondria, gene expression profiling in brain slices from Tg2576 mice showed an upregulation of genes involved with mitochondrial energy production and apoptosis in comparison to age-matched litter controls (Reddy et al., 2004). Furthermore, in Tg2576 mice and mouse N2a (Neuro-2a) cells expressing human mutant APP or wild-type APP, both Aβ monomers and oligomers were found to be associated predominantly with the inner mitochondrial membrane and matrix in mutant APP expressing cells but not in wild-type APP cells, confirming a direct relationship between Aβ and mitochondria and it is hypothesised that this IMM localisation of Aβ may perturb the electron transport chain and energy metabolism (Manczak et al., 2006). In support of this, there was a decrease in cytochrome c oxidase activity, a major enzyme component of the electron transport chain, in Tg2576 mice (Manczak et al., 2006).

Additionally, in fibroblast cells from AD patients, mitochondria were more interconnected than in wild-type controls which was suggestive of a shift in mitochondrial dynamics towards fusion events i.e. less fission (Wang et al., 2008). In AD fibroblasts, Drp1 levels were significantly decreased while optic atrophy protein

1 (OPA1) levels, a protein involved with mitochondrial fusion, remained the same (Wang et al., 2008).

In summary, the evidence suggests that a dysfunction to mitochondria, involving both structural and functional deficits, is a common early pathogenic event in neurodegenerative disorders and the mitochondrial defects conform with the amyloid cascade hypothesis due to the observed relationship between Aβ and the mitochondria.

1.2.2 Dysregulation of calcium homeostasis

Although mutant genes associated with neurodegeneration are often ubiquitously expressed, only a subset of neurons, characteristic to each specific disease are seen to degenerate. In ALS, it has been hypothesised that the specific vulnerability of motor neurons may be due to a lower Ca^{2+} buffering capacity (Palecek et al., 1999). In support of this, oculomotor neurons, that are more resistant to ALS pathology, have higher calcium binding capabilities (Vanselow and Keller, 2000). The high density of Ca^{2+} permeable AMPA (α-amino-3-hydroxy-5-methyl-4-isoxazolepropionic acid receptor) receptors on motor neurons, in combination with the low Ca^{2+} buffering capacity, may induce a particular sensitivity to excitotoxic conditions (Van Den Bosch et al., 2000; Grosskreutz et al., 2010).

In familial presenilin-linked AD, there is increased activity and/or expression of calcium receptors including ryanodine receptors (RyR) and inositol 1,4,5-triphosphate receptors (IP_3R), causing excessive release of Ca^{2+} from ER calcium stores (Chan et al., 2000; Hayrapetyan et al., 2008; Cheung et al., 2010). Similarly, in human induced pluripotent stem cell (iPSC) neurons exposed to tau oligomers, the formation of aggregated, hyperphosphorylated pathogenic tau was induced with a consequent elevation of intracellular Ca^{2+} levels (Usenovic et al., 2015). In the previous section, I have already mentioned how elevated cytosolic Ca^{2+} levels can cause excessive mitochondrial calcium uptake and the release of pro-apoptotic factors but in addition to this, increased Ca^{2+} ion concentrations can disrupt neuronal signal transmissions. Neuronal calcium signalling is a key modulator of

neurotransmitter release and in neurons exposed to pathogenic tau oligomers there was a significant increase in inhibitory neuronal GABA (gamma-aminobutyric acid) release, following the consequent rise in Ca^{2+} levels (Usenovic et al., 2015). Furthermore, in iPSCs from frontotemporal lobar degeneration tauopathy (FTLD-Tau) patients, increases in intracellular calcium levels in response to electrical stimulation were greater than control neurons, suggesting increased excitability (Imamura et al., 2016).

1.2.3 Protein aggregation and perturbed degradative pathways

A common hallmark of many neurodegenerative disorders is the appearance of protein inclusions within degenerating neurons. Skein-like inclusions that positively label for ubiquitin and small cytoplasmic, ubiquitin-negative Bunina bodies are often found within spinal cord and brainstem motor neurons of ALS patients and are considered to be specific hallmarks of the disorder (Kato, 2008). Most of the ALS-linked gene mutations encode for proteins with a high propensity to aggregate and these are often found within protein inclusions [As reviewed by (Bendotti et al., 2012)]. Similar to skein-like inclusions, PD associated Lewy bodies containing α-synuclein also contain some cytoskeletal and proteasomal proteins and can be positively labelled for ubiquitin (Ross and Poirier, 2004). Although the exact role of protein aggregates in neurodegeneration has not been elucidated, a positive correlation has been identified between the proportion of skein-like inclusion containing neurons and the extent of neuronal cell death (van Welsem et al., 2002). In contrast, there is only a very weak correlation between neuritic plaque density in post-mortem tissue of AD patients and ante-mortem cognitive decline (Terry et al., 1991). Cells have two main degradative pathways in place to clear insoluble protein aggregates and dysfunctions to these clearance systems are often observed in neurodegeneration. Opposing points of view state that protein aggregates may be a secondary pathogenic event as a consequence of defects in the cellular degradative pathways or they themselves may induce defects to the clearance systems by a toxic gain-of-function mechanism or by sequestering core degradative proteins (Navone

et al., 2015). The following sections will outline the two major cellular degradative systems.

1.2.3.1 Ubiquitin-Proteasome system (UPS)

The UPS is a complex, multi-component process whereby abnormal or misfolded proteins are tagged with ubiquitin and degraded within a central cavity of a large protease complex called the proteasome. The fact that many of the protein inclusions observed within degenerating neurons label positively for ubiquitin has implicated this pathway in disease pathogenesis (Leigh et al., 1988; Kato, 2008). More direct evidence for a role of the UPS in neurodegeneration comes from transgenic mice with a knock-down of the critical UPS component regulatory particle triple-ATPase subunit 3 (Rpt3) which is a major subunit of the 26S proteasome (the major cellular mammalian protease) (Tashiro et al., 2012; Bedford et al., 2010). These mice develop a degenerative motor neuron phenotype with the appearance of ALS-associated protein aggregates, illustrating how a dysfunction of the UPS can directly lead to neurodegeneration (Tashiro et al., 2012). Pharmacological inhibition of UPS activity also results in an accumulation of protein aggregates while overexpressing proteins with a propensity to aggregate can suppress UPS activity, suggesting that misfolded protein aggregates may be both a cause and a product of UPS suppression in a positive-feedback mechanism (Moumen et al., 2011; Kuijpers et al., 2013a). Additional evidence for an impairment of UPS activity in neurodegeneration comes from neurodegenerative-linked genetic mutations in proteins associated with the UPS for example, mutations in VCP or ubiquilin 2 (UBQLN2) result in a familial form of ALS (Johnson et al., 2010; Deng et al., 2011). VCP is a chaperone protein involved with the recognition and targeting of misfolded proteins in the ER or mitochondrial membranes or within protein complexes for proteasomal degradation (Yamanaka et al., 2012; Stolz et al., 2011). VCP was also detected at high levels in protein inclusions in VAPB-linked ALS suggesting that an impairment of the UPS chaperone protein function may play a more general role in ALS pathogenesis (Kuijpers et al., 2013a). A recent study has shown that a neuronal specific knock-down of the VCP associated co-factors ubiquitin fusion degradation 1

(Ufd1) or nuclear protein localization homolog 4 (Npl4) induces a neurodegenerative phenotype in *Drosophila* models, providing further evidence that dysfunctional UPS activity may be a primary pathogenic event in neurodegeneration (Byrne et al., 2017).

1.2.3.2 Autophagy

Autophagy is an effective clearance pathway for protein aggregates and their oligomeric precursors, clearing both spontaneously generated misfolded proteins and those aggregate-prone proteins associated with neurodegenerative diseases (Levine and Kroemer, 2008; Navone et al., 2015). In neurons, autophagosomes form preferentially at the axon tip where they sequester ubiquitinated protein aggregates and migrate towards the cell soma, assisted by dynein motor proteins for fusion with lysosomes (Navone et al., 2015). Mice with a knock-down of the essential autophagy-related 5 (Atg5) protein in neurons presented with progressive locomotor defects and in Atg5 knock-out cells, an accumulation of protein inclusion bodies was detected indicating that a dysfunction to basal autophagy can induce a degenerative phenotype (Hara et al., 2006).

Genetic mutations underlying inherited forms of neurodegenerative diseases provide compelling evidence for a link between autophagy and disease pathology. As previously mentioned, familial PD is associated with mutations of PINK1 and Parkin which play a role in selective mitophagic clearance of damaged mitochondria (Shimura et al., 2000; Valente et al., 2004). Similarly, mutations in optinuerin are associated with ALS and impair the recruitment of the autophagic machinery to damaged mitochondria as well as impairing autophagosome maturation (Maruyama et al., 2010; Wong and Holzbaur, 2014). In addition to familial cases of neurodegeneration, autophagy is also linked to sporadic forms of disease e.g. in sporadic ALS patients, autophagy is upregulated as shown by an increased number of autophagosomes within patient motor neuron cells (Sasaki, 2011).

In most circumstances, autophagy plays a protective role within the cell however, pathways regulating autophagy are intricately linked to those regulating apoptotic

cell death and molecular inducers of one pathway may activate the other (Maiuri et al., 2007). Additionally, it can be difficult to distinguish an upregulation of autophagosomes as being a pro-survival mechanism or as a consequence of defective autophagic clearance and therefore, there is some controversy surrounding the exact role of autophagy in neurodegenerative events.

1.2.4 Alterations in lipid metabolism

The tight regulation of cell membrane lipid composition is essential for maintaining the structural integrity and function of cell membranes. Alterations to lipid levels or lipid processing have been identified in patients with a variety of neurodegenerative diseases suggesting that dysfunctional lipid metabolism may be involved in the neuropathological process.

Sphingolipids are a group of lipids derived from sphingosine that are enriched within the nervous system and play important structural and signalling roles (Haughey et al., 2010). Ceramide is a core component of complex sphingolipids and is comprised of several subspecies that differ in their number of carbons. The ratios of these ceramide subgroups to one another is very tightly regulated and although this ratio does not differ in tissue undergoing neurodegeneration, an overall elevation of ceramide levels has been detected in post-mortem brain tissue from AD patients (Filippov et al., 2012). Additionally, the expression of two sphingomyelinase genes, involved in ceramide biosynthesis from the catabolic breakdown of sphingomyelin, was significantly upregulated in AD samples (Filippov et al., 2012). Elevated levels of ceramide have been shown to decrease respiratory cycle protein complex activity and alter mitochondrial membrane potential and permeability (Kogot-Levin and Saada, 2014). Ceramide can also induce neuronal death by activating ceramide associated protein kinases (CAPK) and phosphatases (CAPP) to trigger apoptotic death signalling pathways (Haughey et al., 2010) Furthermore, AD patients also show significantly reduced plasma levels of phosphatidylcholine (Mapstone et al., 2014) and decreased levels of phosphatidylinositol in the hippocampus (Prasad et al., 1998). The decrease in phospholipid species is likely due to an increase in

phospholipid processing as increases in the phospholipid catabolite, glycerophosphocholine, are also detected in AD patients (Nitsch et al., 1992).

A similar reduction in phospholipids and sphingolipids is detected in spinal cords of SOD1 mouse models of ALS, at both the symptomatic and pre-symptomatic stages of disease, with a prominent change in sphingolipid metabolism (Henriques et al., 2015). Glucosylceramide synthase, involved with glycosphingolipid biosynthesis, shows upregulated expression levels in the muscles of ALS patients and co-localises with TDP-43 inclusion bodies in degenerating cells (Henriques et al., 2015). As the occurrence of lipid metabolism defects takes place before the onset of symptoms, it suggests that these defects may be an early, primary pathogenic event in disease progression.

1.2.5 ER Stress

As prolonged ER stress can induce apoptosis, it is hypothesised that severe ER stress proceeds various cell insults built up over time and is responsible for the selective death of neurons in neurodegenerative disorders. In spinal cord motor neurons of sALS patients, all three UPR pathways described above were found to be activated (Atkin et al., 2008). Furthermore, expression levels of eIF2α and PDI were elevated (Ilieva et al., 2007). In $SOD1^{G93A}$ and $SOD1^{G85R}$ transgenic mouse models of ALS, the accumulation of SOD1 protein triggers an ER stress response exclusively in the spinal cord at the final stages of disease progression (Kikuchi et al., 2006). SOD1 may also increase the severity of the ER stress by inhibiting the protein folding activity of PDI (Atkin et al., 2006). In mice with frontotemporal dementia pathology there is continuous activation of the PERK pathway resulting in a reduction of global protein synthesis in the central nervous system (CNS) leading to neuronal cell death (Radford et al., 2015).

1.2.6 Fragmentation of the Golgi apparatus

Morphological and functional alterations to the Golgi are a hallmark of several neurodegenerative disorders. In sALS spinal cord motor neurons, the Golgi appears as disconnected components dispersed throughout the cell. The number of

immunolabelled components doubled in degenerating motor neurons in comparison to control cells, but the average size was dramatically reduced (Gonatas et al., 1992). Similar fragmentation of the Golgi cisternae was observed in transgenic SOD1 mouse models of ALS which was detectable several months before the onset of motor deficits (Mourelatos et al., 1996). Furthermore, in cells expressing Parkinson's linked mutant α-synuclein protein, Golgi defects occurred before the appearance of protein aggregates (Gosavi et al., 2002) and in Alzheimer's, Golgi fragmentation occurred within hippocampal neurons of AD patients, when not in the presence of neurofibrillary tangles (Stieber et al., 1996). Overall, the evidence suggests that fragmentation of the Golgi apparatus is a common, preclinical hallmark of many neurodegenerative diseases.

From the evidence presented above, there are a number of clear and distinct pathways that are commonly perturbed in neurodegenerative disorders with early insults such as mitochondria abnormalities or defects in cellular degradative pathways leading to the induction of ER stress and subsequent apoptotic cell death. However, it is not always clear how the expression of a single neurodegenerative-linked mutant protein could perturb so many distinct cellular processes. It is possible that these molecular mechanisms of neurodegeneration could converge on a dysfunction to organelle membrane contact sites. The evidence linking organelle contact sites and neurodegeneration will be discussed in the proceeding sections.

1.2.7 ER-mitochondria contacts and neurodegeneration

There is a clear overlap between many of the processes regulated by ER-mitochondria interaction sites and those pathways that are commonly implicated in the neurodegeneration. Specific examples of defective ER-mitochondria contacts in AD, PD and ALS pathogenesis are presented below.

1.2.7.1 ER-mitochondria contacts in Alzheimer's disease (AD)

The cleavage of APP to Aβ occurs at the MAMs where γ-secretase activity is predominantly localised (Area-Gomez et al., 2009). In PSEN1 and/or PSEN2 knockout

MEFs there was a significant increase in MAM activity as measured by elevated levels of cholesteryl ester synthesis and phospholipid synthesis (Area-Gomez et al., 2012). In addition to increased MAM function, PSEN1/2 knockout cells showed an increase in the percentage surface area of mitochondria in close apposition to the ER and this was also observed in fibroblast cells from both familial AD and sporadic AD patients (Area-Gomez et al., 2012). In contrast, another study showed that ER-mitochondria associations were increased upon overexpression of wild-type or FAD-linked PS-2 with altered mitochondrial calcium homeostasis whereas altering the levels of PS-1 expression had no impact on the extent of ER-mitochondria associations (Zampese et al., 2011). Although PS-1/2 has no direct tethering role at the MAMs, the regulation of ER-mitochondria associations by PS-2 seems to be dependent on the presence of MFN2 at these junctions suggesting that PS-2 may interact with MFN2 at the MAMs to impact its role as a negative regulator of ER-mitochondria contacts (Filadi et al., 2016). To further strengthen the link between the γ-secretase complex and MFN2, it was shown that Aβ production and processing was decreased in MFN2 knockdown cells, despite there being an increase in the amount of close ER-mitochondria associations, and this effect was due to a defect in γ-secretase complex maturation and activity (Leal et al., 2016).

Preceding the cleavage event by γ-secretase to generate Aβ, an initial cleavage event of APP is carried out by β-secretase complex to generate a 99-aa C-terminal fragment (C99) and it has been suggested that increased levels of C99 may contribute to AD pathogenesis (Lee et al., 2006) **(Fig 1.4)**. A recent study has demonstrated that C99 fragments are enriched at the MAMs, in agreement with γ-secretase activity occurring in these compartments, and levels of C99 were significantly increased in tissue from AD patients and in mutant PS-1^{M146V} mouse models, especially in the MAM fraction (Pera et al., 2017). In PS-1/PS-2 double knock-out cells that have increased ER-mitochondria associations and increased levels of C99, the inhibition of β-secretase activity to halt C99 production could rescue this increased apposition phenotype, suggesting that the accumulation of C99 at the MAMs can increase ER-mitochondria contacts (Pera et al., 2017). Furthermore, there was a reduction of the

conversion of cholersterol to cholersteryl esters upon treatment with a β-secretase inhibitor, indicating that C99 can enhance MAMs both physically and functionally (Pera et al., 2017). C99-mediated upregulation of ER-mitochondria interactions was further associated with increased phosphatidylserine and sphingomyelinase activity at the MAMs with an associated increase in ceramide levels at the mitochondria (Pera et al., 2017). Therefore, it has been hypothesised that the respiratory defects observed in AD, could be accounted for by C99-mediated upregulation of ER-mitochondria associations and consequent perturbations to lipid biosynthesis and enhanced ceramide levels.

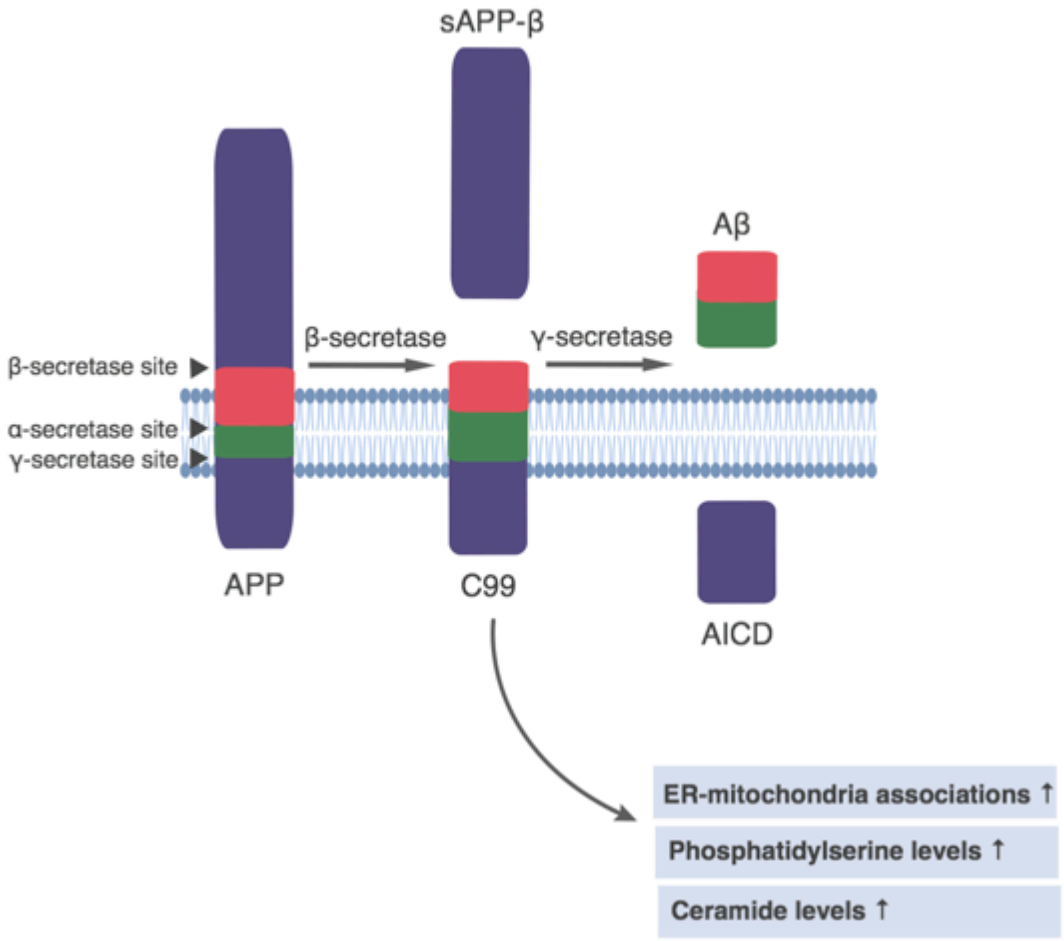

Fig 1.4: C99 fragment generation in the amyloidogenic pathway. APP is initially processed by the β-secretase complex in the amyloidogenic pathway to generate the soluble amyloid precursor protein β (sAPP-β) and the C-terminal C99 fragment. Increased levels of C99 promote an increase in ER-mitochondria associations with a consequent elevation in phosphatidylserine and ceramide production. Further

processing of C99 by the γ-secretase complex generates Aβ and the AβPP intracellular domain (AICD). Illustrations was generated in BioRender.

Due to the fact that alterations to the MAMs are observed in both familial and sporadic AD cases with no known mutations in APP, PS-1 or PS-2, (Area-Gomez et al., 2012) it has led to the suggestion that MAM dysfunction may be a common denominator underlying AD pathogenesis. Indeed, many of the cellular pathways that are seen to be perturbed in AD can be attributed to the functions of the MAMs including abnormal cholesterol synthesis (Stefani and Liguri, 2009), dysregulated calcium signalling (Bezprozvanny and Mattson, 2008) and mitochondrial abnormalities (Su et al., 2010), suggesting that dysfunction to these pathways could be secondary pathogenic effects arising from disruptions to the MAMs (Pera et al., 2017).

1.2.7.2 ER-mitochondria contacts in Parkinson's disease (PD)

As described previously, PINK1 accumulates on the surface of damaged mitochondria and recruits parkin to target the organelle for mitophagic clearance. Parkin can also be recruited by the pro-autophagic Beclin-1 protein that is a constituent of the PI3K complex (Choubey et al., 2014). PINK1 and Beclin-1 were both identified at the ER-mitochondria interface and their levels in the MAM fraction are enhanced upon carbonyl cyanide m-chlorophenyl hydrazone (CCCP) treatment, a chemical uncoupler of the proton gradient established during the electron transport chain that consequently dissipates the mitochondrial membrane potential and can be used to induce mitophagy (Lim et al., 2001; Gelmetti et al., 2017). The relocalisation of beclin-1 to the MAMs is dependent on the presence of PINK1 as beclin-1 levels failed to increase following CCCP exposure in PINK1 knock-down cells (Gelmetti et al., 2017). Similarly, parkin also relocalises to the MAMs after the induction of mitophagy in a PINK1-dependent manner (Gelmetti et al., 2017). Previous work has shown that increasing the levels of parkin favours increased ER-mitochondria associations while knocking-down expression reduces contacts (Cali et al., 2013). The exact role of PINK1 and parkin on ER-mitochondria associations is

unclear however as other studies have shown a tightening of the MAM junctions in parkin knock-out mice, primary fibroblasts from parkin-linked PD patients and neurons derived from iPS cells from a patient with parkin mutations (Gautier et al., 2016). The ER-mitochondria tether MFN2 is a substrate of parkin, through which it is ubiquitinated and degraded (Ziviani et al., 2010). *Drosophila* loss-of-function mutants of PINK1 and parkin show an accumulation of MFN2 and in increase in ER-mitochondria contact points indicating that the influence PINK1 and parkin exert on the nature of the contacts may be through a MFN2-dependent mechanism (Celardo et al., 2016). The increase in MAMs was accompanied by activation of the PERK ER stress pathway and knocking down MFN2 expression could attenuate the PERK signalling pathway (Celardo et al., 2016) **(Fig 1.1)**.

In addition to PINK1 and parkin, the overexpression of α-synuclein has also been seen to cause a significant increase in mitochondrial calcium levels and uptake ability as a consequence of increased ER-mitochondria contacts in cell culture (Cali et al., 2012). In contrast, siRNA-mediated knock-down of α-synuclein in mammalian cells decreased the ability to uptake Ca^{2+} and altered the structure of the mitochondrial network to give a fragmented appearance suggesting that endogenous levels of α-synuclein are required to maintain calcium homeostasis (Cali et al., 2012).

1.2.7.3 ER-mitochondria contacts in amyotrophic lateral sclerosis (ALS)

Mutations in the sigma-1 receptor protein are associated with a juvenile form of inherited ALS (ALS16) (Al-Saif et al., 2011). As mentioned previously, this protein is enriched at the MAMs and regulates calcium exchange between the ER and mitochondria (Hayashi and Su, 2007). In spinal cord tissue samples from sALS patients, sigma-1 receptor levels were significantly reduced in comparison to healthy control samples and in primary neuronal cultures, a knock-down of sigma-1 receptor protein expression resulted in a reduction of ER-mitochondria contact sites (Prause et al., 2013; Bernard-Marissal et al., 2015).

Our lab has a particular research interest in the ALS-linked VAPB protein that is believed to be involved in tethering the ER and mitochondria at close proximity by

forming a link with the outer mitochondrial membrane protein tyrosine phosphatase interacting protein 51 (PTPIP51) (De Vos et al., 2012; Stoica et al., 2014). The VAMP-associated protein (VAP) family are a group of integral ER membrane proteins all of which are structured with an N-terminal major sperm protein (MSP) domain, a central coiled-coil domain and a C-terminal hydrophobic transmembrane domain (TMD) **(Fig 1.5A)** (Nishimura et al., 1999). VAP was first identified as a 33-kilodalton protein, VAP-33, interacting with vesicle associated membrane protein (VAMP)/synaptobrevin in *Aplysia californica* (Skehel et al., 1995). Subsequently, the mammalian VAP homologues, VAPA and VAPB, sharing 63% sequence identity, were cloned and an alternative splice form of VAPB termed VAPC was identified, consisting of the first 70 amino acids of VAPB plus an additional 27 amino acids (Nishimura et al., 1999). In addition to interacting with VAMP, mammalian VAPA and VAPB undergo homo- and hetero-dimerization and deletion of the TMD from either protein prevents this interaction (Nishimura et al., 1999). Northern blot analysis revealed that VAPB is ubiquitously expressed in all mouse tissue examined and predominantly shows a reticular pattern but also appears to associate with microtubule and cytoskeletal proteins (Skehel et al., 2000). VAPA is also found on the ER but appears to be present on distinct regions of the ER to VAPB, with only a modest level of co-localisation between the two VAP proteins (Gkogkas et al., 2008). Mammalian VAP proteins have also been observed on other intracellular membranes such as the Golgi apparatus, recycling endosomes and the neuromuscular junctions (Soussan et al., 1999; Pennetta et al., 2002). Specifically in the CNS, VAPB is highly abundant and is particularly enriched in motor neurons of the spinal cord and caudal brainstem (Teuling et al., 2007).

Altering the levels of VAPB or its binding partner PTPIP51 in cultured mammalian cells perturbed contact sites and influenced mitochondrial calcium levels, supporting VAPBs role as an ER-mitochondria tether (De Vos et al., 2012; Stoica et al., 2014). The identification of TDP-43 as a regulator of the VAPB/PTPIP51 interaction has highlighted the relevance of VAPB to the wider field of ALS pathogenesis (Stoica et al., 2014). As mentioned in **section 1.2.1.2**, mutations in TDP-43 are associated with

familial forms of ALS but this protein is also found as a significant component of protein aggregates in several other forms of ALS and FTD and as such, TDP-43 aggregates are considered to be a pathological hallmark of the disease (Sreedharan et al., 2008; Neumann et al., 2006). Overexpression of wild-type TDP-43 or ALS-linked mutant TDP-43 (TDP-43^{Q331K}, TDP-43^{A382T} or TDP-43^{G348C}) disrupted ER-mitochondria contact sites while siRNA-mediated knock-down of TDP-43 had no influence over the MAMs (Stoica et al., 2014). TDP-43 does not directly bind to either VAPB or PTPIP51 but rather, influences their association through the activation of glycogen synthase kinase-3β (GSK-3β) however, the mechanism by which this regulates VAPB/PTPIP51 binding has not yet been elucidated (Stoica et al., 2014). The role of VAPB at the MAMs is discussed in greater detail in **chapter five** of this thesis.

1.2.7.4 Other forms of inter-organelle contact sites and neurodegeneration

In addition to ER-mitochondria contacts, ER-endosome contact defects may also associated with neurodegeneration. Niemann-Pick disease type C is characterised by progressive neuronal degeneration beginning in childhood and is characterised by abnormal lipid and cholesterol compositions of late endosomes and lysosomes (Mukherjee and Maxfield, 2004). Furthermore, a polymorphism in the ER-endosome tethering protein Protrudin has been linked with hereditary spastic paraplegia (Mannan et al., 2006) and a knock-out of expression of the ALS-linked VAP proteins resulted in endosomal trafficking and Golgi defects, common hallmarks of neurodegenerative disorders (Dong et al., 2016). The pathology of these disorders may, in part, arise from defects to ER-endosomal contact sites.

The proper maintenance of peroxisome function is important for neuronal development and defects in peroxisome biogenesis, as regulated by ER-peroxisome junctions, has been linked to neurodegenerative diseases including Zellweger syndrome and X-linked adrenoleukodystrophy (Wanders and Poll-The, 2017).

1.3 The VAP protein family

From the evidence presented above, it is clear that the VAMP-associated protein (VAP) protein family plays a critical role in regulating a variety of organelle membrane contact sites. As previously mentioned, VAPs consist of an N-terminal MSP domain, a central coiled-coil domain and a C-terminal transmembrane domain. The transmembrane domain is embedded in the ER membrane while the N-terminus of VAP is cytosolic. These protein domains will be discussed in further detail in the following sections.

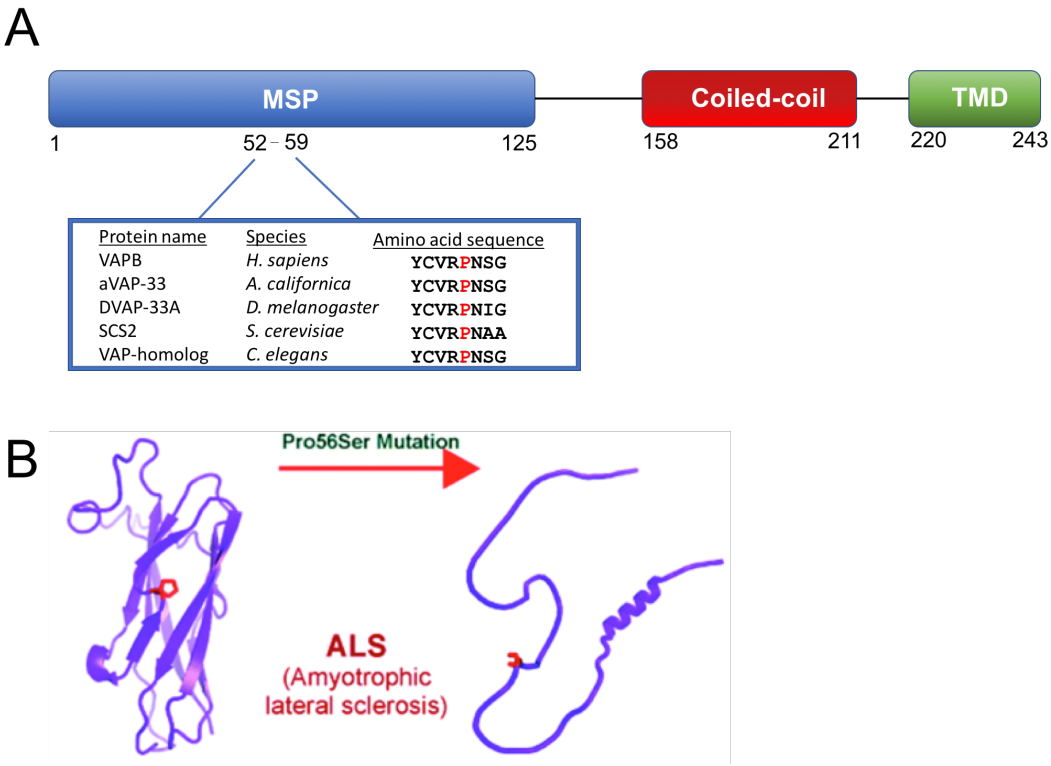

Fig 1.5: Schematic representation of the VAP protein domains and location of the ALS-linked point mutation. (A) All VAP proteins possess an N-terminal major sperm protein (MSP) domain (amino acids 1-125), a central coiled-coil domain (amino acids 158-211) and a C-terminal transmembrane domain (TMD) (amino acids 220-243). Boxed region indicates a representative 8 amino acid sequence taken from within the 16 amino acid VAP MSP consensus sequence that is highly conserved between species, aligned by CLUSTAL W (Lev et al., 2008). The location of the proline residue associated with ALS8 is highlighted in red. Image adapted from (Lev et al., 2008). **(B)** The structure of VAPB MSP domain is composed of seven-stranded immunoglobulin-

like β strands that form a highly-coiled structure. The proline to serine point mutation perturbs the native coiled structure and renders the protein insoluble (Shi et al., 2010).

1.3.1 VAP transmembrane domain

The VAP C-terminal transmembrane domain (amino acids 220-243) anchors the protein to its target membrane location and the expression of VAP with a deletion of the TMD has a diffuse, cytosolic distribution (Teuling et al., 2007). The TMD of VAPs also possess a GXXXG dimerization motif consisting of two glycine residues separated by three amino acids (Kim et al., 2010). This motif mediates the interaction of two transmembrane helices and has been implicated in TMD interactions of more than 20 different proteins (Russ and Engelman, 2000; Teese and Langosch, 2015). This dimerization motif is crucial for the oligomerisation of VAP TMDs but is dispensable for the oligomerization of full-length VAPs, which suggests the involvement of other structural motifs (Kim et al., 2010).

1.3.2 VAP coiled-coil domain

The central coiled-coil domain (amino acids 158-211) of VAP proteins is a common motif found in many soluble NSF (N-ethylmaleimide sensitive fusion protein) attachment protein receptor (SNARE) proteins. SNARE proteins are a class of integral membrane proteins that provide the fundamental machinery for vesicular trafficking and membrane fusion and are sub-divided into v-SNAREs on the transport vesicles that recognise complementary t-SNAREs on the target membrane sites which provides specificity to fusion events (Sollner et al., 1993). The coiled-coil domain is also a highly versatile folding motif and mediates oligomerization in a large number of proteins (Burkhard et al., 2001). In VAPB, deletion of the coiled-coil domain prevented its dimerization highlighting the importance of this domain in VAP oligomerization in addition to the GXXXG motif of the TMD (Kim et al., 2010).

1.3.3 VAP MSP Domain

The MSP domain sequence (amino acids 1-125) is highly conserved among species and is named due to its similarity to the nematode major sperm protein (Nishimura et al., 1999). MSP is a dimeric protein comprised of two helical subfilaments spiralling

around each other and functions in the locomotion of nematode sperm cells (Stewart et al., 1994; Bottino et al., 2002). Additionally, MSP is secreted from sperm cells where it acts as a ligand for VAB-1 Ephrin receptors to induce oocyte maturation (Miller et al., 2003). The MSP domain of VAP proteins is also cleaved and secreted and in mammalian cells it competitively binds to the EphA4 receptor that is abundantly expressed throughout the nervous system and skeletal muscle (Tsuda et al., 2008; Lai et al., 2001). Cleaved forms of VAPA are detectable in almost all tissue types however the proteolytic cleavage of the VAPB MSP domain seems to selectively occur in neurons (Gkogkas et al., 2008). Furthermore, cleaved VAPA MSP domains were readily identified in both embryonic and adult rat brain lysates but the predominant VAPB signal in embryonic tissue was the full-length protein indicating that the cleavage of the MSP domain may be developmentally regulated (Gkogkas et al., 2011).

1.4 VAPs and neurodegeneration – Functional consequences of the *VAPB*^{P56S} mutation

As described above, there is a strong link between organelle contact sites and neurodegeneration with many disease-linked proteins being identified as having a direct impact on the regulation of membrane contacts. In support of this, the ER-mitochondria tether VAPB was linked with neurodegeneration upon the identification of a proline to serine (P56S) point mutation within the highly conserved MSP domain. This mutation was originally found in seven Brazilian families exhibiting phenotypes ranging from an atypical form of ALS termed ALS type 8 (ALS8), to late-onset slowly progressive ALS or late-onset spinal muscular atrophy (SMA), inherited in an autosomal dominant manner (Nishimura et al., 2004). In wild-type VAPB, proline 56 lies within a conserved motif distal to the protein dimerization face and forms an unusual cis-peptide bond conformation that is essential for maintaining the S-shaped loop and highly-folded structure of the MSP domain, constituted by seven-stranded immunoglobulin-like β strands (Shi et al., 2010). As a consequence of the proline to serine substitution seen in ALS, the protein lacks its native tightly-packed structure and is rendered

insoluble in buffer and prone to aggregation (**Fig1.5(B)**) (Shi et al., 2010). In this thesis, we have a specific focus on the VAP protein family to investigate how a mutation in a protein with a MAM-specific function can lead to neurodegeneration. The functions of VAP proteins in the context of the pathogenic *VAPB*^{P56S} mutation will be discussed in the following sections.

The P56S mutation disrupts the subcellular localisation of VAPB, causing it to form large intracellular aggregates (Nishimura et al., 2004). The mutation also reduces the solubility of VAPB and induces its misfolding and polyubiquitination (Kanekura et al., 2006). However, it is not entirely clear whether VAPB-P56S acts in a gain-of-function or loss-of-function manner or in some combination of the two. In cells expressing VAPB-P56S, there is a significant recruitment of endogenous wild-type VAPA and VAPB within the cytoplasmic aggregates which could account for the dominant nature of the mutation in ALS patients (Teuling et al., 2007). VAPB-P56S undergoes dimerization similar to wild-type VAPB and deletion of the coiled-coil domain reduces its dimerization capabilities and in conjunction with a mutation of the GXXXG motif, completely abolishes it (Kim et al., 2010). However, the reduction in dimerization is not as significant as that seen with wild-type VAPB and therefore, it has been suggested that an enhancement to the dimerization ability of VAPB-P56S could account for the sequestration of endogenous VAP proteins within aggregates which could then phenocopy a loss of VAP function (Kim et al., 2010). In pull-down assays in mammalian cell lines, it was demonstrated that the P56S mutation inhibits the binding of VAPB to FFAT motif-containing proteins (Teuling et al., 2007). As VAPB interacts with a variety of proteins via the FFAT domain to mediate functions including the non-vesicular transport of lipids at membrane contact sites, it could indicate that the P56S mutation operates through a loss of normal VAP function.

Interestingly, the expression of the ALS-linked VAPB mutation in the mammalian cell lines HeLa or Cos-1 did not significantly increase cell death however, a greater rate of cell death was observed in comparison to controls when expressed in primary neurons which conforms to the specific vulnerability of neuronal cells in ALS

pathology (Teuling et al., 2007). Knocking-down of VAPB expression caused no significant changes in neuronal death but a loss of VAPA reduced survival and this effect was enhanced even further upon silencing of expression of both VAPA and VAPB which supports that the pathology of VAPB-P56S is through a loss of VAP function (Teuling et al., 2007). A study by Langou *et al* however, showed a selective vulnerability of motorneurons to an overexpression of either wild-type or mutant VAPB but no change in survival with an overexpression of VAPA (Langou et al., 2010). The overexpression of wild-type or mutant VAPB induced a consequent increase in IRE1 phosphorylation and treatment of the motorneuronal cultures with the ER stress inhibitor salubrinal prevented the VAPB-induced cell death suggesting that VAPB-P56S could cause cell death through a gain-of-function mutation inducing an ER stress response (Langou et al., 2010).

1.4.1 VAPs and the regulation of the unfolded protein response

As described above, the unfolded protein response is a cellular mechanism induced by ER stress to try and alleviate protein overload in the ER lumen. The exact role of VAP proteins in the UPR is controversial and conflicting evidence exists on the role the P56S mutation plays in this process. While Langou *et al* showed an ER stress response to an AAV-mediated overexpression of wild-type and mutant VAPB, another group demonstrated that an overexpression of wild-type VAPA or VAPB triggers an unfolded protein response via IRE1-mediated XBP1 splicing but expressing VAPB-P56S to the same level does not (Kanekura et al., 2006; Langou et al., 2010). Furthermore, silencing VAP expression inhibited the activation of UPR in response to chemical-induced ER stress indicating that VAPB is a positive regulator of the UPR (Kanekura et al., 2006). This positive regulation of the IRE1/XBP1 pathway is dependent on the ability of VAP to interact with FFAT motifs as the overexpression of two mutant VAPB constructs deficient in FFAT binding did not induce XBP1 splicing (Suzuki et al., 2009).

The ER stress protein ATF6 was also identified as an interactor of both VAPA and VAPB via the MSP domains from a yeast two-hybrid screen (Gkogkas et al., 2008). Using a luciferase-based transcriptional assay, it was revealed that ATF6-dependent

transcriptional levels were reduced upon overexpression of VAPB or VAPB-P56S and additionally, there was a significant reduction in tunicamycin-induced activation of ATF6-dependent transcription (Gkogkas et al., 2008). In contrast, silencing of VAPB expression increased the levels of ATF6-dependent transcription (Gkogkas et al., 2008). This data suggests that VAPB is a negative regulator of the ATF6 pathway of the UPR and the VAPB-P56S mutation can inhibit this process at much lower protein levels than wild-type VAPB (Gkogkas et al., 2008).

In C2C12 cells, a mouse myoblast cell line, expression of VAPB-P56S inhibited the activation of the IRE1-XBP1 pathway following the induction of ER stress and overall XBP1 levels were reduced during differentiation from expression of mutant but not wild-type VAPB (Tokutake et al., 2015). The collective data suggests that a dysfunction of UPR may be a pathogenic consequence of the VAPB-P56S mutation however, the exact nature of VAPB as a positive or negative regulator of this response is still uncertain. It also appears that expression of VAPB-P56S may lead to a higher susceptibility to ER stress related cell death as shown by a significant reduction in cell viability of cells expressing VAPB-P56S in comparison to controls when incubated with the ER stress inducer thapsigargin, an inhibitor of Ca2+ ATPase (SERCA) that depletes ER calcium stores (Suzuki et al., 2009; Rogers et al., 1995).

1.4.2 VAPs and the maintenance of ER structure

The endoplasmic reticulum is a continuous network of interconnected tubules extending throughout the cytoplasm that is divided into structurally distinct regions, namely the nuclear envelope, rough ER containing the ribosomes and smooth ER (Terasaki et al., 1994; Voeltz et al., 2002). The ER is a highly dynamic organelle, moving along microtubule and cytoskeletal elements and rearranging in response to certain physiological conditions or changes in the levels of specific ER resident proteins [as reviewed by (Powell and Latterich, 2000)]. An interaction of VAPB with the phosphatidylinositol transfer protein Nir2 was already described above as playing a role in ER to Golgi lipid transport however, this interaction with the Nir protein family including Nir1 and 3 via their FFAT motif also affects the structural integrity of the ER (Amarilio et al., 2005). The overexpression of VAPB with Nir2

results in the appearance of large granular structures composed of multiple membrane arrays originating from the ER which inhibits protein export from the ER. When VAPB and Nir3 are overexpressed together, it results in a striking re-localisation of VAPB and modifies the ER into a tubular-like structure. Similarly, microtubule structure was reorganised and aligned with VAPB and Nir3 staining, suggesting that the VAPB-Nir3 interaction connects the ER and microtubule networks (Amarilio et al., 2005). Overexpression of VAPA or a VAPA FFAT binding mutant disrupted ER morphology, suggesting that similar to the VAPB-Nir interactions, the binding of VAPA to different cytosolic proteins containing an FFAT-motif plays a role in regulating and maintaining ER structure (Kaiser et al., 2005). Overexpression of the mutant VAPB^{P56S} induces the formation of aggregates that are continuous with the ER membrane but seem to exclude membrane proteins of the rough ER (Fasana et al., 2010). High resolution electronic microscopy images of these aggregates revealed the presence of electron-dense structures surrounding the nucleus composed of parallel ER cisternae, a structural feature which had not been previously described and was termed to be a novel form of organised smooth ER (OSER) (Fasana et al., 2010). Although it had been shown that the presence of the P56S mutation in VAPB distorts the helical conformation of the MSP domain, a later study demonstrated that in the presence of the lipid dodecylphosphocholine (DPC), the P56S-MSP domain transforms into a highly helical formation and it was stated that this may rationalise the mutant proteins specific ability to restructure the ER membrane (Qin et al., 2013).

1.4.3 VAPs and vesicular protein trafficking

The early secretory pathway involves the transport of newly synthesised proteins to the cis-Golgi membrane for further processing and delivering to their target locations. Yip1-interacting factor homologue A (YIF1A) is a transmembrane protein that was identified as an interactor of VAPs and plays a role in the early secretory pathway (Matern et al., 2000; Kuijpers et al., 2013b). YIF1A has a reticular pattern of distribution within neurons and partially co-localises with VAPB however, when vesicular trafficking is blocked, YIF1A accumulates at the Golgi and is found

predominantly at the ER-Golgi intermediate compartment (ERGIC). When VAPA or VAPB expression is silenced, YIF1A re-localises to the Golgi and conversely, when VAPB is overexpressed it binds YIF1A to the ER and inhibits its cycling to the Golgi suggesting that the distribution of YIF1A is dependent on the expression of VAP proteins. In VAP or YIF1A knockdown neurons, an impairment of transport to the dendrites was observed with a consequent reduction in dendritic tree branch number and length (Kuijpers et al., 2013b). When VAPB-P56S is expressed in cells, YIF1A can be identified as a component of the intracellular aggregates, causing it to lose its localisation to the ERGIC even after pharmaceutical inhibition of vesicular trafficking (Kuijpers et al., 2013b). Therefore, defects in the early secretory pathway could represent a pathogenic event in ALS8.

A distinct function of VAPA in vesicular protein trafficking has been identified whereby an overexpression of VAPA, but not VAPB, inhibits the incorporation of ER proteins within membrane vesicles during ER to Golgi transport (Prosser et al., 2008). Furthermore, VAPA overexpression repressed the lateral diffusion of membrane proteins to ER exit sites through its MSP-domain mediated interaction with the microtubule network that could create impassable objects (Prosser et al., 2008).

1.4.4 VAPs and bouton formation at NMJs

In *Drosophila melanogaster* models, the *Drosophila* homologue of mammalian VAP, DVAP-33A is present at the neuromuscular junctions (NMJs) and plays a role in synaptic bouton budding (Pennetta et al., 2002). During larval development, bouton number, in part, increases by asymmetric division of pre-existing boutons (Zito et al., 1999). Knocking down DVAP-33A expression caused a decrease in the number of boutons but an increase in their size while conversely, overexpressing DVAP-33A increased bouton number but they were smaller in size (Pennetta et al., 2002). Compensatory quantal size changes were identified in response to alterations in synaptic bouton size and number and therefore, normal synaptic transmission was maintained in both DVAP-33A null and overexpression models (Chai et al., 2008). In transgenic flies expressing Vap^{P58S} within neurons, the equivalent mutation to the mammalian ALS-linked point mutation, there was a significant increase in average

synaptic bouton size, similar to the phenotype observed from a knock-down of VAP expression (Ratnaparkhi et al., 2008). Furthermore, in a *Drosophila* mutant lacking full-length endogenous VAP protein, neuronal expression of wild-type VAP but not VAP-P58S could rescue abnormalities in bouton size, providing supporting evidence that the ALS8 point mutation may act in a dominant negative manner (Ratnaparkhi et al., 2008).

1.4.5 VAPs and mitochondrial motility and function

In *Drosophila* models, VAP has been shown to associate with microtubules and a knock-out of expression perturbed the organisation of the microtubules at the NMJs (Pennetta et al., 2002). Similarly, overexpression of VAP-P58S but not wild-type VAP induced microtubule disorganisation comparable to that of null mutants (Ratnaparkhi et al., 2008). In neurons, expression of VAPB-P56S caused a significant reduction in mitochondria motility and the anterograde movement of mitochondria along the axon was particularly affected (Morotz et al., 2012). This was due to a disruption in the interaction of tubulin with the OMM protein Miro1 that mediates mitochondrial movements in response to calcium levels (Morotz et al., 2012).

Furthermore, in *C. elegans* mutant VAP models, the mitochondrial network was composed of thin, highly branched tubular networks which is in stark contrast to the largely unbranched tubules of wild-type *C. elegans*. This change in morphology was accompanied by a significant reduction in resting membrane potential and impaired generation of ATP and ROS (Han et al., 2012).

1.4.6 VAPs and cellular degradative pathways

As previously described, ALS is characterised by the presence of ubiquitinated aggregates and the expression of VAPB-P56S leads to the presence of intracellular aggregates that are continuous with the ER. It was shown that VAPB-P56S aggregates are positive for ubiquitin and treatment of cells expressing mutant VAPB with an inhibitor of the proteasome almost completely attenuated the degradation of the mutant protein suggesting that mutant VAPB is a target of the UPS (Papiani et al., 2012). In contrast, treatment of cells with an inhibitor of autophagy had no

significant effect on the level of aggregates (Papiani et al., 2012). Co-expression of VAPB-P56S with an ALS-linked mutant VCP increased the levels of aggregated protein, further implicating mutant VAPB as a target of the UPS (Papiani et al., 2012).

The alpha 5 subunit of the proteasome and several subunits of the 20S proteasome particle were identified as constituents of VAPB inclusions and co-immunoprecipitated with the mutant protein, suggesting that VAPB-P56S aggregates can impair UPS activity (Moumen et al., 2011). In addition, over-expression of wild-type or mutant VAPB resulted in elevated levels of three fluorescent substrates of the UPS whereas overexpression of VAPA or SOD1 had no significant effect, indicating that the P56S mutation induces a global defect in UPS activity (Moumen et al., 2011).

Recently, it was shown that VAPA/B interact with the autophagy-related proteins FIP200 (focal adhesion kinase family interacting protein of 200 kD) and ULK1 to mediate the initiation of autophagosome formation and depletion of VAPs within cells inhibited autophagy by preventing the progression of the isolation membranes into fully formed autophagosomes (Zhao et al., 2018).

1.5 Additional pathogenic VAPB mutations

1.5.1 *VAPB^{T46I}*

After the identification of the P56S mutation in VAPB, a second mutation in VAPB was detected in a familial ALS patient with a threonine to isoleucine point mutation at codon 46 (*VAPB^{T46I}*) (Chen et al., 2010). Like the P56S mutation, the T46I mutation occurs within the highly conserved VAP consensus sequence of the MSP domain and induces the mislocalisation of the protein from the ER into large protein aggregates. Expression of VAPB-T46I upregulates pro-apoptotic markers in transfected cells and was capable of inducing protein aggregation in neighbouring, non-transfected cells. Furthermore, co-expression of VAPB-T46I with wild-type VAPB inhibits the wild-type protein's activation of the IRE1 pathway (Chen et al., 2010).

1.5.2 *VAPB*^{V234I}

An additional pathogenic mutation in VAPB, a valine to isoleucine point mutation at amino acid position 234 (*VAPB*^{V234I}) was identified in one ALS patient who also had a C9Orf72 repeat expansion (van Blitterswijk et al., 2012). Unlike the P56S and T46I mutations, this point mutation occurs within the transmembrane domain of VAPB. In *Drosophila* models, expression of the equivalent *Vapb*^{V260I} mutation disrupted microtubule organisation and induced locomotor defects in larvae (Sanhueza et al., 2014).

1.6 VAPA and neurodegeneration

Although VAPA and VAPB share extensive sequence similarity and function in the same cellular pathways, mutations in VAPA have not been linked to neurodegeneration. The equivalent P56S point mutation in VAPA, VAPA-P56S, does form aggregates that are similar in appearance to VAPB-P56S aggregates however, a significant proportion of VAPA-P56S still localises to the ER in addition to the aggregated protein (Teuling et al., 2007). Moreover, in contrast to VAPB-P56S, mutant VAPA does not induce the aggregation of wild-type VAPA and VAPB proteins and shows greater solubility (Suzuki et al., 2009; Prosser et al., 2008). Within the VAP consensus sequence of the MSP domain, VAPB possesses two proline residues while VAPA contains 3 and it is believed that this extra proline residue infers the resistance of VAPA to the P56S mutation. In support of this, a double point mutation replacing the extra proline residue in VAPA (*VAPA*^{P56S,P63A}) caused the protein to relocalise into large membranous aggregates that were indistinguishable from VAPB-P56S while VAPA-P56S alone showed a reticular pattern of staining (Nakamichi et al., 2011).

In summary, a number of the pathways disrupted by the expression of VAPB-P56S specifically are common pathogenic hallmarks of neurodegenerative disorders and indeed, a large proportion of these pathways are also regulated by organelle contact sites. Therefore, it is plausible to hypothesise that a dysfunction to organelle contact sites and predominantly ER-mitochondria contacts, induced by the expression of

VAPB-P56S, could represent an early pathogenic event in ALS8, preceding the cellular perturbations described above.

1.7 Aims and approaches

In light of all the evidence presented above, the overall aim of this thesis was to develop a high-throughput, bi-fluorescence complementation (BiFC) system for the detection and visualisation of membrane contact sites that can be used in both fixed and living cells, with a particular focus on ER-mitochondria interactions. We aimed to validate this technique for the quantification of contact sites by replicating known changes to ER-mitochondria contacts, the data of which is presented in chapter three of this thesis. The majority of the data presented in chapter three has been published in (Harmon et al., 2017).

As our BiFC reporter proteins detect ER-mitochondria junctions of a maximum distance of <10 nm, we aimed to use this technique to try and correlate the fluorescent signal with known functions of the MAMs to elucidate the specific functional significance of these particularly tight contact sites, which we have reported on in chapter four.

Finally, using the BiFC approach and other molecular techniques, we investigated the role of VAPs and the mutant VAPB-P56S protein on ER-mitochondria contact sites in cells and in transgenic rat models in order to gain some insight into the molecular mechanisms of ALS8 pathogenesis, detailed in chapter five.

Chapter 2
Materials and Methods

2.1 Plasmids and primers

2.1.1 Venus expression plasmids: Full-length coding sequences for mouse VAPA and VAPB were previously amplified by polymerase chain reaction (PCR) and sub-cloned into pcDNA3.1(zeo)-Venus[1] plasmids (Remy et al., 2002) as described in (Gkogkas et al., 2008) to generate full-length Venus1-VAPB (V1-VAPB) and Venus1-VAPA (V1-VAPA) plasmids respectively. Previous work in the Skehel lab generated V1-ER expression plasmids, derived from V1-VAPB by deletion PCR mutagenesis with the primers gggtcctccggaatgggcctgagcgcccggctgct and cattccggaggacccaccacctccagagc to generate a Venus1 fragment fused at its C-terminus to the C-terminal 25 amino acids from mouse VAPB, GLSARLLALVVLFFIVGVIIGKIAL, with a 14 amino acid linker sequence, as published in (Harmon et al., 2017)(**Fig 2.1**).

Venus2-Mito (V2-Mito) was generated from human TOMM20 (Translocase of Outer Mitochondrial Membrane 20) cDNA by PCR using primers 5'-cggcggccgctccggaccatggtgggccggaacagcgcc-3'

and 5'-atctagattaatcgattgcagacccgatgccgctgc-3' to amplify the first 34 amino acids MVGRNSAIAAGVCGALFIGYCIYFDRKRRSDPN (**Fig 2.1**). The PCR product was digested and ligated to *NotI* and *ClaI* restriction sites of a pcDNA3.1 Venus[2]-zip plasmid (Kindly gifted by S.W.Michnick)(Harmon et al., 2017).

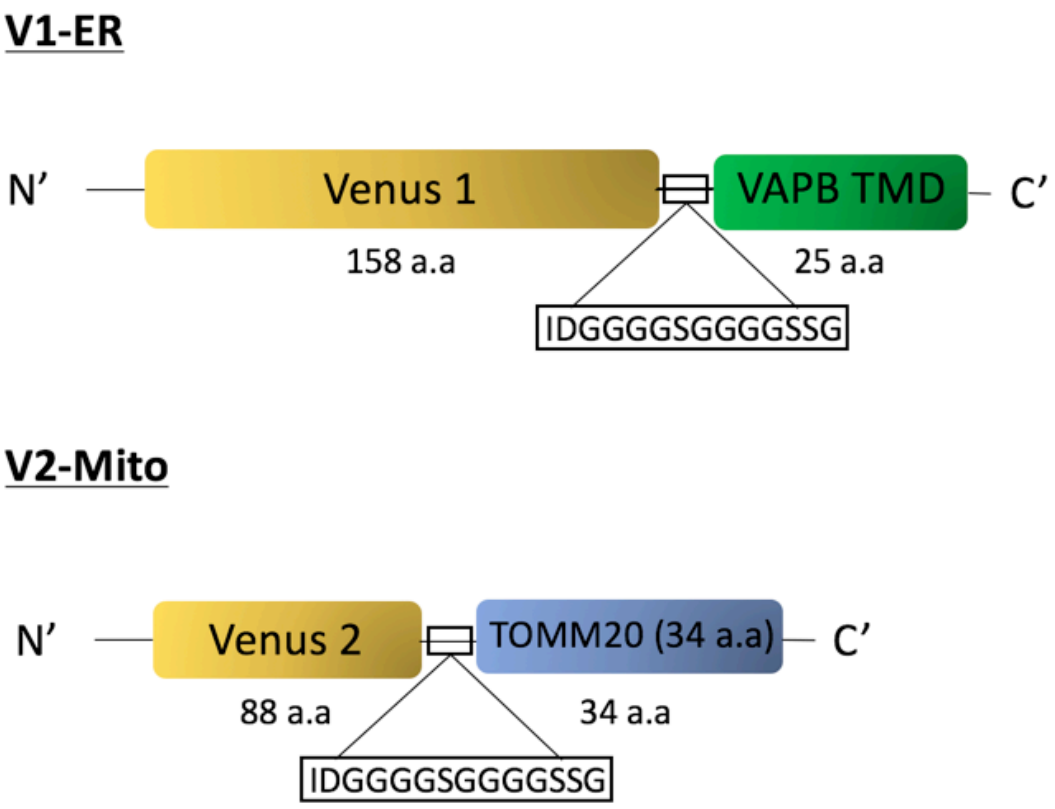

Fig 2.1: Protein maps of V1-ER and V2-Mito constructs. V1-ER construct consists of an N-terminal Venus 1 fragment of 158 amino acids and a 14 amino acid poly-G linker sequence fused to the 25 amino acids of the VAPB transmembrane domain. V2-Mito is comprised of an N-terminal Venus 2 fragment, 88 amino acids in length, fused to the N-terminal 34 amino acids of TOMM20 with a 14 amino acid linker sequence in between.

In order to detect and quantify ER-endosome contacts, Venus2-VAMP4 and Venus2-VAMP4-CT plasmids composed of the full-length VAMP4 sequence or just the C-terminal endosomal targeting sequence were previously generated in the lab by Ms. Emma Lund (unpublished data). Briefly, a VAMP4-pHluorin template plasmid (kindly provided by Prof. Mike Cousin, University of Edinburgh, as published in (Nicholson-Fish et al., 2016)) was used to PCR amplify the full-length VAMP4 sequence using a forward primer sequence 5'-ggtgggtcctccggaatgcctcccaagtttaagcgccac-3' and a reverse primer sequence 5'-ttcgccaactaatttttaagtacggtatttcatgactataag-3' which

was subsequently cloned into the Venus vector backbones using Gibson Assembly cloning as per manufacturer's instructions (New England Biolabs). For generation of the VAMP4-CT sequence, a 51 amino acid gBlock sequence, SGGGGSSGMWWRGCKIKAIMALAAAILLLMIITQIILHLKK*KLVGER*SR was ordered from Integrated DNA Technologies whereby an * indicates a stop codon, and subsequently cloned into the Venus vectors using the Gibson Assembly kit.

2.1.2 Other expression vectors: pECFP-Golgi and pDsRed2-ER (Clontech) were used to label the Golgi and ER respectively. CMV-Globin (kindly provided by Prof. Giles Hardingham, University of Edinburgh) was used as a balancer transfectant where equivalent total DNA concentrations across different experimental groups was required.

For the overexpression of VAPB, double-tagged constructs were previously cloned in the Skehel lab to generate plasmids expressing wild-type VAPB, VAPB-P56S or VAPB-N29S with an N-terminal Myc epitope and a C-terminal HA epitope at the C-terminus of VAPB to generate the Myc-VAPB-HA, Myc-VAPB-P56S-HA and Myc-VAPB-N29S-HA constructs respectively.

A mitochondrially targeted, genetically encoded pMito-RCaMP (Akerboom et al., 2013), previously cloned in the lab from a pMito-GCaMP6 template (Chen et al., 2013), and a cytoplasmically targeted pGCaMP2-Cyto (Tallini et al., 2006) were used for mitochondrial calcium imaging experiments (both kindly provided by Prof. Giles Hardingham).

mCherry-ATG14-C-18 was a gift from Michael Davidson (Addgene plasmid # 54989). pJ603-NGFP-p55 encoding for POLG2-GFP was kindly gifted from Dr. William Copeland, National Institute of Environmental Health Sciences (Young et al., 2015).

pAAV-EF1α-DIO-hM3D(Gq)-mCherry (referred to in the rest of this thesis as EF1α-DIO-Gq-mCherry) is a double floxed Gq-coupled hM3D DREADD receptor fused with a fluorescent mCherry probe under the control of a ubiquitous EF1α promoter in which the expression depends on Cre and was gifted by Bryan Roth (Addgene

plasmid #50460) which in turn was kindly gifted to use by Prof. Giles Hardingham, University of Edinburgh. The pAAV-Ef1α-Cre plasmid used in combination with this to activate expression was gifted by Karl Deisseroth (Addgene plasmid #55636) and was also kindly provided to use by Prof. Giles Hardingham's group.

2.2 Cloning and PCR

2.2.1 Cloning of plasmids expressing POLG2-DsRed2: POLG2-DsRed2 and $POLG2_{1-25}$-DsRed2 expression plasmids were generated by in-fusion cloning from 1 ng of a pJ603-NGFP-p55 template containing a GFP open reading frame fused in-frame between the N-terminal 25 codons of POLG2, encoding for the predicted mitochondrial targeting sequence, and the remaining C-terminal POLG2 sequence (as published in (Young et al., 2015). Linearized vector backbone sequence containing the POLG2 cDNA without the GFP ORF was amplified by PCR reaction using the primer pairs agatgcggggcagccggagctgttg and actcgacccccaaacccagacaaca. DsRed2 insert sequences were amplified by PCR from 1 ng of an ER-DsRed2 (Clontech) vector template using the forward primer gtttgggggtcgagtaatggcctcctccgagaacgtcatc with either a reverse primer of sequence ggctgccccgcatctctacaggaacaggtggtggcggccc to include the DsRed2 stop codon or with a reverse primer of sequence ggctgccccgcatctcgagccaggaagaggtggtggcgg to incorporate a point mutation in the stop codon, replacing it with a serine. The presence of a stop codon results in the translation of only the first N-terminal 25 amino acids of POLG2 ($POLG2_{1-25}$-DsRed2). Insert sequences were amplified with 5' 15-bp extensions complementary to the ends of the amplified, linearized vector sequence for In-Fusion cloning.

2.2.2 Polymerase chain reaction (PCR): PCR reactions were carried out in a total volume of 25 µl using Phusion high fidelity DNA polymerase (Thermo Fisher Scientific) or Taq DNA polymerase (2.5 units/µl) (Qiagen) along with 0.5 µM of each primer, 200 µm of each dNTP and Phusion HF buffer providing 1.5 mM

$MgCl_2$ (Thermo Fisher Scientific). DNA was amplified in a thermocycler at the following settings:

- Initial denaturation step of 98°C for 30 seconds
- 20-25 cycles of
    - Denaturation at 98°C for 15 seconds
    - Annealing at 55-56°C (ranging from 15 seconds to 30 seconds)
    - Extension at 72°C (15 seconds to 7 minutes)
- Final extension step of 72°C for 10 minutes.

2.2.3 Gel electrophoresis: PCR products were run on a 0.7-3.5% (w/v) TAE agarose gel depending on the size of the band of interest, made from NuSieve 3:1 Agarose. In most cases, gels were run at 65 V except for when the splicing of XBP1 mRNA was being investigated whereby gels were run at 45 V to obtain better separation of DNA bands. PCR products were visualised through staining with SyberSafe (Invitrogen) and detection under UV light, using a UVITEC light box (Thistle Scientific).

2.2.4 Gel purification: PCR bands of interest were cut out of the gel using a sterile scalpel blade and purified using the Zymoclean Gel DNA Recovery kit as per manufacturer's instructions (Zymo Research). In summary, gel slices were mixed with agarose dissolving buffer and incubated in a 50°C water bath for 15 minutes. DNA was then purified by a series of centrifugation steps using the Zymo-spin columns followed by wash steps with DNA wash buffer. Purified DNA was eluted in 10 µl of DNA elution buffer.

2.2.5 In-fusion cloning: DsRed2 insert sequences were cloned into POLG2 vector backbone sequences using the In-Fusion HD cloning kit as per manufacturer's instructions (Clontech), scaled down to a total reaction volume of 5 µl per reaction mix. Cloning was performed with an insert to vector molar ratio of 2:1 for 15 min in a water bath set to 50°C.

2.2.6 Bacterial transformation: Bacterial transformation of In-Fusion cloning products into competent *E.Coli* cells were carried out by the following steps:

- 2.5 µl of each cloning reaction was mixed with 25 µl of NEB 10-beta competent *E.coli* (NEB) and kept on ice for 30 min.
- *E.coli* cells were then heat-shocked at 42°C for exactly 40 seconds before being placed back on ice for a further 2 min.
- Proceeding this, 200 µl of SOC outgrowth media (NEB) was added to the cells which were shook for 45 min at 150 rpm at 37°C.
- The entire reaction mix was spread on LB agar plates containing ampicillin 100 µg/ml and incubated overnight at 37°C.

2.2.7 DNA extraction: Single bacterial colonies were selected and grown overnight in LB media with 100 µg/ml ampicillin, shaken at 200 rpm at 37°C. DNA extraction was carried out using a QIAGEN plasmid miniprep kit as per manufacturer's instructions. The correct plasmid sequence was confirmed by Sanger sequencing at the Edinburgh Genomics GenePool facility.

2.3 Cell culture and transfection

2.3.1 Mammalian cell culture and maintenance: NSC34 (Cashman et al., 1992), COS-7 (Gluzman, 1981) and HEK293 (Graham et al., 1977) were grown at 37°C with 5% CO_2 in Dulbecco's modified Eagle's medium (DMEM) containing high glucose and supplemented with 10% (v/v) fetal bovine serum and 1% (v/v) antibiotic-antimycotic (Thermo Fisher Scientific). In preparation for imaging, cells were plated on 13 mm glass coverslips that had been coated with poly-L-lysine (50 µg/ml) and bovine plasma fibronectin (10 µg/ml) (Life Technologies) for at least 2 hours each.

2.3.2 DNA transfection: Plasmid transfections were carried out using Lipofectamine 2000 (Invitrogen) in Opti-MEM media (Thermo Fisher Scientific). For 12-well plates containing 1 ml DMEM, 50 µl of Opti-MEM containing the DNA mix and 50 µl of

Opti-MEM containing Lipofectamine 2000 was made and let sit for 5 min. The DNA and Lipofectamine mixes were then added together and mixed by gentle flicking of the tube and let stand at room temperature for 20 min. For NSC34 cells, a Lipofectamine:DNA ratio of 1:1 µl:µg was used while for HEK293 and COS-7 cells a ratio of 0.5:1 µl:µg was used. Media was changed 4 hours post-transfection to remove traces of Lipofectamine. V1-ER and V2-Mito reporter plasmids were transfected in a 1:1 ratio. In cases where particular protein levels were titrated within a single experiment, CMV-Globin plasmid was used as balancer DNA to ensure that equal concentrations of total DNA were transfected per well. Cells were fixed 48 h post-transfection with 4% (w/v) Paraformaldehyde in Phosphate-buffered saline (PBS)(Roche) or with ice-cold methanol for 5 min at -20°C. Different fixation methods were used depending on what antibodies were required (as indicated in **table 2.1**). Coverslips were mounted on glass slides using ProLong Diamond Antifade mountant (Thermo Fisher Scientific) or Vectashield with DAPI (Vector Laboratories, Inc. Burlingame, CA 94010) and left overnight in a darkened area before imaging.

2.3.3 siRNA transfection: Silencing of protein expression was performed by siRNA transfection using Lipofectamine RNAi Max (Invitrogen) and Opti-MEM media (Thermo Fisher Scientific). A total siRNA concentration of 50 nM was used and protein was harvested 48 h post-transfection. All surfaces were decontaminated prior to transfection using RNase AWAY decontamination reagent (Invitrogen). siRNA plasmids used were as follows:

Mouse MFN2 ON-TARGETplus SMART pool (Dharmacon).

ON-TARGETplus control non-targeting pool was used for control transfections (Dharmacon).

Proprietary stealth siRNA and scramble sequences from Invitrogen were used for the knock-down of mouse VAPA and VAPB. VAPA product numbers 887S and 657S. VAPB product numbers 675S and 1465S. 25 nM of each siRNA pair was transfected.

Validation and quantification of protein knock-down was determined by western blotting.

2.3.4 Stable cell line generation: NSC34 cells stably expressing V1-ER/V2-Mito, V1-VAPB/V2-Mito or V1-VAPA/V2-Mito respectively were generated by Lipofectamine transfection followed by Zeocin (Invitrogen) selection at 200 μg/ml. Clonal populations were obtained by serial dilutions of stably transfected cells in 96-well plates (Greiner Bio-One) under Zeocin selection.

2.3.5 RNA extraction and PCR: Total RNA was extracted from NSC34 cells using the RNeasy mini kit (Qiagen) as per manufacturer's instructions. In short, cells are trypsinized from a 12-well plate and lysed in the presence of a lysis buffer to extract RNA while simultaneously deactivating RNases. The lysate is homogenised by centrifugation through a QIAshredder spin column and subsequently spun through a silica RNeasy spin column to purify RNA. Following wash steps, RNA is eluted in 50 μl of RNase-free water. Reverse-transcription PCR was performed using the Omniscript reverse transcription kit (Qiagen) to generate cDNA, followed by PCR amplification using Phusion high fidelity DNA polymerase (Thermo Fisher Scientific) or Taq DNA polymerase (Qiagen). PCR products were visualised on a 3.5% (w/v) TAE agarose gel stained with SyberSafe (Invitrogen) and detected under UV light, using a UVITEC light box (Thistle Scientific).

2.3.6 Cell treatments: ER Stress was induced by treating cells with 2 μg/ml or 10 μg/ml tunicamycin (Calbiochem) for 6 h before fixation of the samples. An equivalent volume of DMSO was used as a vehicle only control. For the induction of serum deprivation, cells were grown in serum-free DMEM for 24 h post-transfection. To increase mitochondrial membrane potential, cells were treated with 5 μg/ml oligomycin (Sigma) for 24 h post-transfection.

2.4 Immunocytochemistry

2.4.1 Immunofluorescent (IF) staining: Following fixation of cells, cells were washed with PBS and then permeabilised with 0.4% (v/v) Triton X-100 for 10 min at room temperature, except in cases where cells were fixed in ice cold methanol where no extra permeabilisation step was carried out. Cells were then incubated in a PGAS blocking solution composed of PBS, 0.2% (v/v) fish gelatin and 0.02% (w/v) saponin and filtered through a stericup 0.22 µm pore size (Merck Millipore) at 4°C for at least 2 hours. Cells were incubated with the primary antibody in PGAS solution, in a humidified chamber for 30-60 min at room temperature followed by three washes in PGAS solution. Secondary antibodies were incubated with cells in PGAS solution at a 1/250 dilution for 30 min at room temperature in the dark. Finally, cells were washed 3 times in PGAS solution with a subsequent 3 washes in PBS before being mounted for imaging.

2.4.2 Antibodies for IF: Secondary antibodies used were donkey anti-mouse Cy2 (715-225-150), Cy3 and Cy5-coupled goat anti-mouse (115-165-146, 115-175-156), Cy3 and Cy5-coupled donkey anti-rabbit (711-165-152, 711-175-152) (Jackson ImmunoResearch). Primary antibodies used for immunocytochemistry are listed in **table 2.1** below. Anti-ATG5 (C-terminal) primary antibody (Sigma) was a generous gift from Dr. Noor Gammoh (The University of Edinburgh).

Table 2.1: Antibodies used for immunocytochemistry.

Name	Class	Host	Antigen	Catalogue number	Dilution	Fixation method
Anti-ATPB (abcam)	Monoclonal	Mouse	Whole heart mitochondria (human)	Ab14730	1:250	4% (w/v) PFA
Anti-GFP (Life Technologies)	Polyclonal	Rabbit	GFP isolated from *Aequorea victoria*	A6455	1:400	4% (w/v) PFA
Anti-ERp72 (Enzo Life Sciences)	Polyclonal	Rabbit	a.a. 623-638 of ERp72	ADI-SPS-720	1:100	Methanol
Anti-EEA1 (Cell Signaling Technology)	Polyclonal	Rabbit	Synthetic peptide corresponding to residues surrounding Gly14 of human EEA1	2411S	1:100	4% (w/v) PFA
Anti-c-Myc clone 9E10 (Invitrogen)	Monoclonal	Mouse	Synthetic peptide a.a 408-438 of human c-Myc	MA1-980	1:500-1000	4% (w/v) PFA
Anti-ATG5 (C-terminal) (Sigma)	Polyclonal	Rabbit	Amino acids 262-275 of mouse ATG5	A0731	1:200	4% (w/v) PFA followed by methanol treatment for 2 min

2.5 Immunoblotting

2.5.1 Western Blotting: Protein was harvested from cells 48 h post-transfection using SDS sample buffer composed of 80 mM Tris-HCl pH6.9, 2% (w/v) SDS, 100 mM DTT, 10% (v/v) glycerol, or in RIPA lysis buffer made up of 1% NP40 (v/v), 0.1% SDS (w/v), 150 mM NaCl, 0.5% (w/v) sodium deoxycholate, 50 mM Tris pH 8 with complete protease inhibitor (Roche). Total protein was quantified by Pierce BCA protein assay kit (Thermo Fisher Scientific). Samples were heated at 85°C for 15 min and then run on an NuPAGE 4-12% Bis-Tris gel (Invitrogen) in MES SDS running buffer (Invitrogen) at 120 V. Proteins were transferred to a PVDF Immobilon-P (EMD

Millipore) membrane soaked in methanol and then in NuPAGE transfer buffer containing 10-20% (v/v) methanol. Protein transfer was performed at 100 V for 60 min in the presence of an ice-block and constant magnetic stirring. Non-specific antibody binding was inhibited by blocking PVDF membranes in PBS containing 5% (w/v) non-fat dry milk and 0.1% (v/v) Tween-20 for at least 60 min at room temperature while rocking. Primary antibodies (as listed in **table 2.2**) were incubated with the membrane in blocking solution at 4°C overnight, followed by 3 washes at room temperature with PBS containing 0.1% (v/v) Tween-20. Proceeding this, membranes were incubated with horseradish-peroxidase conjugated secondary antibodies in blocking solution at a 1/5000 dilution at room temperature for 1 hour, followed by enhanced chemiluminescent substrate (ECL) detection made up of a 1:1 ratio of hydrogen peroxide and Luminol or, in cases where protein concentrations were very low, Amersham ECL western blotting detection reagent (GE Healthcare) was used. Blots were exposed on X-ray film (FUJIFILM). Densitometry analysis of blots was carried out on FIJI image analysis software.

2.5.2 Antibodies for Western blotting: Secondary antibodies used were horseradish-peroxidase conjugated goat anti-rabbit (111-035-003) and goat anti-mouse (115-035-146) (Jackson ImmunoResearch). Primary antibodies used for Western blotting are listed in **table 2.2** below.

Table 2.2: Antibodies used for Western blotting.

Name	Class	Host	Antigen	Catalogue Number	Dilution
Anti-MFN2 (Abcam)	Monoclonal	Mouse	Amino acids 661-758 of human MFN2	Ab56889	1:5000
Anti-α-Tubulin (EMD Millipore)	Monoclonal	Mouse	Amino acids 426-450 of human α-tubulin	05-829	1:50,000
Anti-c-Myc clone 9E10 (Invitrogen)	Monoclonal	Mouse	Amino acids 408-438 of human c-Myc	MA1-980	1:20,000
Anti-Histone H3 CT (Merck Millipore)	Polyclonal	Rabbit	Synthetic peptide corresponding to the C-terminus of human Histone H3	07-690	1:100,000
Anti-VAPA (Murex Bioservices)	Polyclonal	Rabbit	As published in (Skehel et al., 2000)	N/A	1:1000-10,000
Anti-VAPB clone #6 (Murex Bioservices)	Monoclonal	Rabbit	Bacterially expressed VAPB MSP domain (unpublished).	N/A	1:500-5,000
Anti-VAPB clone #38 (Murex Bioservices)	Polyclonal	Rabbit	Bacterially expressed carboxy terminal deleted soluble VAPB (unpublished).	N/A	1:500-5,000

2.6 Ca^{2+} Measurements

NSC34 cells were transiently transfected to express a mitochondrially-targeted fluorescent Mito-RCaMP probe whereby regions of higher fluorescence intensity are indicative of higher calcium concentrations (Akerboom et al., 2013). 3D live-cell images were obtained by confocal microscopy. Mean fluorescence intensity value of each of the disconnected components of the mitochondria network signal was quantified on Imaris. To quantify fluorescence intensity specifically of mitochondrial regions associated with BiFC puncta, the Venus signal was used as a mask for the mitochondria channel and all pixel intensity values outside of this mask were set to 0. The mean fluorescent intensity value for all remaining mitochondrial signal was

then quantified and expressed relative to the mean total mitochondrial intensity value.

For Gq DREADD receptor optimisation experiments, NSC34 cells were transfected with 0.05 μg EF1α-DI0-Gq-mCherry, 0.5 μg AAV-EF1α-Cre and 0.45 μg GCaMP3-cyt per well in a 12-well plate. For optimisation, cells were imaged with a DFC350 FX digital camera on a Leica AF6000 LX microscope on a 20X objective. To induce DREADD receptor activation, 1 μM of Clozapine N-oxide (CNO) diluted in live-cell imaging media. Cells were imaged using a standard GFP filter set. Images were taken every 3 seconds. Change in mean fluorescence was measured according to the equation F/F_0 where F = fluorescence intensity value and F_0 = the mean intensity value of baseline fluorescence before the addition of CNO, averaged over three images. As a negative control, cells were imaged for the same length of time without the addition of CNO. Analysis of fluorescence intensity values was carried out with Leica Application suite X imaging software.

For quantification of BiFC puncta in response to Gq DREADD mediated Ca^{2+} release, NSC34 cells were transfected with V1-ER/V2-Mito reporter plasmids in addition to 0.1 μg EF1α-D10-Gq-mCherry and 0.5 μg AAV-EF1α-Cre in a live-cell, glass-bottomed imaging dish (Mattek) equalling 2 μg total DNA. Cells were imaged live on a Nikon A1R FLIM microscope for 1 min before the addition of 1 μM CNO. Images were acquired every 3.81 seconds. Changes in the number of BiFC puncta were measured as described in section **2.9.5.**

2.7 Sub-cellular organelle fractionation

Transgenic homozygous or heterozygous rat models for the *Vapb*^{P56S} mutation and homozygous *Vapb* knock-out rats were previously generated using long single-stranded DNA (lssDNA) to the rat *Vapb* gene to insert the P56S mutation into a floxed exon 2 of rat *Vapb* via the CRISPR/Cas gene editing system by Tomoji Mashimo (as mentioned in (Meek et al., 2017)). Sub-cellular organelle fractionation of brain and liver tissue from wild-type, heterozygous *Vapb*^{P56S} and homozygous *Vapb* knock-out

transgenic rats was carried out using the protocol as published in (Wieckowski et al., 2009). All of the described steps were carried out on ice or in centrifuges chilled to 4°C. In summary, brain and liver tissue was extracted from 2 month old or 5 month old animals as indicated in the specific figure legends and immediately placed in isolation buffer composed of 225 mM mannitol, 75 mM sucrose, 0.5% (w/v) BSA, 0.5 mM EGTA and 30 mM Tris-HCl pH 7.4. Animals were housed and sacrificed in accordance with UK Home Office guidelines. Tissue was washed 3 times in wash buffer (225 mM mannitol, 75 mM sucrose and 30 mM Tris-HCl pH 7.4) before being homogenised manually. The homogenate was centrifuged at 740*g* for 5 min at 4°C and the pellet was discarded. This was followed by an additional spin at 740*g* for 5 min after which the supernatant was centrifuged at 9,000*g* for 10 min. Both the supernatant (lysosomal and ER fraction) and pellet (crude mitochondria fraction) obtained from this step were collected for further processing. The supernatant was centrifuged at 20,000*g* for 30 min to separate the lysosomal fraction (pellet) and ER fraction (supernatant) after which a further centrifugation step of the supernatant at 100,000*g* for 1 hour was performed to isolate the ER fraction as a pellet. The ER fraction was resuspended in a resuspension buffer consisting of 250 mM mannitol, 5 mM HEPES (pH 7.4) and 0.5 mM EGTA. The crude mitochondria pellet was resuspended with a soft paintbrush in 20 mL of buffer consisting of 22 mM mannitol, 75 mM sucrose, 0.5% (w/v) BSA and 30 mM Tris-Hcl pH 7.4 and centrifuged twice at 10,000*g* for 10 min, discarding the supernatant. This pellet was resuspended in 2 mL of resuspension buffer and a small aliquot of this was taken as the crude mitochondrial fraction. Percoll medium consisting of 225 mM mannitol, 25 mM HEPES (pH 7.4), 1 mM EGTA and 30% Percoll (v/v) was made up and 4 mL of this was placed in polyallomer ultracentrifuge tubes (13 x 51mm) (Beckman). 1mL of the mitochondrial suspension was layered on top of this and tubes were weighed to ensure that they were all equivalent weights before ultracentrifugation. Tubes were centrifuged at 95,000*g* for 30 min in a Beckman Coulter Optima MAX Ultracentrifuge in an MLS-50 aluminium swinging-bucket rotor (Beckman Coulter). A band of purified mitochondria is present near the bottom of the tube while a second band containing

the MAM fraction is located above this about two thirds of the way up the tube (**Fig 2.2)**. Both fractions were collected with a Pasteur pipette, diluted five-fold in resuspension buffer and centrifuged at 6,300*g* for 10 min. MAM fraction supernatants were transferred to Beckman ultracentrifuge tubes and spun at 100,000*g* for 1 hour. The supernatant was discarded and the MAM pellet was resuspended in 50 µl of resuspension buffer. The pure mitochondria pellet was resuspended in the resuspension buffer and centrifuged one final time at 6,300*g* for 10 min. The supernatant was discarded and the pellet was resuspended with a soft paintbrush in 50 – 100 µl of resuspension buffer. The relative purity of the ER, crude mitochondrial, pure mitochondrial and MAM fractions was tested by western blotting.

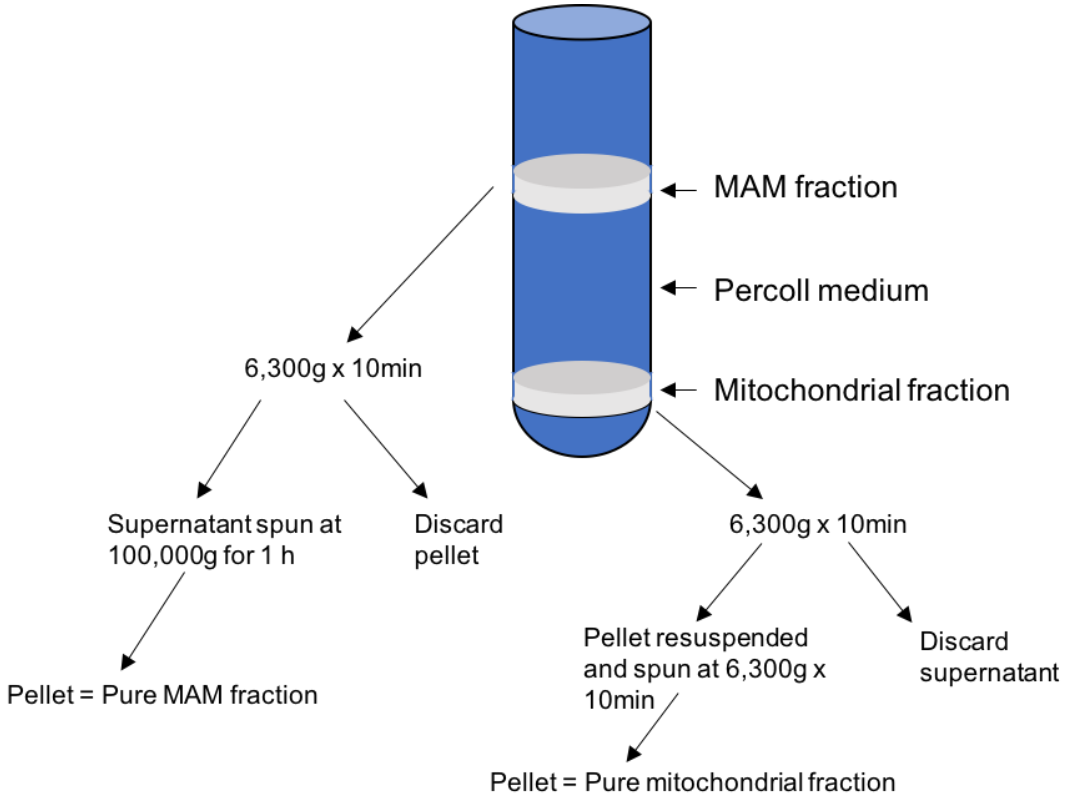

Fig 2.2. Schematic diagram of steps performed to purify MAM and mitochondrial fractions. Following centrifugation in Percoll medium, the MAM and mitochondrial fractions appear as dense bands as indicated in the diagram. Further centrifugation steps allow for the purification of both of these fractions. Adapted from (Wieckowski et al., 2009).

2.8 Microscopy

2.8.1 Confocal microscopy: A Nikon A1R FLIM microscope was used to acquire all confocal images. Excitation laser wavelengths used were for CFP and DAPI 401.5 nm, GFP, YFP (Venus) and Cy2 488 nm, Cy3, DsRed2 and mCherry 56 1nm, and Cy5 641 nm. Microscope control and image acquisition were performed with the NIS-Elements-v4.13 software. High-resolution imaging of single-cells was carried out using a 60X Plan ApoVC NA 1.4 oil objective with a z-step size of 150 nm. For **Fig 3.7B** and **Fig5.1B** images were acquired with a 20X Plan Apo NA 0.75 objective lens using the same laser power, detector gain and acquisition parameters.

2.8.2 Live-cell imaging: Cells were plated on poly-D-lysine/fibronectin coated 35 mm glass-bottomed culture dishes with a 14 mm microwell diameter and glass thickness No. 1.5 (MatTEK). Prior to imaging, DMEM was replaced with optically clear, HEPES buffered live-cell imaging solution (Thermo Fisher Scientific). Live-cell imaging was performed on a Nikon A1R confocal microscope in a heated chamber at 37°C with 5% CO_2 (Okolab) using a 60X oil objective lens (Plan ApoVC NA 1.4 oil). For live- cell imaging, mitochondria were labelled using 25 nM red fluorescent MitoTracker CMXRos dye or MitoTracker Deep Red FM far red fluorescent dye (Thermo Fisher Scientific) for 30 min in pre-warmed DMEM followed by three five minute washes with pre-warmed live-cell imaging solution.

2.8.3 CW-gSTED microscopy: Continuous wave gated stimulated emission depleted (CW-gSTED) microscopy was performed on a Leica SP5 confocal laser scanning microscope equipped with a 592 nm depletion laser and 100 x 1.4 NA HCX PL Apo oil immersion objective lens. YFP fluorophores were excited by a white laser tuned to 514 nm with an 80MHz pulse rate. STED was achieved by concurrent 592 nm depletion aligned to the excitation laser. 524-580nm emission was isolated by an acousto-optical beamsplitter and detected with a Leica HyD hybrid detector gated to detect 0.5-8 ns following each excitation pulse. Single slice images were acquired with a 0.02 μm pixel size to achieve Nyquist sampling.

2.9 Image Analysis

2.9.1 Deconvolution: Deconvolution of confocal images was carried out on Huygens Essential deconvolution software (Huygens Software 4.5.1p3) before subsequent analysis.

2.9.2 Colocalisation Analysis: Colocalisation analyses were performed on 3D stack, deconvolved images using ImarisColoc feature of Imaris image analysis software (Bitplane Inc, software available at http://bitplane.com). The extent of colocalisation was quantified by Pearson's Correlation Coefficient (PCC) and Mander's Correlation Coefficient (MCC) and results were exported in Microsoft Excel. Images were thresholded manually by pixel intensity values.

2.9.3 Quantification of BiFC signal: BiFC puncta were quantified using the 3D volume rendering function of Imaris and thresholded by pixel intensity value. The "total number of disconnected components" measurement value was then used to automate counting of fluorescent puncta. Total BiFC volume or mitochondria volume was quantified in the same manner using the 3D volume rendering function followed by the "volume" measurement value.

For quantification of fluorescent signal overlap of BiFC puncta and fluorescently tagged organelles **(Fig3.8),** the "Spots" function of Imaris was used to quantify the number of fluorescent puncta based on a maximum intensity pixel value. Using this same threshold value, a colocalisation channel was built between the BiFC signal and the fluorescently labelled organelle. Finally, the number of spots in the colocalisation channel was counted in the same way and the number of puncta with a point of colocalisation with the specific organelle signal was expressed as a percentage of total BiFC puncta.

2.9.4 STED image quantification: Deconvolution of STED images was not performed due to the relative low strength of the fluorescent signal. Measurements of the diameter of fluorescent puncta was carried out using the "straight line" tool in Fiji (ImageJ) (Schindelin et al., 2012; Schneider et al., 2012). Simply, a straight line was

manually drawn across the widest-most point of each BiFC puncta and the length of the line was calculated in μm.

2.9.5 Live-cell imaging quantification: Imaris image analysis software was used to automate the quantification of the number of BiFC puncta per frame using the 3D volume rendering function on the Venus channel, thresholded by fluorescence intensity value, to detect the total number of BiFC puncta. Measurement values of the number of disconnected components per time point were then automated by the software.

For measuring the distance and speed travelled by the BiFC puncta, each individual object was organised based on track duration i.e. the length of time each individual puncta was visible within the focal plane of the live-cell video. A selection bias was added such that only distance and speed measurements for those puncta present for a large proportion of the video were taken, to exclude any BiFC puncta that only appear in-focus for a very brief amount of time. For each of the selected BiFC puncta, the mean speed value in μm/s and the mean displacement length from the first frame where the object appears until the final frame that it is in focus in μm.

For measuring the distance travelled by the BiFC puncta and its associated mitochondria, the "straight line" tool of ImageJ was used to measure the distance between the starting point of each object and their position in the final frame of the live-cell video.

2.9.6 Fluorescence intensity quantification: For optimisation of Gq-DREADD mediated increases in cytoplasmic calcium levels, changes in cytoplasmically-targeted GCaMP fluorescence was analysed on Leica Application Suite X imaging software. A region of interest was defined for a large selection of cells within the field of view (27 cells) and the mean fluorescence intensity value was quantified for each frame of the live-cell video. Three random spots of background were quantified and averaged to give the mean background signal value which was then subtracted from each of the cells measured.

For all other measurements of fluorescence intensity, quantification was carried out on Imaris. 3D surface rendering was used to add a volume to the fluorescent signal, thresholded by maximum fluorescence intensity value and then the mean fluorescence intensity value could be quantified.

2.9.7 Concentric circle profiling of mitochondrial fluorescence intensity: A concentric circles plugin for ImageJ image analysis software was used to calculate the mitochondrial signal intensity falling on the perimeter of eight, equally spaced concentric circles radiating from the nucleus to the cell perimeter (Available at https://imagej.nih.gov/ij/plugins/concentric-circles.html) (Schindelin et al., 2012).

2.9.8 Distance measurements of spots to surfaces: For calculating the percentage BiFC puncta falling within a certain distance of the nucleus **(Fig4.3C)** and for determining the distance of BiFC puncta to POLG2-DsRed2 puncta **(Fig4.10B)**, the "Spots Close to Surface" tool of Imaris XTension was used. The surface objects (nucleus or POLG2-DsRed2 puncta) were defined by 3D volume rendering using fluorescence intensity values as a threshold. The "spots" function was then used to define each BiFC puncta as a single spot using an estimated XY diameter of 0.5 μm and thresholding by signal intensity values. The number of spots present within a defined distance from the nearest surface could then be determined. Values were exported to Microsoft Excel and presented as the number of spots within a defined distance as a percentage of total spots per cell.

2.10 Statistical analysis

All experiments were replicated a minimum of three times for statistical analysis. All statistics were performed using GraphPad Prism version 6.0 (GraphPad Software, La Jolla California USA, www.graphpad.com). Statistical significance was measured using unpaired two-tailed t-test, paired t-test or one-way ANOVA followed by either Holm-Sidak's or Dunnett's multiple comparison test as indicated in each individual figure legend. To identify outliers, a technique known as ROUT was used that fits a curve using a *Lorentzian* distribution and then identifies outliers of the curve using a

threshold False Discovery Rate (FDR) value which was set at 1% (Motulsky and Brown). This makes the assumption that fewer than 1% of statistically significant values will be false values. Values falling outside of this threshold were removed using the ROUT automated function on GraphPad Prism. All error bars represent the standard error of the mean (SEM). Statistical significance is annotated by * $P < 0.05$, ** $P < 0.01$, *** $P < 0.001$, ns (non-significant) $P > 0.05$. For xy plots, a linear regression best-fit line was fitted and the R-squared value calculated.

Chapter 3
Bi-Fluorescence Complementation Assay (BiFC)

3.1 Background

Membrane contact sites regulate a wide range of physiological processes and perturbations to the formation or maintenance of these contact points can have devastating consequences, as has been observed in various neurodegenerative disorders (as discussed in **section 1.2.3** of **chapter 1**). Therefore, it is of particular research interest to be able to visualise and quantify organelle contact points in cells. Our lab has a specific interest in the detection of MAMs and at the time of commencement of this research project, several strategies to quantify MAMs and other organelle contact sites had been published, which will be summarised below.

3.1.1 Techniques for detecting MAMS

In contrast to the rest of the ER, MAMs are enriched for proteins involved with lipid biosynthesis (Rusinol et al., 1994) and other functions however, the majority of proteins found at these sites are also present along the bulk of the ER and on other organelles, making the identification of specific markers of the MAMs to be a challenge. Interestingly, antibodies against phosphatidylethanolamine N-methyltransferase, an enzyme that synthesises phosphatidylcholine from phosphatidylethanolamine in the liver, specifically labelled the MAMs and not the bulk ER in hepatocytes (Cui et al., 1993). However, this antibody has been of limited value as a marker of MAMs in other cell types (Vance, 2014).

Many studies use high resolution electron microscopy images to detect and quantify MAMs (Vance, 1990; Giacomello and Pellegrini, 2016; Csordas et al., 2006) which appear as close parallel juxtaposition of the OMM and ER membrane that can extend for hundreds of nanometres (Sood et al., 2014)**(Fig 3.1A)**. While this technique provides detailed structural and morphological data on ER-mitochondria contact

sites, in addition to being technically challenging, it can only be carried out on fixed cells and has limited value in studying contact dynamics.

In contrast to EM, fluorescent-based methods for detecting MAMs have the advantage that they can be used in live-cell imaging and can be quantified in a large number of cells with relative ease. One simple method that has been used to measure changes in ER-mitochondria associations is to quantify the signal co-localisation of fluorescently labelled ER and mitochondria membranes whereby an increase or decrease in the extent of co-localisation is representative of increased or decreased contacts respectively (Bravo et al., 2011; de Brito and Scorrano, 2008; Filadi et al., 2015)**(Fig3.1B)**. However, unless super-resolution microscopy techniques are utilised, this method is restricted by the diffraction limit of light microscopy [as reviewed by (Heilemann, 2010)], and so will quantify signals as overlapping if they are within approximately 200-250 nm of each other, well beyond the defined distance of ER-mitochondria junctions. Furthermore, this method is sensitive to any alterations in organelle morphology (Filadi et al., 2015).

Csordas *et al* quantified MAMs by taking advantage of FRET analysis using a donor CFP- and acceptor YFP-tagged, rapamycin-inducible ER-mitochondria linker pair system in which the addition of rapamycin induced covalent linkage between the protein pairs at areas of close apposition and an increase in fluorescence (Csordas et al., 2010). An increase in ER-mitochondria associations can be implied from an increase in the donor and acceptor fluorescent probe emissions. FRET has a higher resolution than fluorescence co-localisation however, spots of fluorescent signal only briefly labelled pre-existing ER-mitochondria contact sites before a "zippering" type mechanism took over whereby the artificial tightening of the contact sites by the linker proteins brought more of the donor pairs within close proximity to one another, resulting in a gradual expansion of the fluorescent signal around the surface of the mitochondria until it appeared to cover the majority of the OMM (Csordas et al., 2010). The addition of rapamycin itself may also induce increased ER-

mitochondria contacts as it initiates autophagy and as previously described, the formation of autophagosomes may partly occur at the MAMs.

An *in situ* proximity ligation assay was used to quantify interactions between VDAC1 and IP_3R receptors at the MAMs by probing the proteins with secondary antibodies conjugated to oligonucleotide extensions (Tubbs et al., 2014). The principle behind this technique is that when the oligonucleotides are within close proximity to one another they hybridise, allowing their visualisation by subsequent hybridisation of a fluorescently-labelled complimentary oligonucleotide to give a discrete spot of fluorescent signal (Tubbs et al., 2014). This method has the advantage of visualising MAMs without subjecting cells to any potential artefacts of protein overexpression and the signal can be amplified so that even weak interactions can be quantified. However, this technique relies on the specificity of antibody binding and the distance permitting oligonucleotide hybridisation depends on both target protein conformation and size including the bound antibody which could surpass the defined distance of these junction sites (Tubbs et al., 2014). Furthermore, it requires fixation of samples and may be affected by the expression levels of the target proteins.

Dimerization-dependent fluorescent proteins (ddFP) are fluorescent protein variants involving the reversible interaction of two non-fluorescing monomers to form a fluorescent protein complex **(Fig3.1C)**. In one study, monomeric pairs were fused to TOMM20 OMM protein and the ER protein calnexin respectively (Alford et al., 2012). Expression of either fusion protein alone yielded no fluorescent signal but co-expression gave a fluorescent signal that partially colocalised with both the mitochondria and the ER (Alford et al., 2012). This technique has the benefit of being applicable in live-cell imaging, has improved resolution over confocal microscopy and can be adjusted to give new colour variants however, it may be susceptible to artefacts induced by protein overexpression and first generation ddFPs had low brightness and contrast, limiting their value in live-cell imaging (Alford et al., 2012).

An alternative to fluorescent-based methods has been used to quantitatively measure the number of ER-mitochondria contact sites in live-cells using split-*Renilla*

luciferase constructs with each half being targeted to the ER and mitochondria respectively (Lim et al., 2015). When the two halves are in close proximity i.e. at the MAMs the luciferase reporter protein is restored and light is emitted. The advantage of this technique is that the quantification of ER-mitochondria associations can be automated over a large population of cells very rapidly but it does not allow visualisation of the MAMs nor provide any structural information within an individual cell and requires the addition of a substrate to the cell media.

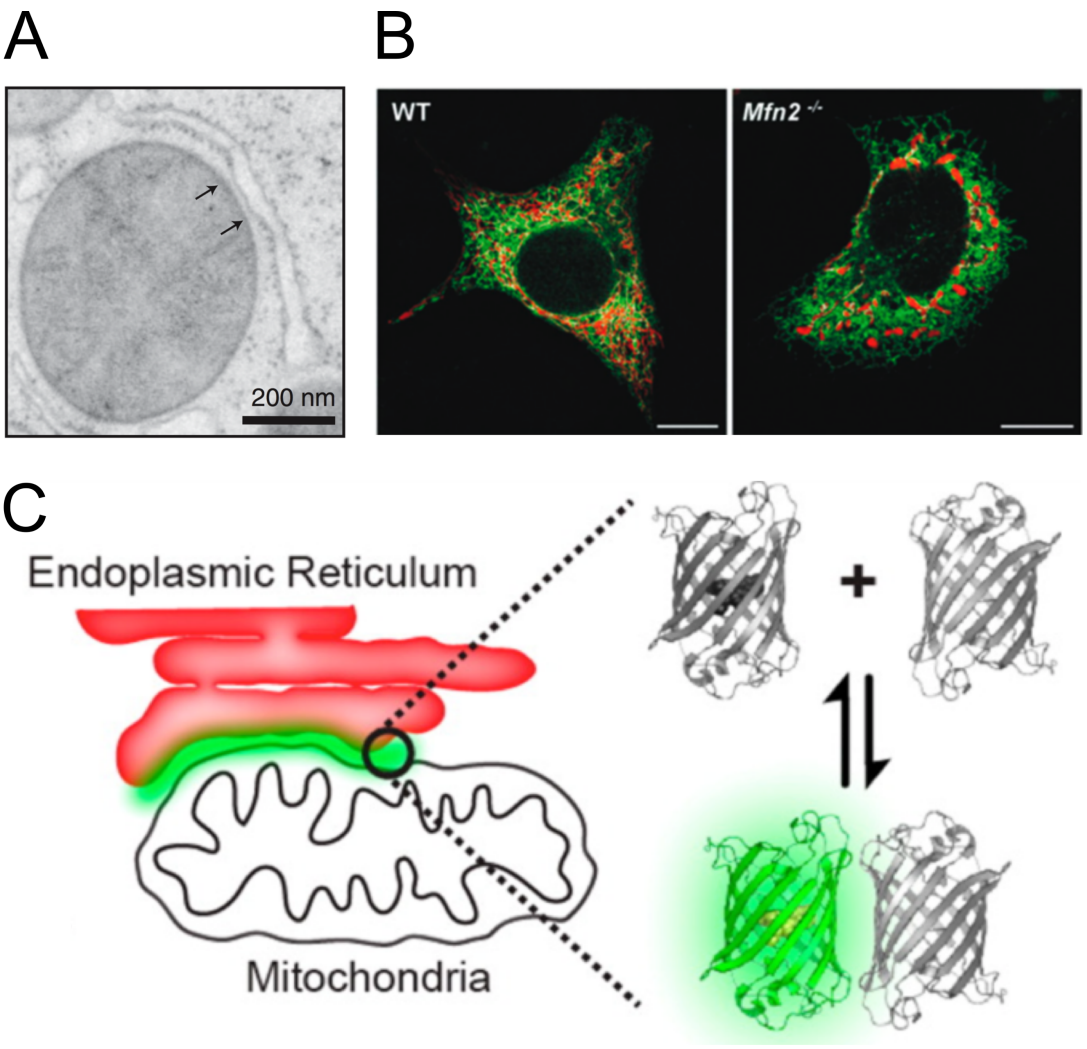

Fig 3.1: Representation of some of the techniques used to quantify MAMs. (A) EM image of MAMs as published in (Sood et al., 2014). **(B)** Co-localisation analysis of fluorescently labelled ER and mitochondria illustrating a reduction in the extent of co-localisation induced by a knock-down of Mfn2 expression as published in (Filadi et al., 2015). **(C)** Schematic representation of the principle of dimerization-dependent fluorescent proteins. The interaction of the non-fluorescing monomers

at the MAMs forms a fluorescent protein dimer. Reprinted with permission from (Alford et al., 2012). Copyright 2012 American Chemical Society.

3.2 Chapter aims

As outlined above, there are a number of currently available techniques to investigate ER-mitochondria contact sites but there are several limitations associated with these methods, particularly in their usefulness in studying contact dynamics in living cells.

Therefore, the initial aim of the thesis was to develop a Bi-Fluorescence Complementation (BiFC) assay based on split fluorescent Venus fragments targeted to the ER and OMM respectively. Venus is a modified version of YFP (Yellow Fluorescent Protein) containing an F46L mutation to enhance its stability (Nagai et al., 2002). The principle of this technique is that neither Venus fragment alone will fluoresce but when brought within close proximity to one another such as at the MAMs, it will result in the restoration of the reporter protein and the emission of a fluorescent signal **(Fig 3.2)**. This will allow for the visualisation and quantification of close ER-mitochondria associations that could be used in both fixed and living-cells. After development of the technique, the aim was to validate its effectiveness by attempting to replicate known changes in ER-mitochondria contacts as previously observed with high-resolution EM studies.

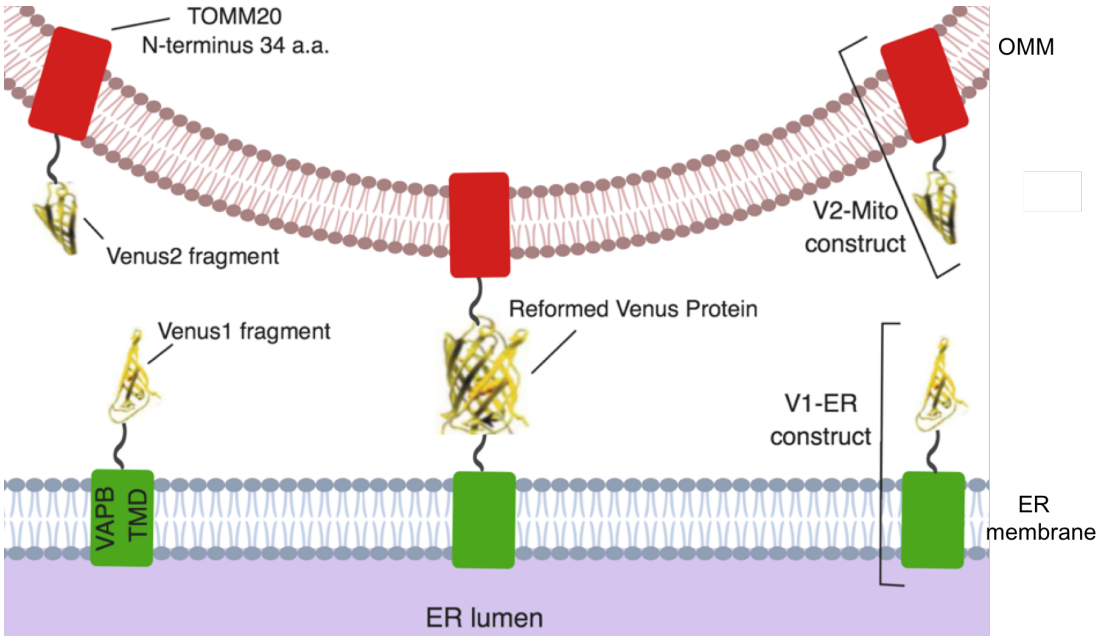

Fig 3.2: Schematic illustration of the principle of the bi-fluorescence complementation (BiFC) assay. Split venus fragments are targeted to the ER and outer mitochondrial membrane respectively. When these fragments are brought within close proximity it results in the reformation of the fluorescent Venus protein and the emission of a detectable fluorescent signal. Illustration was produced on BioRender [Available at https://app.biorender.io].

3.3 Results

3.3.1 Venus reporter fusion proteins are correctly targeted to the ER and mitochondria.

To allow the BiFC system to report on membrane contact sites between the ER and mitochondria, the Venus1 and Venus2 fragments were targeted separately to these organelles. Previous work in the Skehel lab targeted the N-terminal Venus1 fragment to the cytoplasmic face of the ER membrane by fusion to the either the full-length sequence or just the ER-targeting C-terminal 25 amino acids of mouse VAPB, containing the GxxxG dimerization motif, to produce V1-VAPB (Gkogkas et al., 2008) and V1-ER (Harmon et al., 2017) reporter plasmids respectively. The C-terminal Venus2 fragment was fused to the first 34 amino acids of TOMM20 in order to target it to the OMM, generating the V2-Mito plasmid. Alternating between the use of the

smaller V1-ER fusion protein or the larger V1-VAPB protein in conjunction with the complementary V2-Mito fragment means that ER-mitochondria junctions of different sizes can be reported on. The correct localisation of the Venus reporter proteins to the ER and mitochondria was confirmed by immunofluorescent staining with a polyclonal anti-GFP antibody that recognises both fragments of the Venus protein, in the mouse motor neuron-like cell line, NSC34 **(Fig 3.3)**. Co-localisation of the anti-GFP signal with a fluorescent ER-DsRed2 and anti-ATPB mitochondrial marker was quantified by Pearson's Correlation Coefficient (PCC) **(Table 3.1)**. V1-VAPB and V1-ER showed a high level of co-localisation with the ER marker but not with the mitochondrial protein ATPB. In contrast, V2-Mito co-localised with the mitochondrial protein but had a very low level of co-localisation with the ER. The results indicate that the Venus reporter proteins are correctly targeted to the appropriate organelles.

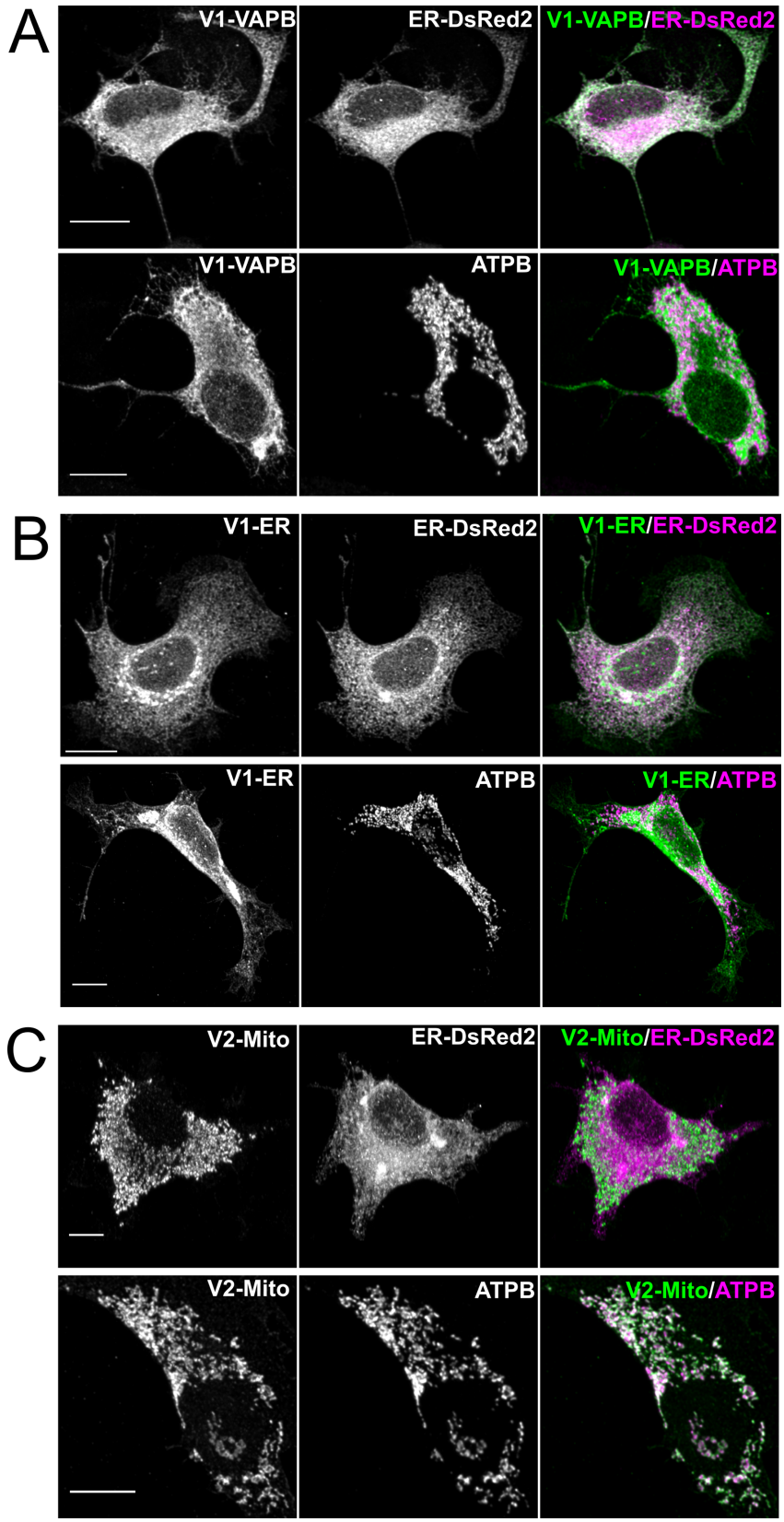

Fig 3.3: The split Venus fusion proteins are correctly targeted to the ER and mitochondria respectively. NSC34 cells transiently transfected with **(A)** V1-VAPB, **(B)**

V1-ER, or **(C)** V2-Mito, were probed with a polyclonal anti-GFP antibody which recognises both Venus fragments. The ER was labelled by co-transfection of an ER-DsRed2 plasmid and mitochondria were labelled by immunofluorescent staining with an anti-ATPB antibody. Co-localisation of the Venus proteins with the organelle markers were analysed by Pearson's Correlation Coefficient (PCC) **(Table 3.1)**. n = 3 independent experiments (9-10 cells total). Scale bars, 10 μm. As published in (Harmon et al., 2017).

Table 3.1: Fluorescent signal co-localisation of Venus probes and organelle markers quantified by PCC. Values indicate mean PCC ± SEM for the co-localisation of the indicated fluorescent labels. n = 3 independent experiments (9-10 cells per experimental group).

Fluorescent labels	PCC
V1-VAPB / ER-DsRed2	**0.876 ± 0.009**
V1-VAPB / ATPB	**0.035 ± 0.010**
V1-ER / ER-DsRed2	**0.870 ± 0.017**
V1-ER / ATPB	**0.070 ± 0.020**
V2-Mito / ER-DsRed2	**0.050 ± 0.011**
V2-Mito / ATPB	**0.910 ± 0.008**

3.3.2 Co-expression of complementary Venus reporter fusion proteins generates detectable BiFC signals consistent with a MAM localisation

Expression of either Venus fragment alone in NSC34 cells yields no detectable fluorescent signal but when co-expressed, the Venus fusion proteins readily produce a pattern of fluorescent signal that varies greatly depending on the combination of the Venus fusion protein used **(Fig3.4)**. This result indicates that any fluorescent signal obtained solely represents sites of reformed Venus reporter proteins. Co-expression of V1-VAPB and V2-Mito yields a fluorescent signal that surrounds a large proportion of the surface area of almost all mitochondria of the cell **(Fig 3.5A).** In contrast, when V1-ER and V2-Mito are co-transfected, it generates discrete fluorescent puncta that are closely associated with a subset of mitochondria. These

BiFC puncta are restricted to the sites of close apposition of the ER and mitochondria as shown by immunostaining for ERp72 and ATPB and therefore, are consistent with a MAM localisation **(Fig 3.5B).**

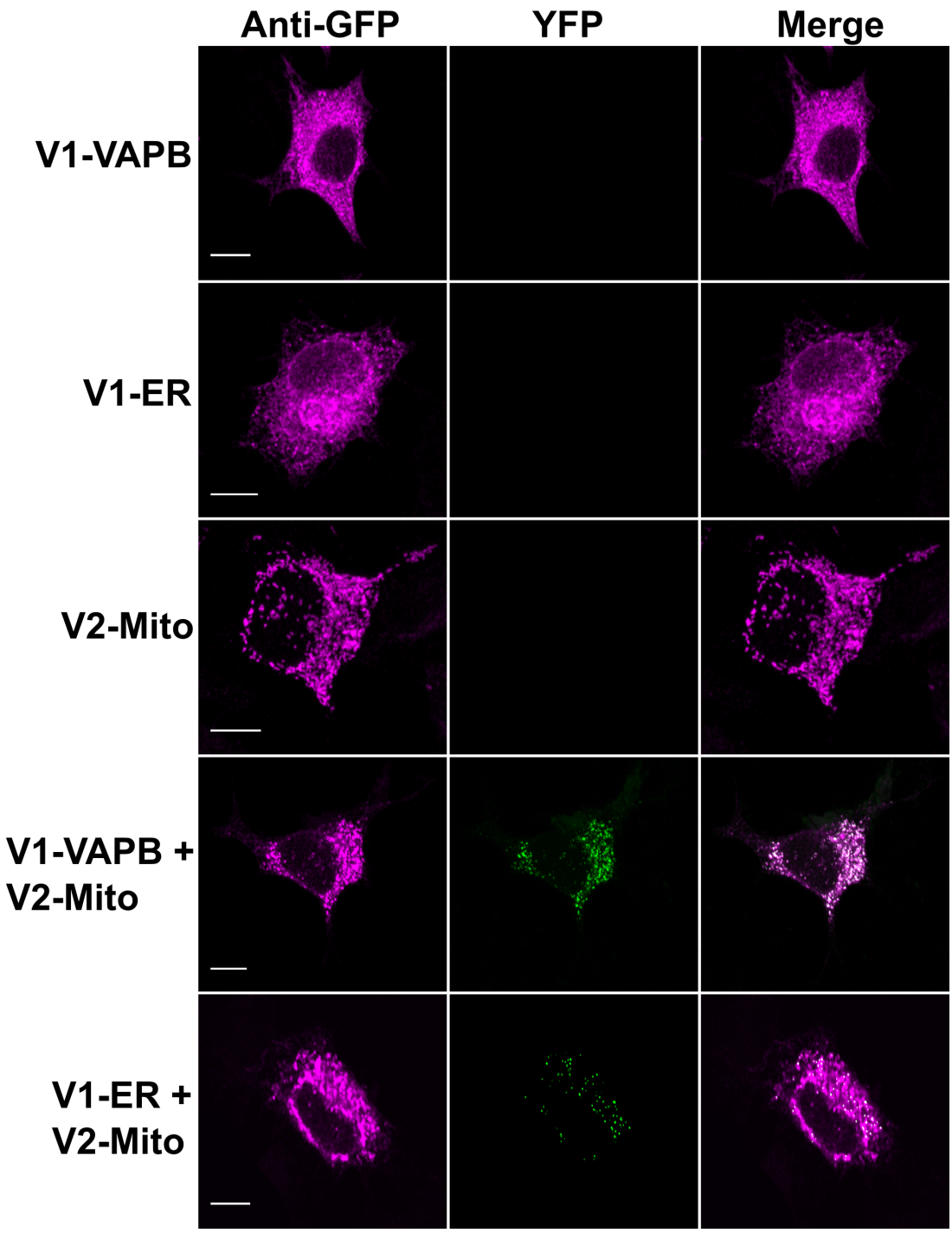

Fig 3.4: Co-expression of complementary Venus reporter fusion proteins yields a detectable fluorescent signal. Co-transfection of V1-VAPB/V2-Mito or V1-ER/V2-Mito produces readily detectable fluorescent signal whereas transfection of either

plasmid alone yields no detectable signal. Expression of the Venus proteins was confirmed by immunostaining with an anti-GFP antibody that can detect both Venus fragments. As published in (Harmon et al., 2017).

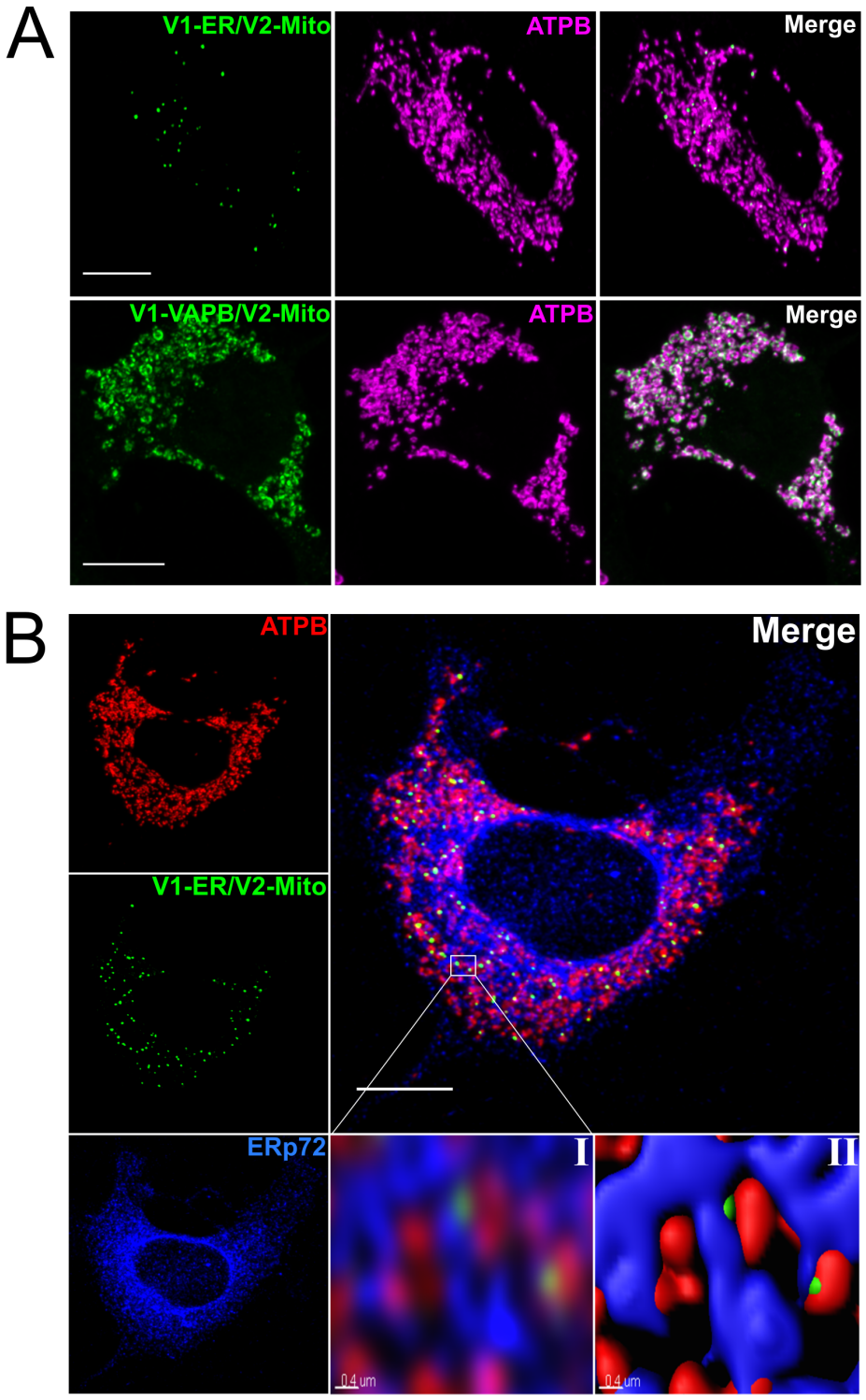

Fig 3.5: Co-expression of complementary V1-VAPB or V1-ER with V2-mito in NSC34 cells generates distinct patterns of BiFC signal depending on the V1-fusion protein used. (A) Representative images of NSC34 cells transfected with V1-ER/V2-Mito (Top row) or V1-VAPB/V2-Mito (Bottom row). BiFC signal is associated with the mitochondria as indicated by ATPB labelling. **(B)** Labelling of the ER (anti-ERp72, *blue*)

and mitochondria (anti-ATPB, *red*) illustrate that BiFC puncta occur at regions of overlap of ER and mitochondria signal. **(B.I)** Higher magnification of boxed region from merged panel. **(B.II)** 3D volume rendering of magnified region using Imaris image analysis software. Scale bars 10 μm, or 0.4 μm in panels B.I and B.II. As published in (Harmon et al., 2017).

For the experiments presented in the rest of this chapter, the shorter V1-ER reporter protein in combination with V2-Mito was used due to the discrete punctate pattern of fluorescence obtained and to avoid any potential artefacts of VAPB overexpression. The BiFC puncta observed upon co-expression of these Venus fusion proteins was not unique to NSC34 cell lines and was also observed in the primate COS-7 and human HEK293 cell lines **(Fig3.6)**. No gross changes to organelle morphology were observed in any of the cell lines tested.

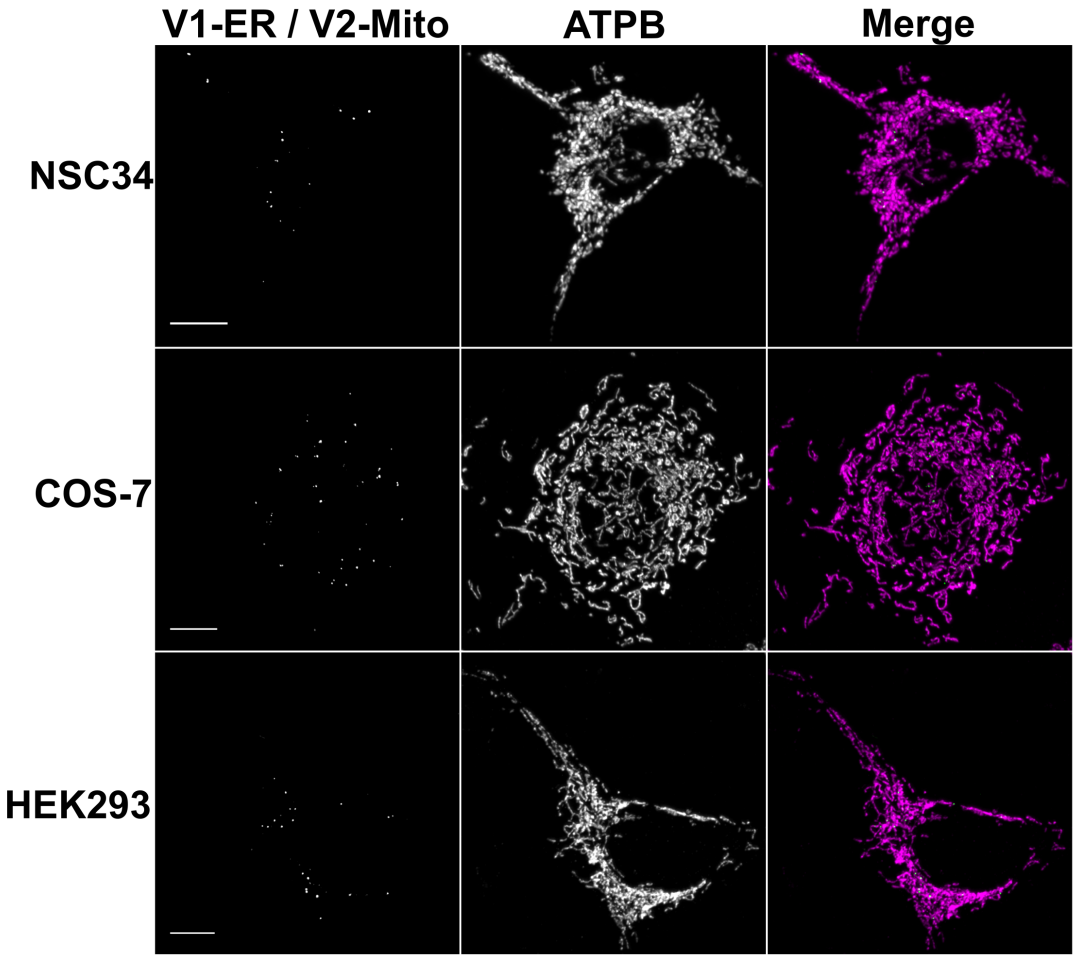

Fig 3.6: The pattern of BiFC signal is comparable between different cell types. Co-expression of V1-ER/V2-Mito generates a similar pattern of discrete BiFC puncta closely associated with a subset of mitochondria (as labelled by anti-ATPB) in mouse NSC34 cells, primate COS-7 cells and human HEK293 cells. As published in (Harmon et al., 2017).

3.3.3 Increasing levels of Venus reporter proteins does not alter the pattern or number of BiFC puncta

One of the concerns associated with this technique is that the expression of V1-ER and V2-Mito may artificially induce or tighten ER-mitochondria contact sites. If this was the case, we hypothesised that increasing the relative protein levels of V1-ER and V2-Mito may increase the mean number of BiFC puncta per cell or alter the pattern of fluorescent signal. Differing total DNA concentrations of V1-ER and V2-

Mito in a 1:1 ratio were transfected in NSC34 cells and the mean number of BiFC puncta per cell (each being taken to represent one ER-mitochondria contact site) was quantified **(Fig3.7A).** The fluorescent Venus signal always appeared as discrete puncta associated with a subset of mitochondria regardless of the concentration of DNA transfected. No significant difference was detected between any of the experimental groups. An equivalent increase in protein levels resulting from increased concentrations of DNA was determined by anti-GFP immunostaining **(Fig3.7B)**. For subsequent experiments, a concentration of 1 µg total DNA was transfected. As will be seen in **section 3.3.6** below, the Venus reporter signal increases in response to chemical and stress-induced changes to the cell, indicating that expression of the Venus reporter plasmids alone at this concentration does not saturate the number of ER-mitochondria contact sites formed in the cell.

Furthermore, we generated an NSC34 cell line stably expressing V1-ER and V2-Mito plasmids and long-term expression of the Venus fusion proteins did not alter the discrete fluorescent puncta pattern as observed in transiently transfected cells (data not shown). Combined, these results show that increasing protein levels or time of expression does not alter the BiFC signal and therefore, suggests that expression of V1-ER and V2-Mito is not artificially inducing contacts but rather, is labelling pre-existing sites of close apposition between the ER and mitochondria.

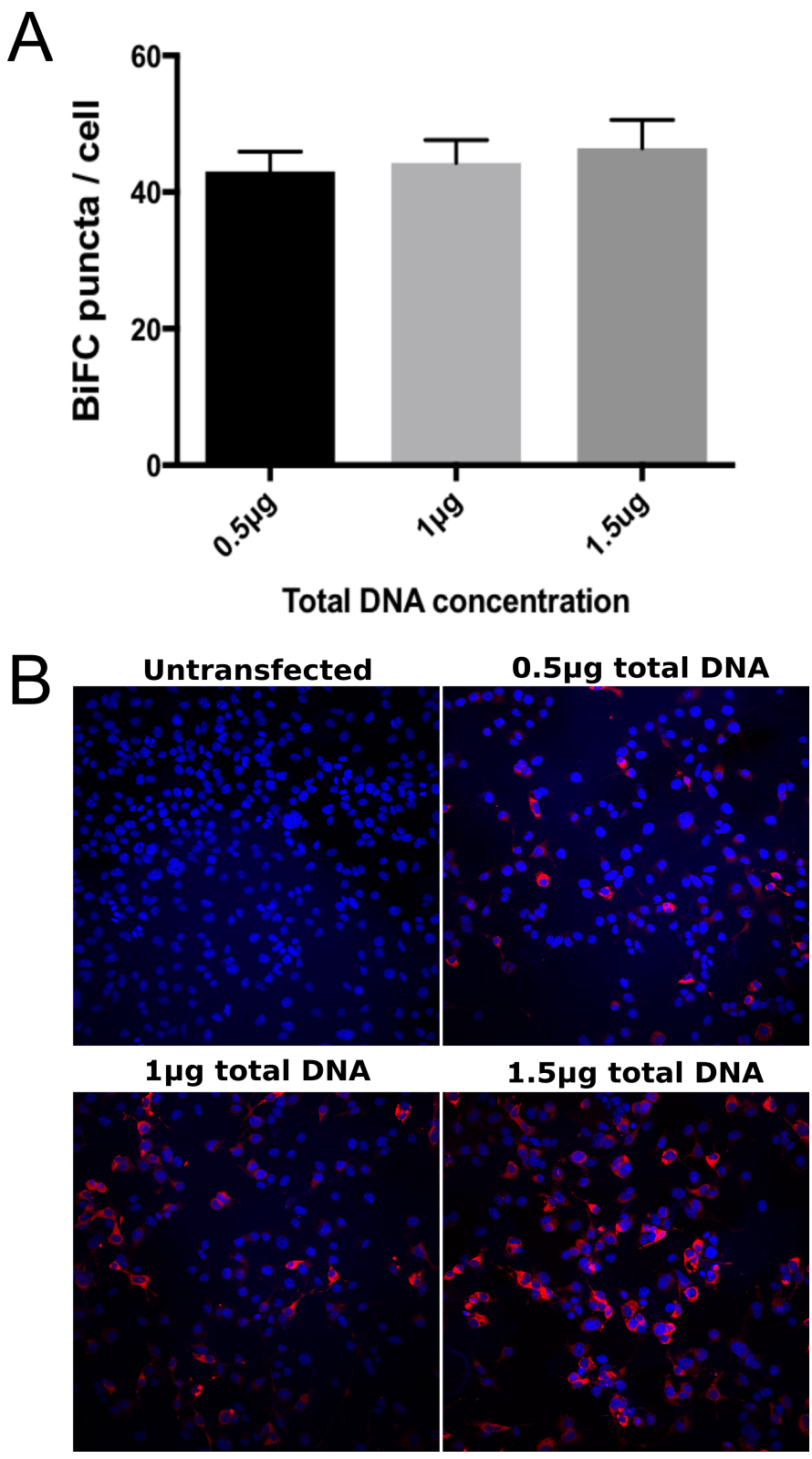

Fig 3.7: Increasing the concentration of Venus reporter proteins does not influence the number of BiFC puncta per cell. (A) NSC34 cells were transfected with 0.5 µg, 1

μg or 1.5 μg total DNA concentration at a 1:1 ratio of V1-ER: V2-Mito and imaged by confocal microscopy. The mean number of BiFC puncta per cell was quantified. Statistical significance was determined by one-way Anova followed by Holm-Sidak's multiple comparison test. Values indicate the mean number of BiFC puncta per cell. n = 3 independent experiments (23-27 cells total). Error bars represent SEM. **(B)** An equivalent increase in protein levels produced from increased concentrations of DNA transfected was shown using anti-GFP immunostaining (*red*) to illustrate an increase in the number of cells showing detectable fluorescence. Cell nuclei were labelled with DAPI (*blue*). Images were acquired by confocal microscopy with a 20x objective using identical acquisition settings per experimental group. As published in (Harmon et al., 2017).

3.3.4 BiFC puncta are highly associated with the ER and mitochondria but not with other organelles of the cell

The reformation of the Venus reporter proteins only depends on spatial proximity and therefore, it is possible that a positive fluorescent signal could be observed at other sites where these proteins may be in close apposition. To investigate this, the percentage of BiFC puncta with a point of co-localisation to various organelle markers was quantified **(Fig3.8, Table 3.2)**. The vast majority of the Venus signal was associated with ER and mitochondria markers with very few puncta co-localising with EEA1 positive endosomes, the Golgi apparatus or the nucleus. Due to the diffraction limit of confocal microscopy, BiFC puncta would score positive for co-localisation if they are within approximately 200 nm of the organelle marker.

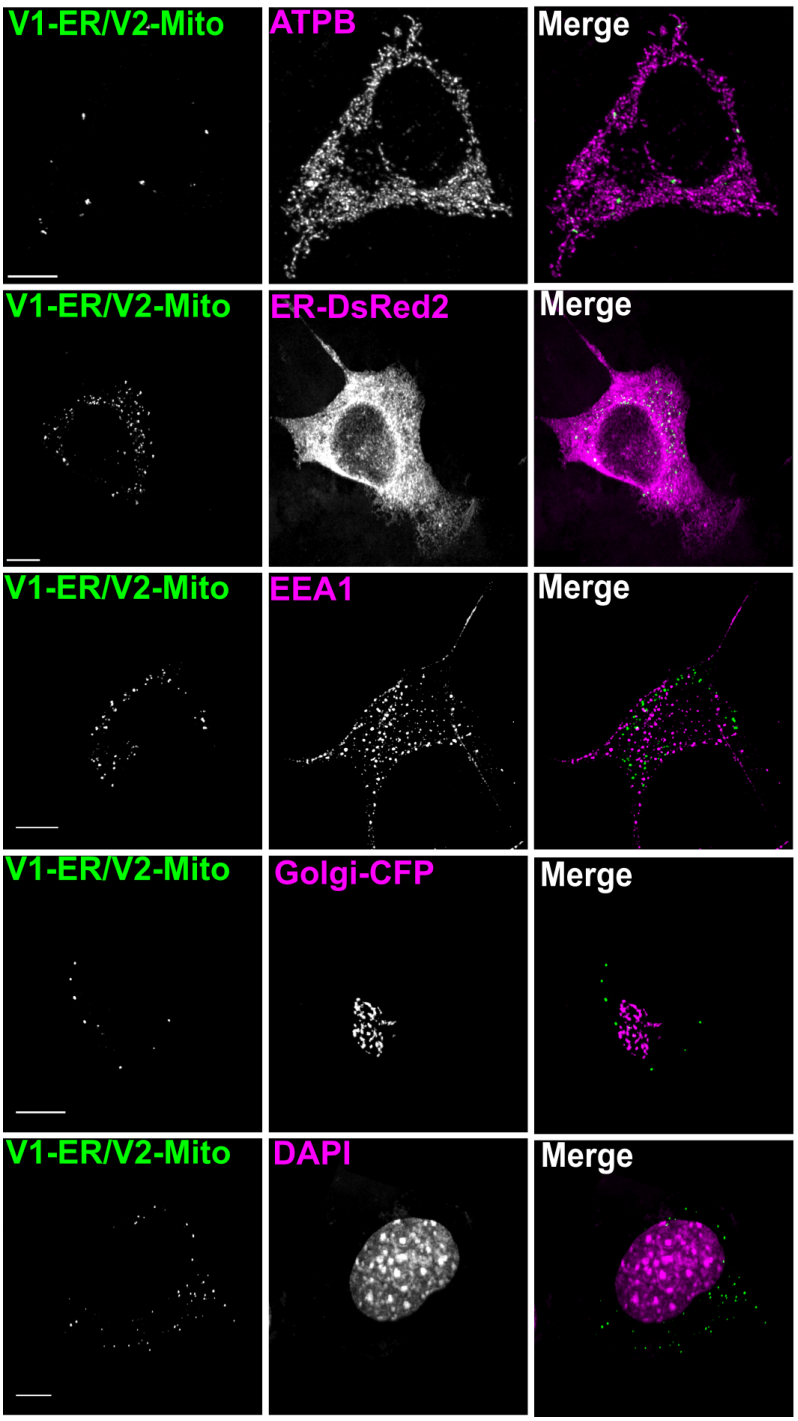

Fig 3.8: BiFC puncta are highly associated with the ER and mitochondria and not with other organelles of the cell. Representative images of NSC34 cells transiently expressing V1-ER/V2-Mito plasmids with various organelle markers. The ER and Golgi were labelled by co-transfection of ER-DsRed2 and Golgi-CFP expression plasmids respectively (Clontech). Early endosomes and mitochondria were labelled by immunostaining with anti-EEA1 (endosomes) or anti-ATPB (mitochondria). The cell nucleus was labelled with DAPI. Imaris image analysis software was used to

quantify the total number of BiFC overlapping with the corresponding fluorescent organelle signal as detailed in **chapter 2, section 2.9.3**. Scale bars, 10 μm. n = 3 independent experiments (10-15 cells per experimental group). As published in (Harmon et al., 2017).

Table 3.2. Quantification of number of BiFC puncta overlapping with corresponding fluorescent organelle marker. Values indicate % BiFC puncta overlapping with the specific organelle marker ± SEM. n = 3 independent experiments (10-15 cells per experimental group).

Protein/organelle labelled	% BiFC puncta co-localised with organelle marker
ATPB (Mitochondria)	**97.07 ± 1.34**
ER-DsRed2 (ER)	99.07 ± 0.27
EEA1 (Endosomes)	10.74 ± 2.36
Golgi-CFP (Golgi Apparatus)	8.95 ± 3.47
DAPI (Nucleus)	6.81 ± 0.57

3.3.5 Super-resolution STED microscopy indicates that the BiFC puncta are continuous structures

Although the BiFC puncta appeared as discrete structures, due to the diffraction limitations of confocal microscopy, it could not be ruled out that these structures could be composed of close, unresolvable objects. To investigate this, NSC34 cells expressing V1-ER and V2-Mito reporter plasmids were imaged by super-resolution stimulated emission depletion (STED) microscopy that is capable of imaging structures below the diffraction limit of conventional light microscopy. Puncta imaged with the STED laser had improved resolution and were heterogeneous in shape **(Fig3.9A)**, however they remained as discrete, singular structures for the most part and therefore it was concluded that diffraction limited scanning laser confocal microscopy was sufficient for quantifying the number of BiFC puncta within a cell. Measuring the size of these objects revealed that puncta ranged between approximately 100-700 nm in length with a mean diameter of 310 nm **(Fig3.9B).**

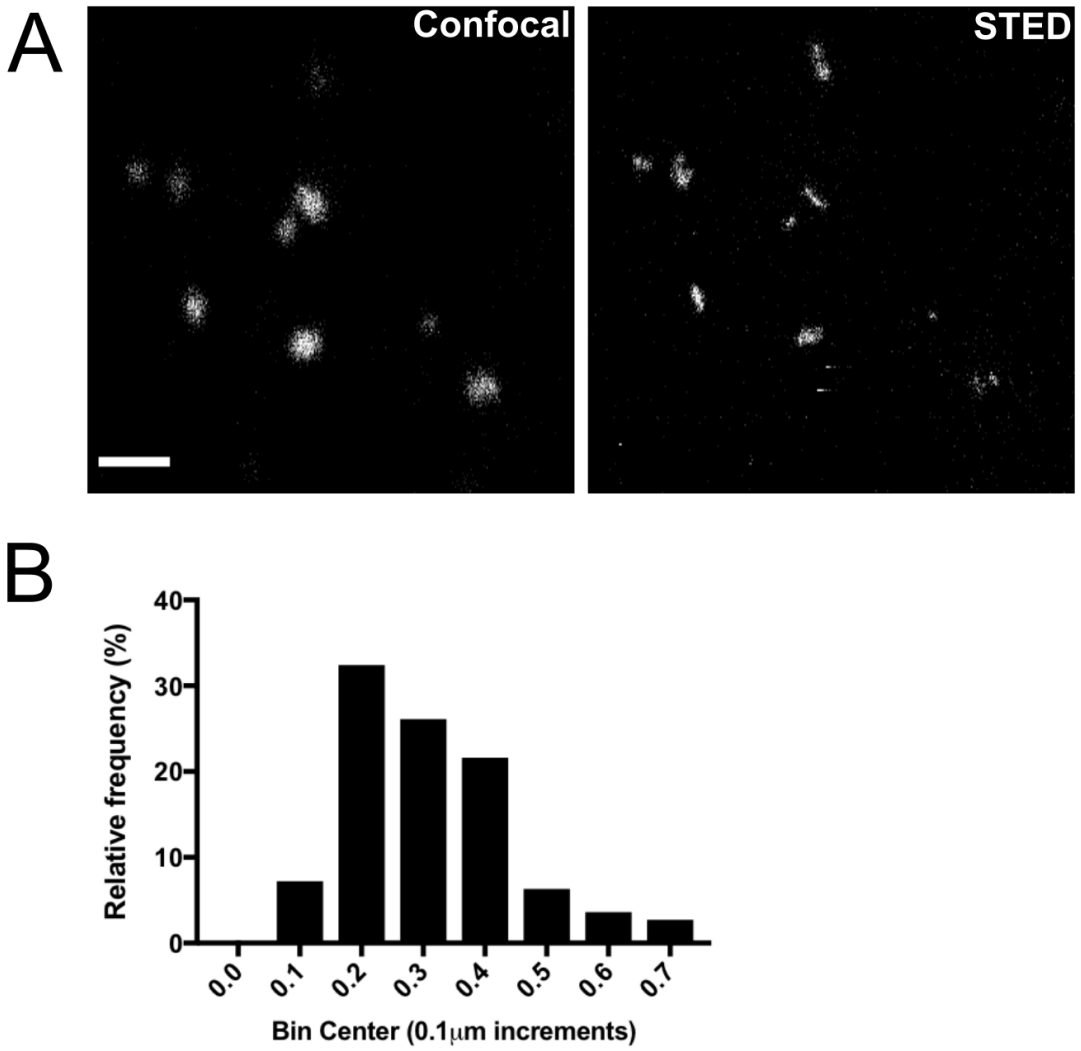

Fig 3.9: Super-resolution STED microscopy illustrates that BiFC puncta are discrete singular objects. (A) Representative image of an NSC34 cell transiently expressing the Venus reporter proteins imaged with a confocal versus STED microscope. Scale bar, 1 µm. **(B)** Frequency distribution graph illustrating the relative frequency of BiFC puncta size with bin centres in 0.1 µm increments. Puncta were measured using the "straight line" tool on ImageJ across the widest point of each individual punctum. n = 111 BiFC puncta (7 cells total). Mean value = 0.31 µm. As published in (Harmon et al., 2017).

3.3.6 ER stress and serum deprivation significantly increases the mean number of BiFC puncta per cell

ER-mitochondria contacts are dynamic in nature and have been shown to change in response to certain stress conditions (Bravo et al., 2011; Csordas et al., 2006). In order to validate the BiFC method and test if it was sensitive to stress-induced changes, NSC34 and COS-7 cells were transfected with the Venus reporter plasmids and treated for 6 hours with 2 µg or 10 µg tunicamycin, an inhibitor of N-linked glycosylation that consequently induces an ER stress response and G1 cell cycle arrest (Han et al.) **(Fig3.10A)**. As the previous super-resolution STED microscopy data illustrated that the BiFC puncta are discrete, singular objects, the mean number of BiFC puncta per cell was quantified such that each individual fluorescent spot was taken to represent one site of ER-mitochondria contact. The induction of ER stress at both concentrations of tunicamycin significantly increased the mean number of BiFC puncta per cell in comparison to DMSO treated controls **(Fig3.10B)**. An increase in the total volume of Venus signal as a percentage of total mitochondrial volume in both cell types was also observed, demonstrating that the increased numbers of fluorescent puncta were not due to an increase in mitochondrial network **(Fig3.10C).** The induction of ER stress was confirmed by detection of spliced XBP1 mRNA and it is noteworthy that transfection of the V1-ER and V2-Mito plasmids alone did not induce any ER stress on the cell **(Fig3.10D)**.

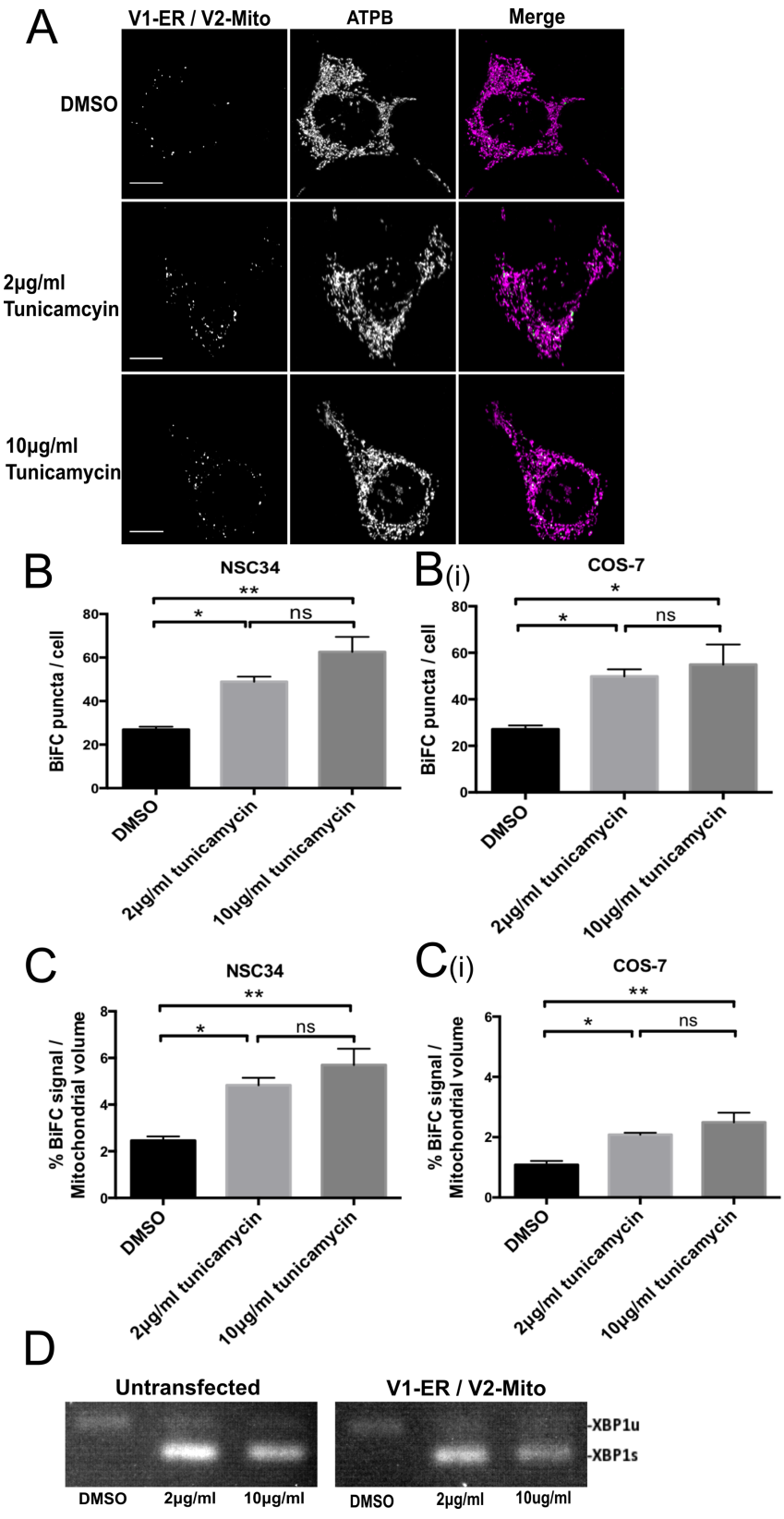

Fig 3.10: ER stress significantly increases the mean number of ER-mitochondria contacts per cell. (A) Representative images of NSC34 cells transfected with V1-

ER/V2-Mito plasmids treated with DMSO, 2 µg/ml or 10 µg/ml tunicamycin. The induction of ER stress significantly increases the mean number of BiFC puncta per cell in **(B)** NSC34 and **(B_i)** COS-7 cells and **(C)** significantly increases the total volume of BiFC signal as a percentage of total mitochondria volume in all cell types. n = 3 independent experiments (32-34 cells for NSC34, 29-32 cells for COS-7). Values indicate overall mean values from the three independent experiments. Error bars indicate SEM. Statistical significance was measured using one-way ANOVA followed by Holm-Sidak's mutiple comparison test, ns (non-significant), *p < 0.05, **p < 0.01. **(D)** ER stress was confirmed by the detection of spliced Xbp1 mRNA in NSC34 cells by gel electrophoresis and under UV light. Scale bars, 10 µm. Image adapted from (Harmon et al., 2017).

Previous studies also showed that the extent of interaction between the ER and mitochondria varies in response to serum deprivation (Csordas et al., 2006). To further test the validity of our approach, we also investigated a change in the number of BiFC puncta in cells grown in serum-free media for 24 hours. Mirroring the effect seen with ER stress induction, the mean number of BiFC puncta per cell, as well as the total volume of Venus signal as a percentage of total mitochondrial volume, significantly increased in comparison to cells grown in media supplemented with 10% (v/v) foetal bovine serum **(Fig3.11)**. These changes were in agreement with previously published studies (Csordas et al., 2006).

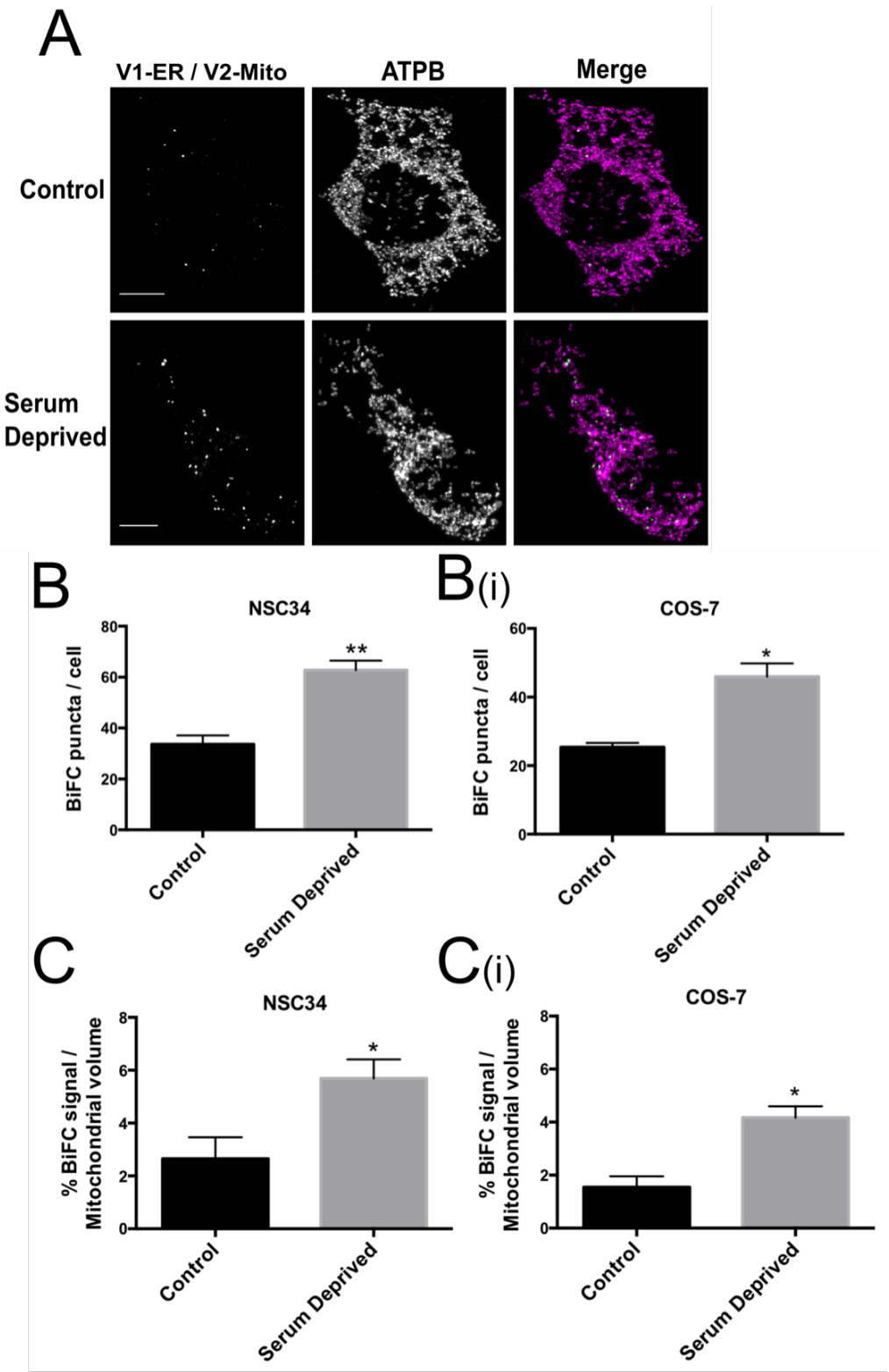

Fig 3.11: Serum deprivation increases the number of ER-mitochondria contacts per cell. (A) Representative images of NSC34 cells transfected with V1-ER/V2-Mito reporter plasmids grown in DMEM supplemented with 10% (v/v) FBS or in serum-free DMEM for 24 hours post-transfection. Serum deprivation significantly increases

the mean number of BiFC puncta in **(B)** NSC34 cells and **(B_i)** COS-7 cells and **(C)** significantly increases the total volume of BiFC signal as a percentage of total mitochondrial volume in both cell types. n = 3 independent experiments (36-37 cells for NSC34, 32-35 cells for COS-7). Values indicate overall mean values from 3 independent experiments. Error bars represent SEM. Statistical significance was measured using unpaired two-tailed t-test, *p<0.05, **p<0.01. Scale bars, 10 µm. Image adapted from (Harmon et al., 2017).

In order to test the strength of the BiFC technique in comparison to one of the existing methods for detecting ER-mitochondria associations, we exposed cells with fluorescently labelled ER and mitochondria to the same stress conditions tested above. In this method, any changes in overall co-localisation between the ER and mitochondria signals is indicative of an increase or decrease in ER-mitochondria contacts. In cells treated with tunicamycin there was a significant increase in the extent of co-localisation between the ER and mitochondria signals in agreement with the change observed with the BiFC technique **(Fig3.12A)**. However, using this method, no significant change in co-localisation was detected in serum deprived cells **(Fig3.12B)**. This suggests that the BiFC method is capable of detecting changes, also observed with high resolution EM techniques (Csordas et al., 2006), that simple co-localisation analyses may not be sensitive enough to detect.

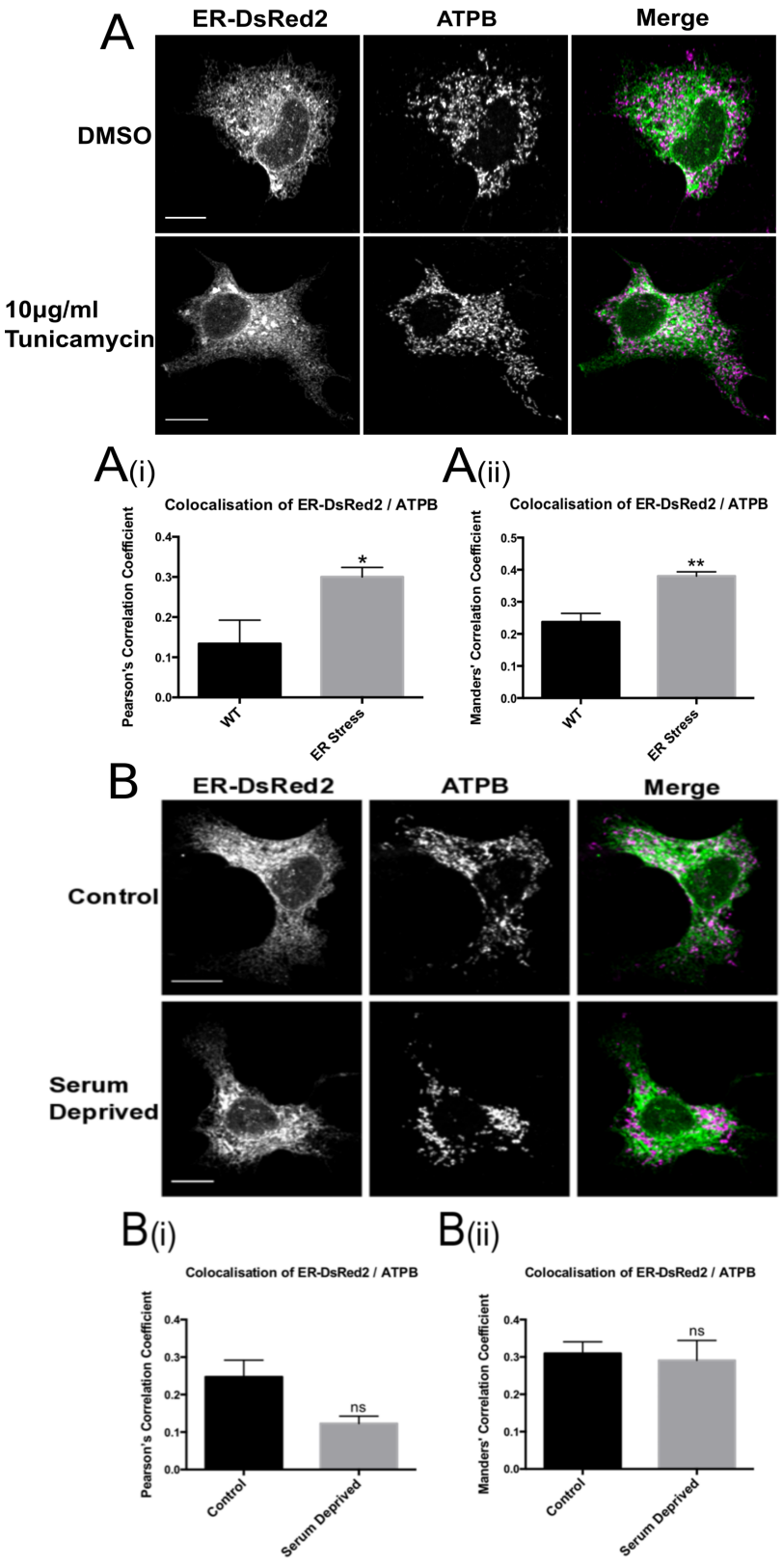

Fig 3.12: Colocalisation analysis of fluorescently labelled ER and mitochondria shows an increase in ER-mitochondria contacts in cells treated with tunicamycin

but not in serum-deprived NSC34 cells. (A) Representative image of NSC34 cells transfected with ER-DsRed2 (Green) and immunostained with anti-ATPB (Magenta) to label the ER and mitochondria respectively, treated with DMSO or 10 µg/ml tunicamycin. Co-localisation of ER and mitochondria signals was quantified by **($A_{(i)}$)** Pearon's Correlation Coefficient (PCC) and **($A_{(ii)}$)** Mander's Correlation Coefficient (MCC). n = 4 independent experiments (26 cells total). **(B)** Co-localisation of ER and mitochondria signals was also quantified in control NSC34 cells versus serum deprived cells showing no significant change in co-localisation as measured by either **($B_{(i)}$)** PCC or **($B_{(ii)}$)** MCC. n = 3 independent experiments (19 cells total). Values indicate the overall mean co-localisation values. Statistical significance was measured using unpaired two-tailed t-test, ns (non-significant), *p<0.05, **p<0.01. Error bars represent SEM. Scale bars, 10 µm. Image adapted from (Harmon et al., 2017).

3.3.7 siRNA knockdown of Mitofusin-2 expression increases ER-mitochondria interactions.

Mitofusin-2 (MFN2) is a well-studied tether of ER-mitochondria contacts, forming homo- and heterodimers with MFN1 on the outer mitochondrial membrane (de Brito and Scorrano, 2008). However, the exact role of this protein in regulating associations is controversial. Early reports using fluorescence co-localisation analyses reported that MFN2 is a positive regulator of ER-mitochondria contact sites with an overexpression of the protein leading to an increase in associations while knocking-down expression reduced the number of contacts (de Brito and Scorrano, 2008). Subsequent studies however, suggested that MFN2 may exhibit a negative regulation over organelle junctions and knocking-down of MFN2 actually increases the number of contacts as shown by EM (Leal et al., 2016; Filadi et al., 2015). It has been suggested that these discrepancies in observations may be due to the sensitivity of the fluorescence co-localisation method to changes in organelle morphology (Filadi et al., 2015).

Here, our BiFC method was used to investigate any changes in ER-mitochondria contacts brought upon by siRNA mediated silencing of MFN2 expression in NSC34

cells stably expressing the V1-ER/V2-Mito reporter plasmids. A significant increase in the number of BiFC puncta resulting from an approximately 80% reduction in MFN2 protein levels was observed (Fig 3.13). This increase in contacts is in agreement with the previously published EM studies, suggesting that MFN2 may be a negative regulator of ER-mitochondria contacts (Leal et al., 2016; Filadi et al., 2015).

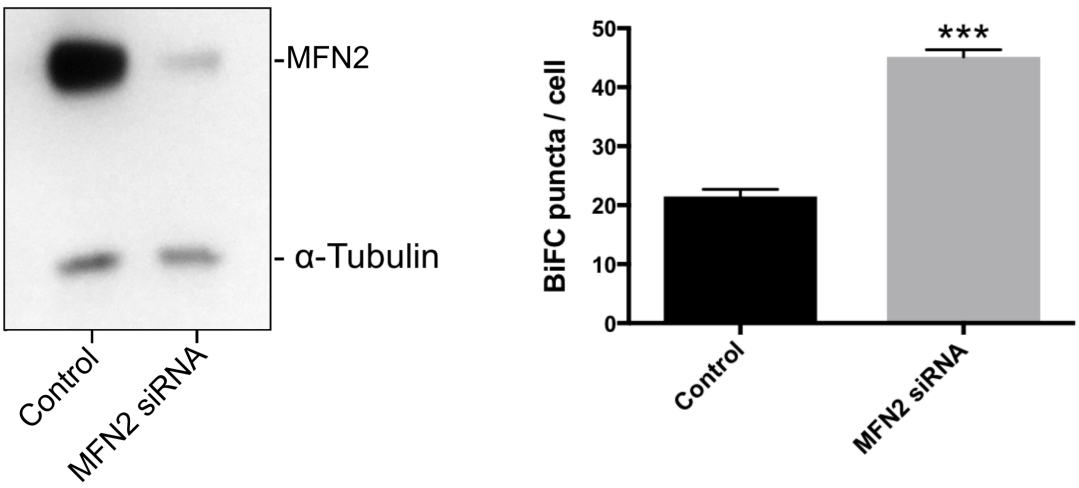

Fig 3.13: Silencing of MFN2 expression significantly increases the number of ER-mitochondria contacts. Transfection of siRNA against MFN2 reduced relative protein levels to approximately 20% in NSC34 cells stably expressing V1-ER/V2-Mito as confirmed by western blot. α-Tubulin was used as a loading control. Knock-down of expression was associated with a significant increase in the mean number of ER-mitochondria contacts per cell. n = 3 independent experiments (30-32 cells total). Values indicate the overall mean values of the three independent experiments. Error bars represent SEM. Statistical significance was determined by unpaired two-tailed t-test, ***p<0.001. Image as published in (Harmon et al., 2017).

3.3.8 The BiFC technique can be adapted to report on ER-endosome contact sites

As the BiFC technique only relies on spatial proximity of the complementary fragments, easy adaptations can be made by varying the targeting sequences of the Venus fusion reporter proteins to label different organelle contact sites. Previous work in the Skehel lab, carried out by Ms. Emma Lund, generated Venus-2 fragments fused to the full-length endosomal protein VAMP4 sequence (V2-VAMP4) or just to the C-terminal endosomal targeting sequence (V2-VAMP4-CT) as outlined in chapter 2. It was hypothesised that transfecting V2-VAMP or V2-VAMP4-CT in combination with the V1-ER plasmid would label sites of close apposition between the ER and endosomes. Co-expression of V1-ER with the shorter length V2-VAMP4-CT plasmid generated discrete fluorescent puncta that was reminiscent of the pattern of fluorescence seen with the V1-ER/V2-Mito combination **(Fig3.14)**. However, when V1-ER was co-expressed with the full-length V2-VAMP4 reporter protein, a typical cell had large fluorescent aggregates that were mostly localised around the nucleus, with only relatively few fluorescent puncta dispersed throughout the periphery of the cell **(Fig3.14)**. The larger length V2-VAMP4 protein could be artificially inducing contacts and may be detrimental to the cell or the presence of the aggregates could indicate a defect in vesicular trafficking. These results mirror those obtained by Ms. Emma Lund in the Skehel lab who illustrated that the presence of the full-length V1-VAPB plasmid in combination with either the full length V2-VAMP4 or V2-VAMP4-CT also led to the appearance of large fluorescent aggregates. The difference in the fluorescent signal detected may be due to the length of the reporter proteins used or by an effect of VAMP4 overexpression (Unpublished data, data not shown).

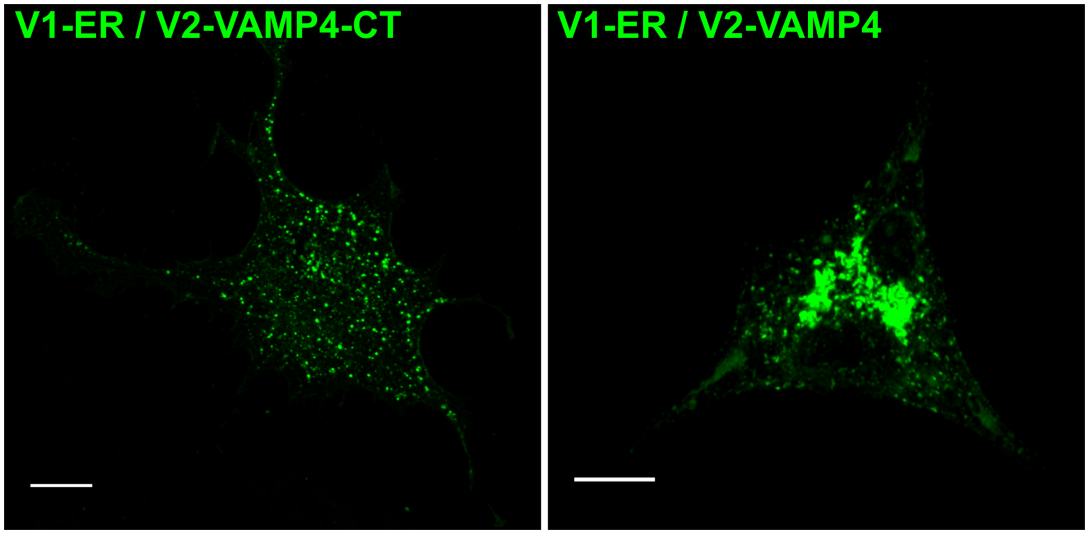

Fig 3.14: Co-expression of V1-ER and V2-VAMP4-CT yields discrete fluorescent puncta. Representative images of an NSC34 cell transfected with V1-ER / V2-VAMP4-CT showing distinct fluorescent puncta dispersed throughout the cell or an NSC34 cell transfected with V1-ER and the larger V2-VAMP4 showing the presence of large fluorescent aggregates surrounding the nucleus.

3.4 Discussion

3.4.1 V1-VAPB and V1-ER differentially label ER-mitochondria contact sites

In this chapter, data is presented on the development and validation of the BiFC system for detecting MAMs by targeting split fluorescent Venus fragments to the cytoplasmic face of the ER and the outer mitochondrial membrane (Harmon et al., 2017). The pattern of fluorescence obtained from co-transfection of the complementary Venus fragments varied greatly depending on whether the Venus fragment fused to the full-length VAPB protein (V1-VAPB) or to just the VAPB transmembrane domain (V1-ER) was transfected. Expression of V1-VAPB with V2-Mito generated a fluorescent signal that appeared to be associated with every mitochondrion of the cell and extended around a large proportion of the mitochondrial surface area. This was in stark contrast to the discrete fluorescent punctate signal detected upon co-transfection of the V1-ER/V2-Mito plasmids that was closely associated to only a sub-set of mitochondria in the cell. The differences in fluorescent signal may be due to VAPB overexpression-induced increases in ER-

mitochondria contacts, as has been previously reported (Stoica et al., 2014) or as a result of the longer length of the V1-VAPB reporter protein, allowing for the detection of wider ER-mitochondria junctions. The effects of the lengths of the reporter proteins on the fluorescent signal obtained could be examined by the addition of non-functional linker sequences to the reporter proteins which may allow for the adaptation of the BiFC system to detect ER-mitochondria junctions of different lengths.

A recent study, published at the same time as our BiFC method, also used a split-GFP based technique to detect ER-mitochondria contact sites (Cieri et al., 2018). Similar to what we observe upon co-transfection of V1-ER and V2-Mito, this group detect discrete fluorescent puncta associated with a subset of mitochondria with their reporter constructs. Furthermore, using this approach, they too could quantify stress-induced changes to the MAMs, providing supporting evidence for the strength of fluorescence complementation assays in the detection of ER-mitochondria associations. Interestingly, this group used two different reporter proteins that varied in the lengths of the amino acid linker sequences, allowing one construct to detect on close junctions of around 10 nm and the other to reporter on wider contact sites of approximately 40 – 50 nm. This result illustrates how altering the length of the reporter proteins used can indeed detect organelle contact sites of different sizes, independent of any functional consequence of specific protein over-expression (Cieri et al., 2018).

3.4.2 The BiFC technique can recapitulate changes in ER-mitochondria contacts in agreement with high-resolution EM studies

Super-resolution imaging of the BiFC puncta indicated that these contacts are heterogeneous in size, ranging from about 100-700 nm in length. This size range is within the scope of what has previously been quantified by EM data, showing that regions of close apposition between the ER and mitochondria can extend for several hundred nanometres around the surface of the mitochondria (Sood et al., 2014). The fact that the BiFC puncta remain, for the most part, as singular objects even with the

improved resolution of the STED images, justifies our use of confocal microscopy to accurately quantify the total number of BiFC puncta per cell. The relative ease by which the data can be analysed highlights one of the great strengths of the BiFC system for the detection of ER-mitochondria contacts.

To validate the usefulness of the BiFC technique, a significant increase in the number of ER-mitochondria contacts induced by ER stress, serum deprivation and knock-down of Mfn2 was detected, which supported the existing literature (Filadi et al., 2015; Csordas et al., 2006). Of all the techniques used to detect MAMs, EM has by far the highest resolution but is technically challenging and can only be carried out on fixed samples. We have shown here that the BiFC technique can report on the same increases in ER-mitochondria contacts as shown by EM, while having a much higher through-put and the benefit of being able to be used in living cells, allowing investigations into MAM dynamics (explored further in chapter 4). This also highlights the advantage of the BiFC system over the proximity ligation assays that are also limited to fixed samples (Tubbs et al., 2014). The strength of the BiFC in comparison to fluorescent co-localisation analysis is clearly demonstrated in **(Fig 3.12B)** where the sensitivity of the co-localisation analysis was insufficient in detecting serum deprivation induced changes in ER-mitochondria associations. Dimerization-dependent fluorescent proteins (ddFPs), similar to the BiFC method, depend on the association of two protein monomers targeted to separate membranes which improves detection limits and can also be used in live-cell imaging (Alford et al., 2012). However, a potential advantage of the BiFC method over ddFPs is improved signal-to-noise ratio as individual venus fragments emit no fluorescence and this could allow for the detection of weaker reporter signals.

The use of the V1-ER and V2-Mito reporter plasmids effectively allows for the detection of tight ER-mitochondria contacts with a maximum predicted junction size of 10 nm. Csordas *et al* (2006) generated artificial protein tethers to tighten ER-mitochondria contacts which consisted of 46 amino acid residues in addition to a red fluorescent protein, creating a construct of approximately 5 nm in length (Csordas

et al., 2006). In combination, the linker sequences of V1-ER and V2-mito adds 85 amino acids in addition to the Venus protein and therefore, these proteins are likely reporting on distances between the ER and OMM of around 6-10 nm, depending on the exact conformations of the reporter proteins. It has been hypothesised that different size junctions between the ER and mitochondria could be reflective of different protein compositions at these sites where specific functions of the MAMs are carried out [As reviewed by (Giacomello and Pellegrini, 2016). The exact functional significance of tight ER-mitochondria contacts <10 nm is yet to be elucidated.

3.4.3 Limitations of the BiFC technique

One concern that arises from the BiFC system is the potential for the Venus fusion proteins to induce the creation of ER-mitochondria contacts rather than only reporting on pre-existing ones, particularly in light of studies showing that artificial protein tethers can be used to induce ER-mitochondria associations (Csordas et al., 2010; Csordas et al., 2006). However, EM data has shown the presence of very tight contacts >6 nm in wild-type, untreated RBL-2H3 cells illustrating that contact sites of this range are not solely an artefact of the BiFC system (Csordas et al., 2006). Furthermore, when Csordas *et al* (2010) used rapamycin inducible ER-mitochondria linkers, there was a rapid induction of ER-mitochondria associations and a "zippering" effect of the proteins around the surface of the mitochondria upon the addition of rapamycin (Csordas et al., 2010). Even after long-term expression in stably transfected NSC34 cells, the fluorescent signal generated from expression of the V1-ER / V2-Mito BiFC reporter proteins always remains as discrete puncta associated with a subset of mitochondria. As shown in **Fig3.3** by anti-GFP immunostaining, the Venus fusion proteins are targeted all along the surface of the respective organelles and therefore, if the association of the complementary Venus fragments was inducing contact formation, one could expect a similar "zippering" effect to be observed. Future experiments using EM to quantify the mean number of ER-mitochondria contact sites <10 nm in untransfected cells and comparing this

to the mean number of contact sites detected by the BiFC technique, would provide supporting evidence on whether the Venus reporter proteins were induced new contact formation or exclusively labelling pre-existing contact sites.

The ability of the BiFC system to detect reductions in ER-mitochondria contacts is unclear from the results of this chapter as all of the stresses tested significantly increased organelle associations. Additionally, the reversibility of the BiFC system is questionable and the dissociation of the complementary fragments has yet to be clearly shown (Kerppola, 2006). However, even if the reformation of the Venus fragments is irreversible, it is still interesting as to why BiFC puncta remain restricted to a subset of mitochondria and this pattern of fluorescence does not vary greatly over time. This could suggest that there are some unique properties of these mitochondria that allow them to form particularly tight contact sites in comparison to the majority of the mitochondrial population or perhaps junctions of this size could be linked to specific functions of the MAMs for example, mitochondria undergoing fission events. The significance of these tight ER-mitochondria contacts will be discussed in further detail in **chapter 4** of this thesis. As described in **section 3.1.1** of this chapter, any of the proteins enriched at ER-mitochondria contact sites are also present along the portions of ER and mitochondrial membranes not lying within close proximity to one another. Therefore, it is not possible to compare the BiFC puncta signal with that of any other MAM-specific protein by immunofluorescent staining. Consequently, the protein compositions of these tight contact sites remain unclear at this time. As the interaction of VAPB with its MAM-binding partner, PTPIP51, relies on the entire cytosolic face of VAPB (De Vos et al., 2012), it implies that PTPIP51 is not necessarily an essential component of the contact sites labelled by the V1-ER reporter protein. However, it is worth noting that the TMD domain of VAPB present in the V1-ER reporter plasmid still possesses the GxxxG dimerization motif that may permit oligomerisation of the reporter protein with endogenous VAPB. This may exert some influence over the localisation of the reporter proteins and the specific contact sites labelled. The introduction of a point

mutation to this motif would determine if the VAPB TMD domain influences the specific MAMs labelled by the BiFC system.

3.4.4 Adaptations to the BiFC technique

Finally, we have shown how a simple adaptation to the technique, changing the mitochondrial targeting sequence to the endosomal targeting sequence of VAMP4 can be used to report on ER-endosome contact sites. In this manner, the BiFC method could be utilised to investigate any kind of organelle contact site. Current work in the Skehel lab is now attempting to incrementally increase the lengths of the linker sequences of the V1-ER fusion proteins to report on junctions of different lengths and finally, ongoing work is trying to replace the split Venus probe with split sf-Cherry probes (Kamiyama et al., 2016). The combination of these adaptations would allow for the simultaneous detection of different organelle contact sites or simultaneous detection of different length junctions, further highlighting the strength and versatility of the BiFC technique.

3.5 Chapter conclusion

In conclusion, the BiFC system is capable of detecting and visualising MAMs in both fixed and living cells and using this technique, we can report on known changes to ER-mitochondria interactions in agreement with previously published, electron microscopy data. This technique offers considerable benefits over pre-existing techniques that have been employed to investigate the MAMs and the system can be adapted to detect ER-mitochondria junctions of different sizes. The V1-ER and V2-Mito fusion proteins report on contact sizes of approximately 6-10 nm and the discrete, punctate pattern of fluorescence generated by co-transfection of these proteins is always, closely associated to a sub-set of mitochondria within a cell. Further work is required to elucidate the functional significance of these particularly tight contacts and to determine any particular properties of this sub-population of mitochondria in relation to Ca^{2+} signalling or biogenesis etc. which will be explored in the next chapter of this thesis.

Chapter 4
Functional significance of tight ER-mitochondria contact sites

4.1 Background

Sites of close apposition between the ER and mitochondria are heterogeneous in their structure and can vary in the overall surface area of the mitochondria membrane that is held in close proximity to the ER (the "length" of the contact site) **(Fig 4.1A)** or the distance at which the organelles are held apart (contact "thickness" or "distance") [As reviewed by (Giacomello and Pellegrini, 2016)] **(Fig4.1B)**. High resolution EM images have shown that the ER membrane can extend around the OMM and retain close contact for several hundred nanometres and has a mean junction distance of around 9-15 nm at the smooth ER, with junction sizes increasing to around 30 nm at the rough ER (Csordas et al., 2006; Sood et al., 2014). However, tighter junctions <6 nm have also been identified as well as much larger contact sites reaching distances of up to 60 nm (Csordas et al., 2006; Wang et al., 2015). Some of this variability in MAM structure may be cell-type specific, however, in the previous chapter we, in addition to several other published studies, have shown that these structures are plastic and can vary in response to metabolic changes of the cell (Bravo et al., 2011; Harmon et al., 2017; Csordas et al., 2006). This suggests that ultrastructural reorganisation of the length and thickness of the MAMs could be an important factor in regulating the specific functions of the contact sites. It is not yet clear what signalling mechanisms induce these changes and the exact mechanisms of contact plasticity have yet to be elucidated but it is plausible to think that a disruption in either of these adaptive processes could be linked to defects in the MAMs as seen in neurodegeneration (Giacomello and Pellegrini, 2016).

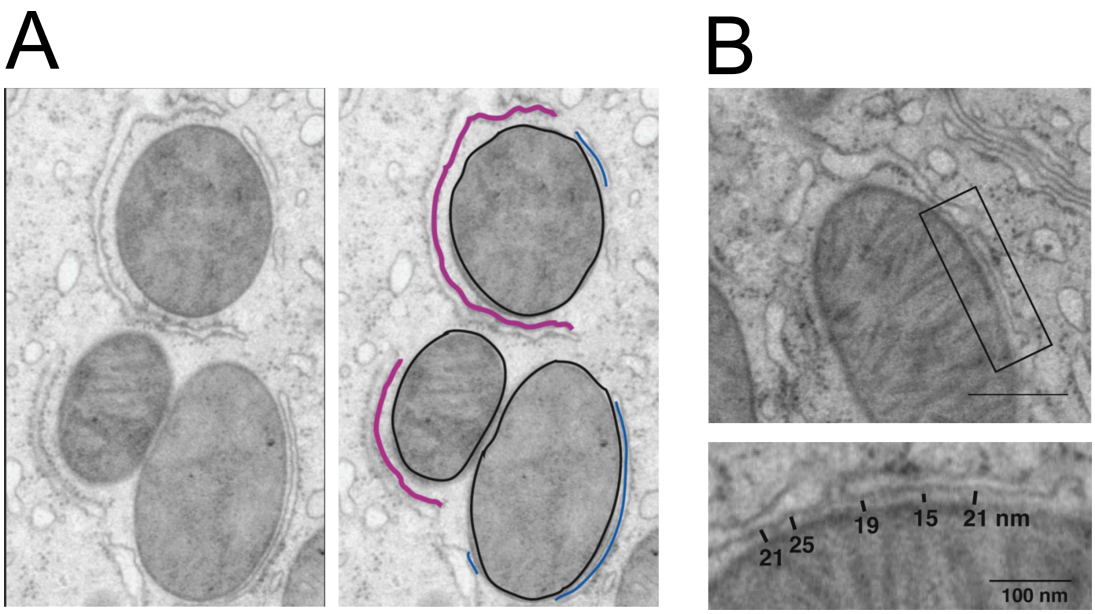

Fig 4.1: ER-mitochondria contact sites are structurally heterogeneous. (A) Cryo-EM images of mouse hepatocytes show variations in the lengths of ER-mitochondria contacts on different mitochondria *(left panel)*. ER-mitochondria contacts formed at the rough ER are highlighted in purple while those formed at the smooth ER are highlighted in blue, illustrating the tighter junctions of those formed between mitochondria and smooth ER *(right panel).* **(B)** Cryo-EM image of mouse liver hepatocyte *(top panel).* Zoomed image of the boxed region shows variation in the thickness of the junction across a contact site *(bottom panel)*. Image adapted with copyright permission from (Giacomello and Pellegrini, 2016) obtained via RightsLink.

Although there is a certain degree of flexibility in the structure of ER-mitochondria contacts, it is possible that this range of variability is restricted by the specific protein composition at these sites. Protein complexes identified as having a tethering role in organelle complexes are heterogeneous in size and the presence of different tethers at contact sites may define the sizes of those particular junctions. For example, the calcium exchange function of the MAMs relies on the formation of a protein complex between IP_3R and VDAC mediated by the chaperone protein grp75 (Szabadkai et al., 2006). Artificial tightening of the ER-mitochondria junction to below 7 nm massively reduced mitochondrial calcium uptake and it is predicted that this distance was too short to properly facilitate the formation of the calcium transport machinery

(Csordas et al., 2010; Giacomello and Pellegrini, 2016). Similarly, contact sites greater than 25 nm in thickness are assumed to be too large to allow for these proteins on opposing membranes to bind (Giacomello and Pellegrini, 2016). This highlights the interesting possibility that if junctions of a particular distance are required to facilitate the formation of certain MAM protein complexes, then perhaps different sized junctions could be attributed to carrying out specific functions. In further support of this, early markers of autophagy can be localised to wide ER-mitochondria contact sites of around 50 nm and it is hypothesised that this large gap might be necessary to facilitate the autophagic machinery and formation of the omegasome (Hamasaki et al., 2013; Giacomello and Pellegrini, 2016). Therefore, it may not be accurate to define MAMs as singular structures carrying out a wide range of functions but rather, as more evidence emerges, it could be possible to sub-classify them based on their size range and functional roles.

4.2 Chapter aims

In the previous chapter, the development of split-Venus fusion proteins that report on ER-mitochondria contacts <10 nm was described. However, the functional significance of MAMs of this tight distance is not well understood. Additionally, it is not clear why the fluorescent signal obtained from co-transfection of the reporter proteins was associated with only a sub-set of mitochondria within a cell. Therefore, the overall aims of this chapter were to investigate the structural and dynamic properties of contacts <10 nm in thickness as reported on by the BiFC technique and to try and attribute contacts of this size to any specific functions of ER-mitochondria contact sites. This was achieved by trying to correlate the localisation of the BiFC puncta with a variety of fluorescently-labelled proteins associated with specific functions of the MAMs. Furthermore, we aimed to elucidate any unique properties of the sub-set of mitochondria associated with contacts of this size by investigating changes in mitochondrial membrane potential and resting calcium concentrations.

4.3 Results

4.3.1 BiFC puncta are stable structures and remain closely associated with the mitochondria in living cells.

As discussed previously, a strong advantage of the BiFC technique over some alternative methods for investigating ER-mitochondria interactions is its ability to be used in living cells, allowing for investigations into MAM dynamics to be carried out. For this purpose, COS-7 cells were chosen due to their flat morphology, minimising the number of BiFC that would move in and out of the focal plane over the duration of the live-cell videos **(Fig4.2A)**. Quantifying changes in the number of BiFC puncta per frame over the course of 10 minute videos, imaged at a single focal plane, revealed that the BiFC puncta are very stable structures and their numbers do not vary much over the duration of the time measured **(Fig4.2B)(Video 4.1, Appendix I)**. Using Imaris image analysis software, the displacement length of each individual fluorescent puncta, from its initial position at the start of the video to its position in the final frame, could be automatically quantified, in addition to the mean movement speed. Plotting these values against one another revealed a mild, positive correlation between the two **(Fig4.2C)**. Due to the highly dynamic nature and constant restructuring of the mitochondrial network, automated tracking of the mitochondria was a challenge. To overcome this, ImageJ was used to manually measure the straight-line distance of individual BiFC puncta, as well as their associated mitochondrion, from the initial to end-point positions over the course of the live-cell video. Not unexpectedly, a very high correlation between the movement of the two structures suggests that the movement of the fluorescent BiFC puncta is dependent on the movement of its associated mitochondrion **(Fig4.2D)**.

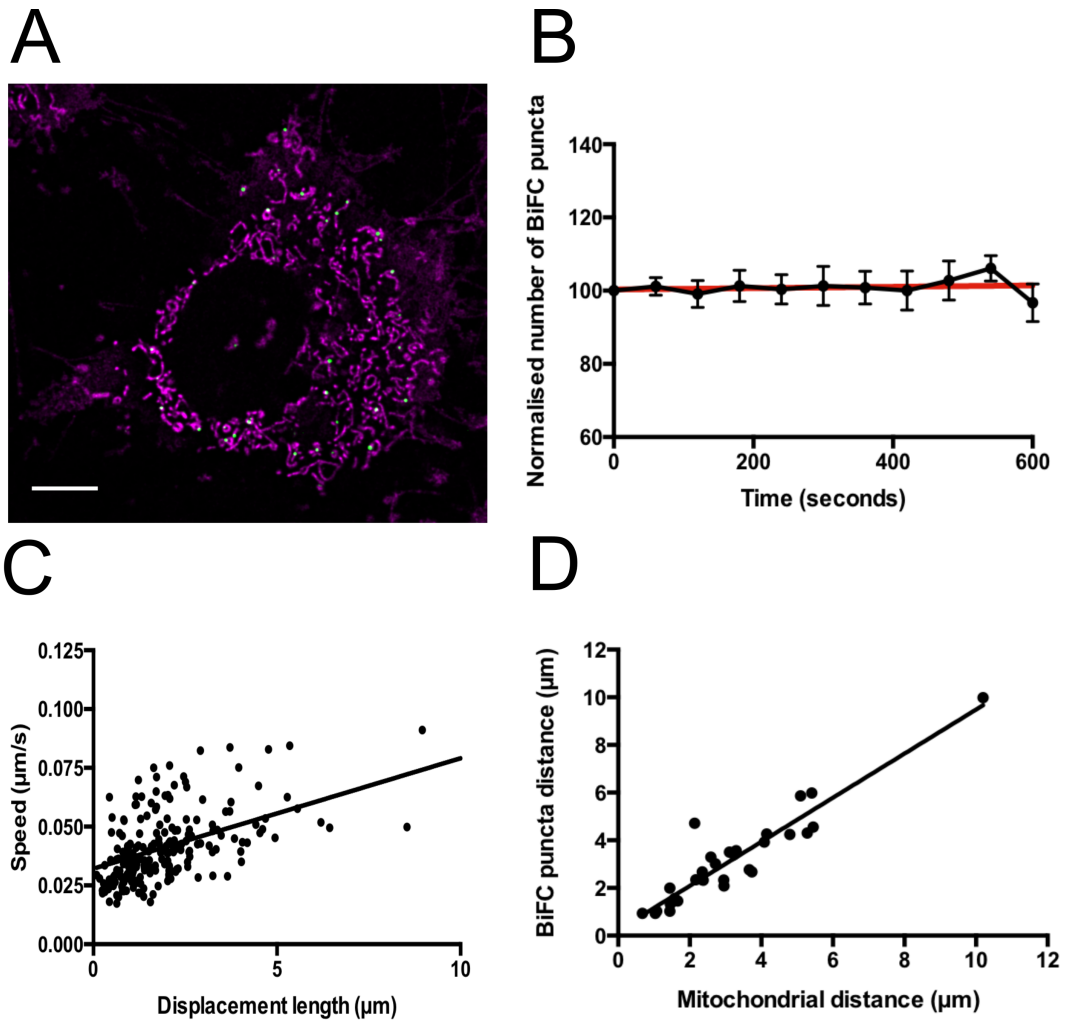

Fig 4.2: BiFC puncta are stable structures and remain closely associated to their corresponding mitochondrion in real-time. (A) Representative still-frame image of a 10 minute live-cell video of a COS-7 cell transiently expressing V1-ER / V2-Mito and stained with MitoTracker Deep Red FM dye. Scale bar, 10 µm. Images acquired at 0.25 FPS **(B)** The number of BiFC puncta per cell in the first frame of the live-cell video was quantified and normalised to give a value of 100%. The number of BiFC puncta in every subsequent frame was then quantified over the course of a 10 minute video and expressed as a percentage of the initial number of BiFC puncta, indicating that these are stable structures and their numbers do not deviate much over the duration of time imaged. Error bars represent SEM. n = 4 independent experiments (18 cells total). Values represent overall mean value from each of the 4 independent experiments per time point. Red line indicates the best-fit line. **(C)** Imaris image analysis software was used to track the displacement length and speed of each individual BiFC puncta per cell (as described in materials and methods) showing a

very mild correlation between the distance travelled and speed of the movement. R-square value = 0.2869. n = 208 BiFC puncta (18 cells total). **(D)** The straight-line distance between the starting position of an individual fluorescent puncta, as well as its' associated mitochondria, and its position in the final frame of the live-cell video was quantified and the relationship between the two was plotted. A very high correlation between the two sets of values suggests that the movement of the BiFC puncta is dependent on the movement of its associated mitochondria. R-square value = 0.8684. n = 30 BiFC puncta (6 cells total).

4.3.2 ER stress does not significantly affect the localisation of the mitochondria or BiFC puncta in NSC34 cells.

Previous work by Bravo *et* al (2011) has shown that upon the induction of ER stress, there is a migration of mitochondria towards the perinuclear area in cultured HeLa cells with a concomitant increase in ER-mitochondria contacts, as well as an increase in resting membrane potential and Ca^{2+} levels of redistributed mitochondria only and no significant changes in the mitochondria which were not seen to migrate (Bravo et al., 2011). In light of our data showing a very high correlation between the movement of a BiFC puncta and its associated mitochondrion **(Fig4.2D)**, we hypothesised that in ER stress induced cells, a migration of the mitochondrial network should be accompanied by an increased proportion of BiFC puncta in the perinuclear area. However, if there was some bias for new contact sites to be formed in a particular subcellular location e.g. at the cell periphery or in the perinuclear area, it could influence this result. To investigate this, the same cells were analysed as shown in the previous chapter in **Fig.3.10** whereby a statistically significant increase in the number of BiFC puncta from tunicamycin treatment had already been determined. A radial profile of mitochondrial fluorescence intensity in treated versus control cells was calculated using a concentric circle plugin of ImageJ whereby the intensity of the fluorescent signal within eight, equally spaced concentric circle regions radiating from the centre of the nucleus towards the cell periphery was quantified **(Fig4.3A)**.

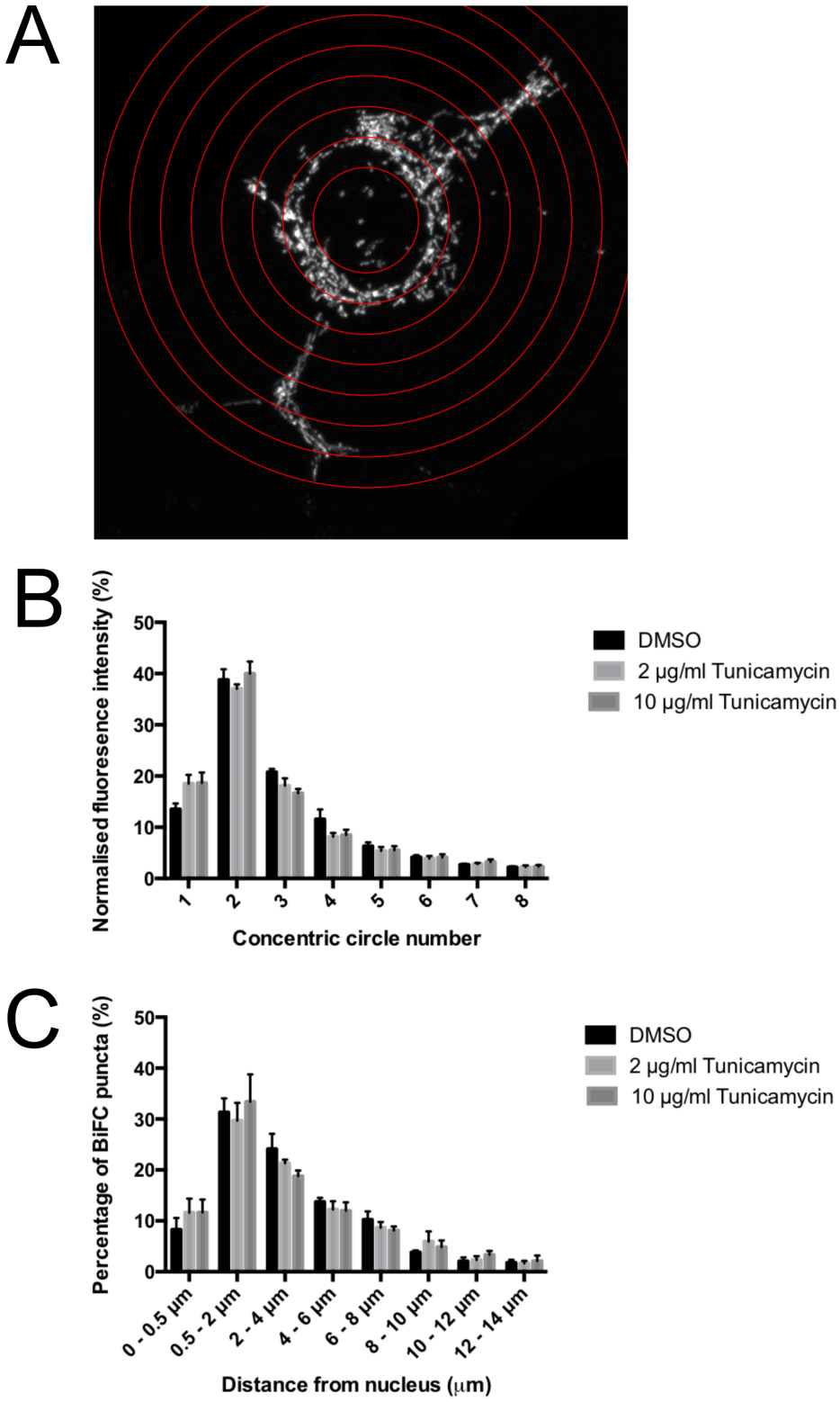

Fig 4.3: ER stress does not significantly alter the distribution of mitochondria or BiFC puncta within NSC34 cells. (A) Representative image of NSC34 cell showing a radial profile of concentric circles in ImageJ image analysis software. Mitochondria are immunofluorescently labelled with anti-ATPB. **(B)** Normalised mitochondrial

fluorescence intensity values calculated along each of the eight concentric circles in cells treated with 2 µg/ml or 10 µg/ml tunicamycin or DMSO as a control. Values represent the overall mean values from 3 independent experiments. n = 3 independent experiments (30-33 cells per experimental group). **(C)** Percentage of BiFC puncta within defined distances of the nucleus in control and treated cells. Values represent the overall mean values of the means of 3 independent experiments. n = 3 independent experiments (30-33 cells per experimental group). Statistical significance was tested using one-way ANOVA followed by Dunnett's multiple comparisons test, comparing the mean values to the mean of the control group for each individual group. $p < 0.05$ for all groups. Error bars represent SEM.

Although a trend was observed whereby there was increased mitochondrial signal in tunicamycin treated cells surrounding the nucleus and a decrease in signal in the central regions of the cell when compared to control cells, suggestive of a migration of the mitochondria towards the nucleus, this was deemed to be non-significant **(Fig4.3B)**. Next, we wished to examine the distribution of BiFC puncta within control and treated cells by calculating the percentage of the total number of contact points that fell within a certain distance of the nucleus (capped at a maximum distance of 14 µm from the nucleus)**(Fig4.3C)**. Here, the same trend was observed whereby an elevated percentage of BiFC puncta were found close to the nucleus in tunicamycin treated cells and a relatively higher percentage of BiFC puncta in control cells was present in the central regions of the cell but again, this was not statistically significant. With higher sample numbers, it is possible that a significant effect would be observed.

4.3.3 BiFC puncta are associated with a sub-population of mitochondria of higher than average resting membrane potential.

As shown previously, the tight ER-mitochondria contact sites reported on by the Venus fusion proteins are consistently associated with only a sub-population of mitochondria, in all cell lines tested. However, it is unclear why the BiFC puncta are associated with these particular mitochondria and whether that is due to some unique properties of these mitochondria or to some specific function of the MAMs actively occurring at these sites is yet to be determined. There are several

fundamental properties on which mitochondria could vary but due to the close relationship between contact thickness and mitochondrial calcium levels (Csordas et al., 2006), we investigated whether any difference in mitochondrial calcium levels could be detected between those that were associated with a BiFC puncta, representing a contact site <10 nm, and those that were not. Furthermore, mitochondrial resting membrane potential is a good indicator of mitochondrial health and is caused by the accumulation of protons in the intermembrane space through the respiratory electron transport chain that generates a charge gradient for ATP production [As reviewed by (Nicholls and Budd, 2000)]. In addition, the aforementioned work by Bravo *et al* (2011) shows that ER stress-induced increases in ER-mitochondria contacts are accompanied by increases in both resting membrane potential and Ca^{2+} levels and therefore, these are the two parameters we chose to investigate in our work.

To measure mitochondrial membrane potential, NSC34 cells were treated with a MitoTracker CMXRos dye. MitoTracker CMXRos is a rhodamine-based dye that does not fluoresce until it becomes oxidised within a living cell and then accumulates electrophoretically within mitochondria in response to a negative membrane potential, such that higher fluorescence intensity is indicative of hyperpolarisation of the mitochondrial membrane (Kholmukhamedov et al., 2013) **(Fig4.4A)**. 3D live-cell imaging of cells then allowed us to measure the fluorescence intensity values of mitochondrial regions associated with a BiFC puncta in comparison to the mean intensity value of the mitochondrial network **(Fig4.4B)**. The results indicate that regions of mitochondria associated with a BiFC puncta have a slight, but significant, increase in fluorescence intensity in comparison to the mean intensity value of the mitochondria network, representing increased membrane potential at these contact sites **(Fig4.4C$_{(i)}$)**. If the normalised mean fluorescence intensity values of each of the disconnected components of the total mitochondrial network are plotted against the normalised intensity values of the regions associated with a BiFC puncta in a frequency distribution graph, it demonstrates that BiFC puncta are not exclusively

associated with regions of higher than average membrane potential and can occasionally be found associated with mitochondria of lower than average membrane potential **(Fig4.4C$_{(ii)}$)**. However, overall there is a shift in the distribution to show a favoured association of the BiFC puncta with mitochondria of higher than average resting membrane potential.

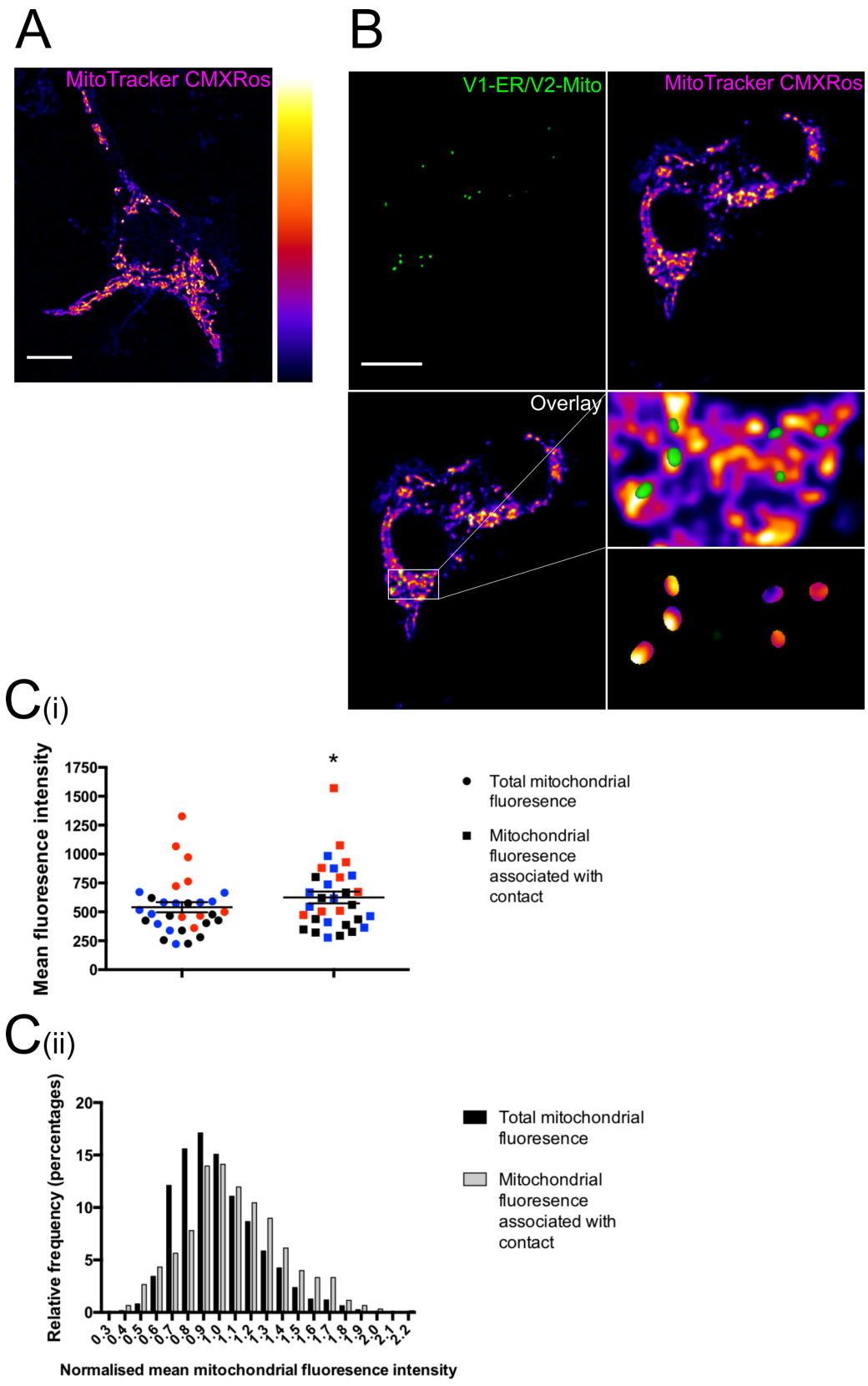

Fig 4.4: BiFC puncta are associated with regions of mitochondria of high membrane potential. (A) Representative image of NSC34 cell labelled with MitoTracker Red

CMXRos dye and pseudo-coloured on ImageJ based on signal intensity according to the key shown. Scale bar, 10 µm **(B)** Using the Venus channel as a mask, mean fluorescence intensity of all regions of mitochondria correlating with a BiFC puncta were quantified and compared to the overall mean fluorescence intensity of the mitochondria signal within a given cell. Bottom right panels represent zoomed in region from overlay image before and after mask is applied. **(C_i)** Mitochondrial fluorescence intensity of regions associated with a BiFC puncta was significantly higher in comparison to overall mean mitochondrial fluorescence intensity. Values from each of three independent experiments are colour-coded. Bars represent overall mean ± SEM. Statistical significance was measured used paired t-test. n = 3 independent experiments (31 cells per experimental group). **(C_{ii})** Distribution graph of the relative frequencies of the mean fluorescence intensity values of each disconnected component of the total mitochondrial channel/regions associated with a BiFC puncta as detected by Imaris. Fluorescence intensity values were normalised to the mean overall mitochondrial fluorescence intensity value which was denoted by a value of 1.

4.3.4 Oligomycin induced increases in mitochondrial membrane potential do not alter the number of BiFC puncta per cell.

Although BiFC puncta were shown to associate with mitochondria of higher than average resting membrane potential, it is not evident whether a higher membrane potential promotes contact formation or whether the formation of a tight physical contact drives an increase in membrane potential. We aimed to test this by chemically increasing the resting mitochondrial membrane potential by treating cells with the proton transporting ATP synthase inhibitor oligomycin (Jastroch et al., 2010). If an increase in resting membrane potential promotes contact formation, one would predict an increase in the number of BiFC puncta per cell however, studies using the mitochondria uncoupler carbonyl cyanide *m*-chlorophenyl hydrazone (CCCP) to induce massive mitochondrial membrane potential depolarisation demonstrated an induction of mitophagy and increase in ER-mitochondria contacts and so perhaps, an oligomycin-induced rise in membrane potential could result in a compensatory reduction in contacts (Gelmetti et al., 2017). NSC34 cells transiently expressing the V1-ER and V2-Mito reporter proteins were treated with a DMSO control or 5 µg/ml oligomycin for 24 hours to investigate any changes in the mean number of BiFC puncta per cell **(Fig4.5A).** Hyperpolarisation of the mitochondrial

membrane induced by oligomycin treatment was proven by an increase in mean fluorescence intensity of cells stained with MitoTracker CMXRos dye **(Fig4.5B).** The results showed no significant change in the mean number of BiFC puncta per cell following oligomycin treatment **(Fig4.5($B_{(i)}$)**. Although non-significant, a difference of 12% in the mean number of BiFC puncta in control versus treated cells was detected and so with a larger sample size, this effect could be significant however, a change of this magnitude is well below the 40-50% change in the number of BiFC puncta we have observed with any of the other stresses tested. Furthermore, as the reversibility of the BiFC technique is questionable, it may not accurately pick up on reductions in ER-mitochondria contacts so in order to test if oligomycin reduces contact sites, we used the fluorescence co-localisation method of measuring MAMs **(Fig4.5C)**. Again, the results showed no significant change in oligomycin treated cells **(Fig4.5$C_{(i)}$).**

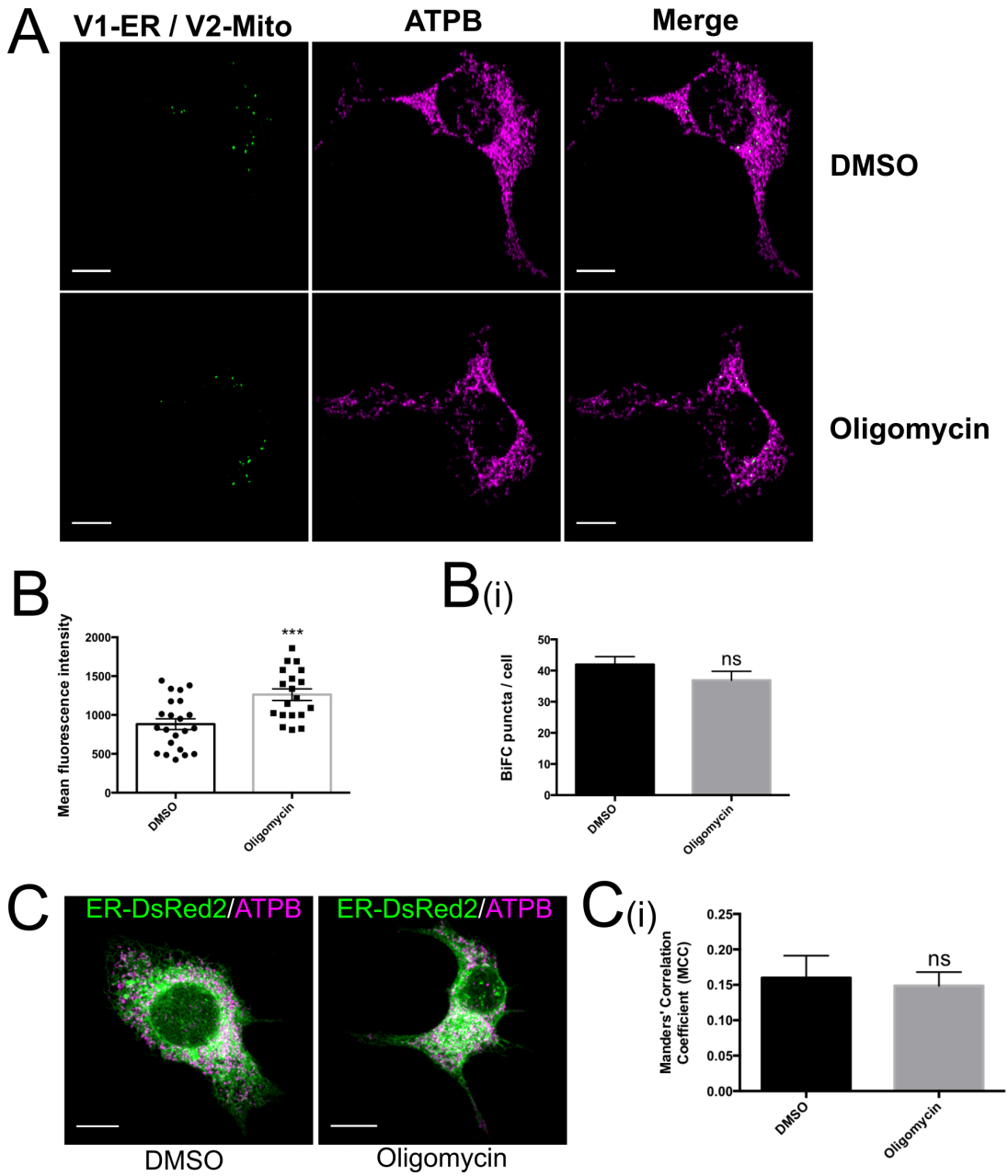

Fig 4.5: Treatment with oligomycin does not change the mean number of BiFC puncta per cell in NSC34 cells. (A) Representative images of NSC34 cells expressing V1-ER and V2-Mito reporter plasmids treated with a DMSO control or 5 µg/ml oligomycin for 24 h post-transfection. Mitochondria were immunolabelled with anti-ATPB. **(B)** A statistically significant increase in fluorescence intensity in cells treated with oligomycin in comparison to those treated with DMSO was observed. n = 19-22 cells per experimental group. **($B_{(i)}$)** No significant change in mean BiFC number per cell was detected in control versus oligomycin treated cells. n = 4 independent experiments (38-56 cells per experimental group). Values indicate overall mean values from the 4 independent experiments. Error bars represent SEM. Statistical significance was determined by unpaired t-test.

ns = non-significant, P>0.05. **(C)** Representative images of NSC34 cells transfected with ER-DsRed2 to label the ER *(green)* and immunolabelled with anti-ATPB to stain the mitochondria *(magenta)*, treated with 5 µg/ml oligomycin or an equivalent volume of DMSO. **($C_{(i)}$)** Fluorescence co-localisation was quantified by PCC. n = 3 independent experiments (15-17 cells per experimental group). Statistical significance was determined by unpaired t-test. ns = non-significant, P>0.05.

In summary, hyperpolarisation of the mitochondrial membrane does not drive the formation of new ER-mitochondria contact sites. No significant reduction in the number of BiFC contact sites was detected through either the BiFC technique or fluorescence co-localisation analysis. We can conclude that the association of the BiFC puncta with mitochondria of high membrane potential is more likely a consequence of tight contact formation as opposed to a driver for increased ER-mitochondria associations.

4.3.5 BiFC puncta are associated with a sub-population of mitochondria with elevated resting calcium concentrations

Differences in mitochondrial Ca^{2+} levels of mitochondria associated with a BiFC puncta in comparison to those that were not, were investigated using a genetically encoded, mitochondrially targeted Mito-RCaMP probe. This class of calcium indicator is based on circularly permuted fluorescent proteins fused C-terminally to a calmodulin domain and to a Ca^{2+}-calmodulin binding peptide, M13, at the N-terminal (Nagai et al., 2001). The binding of Ca^{2+} induces a conformational change to the fluorescent protein, causing an increase in the intensity of the fluorescent signal, proportional to the concentration of Ca^{2+} (Nagai et al., 2001). NSC34 cells transfected with the V1-ER/V2-Mito reporter plasmids and the Mito-RCaMP calcium indicator were imaged live and the fluorescence intensity of regions associated with a BiFC puncta were measured and compared to the overall mean fluorescence intensity value of the mitochondrial network **(Fig4.6A)**. The results show a significantly higher fluorescence intensity value of mitochondrial regions directly associated with a BiFC puncta in comparison to the mean fluorescence intensity value of the total

mitochondrial network, suggesting that BiFC contacts are associated with mitochondria of high calcium concentrations **(Fig4.6B$_{(i)}$)**. When the normalised values are displayed as a frequency distribution graph, the results again demonstrate that although these tight contact sites are not exclusively formed on regions of higher than average Ca^{2+} concentrations, there is a strong shift favouring the association at the areas of high calcium concentration **(Fig4.6B$_{(ii)}$)**.

In summary, the data shows that the BiFC puncta are associated with regions of mitochondria of higher than average resting membrane potential and mitochondrial Ca^{2+} concentrations. This result could indicate that these properties of this sub-population of mitochondria could be encouraging them to form tight associations with the ER however, it could also be the case that elevated membrane potential and Ca^{2+} levels could be a consequence of contact formation rather than a cause and further work would be required in order to determine this.

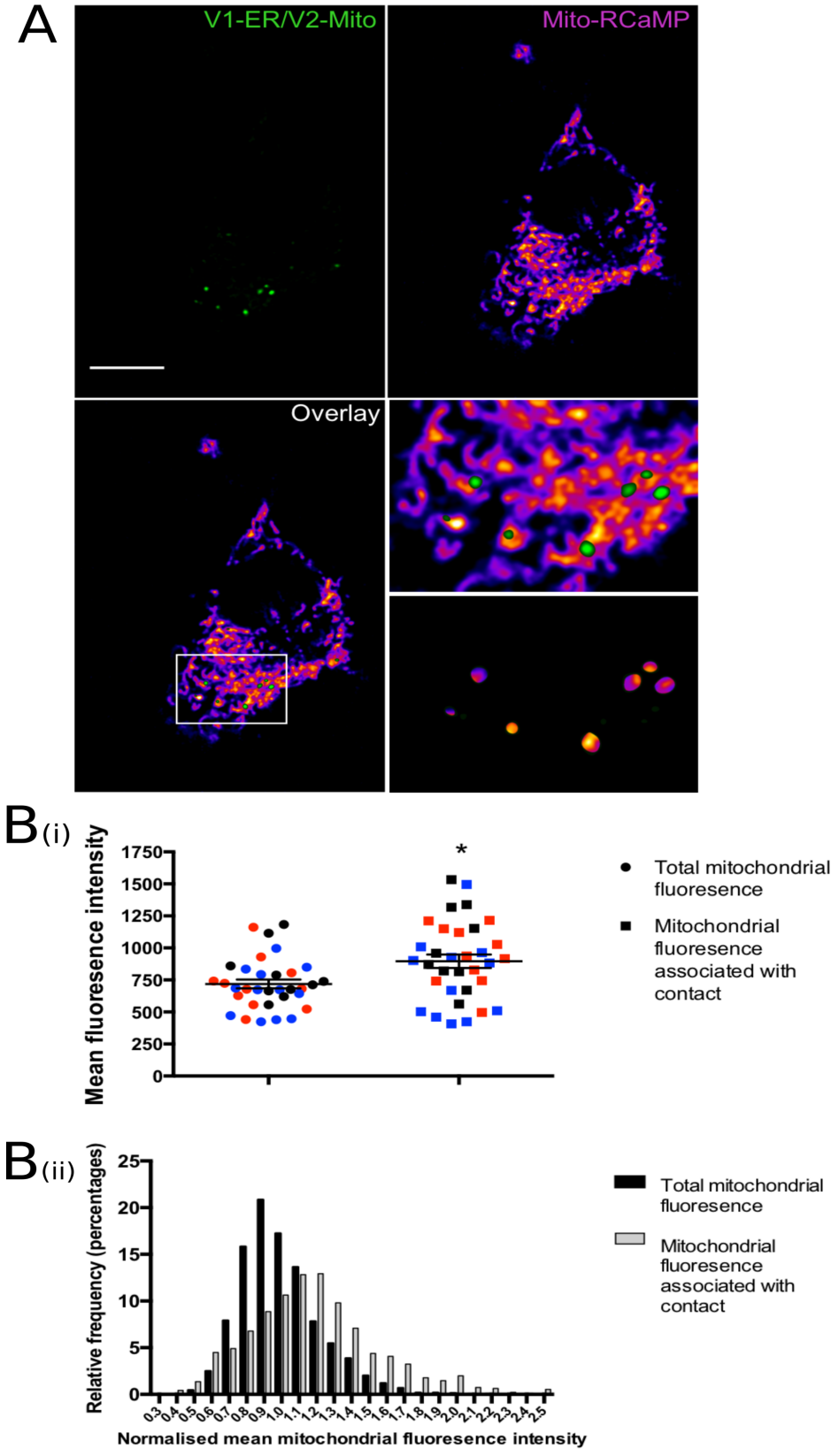

Fig 4.6: BiFC puncta are associated with mitochondria of elevated resting calcium concentrations. (A) Representative image of NSC34 cell transiently transfected with

the Venus reporter plasmids and MitoRCaMP probe. Using the Venus channel as a mask, mean fluorescence intensity of all regions of mitochondria correlating with a BiFC puncta were quantified and compared to the total mean fluorescence intensity of the mitochondria signal within a given cell. Bottom right panels represent zoomed in region from overlay image before and after mask is applied. Scale bar, 10 µm **(B_i)** Mitochondrial fluorescence intensity of regions associated with a BiFC puncta was significantly higher in comparison to overall mean mitochondrial fluorescence intensity. Values from each of three independent experiments are colour-coded. Bars represent overall mean value ± SEM. Statistical significance was measured used paired t-test. n = 3 independent experiments (33 cells per experimental group). **(B_{ii})** Distribution graph of the relative frequencies of the mean fluorescence intensity values of each disconnected component of the total mitochondrial channel/regions associated with a BiFC puncta as detected by Imaris. Fluorescence intensity values were normalised to the mean overall mitochondrial fluorescence intensity value which was denoted by a value of 1.

4.3.6 BiFC puncta are not sensitive to Gq-DREADD receptor mediated elevations in cytoplasmic Ca^{2+} levels.

As previously described, there is an intimate relationship between ER-mitochondria associations and calcium signalling, with tighter contacts enhancing calcium exchange from the ER, leading to increased mitochondria calcium levels at these sites (Csordas et al., 2006). Our data above illustrates that the BiFC signal is associated with mitochondria that have high Ca^{2+} concentrations but doesn't inform us whether elevated mitochondrial calcium levels can encourage the formation of physical contact sites with the ER or whether the organelle coupling causes this increase in mitochondrial Ca^{2+}.

To investigate this, we used Designer Receptor Exclusively Activated by Designer Drugs (DREADD), a platform which involves the modification of protein receptors to be activated exclusively by a synthetic drug known as Clozapine N-oxide (CNO), an agonist of DREADD receptors that is not known to activate any endogenously expressed receptors (Armbruster et al., 2007).

In this study, we used a modified Gq–coupled receptor protein (Armbruster et al., 2007), that is part of the G protein-coupled receptor superfamily that are sensitive to external ligands to activate internal signalling pathways. Specifically, the activation of Gq-coupled receptors stimulates plasma membrane bound phospholipase Cβ to cleave phosphatidylinositol biphosphate (PIP_2) into two secondary messengers which includes IP_3 to activate IP_3R mediated calcium release (Kero et al., 2007). Therefore, upon addition of CNO to our cells we should activate the Gq-coupled DREADD to in turn activate the IP_3R receptors and stimulate calcium release from the ER, resulting in a sharp spike in cytoplasmic Ca^{2+} concentrations. In order to test this, NSC34 cells were transfected with a cytoplasmically targeted fluorescent GCaMP calcium indicator along with the EF1α-DI0-Gq-mCherry DREADD plasmid, the expression of which is dependent on Cre recombinase and an AAV-EF1α-Cre plasmid. During live-cell imaging, using a Leica fluorescent imaging system, the addition of 1 µM CNO resulted in a sharp increase of GFP signal that returned to baseline fluorescence approximately 20 seconds later, as can be seen from the still frame images in **(Fig4.7A)** and in **(VIDEO 4.2, Appendix I)**. Quantification of this change in fluorescence showed a 2-fold increase in the mean, normalised intensity value in cells treated with CNO whereas no change in fluorescence was observed in cells imaged without any addition of CNO **(Fig4.7B)**. The results indicate a rapid, Gq-DREADD mediated increase in cytoplasmic calcium levels after the addition of CNO which then returns to baseline levels as calcium homeostasis is maintained.

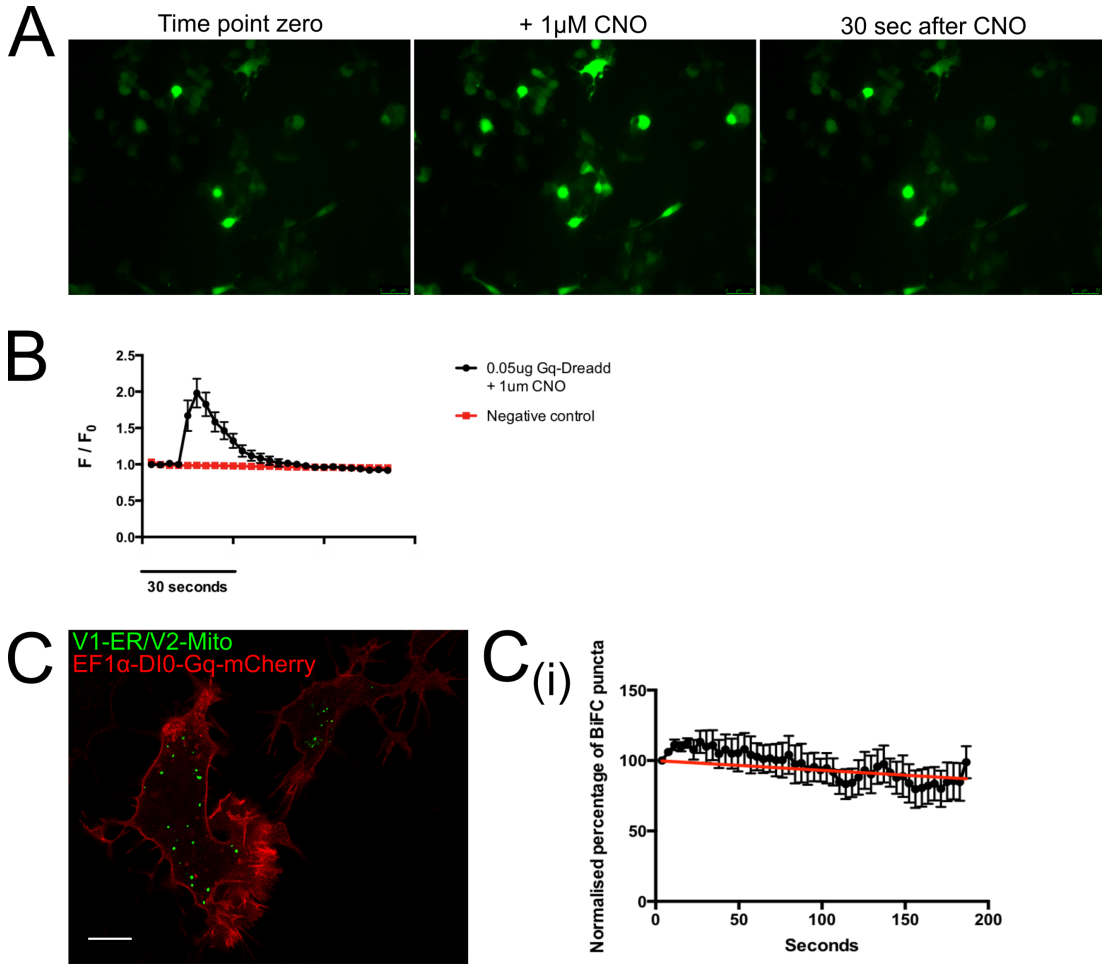

Fig 4.7: Gq DREADD mediated spikes in cytosolic Ca^{2+} levels do not influence the number of BiFC puncta per cell. (A) Single slice images from live-cell optimisation of Gq-DREADD receptor transfection. NSC34 cells transfected with EF1α-DI0-Gq-mCherry, AAV-EF1α-Cre and a GCaMP3-cyt cytoplasmic calcium indicator probe were imaged live to test for elevation in cytoplasmic Ca^{2+} levels mediated by Gq-DREADD receptor activation. 1 µM CNO was added to the cells which resulted in an immediate increase in GCaMP3-cyt fluorescent signal which gradually returned to baseline levels. **(B)** Change in GCaMP3 fluorescence was measured by the equation F/F_0 as outlined in the methods section, demonstrating a 2-fold increase in intensity after the addition of CNO which returns to baseline levels after approximately 20 seconds. Error bars represent SEM. Red line represents the F/F_0 value of untreated cells. n = 27 cells **(C)** Representative still frame image of live-cell NSC34 cell transfected with V1-ER/V2-Mito reporter plasmids *(green)* along with EF1α-DI0-Gq-mCherry *(red)* and AAV-EF1α-Cre plasmids. Scale bar, 10 µm **($C_{(i)}$)** The number of BiFC puncta per time point was analysed by Imaris image analysis software. 1µM CNO was added at 1 min showing no robust change in BiFC puncta number from Gq mediated cytoplasmid Ca^{2+} elevation. n = 8 cells (3 independent experiments). Error bars

represent SEM. Values indicate the mean value of the 8 individual cells, due to low sample size number.

Following on from this, the aim was to see if the BiFC puncta are sensitive to rapid increases in cytoplasmic Ca^{2+}. It was predicted that this could encourage ER-mitochondria associations or tightening of pre-existing contact sites in order to promote mitochondrial calcium uptake leading to rapid increases in BiFC numbers. To test this, NSC34 cells expressing the Venus reporter proteins and the Gq-coupled DREADD receptor showing a plasma membrane localisation, were imaged live and treated with 1 µM CNO after 60 seconds on a Nikon confocal microscope to have a high enough resolution to detect subtle alterations in BiFC number **(Fig4.7C)(Video 4.3, Appendix I).** As this was a different imaging system used to that for the optimisation of the technique, a live-cell imaging dish of cells expressing the DREADD receptor and Cyto-GCaMP calcium indicator was first imaged and treated with CNO to illustrate the same increase in GCaMP fluorescence as with the Leica system (data not shown). Quantification of the number of BiFC puncta per frame showed no immediate changes in BiFC number upon the addition of CNO and overall, there was no real change in the mean number of BiFC puncta over the duration of the video **(Fig4.7C$_{(i)}$).** However, there are some limitations associated with this which will be discussed in further detail in **section 4.3** below.

4.3.7 BiFC puncta do not represent the sites of autophagosome formation

MAMs are believed to be one of the sites contributing membrane for autophagosome formation and in agreement with this, the early autophagy markers ATG5 and ATG14 were shown to re-localise to ER-mitochondria contact sites when autophagy was induced by serum deprivation (Hamasaki et al., 2013). By inducing autophagy in cells expressing our Venus reporter proteins, we aimed to see whether the re-localisation of ATG5 and ATG14 into punctate structures co-localise with the fluorescent BiFC puncta which would indicate that these tight ER-mitochondria

contact sites could represent the sites of autophagosome formation. Alternatively, the sub-population of mitochondria associated with a BiFC puncta could represent a population of damaged mitochondria and therefore one might expect that mitophagic vacuoles could be formed at these sites.

In NSC34 cells grown in serum-free media for 24 h and immunostained with an anti-ATG5 antibody, there was a reorganisation of ATG5 from a diffuse cytoplasmic distribution to punctate structures in agreement with the published literature **(Fig4.8A)**(Hamasaki et al., 2013)**.** For the most part, there was no co-localisation of fluorescent ATG5 puncta with the BiFC puncta **(Fig4.8B).** Similarly, when mCherry-ATG14 was expressed in serum-deprived NSC34 cells, the distribution of the protein re-localises into punctate structures that do not co-localise with BiFC puncta **(Fig4.8C).** We can conclude that the tight ER-mitochondria contact sites reported on by the Venus fusion proteins do not represent sites of autophagosome formation.

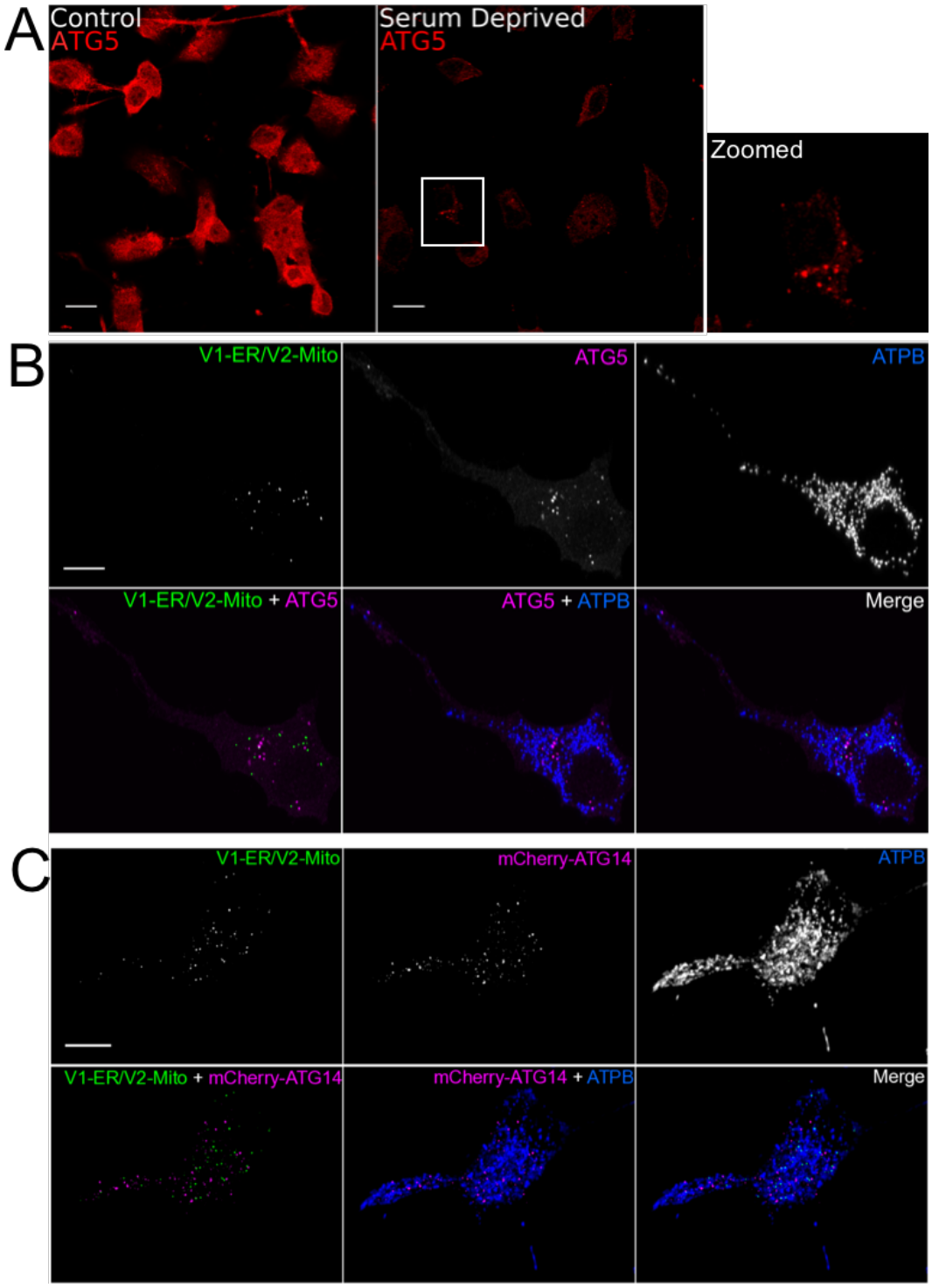

Fig 4.8: BiFC puncta do not correlate with early markers of autophagy induced by serum deprivation. (A) Representative images of NSC34 cells immunostained with an anti-ATG5 antibody grown in control DMEM supplemented with 10% (v/v) FBS or serum deprived in DMEM with no FBS for 24h, showing the re-localisation of ATG5 from a cytosolic pattern to punctate structures. Zoomed image represents area

within boxed region of serum deprived panel. Scale bars, 20 µm **(B)** Serum deprived NSC34 cells expressing V1-ER and V2-Mito reporter plasmids and immunostained for ATG5 and an anti-ATPB mitochondrial marker 24 h post starvation **(C)** Serum deprived NSC34 cells expressing the Venus reporter plasmids and mCherry-ATG14. Scale bars, 10 µm.

4.3.8 BiFC puncta are within close proximity of actively replicating mtDNA nucleoids

In mammalian cells, mtDNA is harboured within circular, closed molecules along the inner mitochondrial matrix known as nucleoids (Brown et al., 2011). The replication of the mitochondrial genome is carried out at these sites by the mtDNA polyermase gamma complex, composed of a p140 catalytic subunit and a p55 accessory subunit encoded for by the *POLG2* gene (Young et al., 2015). Recent evidence has shown that these nucleoids are spatially linked within 1 µm of mitochondrial division events and as described in **section 1.2.2.8** of the introduction chapter, these division events occur at sites of close apposition between the ER and mitochondria (Lewis et al., 2016). Therefore, in order to test if BiFC puncta represented nascent mitochondrial division sites, fluorescently tagged POLG2 was used to label a sub-population of actively replicating nucleoids as demonstrated by Lewis *et al* (2016).

Fluorescently-tagged POLG2 plasmids were cloned as described in **chapter 2, section 2.2** to generate a POLG2-DsRed2 plasmid containing the full-length POLG2 sequence or a $POLG2_{1-25}$-DsRed2 plasmid consisting of only the N-terminal 25 amino acids of POLG2 that make up the mitochondrial targeting domain (Young et al., 2015). To test the sub-cellular localisation of these constructs and to test whether they still specifically labelled replicating nucleoids, they were individually transfected into COS-7 cells along with POLG2-GFP and the extent of co-localisation was quantified by Pearson's Correlation Coefficient **(Fig 4.9, Table 4.1)**. The full-length POLG2-DsRed2 showed a very high level of co-localisation with POLG2-GFP (PCC = 0.798 ± 0.021) indicating that the change in fluorophore did not alter the localisation of the protein. In contrast, $POLG2_{1-25}$-DsRed2 demonstrated only a low level of co-localisation with POLG2-GFP (PCC = 0.291 ± 0.046) but co-localised highly with an

ATPB mitochondrial marker (0.765 ± 0.059), suggesting that the C-terminal domain of POLG2 is essential for its specific targeting to nucleoids.

As the overall aim of the experiment was to investigate an association of the BiFC puncta with replicating nucleoids, we only proceeded with the full length POLG-DsRed2 construct.

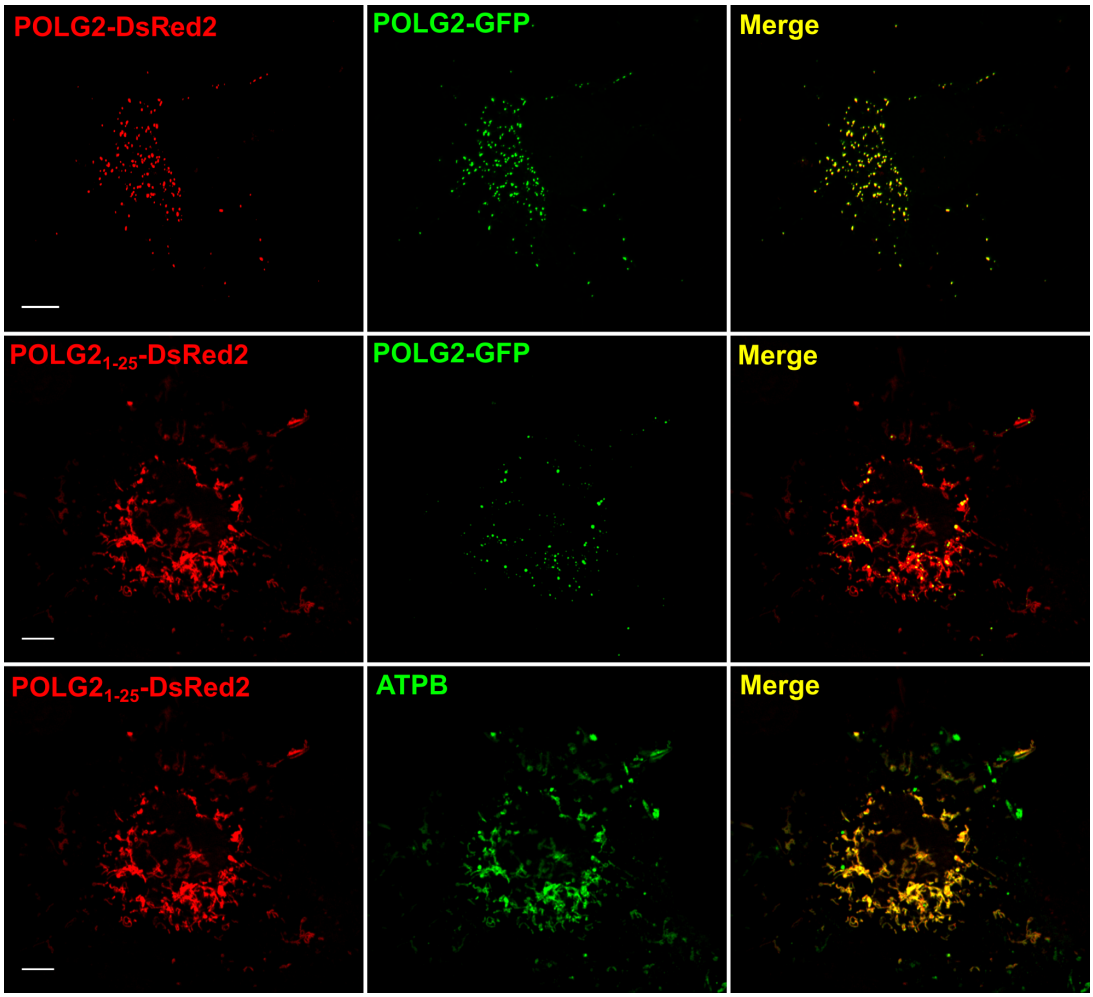

Fig 4.9 Full-length and truncated POLG2-DsRed2 proteins are differentially localised within COS-7 cells. Plasmids were generated containing a DsRed2 ORF fused in-frame between the N-terminal 25 codons making up the mitochondrial targeting domain and the remaining C-terminal cDNA sequence of POLG2 (POLG2-DsRed2) or a DsRed2 ORF including a stop codon was fused after the first 25 codons such that only the POLG2 mitochondrial domain fused to the DsRed2 fluorophore was translated (POLG2$_{1-25}$-DsRed2). POLG2-DsRed2 showed a punctate localisation and co-localised very highly with POLG2-GFP as quantified by PCC (0.798 ± 0.021). In contrast, POLG2$_{1-25}$-DsRed2 demonstrated a low level of co-localisation with POLG2-GFP (0.291 ± 0.046) but a high level of co-localisation with the mitochondrial marker

ATPB as labelled by immunofluorescent staining (0.765 ± 0.059). The results show that the C-terminal domains of POLG2 are required for its specific localisation to replicating nucleoids. Scale bar, 10 µm.

Table 4.1: Fluorescent signal co-localisation quantified by Pearson's Correlation Coefficient (PCC). Values indicate mean PCC ± SEM for the co-localisation of POLG2-DsRed2 with POLG2-GFP or $POLG2_{1-25}$-DsRed2 with POLG2-GFP and the mitochondrial marker ATPB. n = 3 independent experiments (9-11 cells per experimental group).

Fluorescently labelled proteins	PCC
POLG2-DsRed2 / POLG2-GFP	**0.798 ± 0.021**
$POLG2_{1-25}$-DsRed2 / POLG2-GFP	**0.291 ± 0.046**
$POLG2_{1-25}$-DsRed2 / ATPB	**0.765 ± 0.059**

Previously published data had determined that the vast majority of actively replicating nucleoids, as labelled by POLG2-GFP, were found within 1 µm of ER-mitochondria contact sites (Lewis et al., 2016). These images however, were taken by diffraction-limited confocal microscopy and ER-mitochondria contact sites were scored based on co-localisation of an ER and mitochondria marker, at best giving a resolution of around 200 nm and therefore giving no information on the specific thickness of these junction sites. In our study, we wanted to look for a correlation between POLG2 puncta and ER-mitochondria contact sites < 10 nm to determine if tight contacts are functionally linked to mitochondrial division events. We observed that 33.5% ± 4.3 of BiFC puncta were within 200 nm of a POLG2-DsRed2 puncta and 66% ± 6 were within 1 µm as quantified across 13 cells over three independent experiments. The mean number of POLG2 puncta in COS-7 cells was approximately

double the mean number of BiFC puncta and covered double the percentage surface area of the total mitochondrial network in comparison to BiFC puncta (**Table 4.2**).

Table 4.2: Quantification of mean numbers of BiFC and POLG2-DsRed2 puncta per cell and total surface area of BiFC or POLG2-DsRed2 signal as a percentage of the surface area of the total mitochondrial network. Values indicate number of puncta or percentage surface area (%) ± SEM. n = 3 independent experiments (13 cells total).

Mean number of BiFC puncta per cell	Mean number of POLG2-DsRed2 puncta per cell	Mean total surface area of BiFC puncta / mean mitochondrial surface area (μm^2)	Mean total surface area of POLG2-DsRed2 puncta / mean mitochondrial surface area (μm^2)
47 ± 12	**97 ± 14**	**6.6 ± 1 %**	**12.8 ± 3.35 %**

A correlation was observed between the number of POLG2 puncta and the number of BiFC puncta in a cell however, the number of both structures showed high positive correlation with the overall surface area of the mitochondrial network and therefore, we cannot determine from this data alone if the presence of one protein is influencing the levels of the other (**Fig 4.10A**). More likely, the number of these structures is simply dependent on the overall size of the mitochondrial network. As the mean number of POLG2 puncta is a lot higher than the number of BiFC puncta per cell, it is unlikely that BiFC puncta solely represent the sites of mitochondria division. However, it cannot be ruled out that POLG2 puncta are highlighting sites of nascent mitochondrial fission events where constriction of the mitochondria by ER tubules has not yet taken place and therefore, the junction between the ER and mitochondria may not have fallen within the detectable range of the Venus reporter proteins. To investigate this possibility, COS-7 cells expressing the Venus reporter

proteins and POLG2-DsRed2, with the mitochondria labelled by MitoTracker Deep Red FM were imaged live in an attempt to visualise mitochondrial division events (**Fig 4.10B**). Unfortunately, simultaneous three-colour imaging on a laser scanning confocal microscope has relatively slow acquisition speeds and therefore, we were unable to capture any mitochondrial division events with any degree of certainty **(VIDEO 4.4, Appendix I)**. Further work will be required in order to draw a strong conclusion of the association of tight ER-mitochondria contact sites with mitochondrial division events.

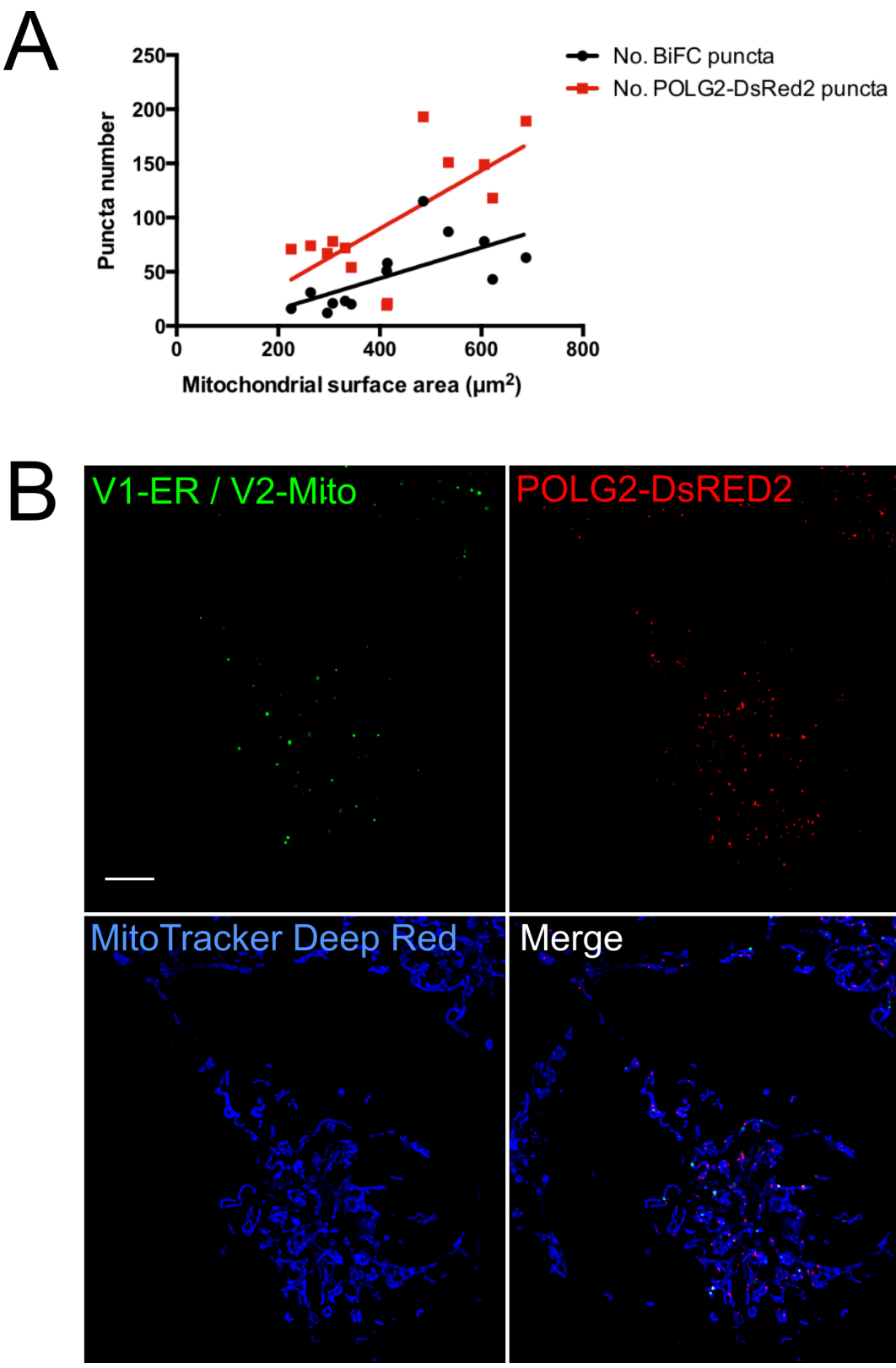

Fig 4.10: A large proportion of BiFC puncta are within close proximity to replicating nucleoids. (A) The number of BiFC puncta and POLG2-DsRed2 puncta show a high positive correlation with the overall surface area of the mitochondrial network. R^2 =

0.4509 for BiFC puncta (p-value 0.0120) and 0.4763 for POLG2-DsRed2 (p-value 0.009). n = 13 cells. **(B)** Representative single frame image of COS-7 cells transfected with V1-ER / V2-Mito (green) and POLG2-DsRed2 (red) and stained with MitoTracker Deep Red (blue). Scale bar, 10 µm.

4.4 Discussion

4.4.1 The BiFC system can be effectively utilised in living cells in the investigation of organelle contact site dynamics

As discussed in **section 4.1** of this chapter, organelle contact sites can respond to certain stress conditions by altering junction length and thickness but the driving force behind this plasticity of MAMs is unclear. However, the variation in MAM length and thickness could be attributed to specific functions of these contact sites. In this chapter, we have presented data on the specific functional significance of tight ER-mitochondria contact sites < 10 nm, as reported on by our BiFC system. To systematically investigate specific functions of the MAMs and determine any unique properties of mitochondria with tight membrane contact sites, we have taken advantage of the capability of the BiFC technique to be used in living cells. As seen with fixed cells, the BiFC puncta are very closely associated with the mitochondria and remain as such throughout the course of live-cell videos taken over a 10 minute period. The BiFC puncta show high photostability as the signal intensity did not diminish during image acquisition, strengthening this techniques usefulness in living systems. Here, we have shown that the BiFC puncta are very stable structures and their numbers do not change over a 10 minute time frame. Of course, as discussed in **section 3.4**, the reversibility of the BiFC technique has not been conclusively shown and therefore, it might not be possible to detect contact dissociation in real-time using this approach (Kerppola, 2006). However, we also do not see any increase in BiFC puncta number, which suggests that these tight contact sites are very defined structures and perhaps, can only be formed at specific membrane regions. Although for the most part, these structures did not move much within a cell, there was a very

high correlation between the movement of the BiFC puncta and the movement of its associated mitochondrion. In support of this, it had been previously been shown by live-cell imaging that the ER and mitochondria remain co-localised as they moved along acetylated microtubules (Friedman et al., 2010). However, the experiment by Friedman *et al* was only suggestive of maintained association between the ER and mitochondria as it relied on diffraction-limited co-localisation in comparison to our results which more definitively shows maintained organelle contact by labelling ER-mitochondria junctions of defined distances (Friedman et al., 2010). The utility of the BiFC system in living-cells in these sets of experiments also highlights the major advantage of this technique over alternative methods such as electron microscopy or the *in situ* proximity ligation assay which are limited to fixed cells (Tubbs et al., 2014).

4.4.2 The formation of tight ER-mitochondria junctions results in an elevation of mitochondrial calcium concentration and hyperpolarisation of the membrane

As mentioned, the punctate pattern of fluorescence generated by expression of the V1-ER / V2-Mito plasmids is consistently associated with a sub-population of mitochondria within the cell. Our data here shows that this sub-set of mitochondria, associated with a tight membrane contact site, have higher than average mitochondrial calcium levels and membrane potential in comparison to the mean values of the whole mitochondrial network. The elevation in mitochondrial calcium concentrations and hyper-polarisation of the membrane may be driving factors that encourage the formation of tight contact sites with the ER membrane or they could be a consequence of contact formation. When cells were treated with oligomycin to hyper-polarise mitochondrial membrane potential, there was no significant change in the number of ER-mitochondria contact sites as quantified by our BiFC method or by fluorescence co-localisation analysis. Similarly, rapid elevations in cytosolic Ca^{2+} mediated by Gq-coupled DREADD receptor activation did not significantly increase the number of BiFC puncta per cell, however, it is has been suggested that because of the time needed for fluorophore maturation after reformation of the split

fluorescent fragments, the BiFC technique is not suitable for detecting rapid changes in real-time (Kerppola, 2006). It is possible that a chronic, more gradual elevation in cytosolic Ca^{2+} could increase the number of BiFC puncta per cell as a mechanism to maintain calcium homeostasis (Wang et al., 2000; Goetz et al., 2007) It is also a possibility that any change in ER-mitochondria associations could specifically effect contact sites with a junction thickness outside of the spatial range of the BiFC reporter proteins, which would suggest that contact sites < 10 nm in thickness are not specifically involved with the calcium exchange function of MAMs. This would be in agreement with previously published data indicating that a tightening of ER-mitochondria junctional complexes to a distance of 7 nm was not permissive to inter-organelle calcium exchange (Csordas et al., 2010). The collective data is suggestive of increased mitochondrial membrane potential and calcium concentrations being a consequence of contact formation, but further experiments could be carried out to strengthen this observation. Indeed, an inversely proportional relationship between the length of an ER-mitochondria contact site and mitochondrial calcium concentrations has been experimentally demonstrated and furthermore, chemically-induced elevations in ER-mitochondria contacts were associated with increases in both mitochondrial calcium concentrations and membrane potential (Bravo et al., 2011; Csordas, 2006).

4.4.3 Contact sites labelled by the Venus reporter proteins may not be permissive for the autophagosome initiation complex

It has been proposed that MAMs are contributors of membrane during autophagosome formation but it is believed that this process is restricted to particularly wide junctions of approximately 50 nm, far beyond the maximum distance the split Venus proteins can report on (Hamasaki et al., 2013; Giacomello and Pellegrini, 2016). In agreement with this, we have shown that ATG5 and ATG14 puncta, early markers of autophagosome formation, do not co-localise with BiFC puncta. This data provides supporting evidence that specific functions of the MAMs

can be attributed to different sized junctions and that ER-mitochondria contact sites < 10 nm are not wide enough to facilitate autophagosome formation.

4.4.4 BiFC puncta may be spatially linked to mitochondrial fission events

Finally, we investigated the association of the BiFC puncta with another function of the MAMs, the regulation of mitochondrial fission events (Friedman et al., 2011). This was carried out by quantifying the number of BiFC puncta within close proximity to replicating nucleoids as labelled by fluorescently tagged POLG2. Previously, it was shown that 73% of POLG2 puncta localised within 1 µm of mitochondrial division events and were spatially linked to ER-mitochondria sites of undefined junction thickness (Lewis et al., 2016). Due to the approximately two-fold difference in the number of POLG2 puncta in comparison to BiFC puncta per cell as we have seen here, it is unlikely that mitochondrial division occurs exclusively at ER-mitochondria contact sites < 10 nm. However, we have demonstrated that 66 ± 6 % of BiFC puncta are within 1 µm of a replicating nucleoid, a figure that is comparable to that seen by Lewis *et al* and 33.5 ± 4.3 % were in very close proximity at only 200 nm apart and therefore, there may be a functional association between tight ER-mitochondria contact sites and mitochondrial fission events. To test this more robustly, this experiment should be repeated using an additional punctate protein marker with no known association with MAMs in order to test the statistical significance of any association between MAMs and POLG2 puncta versus random overlap. Additionally, the laser scanning confocal microscopy (LSCM) system used for these experiments has a relatively slow acquisition speed and therefore it was not possible to accurately capture mitochondrial division events in real-time. Replication of these experiments using a system such as a spinning-disk confocal microscope that scans an image with multiple pin-holes simultaneously and has acquisition speeds in the magnitude of 100-1000 times faster than LSCM systems, would allow us to correlate mitochondrial fission events with BiFC puncta in living cells.

4.5 Chapter conclusion

Overall, the data presented in this chapter suggests that tight ER-mitochondria contact sites < 10 nm in thickness are not associated with autophagosome formation nor are they involved in regulating calcium homeostasis. It may be the case that these processes are functionally linked to wider organelle contact sites and future experiments using BiFC reporter proteins with elongated linker sequences could be carried out to test this hypothesis. A proportion of contact sites labelled by the BiFC system may be spatially linked to replicating nucleoids and possibly, mitochondrial division events but additional experiments will be required in order to strengthen this observation. Furthermore, the formation of these tight contact sites results in an elevation of mitochondrial calcium concentration and hyper-polarisation of the mitochondrial membrane for a sub-population of mitochondria.

As membrane contact sites are dynamic and complex structures, it is unlikely that any one function of the MAMs can be exclusively attributed to ER-mitochondria junctions of a tightly defined thickness range. While these contact sites can vary in their length and thickness, it is important to consider that they may also vary in their protein compositions, a variable that is not discriminated by the BiFC technique. Therefore, MAMs of the same thickness could still be performing different functions depending on the specific protein levels at these sites.

Chapter 5
VAPB and mitochondrial associated membranes

5.1 Background

As outlined in the introduction to this thesis, the VAP protein family are key regulators of organelle contact sites and specifically, VAPB has a very strong link to neurodegeneration through the P56S point mutation resulting in the onset of ALS (Nishimura et al., 2004). Therefore, it is plausible to hypothesise that a dysfunction to MAMs, consequent of the VAPB mutation, may play a role in disease pathogenesis. Percoll gradient fractionation of subcellular organelles revealed that VAPB is enriched specifically in the MAM fraction and associates with the outer mitochondrial membrane protein PTPIP51 to regulate ER-mitochondria associations (De Vos et al., 2012). VAPB-P56S shows increased binding with PTPIP51 over wild-type VAPB with approximately 3-4 times higher levels of PTPIP51 being detected associated with the mutant protein in immunoprecipitation experiments (De Vos et al., 2012). Furthermore, there was a 2-fold enrichment of VAPB-P56S in the MAM fraction compared to the wild-type protein (De Vos et al., 2012). To investigate how expression levels of VAPB may influence the MAMs structurally, Stoica *et al* used high resolution EM studies and quantified areas of the OMM that were within 30 nm of the ER and demonstrated that siRNA-mediated knock-down of VAPB or PTPIP51 reduced associations from approximately 12% of the mitochondrial surface area being in close apposition to around 6% (Stoica et al., 2014). In contrast, overexpression of VAPB or PTPIP51 increased associations to around 20-30% while co-expression of both proteins had a distinct phenotype whereby approximately 50% of the OMM was in contact with the ER (Stoica et al., 2014). Overexpression of VAPB or PTPIP51 was found to inhibit autophagy while loosening ER-mitochondria contacts by siRNA knock-down of VAPB or PTPIP51 was permissive to autophagosome formation and increased the presence of autophagic markers

(Gomez-Suaga et al., 2017). The influence over autophagosome formation was linked to changes in Ca^{2+} exchange from the mitochondria to the ER as a result of altering contact thickness (Gomez-Suaga et al., 2017). The data indicates both a morphological and functional disruption to the MAMs by altering the levels of VAPB or its binding partner, PTPIP51.

Through the generation of various fusion proteins encompassing different domains of VAPB, it was shown that the interaction between VAPB and PTPIP51 relies on the entire cytosolic face of VAPB (Stoica et al., 2014). As discussed in detail in the introductory chapter **(sections 1.3.1 – 1.3.3)**, VAPB is composed of an N-terminal MSP domain and a central coiled-coil domain, making up the cytoplasmic face of the protein, and a C-terminal hydrophobic transmembrane domain (Nishimura et al., 1999). As mentioned previously the MSP domain of VAP proteins is cleaved and secreted and immunoblotting a selection of tissue from an adult male rat showed that the MSP domain of VAPB is cleaved specifically in neuronal tissue while in contrast, cleaved products of VAPA are observed in a number of different tissues but only low levels of truncated protein were detected in forebrain and cerebellum tissue (Gkogkas et al., 2008). The presence of these truncated VAP species appears to be developmentally regulated and are enriched in adult tissue in comparison to embryonic tissue (Gkogkas et al., 2011). While cleavage of wild-type VAPB in neurons can generate an intact MSP domain, the ALS-linked VAPB-P56S protein was resistant to this proteolytic event when expressed in rat primary neuronal cultures (Gkogkas et al., 2011). The presence of the P56S point mutation had previously been shown to disrupt the native structure of the MSP domain while also conferring the ability of the MSP domain to interact with lipids and adopt a highly-helical conformation (Qin et al., 2013; Shi et al., 2010). This structural change may be responsible for the mutant protein's resistance to cleavage of the MSP domain.

Interestingly, expressing fluorescently tagged full-length and truncated CC-CT (coiled-coil-C-terminus) forms of VAPB demonstrated that the two proteins show extensive co-localisation on the ER but there was a proportion of truncated protein

that did not co-localise and may indicate a unique localisation of this protein (Gkogkas et al., 2011). Dissimilar patterns of proteolytic processing of VAPA and VAPB could highlight some yet undiscovered differences between the two proteins or in the case of VAPB, suggests the presence of a neuron-specific protease. An alternative suggestion is that differences in the sub-cellular localisation of these proteins could expose them to different proteolytic complexes (Gkogkas et al., 2011). In peripheral blood leukocytes (PBL) and cerebrospinal fluid (CSF) taken from healthy patients and non-ALS controls, a high concentration of VAPB cleavage products and very low levels of VAPB were detected, suggestive of high proteolytic processing of VAPB (Deidda et al., 2014). This was in stark contrast to SALS patients where VAPB cleavage products were only detected in the CSF of 40% of patients even though no VAPB mutations were detected in these patients (Deidda et al., 2014). This result provides supporting evidence for a wider role of VAPB in ALS pathogenesis, not just restricted to specific ALS8 cases and furthermore, implicates that a disruption to the truncation of VAPB may play a role in disease progression (Deidda et al., 2014). In *C.elegans*, VAP MSP domains secreted from neurons regulates mitochondrial localisation and function in muscle tissue (Han et al., 2012) and impairment of MSP signalling to the muscle causes altered lipid homeostasis and impaired energy metabolism, which could account for the energy metabolism defects observed in ALS patients (Han et al., 2013b). If the cleavage of VAPB or the presence of the truncated protein has a specific effect on ER-mitochondria associations, it has yet to be elucidated.

5.2 Chapter aims

Published EM data has shown a role of VAPB in influencing ER-mitochondria contact sites of <30 nm and a disruption to the MAMs is observed when the levels of this protein are altered (Stoica et al., 2014). In this chapter, we aimed to investigate any changes in tight ER-mitochondria interactions, as reported on by BiFC system, that may arise from altering the levels of VAPA and VAPB. Furthermore, we sought to test the effect of expression of the ALS-linked VAPB-P56S mutant protein on the contact

sites. Finally, sub-cellular organelle fractionation techniques were employed on rat brain and liver tissue to explore the proteolytic cleavage of VAPA and VAPB in more depth.

5.3 Results

5.3.1 Overexpression of VAPB-P56S but not wild-type VAPB significantly increases tight ER-mitochondria contacts

Previously published data has provided supporting evidence that overexpressing VAPB in mammalian cell lines increases the mean percentage area of the OMM that is in close proximity to the ER (Stoica et al., 2014). However, this data does not provide information on whether overexpressing wild-type VAPB promotes the formation of new contact sites or whether it simply tightens pre-existing contact sites that are tethered by the VAPB/PTPIP51 interaction. Immunoprecipitation experiments have shown an increased association of VAPB-P56S with PTPIP51 at the MAMs in comparison to wild-type VAPB and therefore, we could predict that this interaction may also increase ER-mitochondria contacts although this has not been conclusively shown (De Vos et al., 2012). Here, we have overexpressed double epitope-tagged wild-type VAPB, the ALS-linked VAPB-P56S or a non-pathogenic VAPB variant, VAPB-N29S, that was identified in human patients but is not known to cause any disease (unpublished data). In NSC34 cells stably expressing the V1-ER and V2-Mito reporter proteins and immunolabelled with an anti-Myc antibody, we observe the characteristic ER localisation of VAPB and VAPB-N29S while in cells expressing VAPB-P56S there is a clear mislocalisation of the protein from the ER into large aggregates as has been observed in a number of other studies **(Fig5.1A)**(Nishimura et al., 2004; Gkogkas et al., 2008)**.** Increases in the relative protein levels produced from different concentrations of DNA transfected were confirmed by anti-Myc immunofluorescent staining **(Fig5.1B)** and by western blotting **(Fig5.1C).** The data indicates that wild-type VAPB and VAPB-N29S are expressed at equivalent levels whereas a much lower level of VAPB-P56S is detectable from the same concentrations of DNA transfected, an observation which

has also been seen in other published studies (Kanekura et al., 2006). This difference in protein levels is believed to be due to the rapid rate of degradation of mutant VAPB-P56S in comparison to wild-type VAPB by the UPS (Papiani et al., 2012). Quantification of the mean number of BiFC puncta per cell showed a significant increase in cells transfected with both concentrations of VAPB-P56S tested in comparison to control cells transfected with a CMV-Globin vehicle control. No significant change was detected in cells overexpressing wild-type VAPB or VAPB-N29S **(Fig5.1D)**.

In summary, the data shows a significant increase in the number of BiFC puncta induced by expression of the ALS-linked VAPB-P56S but not from wild-type VAPB or VAPB-N29S. However, as these proteins were not expressed to the same levels, we cannot rule out that at equivalent levels of expression, wild-type VAPB may also induce an increase in tight ER-mitochondria contacts. To test this, the levels of Myc-VAPB-HA and Myc-VAPB-P56S-HA DNA were titrated and the relative levels of expression were tested by western blotting. The data indicates approximately equal levels of VAPB and VAPB-P56S are produced when the levels of Myc-VAPB-P56S-HA DNA transfected are ten-fold concentrated (10 ng to 100 ng DNA) **(Fig5.2A)**. We then examined whether lower levels of VAPB would significantly alter the number of BiFC puncta by transfecting 10 ng of Myc-VAPB-HA, 100 ng of Myc-VAPB-P56S-HA to express equivalent protein levels and which we have already shown to significantly increase the BiFC puncta number and 100 ng of Myc-VAPB-HA which previously had no effect on BiFC number. The results showed no significant change in BiFC number from expression of either concentration of VAPB but again, a significant increase was detected from expression of the mutant VAPB-P56S **(Fig5.2B).** The data indicates that expression of VAPB-P56S significantly increases the number of tight ER-mitochondria interactions in NSC34 cells however, it is not clear whether this is through an enhanced physical tethering role at the MAMs or through an indirect, secondary mechanism. Although the evidence is controversial, overexpression of wild-type or mutant VAPB in cells has been seen to trigger UPR through IRE1-mediated XBP1 splicing (Langou et al., 2010) and silencing of VAP expression

prevented the chemical-induced activation of UPR (Kanekura et al., 2006). Our previous data has shown that treating cells with tunicamycin to induce an ER stress significantly increased the mean number of BiFC puncta per cell and therefore, it is possible that VAPB-P56S may be increasing ER-mitochondria associations through the activation of the UPR. To test this, RNA was extracted from NSC34 cells expressing wild-type VAPB, VAPB-P56S or VAPB-N29S and reverse transcriptase PCR was performed to look for the splicing of XBP1 mRNA, indicative of UPR activation. No splicing of XBP1 mRNA was detected in any of the groups and therefore, overexpression of any of the VAPB variants did not seem to induce an ER stress response through the IRE1-XBP1 pathway **(Fig5.2C).** Furthermore, when treated with tunicamycin, splicing of XBP1 mRNA was detectable from all experimental groups and thus, we can conclude that overexpression of wild-type VAPB, VAPB-P56S or VAPB-N29S does not inhibit the chemical-activation of UPR in NSC34 cells **(Fig5.2C).** Therefore, we can conclude that the increase in BiFC puncta caused by overexpression of VAPB-P56S is not due to activation of the IRE1/XBP1 pathway and may be due to some other secondary mechanism or its enhanced binding with PTPIP51.

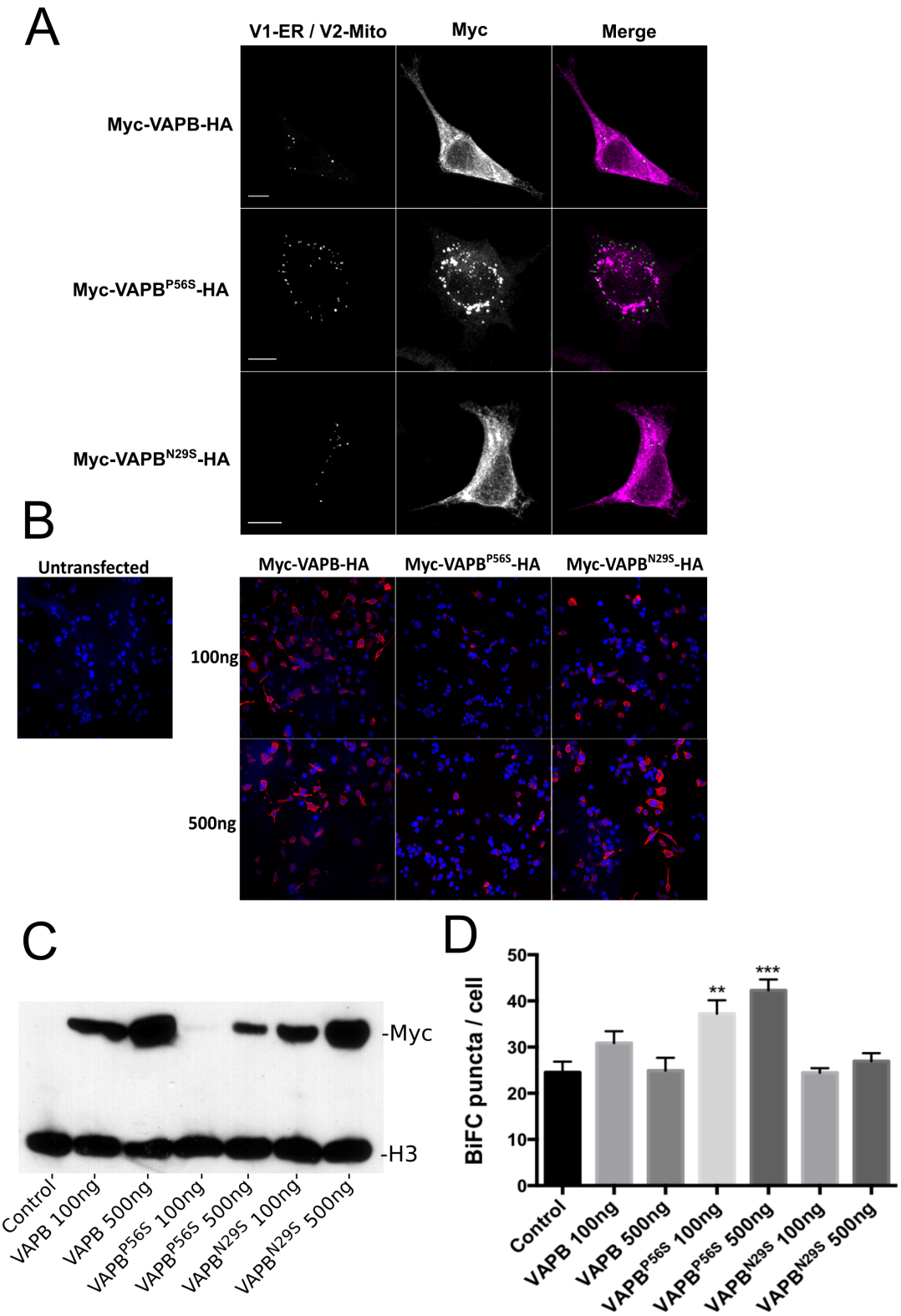

Fig 5.1: Overexpression of VAPB^{P56S} significantly increases the number of tight ER-mitochondria contacts per cell. (A) Representative images of NSC34 cells stably expressing V1-ER / V2-Mito reporter plasmids and transiently transfected with either

Myc- and Ha- tagged wild-type VAPB, ALS-linked VAPB-P56S or a non-pathogenic variant VAPB-N29S. Anti-myc immunostaining (magenta) was carried out to illustrate the mis-localisation of VAPB-P56S from the ER into cytoplasmic aggregates. **(B)** Anti-myc immunostaining (red) of NSC34 cells expressing the different VAPB constructs. Nuclei are labelled with DAPI (blue). **(C)** Western blot analysis of whole cell lysates extracted by SDS detergent, showing relative protein levels produced from equivalent concentrations of transfected DNA. Histone H3 was used as a loading control. **(D)** Overexpression of VAPB-P56S at both concentrations tested significantly increases the mean number of BiFC puncta per cell but no significant change is detected from overexpression of wild-type VAPB or VAPB-N29S. n = 3-4 independent experiments (3 replicates for VAPB-P56S experimental group, 4 replicates for control, wild-type VAPB and VAPB-N29S), 33-47 cells per experimental group. Statistical significance was carried out by one-way ANOVA, comparing the means of each group to the control group, followed by Dunnett's multiple comparisons test. ns (non-significant) $P>0.05$, $^{**}P<0.01$, $^{***}P<0.001$. Values indicate overall mean values from each independent replicate. Error bars indicate SEM.

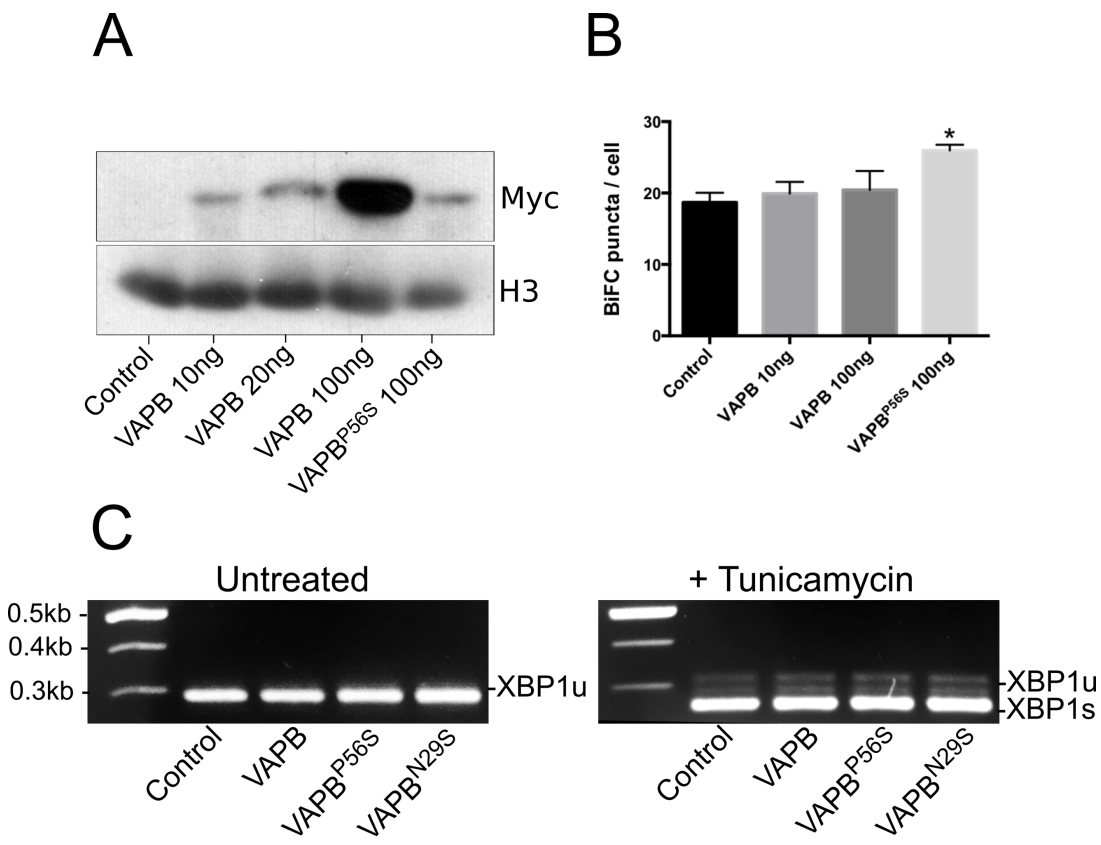

Fig 5.2: At equivalent protein levels, VAPB^{P56S} but not wild-type VAPB significantly increases the mean number of tight ER-mitochondria contacts. (A) Western blot analysis showing the relative protein levels detected from different concentrations of transfected plasmid DNA in NSC34 cells. **(B)** Overexpression of VAPB^{P56S} significantly increases the mean number of BiFC puncta per cell. No significant change was observed from expression of either concentration of wild-type VAPB in comparison to controls. n = 3 independent experiments (29-35 cells per experimental group). Statistical significance was determined using one-way ANOVA, comparing the mean of each experimental group to the mean of the control group, followed by Dunnett's multiple comparisons test. ns (non-significant). $P>0.05$, *$P<0.05$. Error bars represent SEM. Values indicate overall mean values from each of the three independent experiments. **(C)** A lack of XBP1 mRNA splicing from NSC34 cells overexpressing wild-type VAPB, VAPB^{P56S} or VAPB^{N29S} showed that no ER stress was induced from expression of any of the VAPB variants alone. Treatment of cells with 10 µg/ml Tunicamycin for 6 h induced splicing of XBP1 in all experimental groups.

5.3.2 Knock-down of VAP expression has no effect on the number of tight ER-mitochondria contact sites

Although the overexpression of VAPB had no significant impact on the number of tight ER-mitochondria interactions, we wanted to test whether a knock-down of expression of either VAPA or VAPB or both would influence organelle associations. Previous data has illustrated a reduction of approximately 50% in the surface area of the OMM closely opposed to the ER from a VAPB knock-down when contact sites up to 30 nm in thickness were quantified (Stoica et al., 2014).

Western blot analysis using antibodies against whole VAPA and VAPB (VAPB serum #38 was used and is simply referred to as VAPB antibody in the rest of the text) was used to demonstrate a specific knock-down of VAP protein levels in NSC34 cells mediated by siRNA transfections **(Fig 5.3A).** VAPA and VAPB ran slightly higher than would be expected from its primary structure at around 34 kDa but the knock-down of signal in samples treated with the corresponding VAPA or VAPB siRNA demonstrates that this is the correct band. Furthermore, this was also observed in previous experiments carried out by Skehel *et al* (Gkogkas et al., 2011). No change in VAPA levels resulted from a knock-down of VAPB expression and vice versa. Furthermore, depletion of the ER-mitochondria tether MFN2, did not alter either VAPA or VAPB levels, in agreement with data by Stoica *et al* (Stoica et al., 2014). The data indicates that in the NSC34 cell line, the levels of VAP do not seem to be influenced by one another nor are they dependent on the MAM protein MFN2. In our stable NSC34 cell consistently expressing the Venus fusion reporter proteins, siRNA knock-down of VAPA, VAPB or both VAPA and VAPB had no significant impact on the mean number of BiFC puncta per cell **(Fig5.3B).**

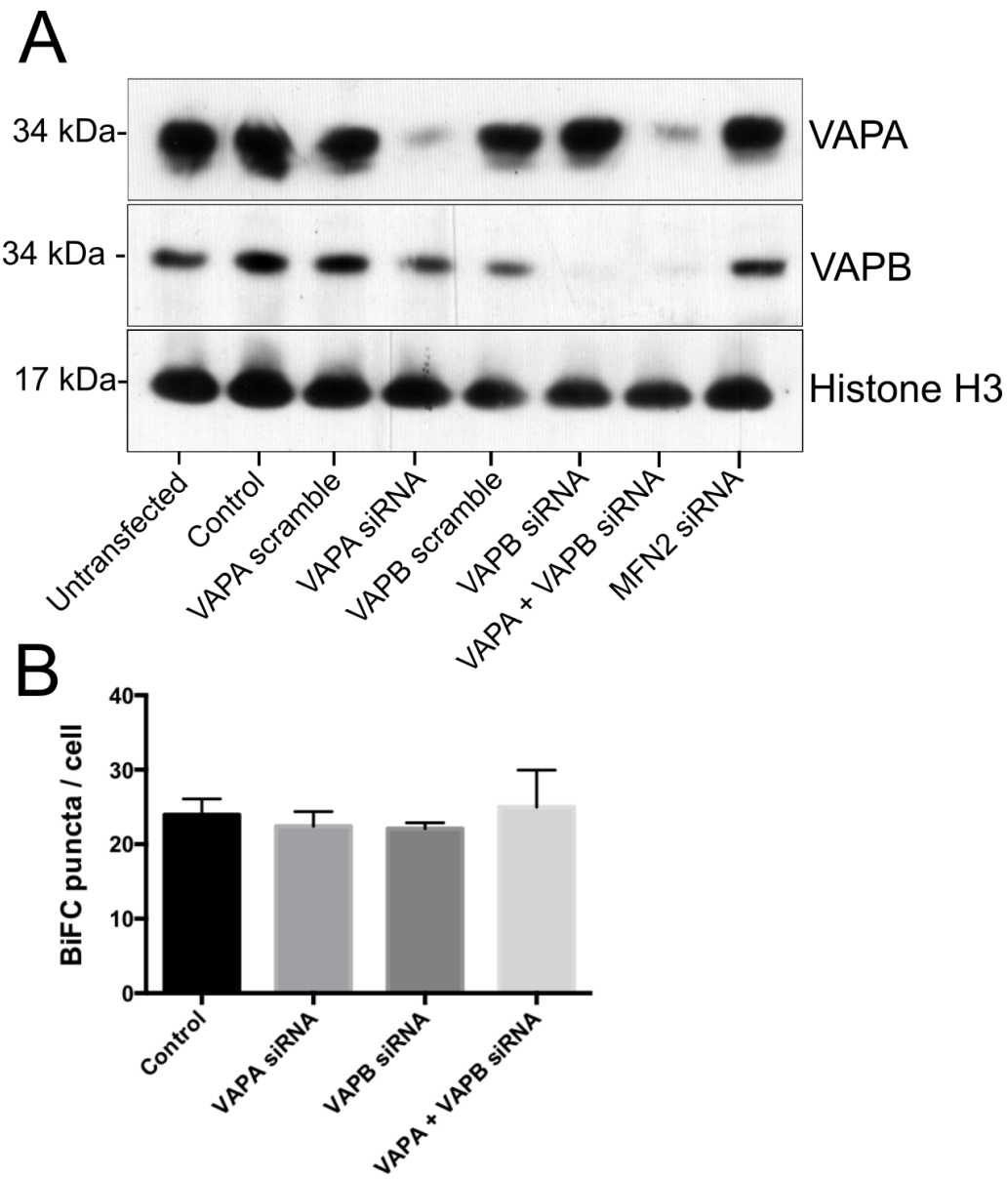

Fig 5.3: Knock-down of VAP expression does not significantly alter the mean number of BiFC puncta in stably transfected NSC34 cells. (A) Western blot analysis showing a knock-down of VAPA expression in lanes treated with VAPA siRNA and both VAPA and VAPB siRNA and a knock-down of VAPB expression in lanes treated with VAPB siRNA and both VAPA and VAPB siRNA. No change in VAPA or VAPB levels was detected from a knock-down of the MAM protein MFN2. Control well represents cells treated with Dharmacon non-targeting siRNA control pool. Histone H3 was used as a loading control. 50 nM of siRNA was transfected per experimental group for 48 h. **(B)** Treatment of NSC34 cells stably expressing V1-ER / V2-Mito reporter proteins with VAPA siRNA, VAPB siRNA or both VAPA and VAPB siRNA showed no significant changes in the mean number of BiFC puncta per cell. n = 3 independent experiments (35-49 cells per experimental group). Statistical significance was tested by one-way

ANOVA comparing the mean of each column to the mean of the control column, followed by Dunnett's multiple comparison test. P>0.05.

It's possible that a knock-down of VAP proteins could be decreasing the number of ER-mitochondria contacts but this may not be detectable by the BiFC method, depending on the reversibility of the technique. To try and overcome this potential limitation, siRNA against VAPA and VAPB was transfected into NSC34 cells, 24 hours before the transient transfection of V1-ER and V2-Mito reporter proteins. By doing so, it would allow any VAP-dependent changes in the MAMs to occur before the expression of the Venus fusion reporter proteins. Western blot analysis showed that in this manner, there was still a strong knock-down of VAPA and VAPB levels from the appropriate siRNA transfections **(Fig 5.4A).** Quantification of the mean number of BiFC puncta per cell again demonstrated no significant change from a loss of VAP expression in comparison to control groups **(Fig 5.4B).**

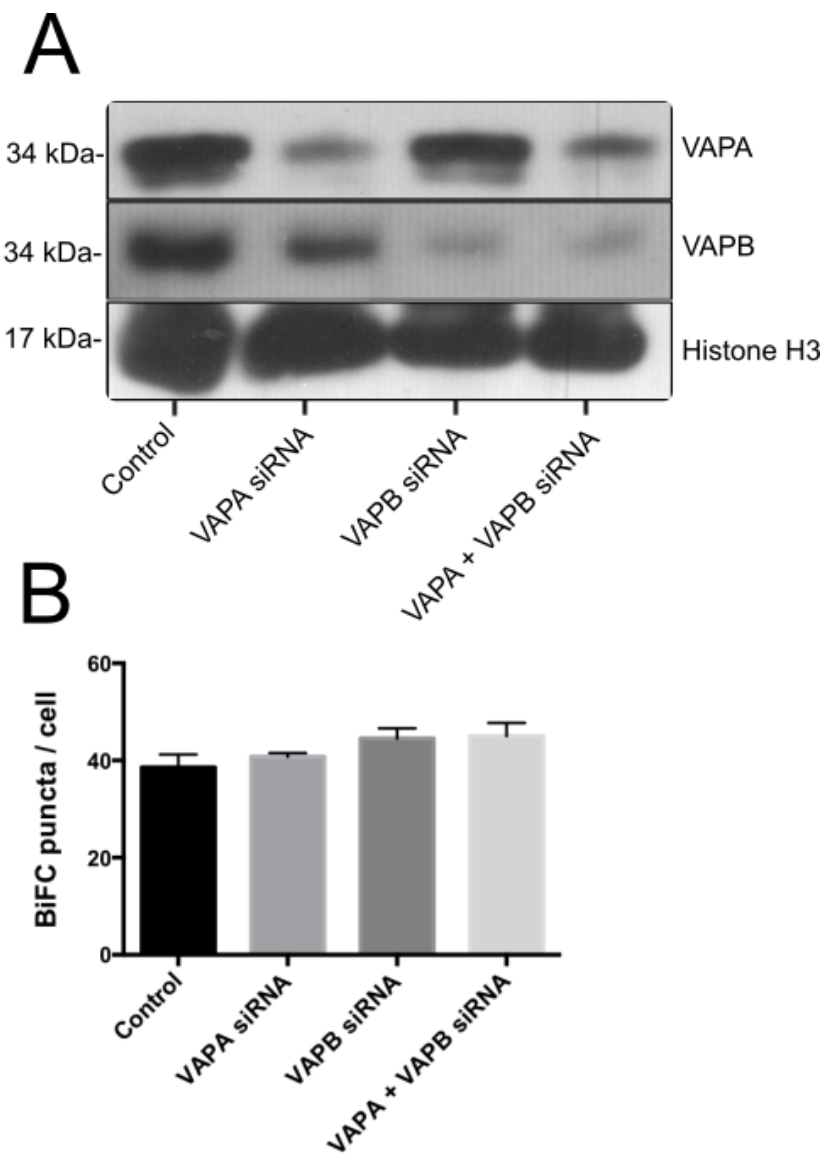

Fig 5.4: siRNA mediated knock-down of VAP protein levels before the transient expression of Venus fusion proteins does not significantly change the number of BiFC puncta in NSC34 cells. (A) Western blot analysis showing that a knock-down of VAPA and VAPB still occurs even when V1-ER and V2-Mito plasmids are transiently transfected 24 hours after the transfection of siRNA. **(B)** No significant change in BiFC puncta number in comparison to control group was detected. Statistical significance was tested by one-way ANOVA comparing the mean of each column to the mean of the control column, followed by Dunnett's multiple comparison test. $P>0.05$. $n = 4$ independent experiments (42-48 cells per experimental group).

Overall, we can conclude that tight ER-mitochondria contacts, approximately 6-10 nm in length, reported on by the Venus reporter proteins are not dependent on the expression of VAP proteins. The previously reported alterations in the MAMs, induced by changes in VAP expression, may allude to a distinct sub-population of MAMs greater than 10 nm in thickness that are mediated by the levels of VAPB (Stoica et al., 2014).

5.3.3 Percoll gradient centrifugation successfully purifies ER, mitochondria and MAM fractions from rat liver tissue homogenates.

Through a series of centrifugation steps in Percoll gradient medium (as described in **section 2.7** of chapter 2 of this thesis), it allows for the biochemical purification of the MAMs from animal tissue homogenates. This permits the detection of protein species specifically within the MAMs in comparison to the bulk ER or mitochondria. In order to optimise the technique and prove the relative purity of the fractions, whole liver and brain tissue was extracted from a 5 month old wild-type rat and the bulk ER, crude mitochondria (consisting of mitochondria and MAMs together), purified mitochondria and purified MAM fractions were isolated and equal protein concentrations of each fraction were loaded on an SDS-PAGE gel and probed for different markers with immunoblotting. The ATP-synthase subunit β (ATPB) is targeted to the inner mitochondrial membrane (Giorgio et al., 2013) and therefore it should be enriched in the mitochondrial fractions and absent from the ER and MAM fractions in liver tissue which can be clearly observed in **Fig5.5A**. In contrast, VAPB was detectable within the ER and MAM fractions as expected and VAPA was also enriched in the MAM and ER fractions with a faint signal in the crude mitochondrial fraction in homogenised rat liver tissue **(Fig5.5A)**. Interestingly, a lower molecular weight protein species was detected by the VAPA antibody specifically in the MAM fraction, which corresponds to the size of the cleaved VAPA protein species previously observed in whole liver tissue in the Skehel lab (Gkogkas et al., 2008). These results indicate that Percoll gradient centrifugation efficiently purifies subcellular organelle fractions however, in fractionated brain tissue from the wild-type rat, there was no detectable signal in the MAM fraction for any of the

antibodies tested (data not shown). To test if this was simply due to low protein concentrations, brain tissue from two wild-type rats was pooled and gram for gram equivalent amounts of starting brain tissue and liver tissue were used for subsequent organelle fractionation. Although the same amount of starting material was used, BSA protein quantification showed lower protein levels in all of the brain fractions in comparison to the equivalent liver fractions, however, we were still able to obtain a detectable brain MAM fraction signal in this case which showed the expected pattern of expression of VAPB and VAPA in agreement with liver fractions (**Fig5.5B)**. In contrast to the liver fractions however, no truncated VAPA species was detected in brain tissue which is in agreement to the published literature (Gkogkas et al., 2008). We did observe a truncated VAPB product of the same molecular weight as the VAPA cleavage product which was confined specifically to the bulk ER fraction and an intermediate product of around 20 kDa that followed the expression pattern of the full-length protein (**Fig5.5B)**. In pure neuronal cultures, protein levels of full-length and truncated VAPB are comparable but when glial cells were also present, relative levels of full-length VAPB were higher (Gkogkas et al., 2011). As we have fractionated whole brain tissue, it is not unexpected that we see relatively lower levels of truncated product (**Fig5.5B)**. It is important to note that these results were obtained from only two animals and therefore, more replications are needed in order to draw a strong conclusion however, the results do highlight an interesting possibility that the proteolytic processing of VAPA and VAPB may occur in different subcellular compartments in brain and liver tissue.

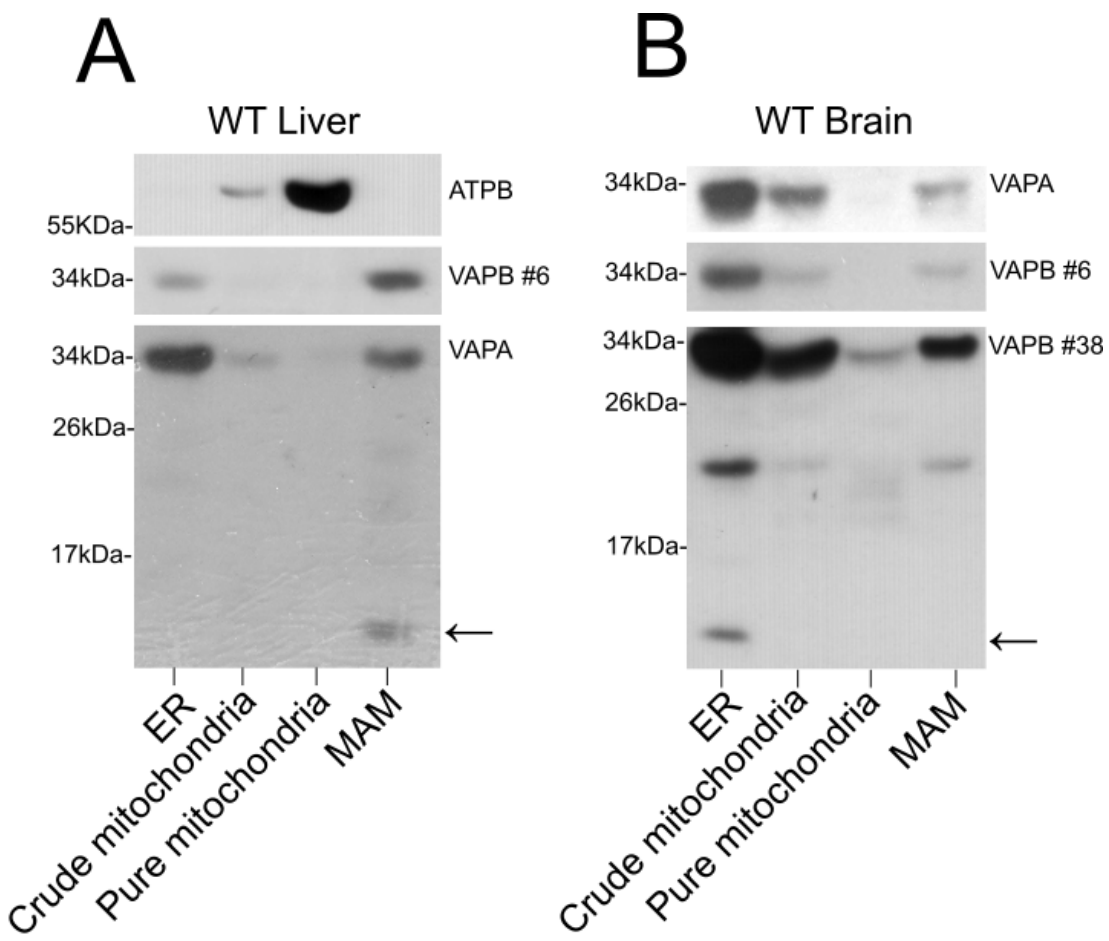

Fig 5.5: Protein species in subcellular fractions generated from wild-type rat liver and brain tissue. (A) Immunoblotting of rat liver fractions indicates the relative purity of each of the fractions, showing the presence of the inner mitochondrial membrane protein ATPB within the crude and pure mitochondrial fractions while VAPB (as labelled by anti-VAPB #6) and VAPA are enriched in the ER and MAM fractions, with a low signal of VAPA being detected in the crude mitochondrial fraction which also contains some MAM proteins. Consistent with all other blots, VAP species ran slightly higher than expected at approximately 34 kDa. Truncated VAPA protein is present specifically within the MAM fraction and is indicated by the arrow symbol. **(B)** In pooled brain tissue from two wild-type animals, VAPA and VAPB proteins (As labelled by both anti-VAPB #6 and #38) are detectable within the appropriate fractions. In contrast to the liver fractions, no truncated VAPA protein is detectable however, truncated VAPB species of around 20 kDa are detectable in the ER, crude mitochondria and MAM fractions while there is a lower molecular weight product, confined to the ER fraction as indicated by the arrow.

5.4 Discussion

5.4.1 Tight ER-mitochondria contact sites appear to be formed independently of VAP protein levels

In the first part of this chapter, data is presented on the influence of VAP protein levels on tight ER-mitochondria junctions as reported on by the BiFC reporter proteins. When wild-type VAPB or a non-pathogenic point mutation of VAPB, VAPB-N29S, were overexpressed in NSC34 cells, there was no significant change in the number of BiFC puncta per cell and immunofluorescent staining revealed a reticular localisation pattern for both proteins. Previous work by Stoica *et al* showed that overexpression of wild-type VAPB did induce an increase in ER-mitochondria associations however, this is not necessarily in contradiction to our data as firstly, this group looked at extensions in the surface area of the mitochondria in close proximity to the ER of pre-existing contact sites, a measurement which is not detectable from the diffraction-limited imaging of cells expressing the BiFC reporter proteins (Stoica et al., 2014). Secondly, this group measured contact sites of up to 30 nm in thickness whereas our reporter proteins would quantify contact sites of approximately 10 nm in thickness (Stoica et al., 2014). Therefore, increases in VAPB may influence ER-mitochondria contact sites but this may be limited to increasing the lengths of pre-existing VAPB-mediated contacts or specifically it could promote the formation of new contact sites >10 nm in thickness, outside of the detectable range of the BiFC reporter proteins. We did observe a significant increase in BiFC puncta upon the expression of the ALS-linked VAPB-P56S, accompanied by the appearance of large intracellular aggregates, even though the relative protein levels of VAPB-P56S were much lower than levels of wild-type VAPB or VAPB-N29S. It is not clear from our data whether this increase is due to direct binding of the mutant VAPB protein with its MAM-tethering partner PTPIP51 or if this is an indirect increase resulting from some secondary mechanism. As discussed in **section 1.4.1** of the introduction of this thesis, although controversial, there is some evidence to suggest that expression of VAPB-P56S induces an ER stress response via the IRE1/XBP1 pathway (Langou et al., 2010). In **section 3.3.6** of chapter 3 of this thesis, we have

shown that the induction of ER stress significantly increases the mean number of BiFC puncta per cell, however our data here shows that overexpression of wild-type or mutant VAPB in NSC34 cells does not induce splicing of XBP1 mRNA and therefore we can conclude that the increase in contact sites is not due to the activation of the IRE1 ER stress response. It has been shown that VAPB-P56S has enhanced binding to PTPIP51 and is present in the MAM fraction at greater levels in comparison to wild-type VAPB (De Vos et al., 2012) and therefore, it is possible that this increase in ER-mitochondria contact sites could be a direct result of increased tethering at the MAMs. However, if this was the case, one might expect that this effect would be recapitulated upon over-expression of wild-type VAPB, particularly as the wild-type protein is expressed at much greater levels. Furthermore VAPB-P56S aggregates do not co-localise well with BiFC puncta, providing supporting evidence that the increase in contacts is more likely due to some secondary effect of VAPB-P56S expression, although further work will be required in order to elucidate the mechanism of action. Future work could involve the over-expression of wild-type VAPB or VAPB-P56S in cells with a knock-out of PTPIP51 expression which would demonstrate that any resulting increase in ER-mitochondria contacts would be independent of VAPB-PTPIP51 binding. Determining the protein composition of tight ER-mitochondria contact sites as labelled by the BiFC system could also provide valuable insight into the VAPB-P56S-mediated increases in puncta number. It is unclear whether VAPB is a component of these tight junctions but future pull-down assays may indicate the extent to which endogenous full-length VAPB oligomerises with the V1-ER construct, which could be suggestive of its presence at sites labelled by the BiFC proteins. Additionally, immunogold labelling of VAPB in combination with high-resolution EM studies could further shine some light on the protein compositions of MAMS <10 nm in thickness. If these contact sites are too tight to permit the formation of the VAPB-PTPIP51 complex, it would indicate that the mutant VAPB –related increases in BiFC number are more likely due to an indirect secondary effect of the mutation rather than as a consequence of direct protein binding.

Similarly, siRNA knock-down of either VAPA or VAPB had no significant impact on the number of BiFC puncta per cell, even when VAP protein levels were knocked-down before the expression of the BiFC reporter proteins to overcome the potential limitation of the irreversibility of the BiFC technique. These results suggest that tight ER-mitochondria contact sites <10 nm are formed independently of VAP protein levels and based on the existing literature, it is more likely that VAPB/PTPIP51 regulates contact sites between 10-30 nm in thickness. EM imaging could be used to provide strength to this observation, simultaneously illustrating that altering VAPB levels regulates contact sites >10 nm as previously shown by Stoica *et al,* while having no effect on the number of contact sites <10 nm (Stoica et al., 2014). However, as this was an siRNA-mediated reduction in VAP protein levels, it is possible that the remaining low VAP protein levels were sufficient to maintain organelle contact formation. Future work using transgenic cell lines with a knock-out of the VAP genes could strengthen the conclusions made from this experiment.

5.4.2 Subcellular organelle fractionation suggests differences in the proteolytic processing of VAP proteins

In addition to optical imaging techniques, MAMs can be purified biochemically in order to quantify MAM proteins specifically in comparison to other subcellular compartments. In the second part of this chapter, data is presented on the subcellular organelle fractionation of rat brain and liver tissue. As stated previously, the data presented here is preliminary due to time constraints and limitations on animal availability. To optimise the technique and prove the relative purity of the fractions, organelle fractionation was performed on liver and brain tissue from a wild-type 5 month old rat and while a strong signal was detectable for all of the antibodies tested within the liver fractions, no protein signal was observed within the MAM fractions of brain tissue. It was unclear at this time whether this was simply a result of low protein concentrations or perhaps there was relatively lower MAMs in brain tissue in comparison to liver. When brain tissue from two wild-type rats was pooled and weighed to ensure equivalent starting weights of brain and liver tissue,

BCA protein quantification of the obtained fractions showed lower protein concentrations within the brain tissue for every fraction when compared to the equivalent fraction in liver tissue, demonstrating that gram for gram, brain tissue has lower protein concentration than liver. A detectable signal could be obtained in the MAM fractions of pooled brain tissue, providing supporting evidence that the previous absence of signal was due to low protein concentrations and is important to bear in mind for future experiments.

Previously, the cleavage of VAPA and VAPB in mammals had only been demonstrated on a whole tissue level (Gkogkas et al., 2008) but our data suggests site specific cleavage of VAPA in the MAM fraction and VAPB within the bulk of the ER **(Fig5.5)**. Although only shown from one animal, it highlights the interesting possibility that the observed differences in the proteolytic processing of the closely related VAP proteins could be due to differences in where this cleavage event takes place or alternatively, it may indicate differences in where the truncated product is retained post-cleavage. This data could also imply that VAP proteins present at the MAMs could behave differently to those localised to the bulk of the ER for example, the binding of VAPB to PTPIP51 on the OMM requires the entire cytosolic domains of VAPB (Stoica et al., 2014) and therefore, it is possible that the formation of this protein complex at the MAMs could inhibit the cleavage event in some manner and hence, we only observe truncated VAPB within the bulk of the ER. If this was the case, it could also offer an explanation as to why the P56S point mutation is resistant to this cleavage event, as the mutation causes an enrichment of the protein within the MAM fraction with enhanced binding to PTPIP51 (De Vos et al., 2012). As the cleavage of VAPB has implications in the wider field of ALS beyond ALS8 specifically (Deidda et al., 2014), elucidating the specific mechanisms of VAPB proteolysis is important and although it is preliminary, the data here presents significant opportunity for further investigation in this area in the future.

The biochemical purification of MAM fractions from rat tissue has presented a significant avenue for future research into the role of VAPs in these subcellular compartments. As our previous data presented an interesting suggestion on possible

subcellular compartment specific processing of VAPA and VAPB, we wanted to further investigate this proteolytic event in transgenic rat models with either a homozygous knock-out of exon 1 of VAPB or expressing the ALS-linked VAPB^{P56S} mutation (as outlined in **chapter 2, section 2.7**) and some preliminary experiments have already been carried out to detect these protein species. Not a lot of information is known about the proteolytic processing of VAPA and VAPB or the role of the truncated proteins at the MAMs, other than that the cleavage of VAPB seems to occur specifically within nerve tissue while processing of VAPA takes place in a much greater variety of tissues (Gkogkas et al., 2008). Additionally, the presence of the P56S point mutation appears to inhibit this proteolytic processing event (Gkogkas et al., 2011). Due to the aforementioned restrictions on animal availability, the experiments could only be carried out on liver tissue for the time being as this was sufficiently concentrated to give detectable signals within the MAM fractions. Early data seems to suggest that a knock-out of VAPB or the presence of the VAPB-P56S mutation does not seem to influence the cleavage of VAPA in liver tissue, as the ~15 kDa truncated protein species is detected within all transgenic models tested but additional experiments are needed in this area.

5.5 Chapter conclusion

Overall, the data presented in this chapter shows that tight ER-mitochondria contacts <10 nm in thickness are not influenced by the overexpression of exogenous VAPA or VAPB but do increase upon the expression of the ALS-linked VAPB-P56S protein. This increase is not due to the induction of ER stress via the IRE1 pathway and further work will be required to determine the exact nature of the increased organelle associations and to deduce the phenotypic consequences of this change. Moreover, the number of BiFC puncta does not change in response to a reduction of VAP protein levels however, as this was carried out by siRNA-mediated protein knock-down, it is possible that remaining VAP protein levels were sufficient for maintaining organelle contact sites. Future work in this area could involve the use of transgenic cell lines with a complete knock out of VAP genes to further assess the impact of VAP knock-out on tight ER-mitochondria contact sites.

The data here also highlights significant avenues for future work into subcellular compartment-specific processing of VAPA and VAPB proteins. Early work suggests the possibility of site specific processing of VAPA and VAPB within different subcellular compartments of brain and rat tissue from animal models. Demonstration of the relative purities of the biochemically isolated MAM fractions also provides the potential for investigation into alterations of protein levels of other MAM proteins in the VAPB knock-out or VAPB-P56S transgenic rat models.

Chapter 6
General discussion and concluding remarks

6.1 The BiFC system successfully reports on tight ER-mitochondria contact sites that may carry out a distinct sub-set of MAM-related functions

The identification of membrane contact sites emphasises the fact that organelles of the cell are not isolated entities but are part of an inter-connected network, coordinating a host of important cellular processes. An emerging body of evidence has linked a dysfunction to organelle contact sites with neurodegeneration as reviewed in this thesis and highlights a commonality between the diverse pathways affected in disease progression and neuronal cell death. As these junctional complexes are in the range of tens of nanometres, existing methods for detecting organelle contact sites are unable to obtain a high enough resolution to accurately define an organelle contact site or in the case of electron microscopy techniques, are unsuitable for the study of membrane contact dynamics in living cells.

In this thesis, data is presented on the development of a bi-fluorescence complementation assay for the detection of membrane contact sites that can be used in both fixed and living cells. Although applied to a diffraction-limited imaging system, this technique effectively allows for the quantification of organelle contact sites up to a predicted thickness of 10 nm, dependent on the total lengths and orientations of the reformed Venus reporter proteins. Future adaptations to this technique could allow for the detection of contact sites of different size ranges by the addition of linker sequences to the reporter proteins. This could have important implications for studying distinct properties and functions of junction sites of varying thickness. The heterogeneity of organelle contact sites and the mechanisms underpinning their flexibility has not been fully elucidated. Here, data is presented to support the hypothesis that contact sites of a particular distance can only accommodate the formation of particular protein complexes and therefore, can be attributed to performing specific functions. This sub-classification of contact sites

has not been extensively investigated in the literature and further research in this area is required (Giacomello and Pellegrini, 2016).

While some of the negative data presented in this thesis is suggestive of which MAM-related functions the BiFC labelled ER-mitochondria contact sites are not involved with, their actual functional role remains unclear. In their review paper, Giacomello and Pellegrini (2016) propose terminology for specific mitochondria-ER contacts (MERCs) that considers the functional role in which they are involved e.g. lipid-MERCs for those involved in lipid transfer or Ca^{2+}-MERCs when describing those mediated calcium exchange (Giacomello and Pellegrini, 2016). Our data suggests that ER-mitochondria sites < 10 nm in size are not involved in autophagosome formation nor do they seem to form to promote mitochondrial calcium uptake but they are found to be associated with a sub-population of mitochondria of higher than average resting membrane potential and calcium concentrations. Determining any unique properties of these tight contact sites has important implications for understanding MAM heterogeneity and the potential pathogenic consequences of alterations to these junctional complexes as observed in neurodegenerative disorders.

In one proposed model for the relationship between MAM size and function, tight ER-mitochondria contacts up to 10 nm in size are specifically permissive to lipid transfer between the organelles (Giacomello and Pellegrini, 2016; Schauder et al., 2014)(**Fig 6.1**). This is based on the hypothesis that lipids are exchanged between closely opposed organelles through hydrophobic tunnels created by the formation of protein complexes involving members of the TULIP (tubular lipid binding) superfamily of lipid-binding proteins (Schauder et al., 2014). A role of TULIP proteins in lipid transfer at membrane contact sites was first implicated from the identification of the ERMES (ER-mitochondria encounter structure) complex in yeast at ER-mitochondria contacts (Kornmann et al., 2009). This complex is an essential component for phospholipid transfer in yeast and three of the core proteins of the ERMES complex belong to the TULIP superfamily (Kornmann et al., 2009; Alva and

Lupas). According to this model of lipid exchange, tight ER-mitochondria contact sites such as those labelled by the BiFC reporter proteins may be functionally involved in lipid transfer between organelles. However, to try and strengthen this observation experimentally through fluorescence microscopy using the BiFC system would present significant challenges. As is the case with other markers of MAMs, although lipid-transport proteins are enriched at these contact sites, they are not exclusively localised here (Stone and Vance, 2000). However, with further structural information on these lipid transport tunnels, it may be possible to specifically label these protein complexes and assess their co-localisation with BiFC labelled contact sites.

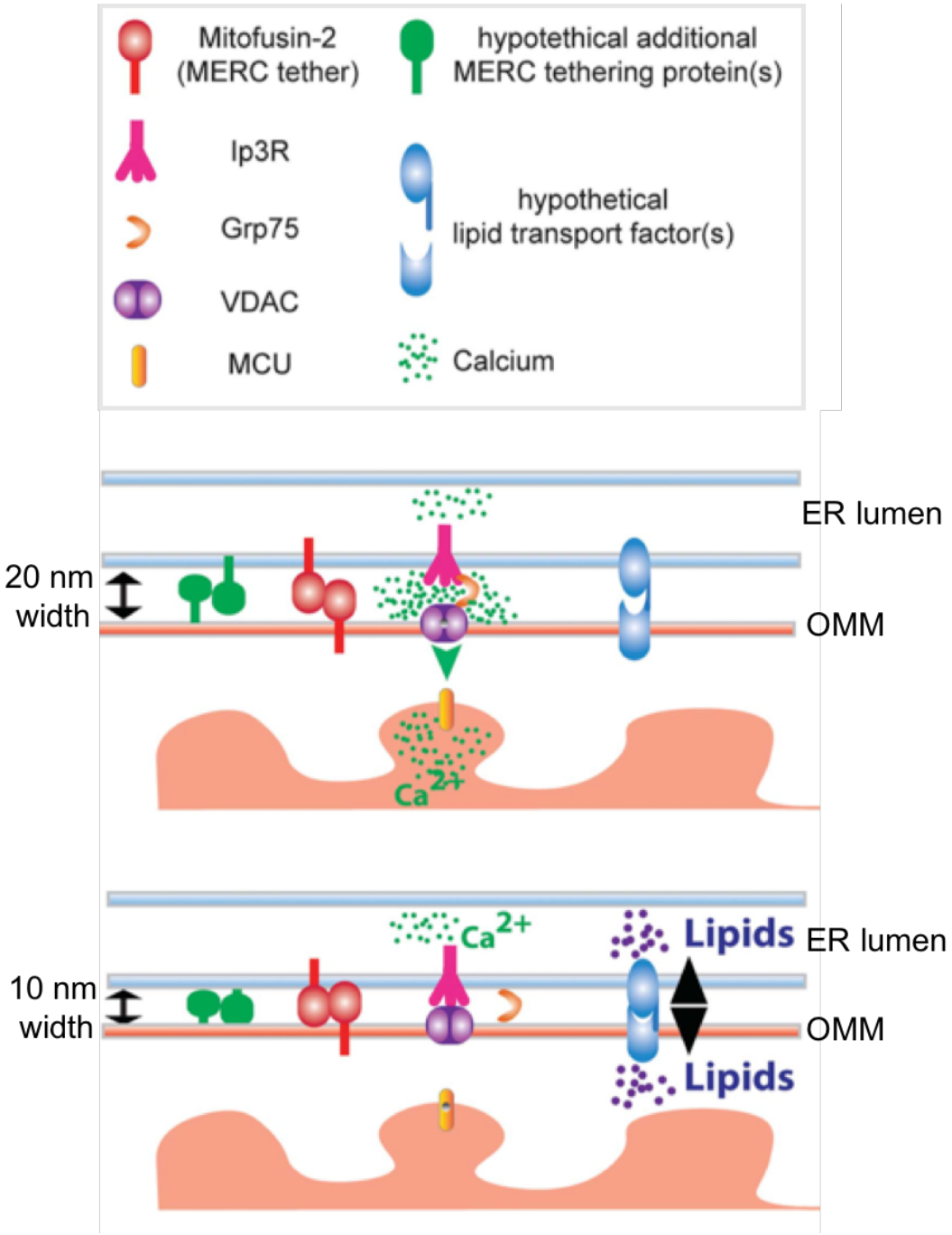

Fig 6.1: Schematic model of the relationship between MAM size and function. Wider junctions are permissive to calcium exchange between the ER and mitochondria but tightening the distance between the organelles, inhibits this process. Tight ER-mitochondria junctions are permissive to the binding of proteins involved in the transport of lipids. Image adapted from (Giacomello and Pellegrini).

6.2 Future adaptations to the BiFC technique may be used to distinguish MAMs based on variability in size or protein composition

Although it may be possible to sub-categorise MAMs based on size, it is improbable that different sized junctions could be attributed to carrying out one function exclusively. This is because in addition to variations in MAM length and thickness, contact sites may also vary in their protein compositions. This highlights a limitation of the BiFC technique in that it only discriminates MAMs based on size and not the protein content. As touched upon briefly in **chapter 3, section 3.4,** current work in the Skehel lab is attempting to clone split sfCherry probes for an adaptation to the BiFC technique to allow for simultaneous detection of two differently coloured reporter proteins. This would allow the applications of this technique to expand towards simultaneous detection of different sized junctions or if fused to particular MAM-associated proteins, it might reveal protein tethers uniquely associated with different contact points. Furthermore, it could also be used for the simultaneous detection of different types of organelle membrane contact sites. In this thesis, we have already demonstrated how fusing one fluorescent Venus fragment to a VAMP4 endosomal targeting sequence instead of an OMM targeting sequence allows for the detection of endosomal contact sites and this same principle could be applied to investigate any variety of inter-organelle contacts.

In addition to variability in the total number of contact points in a cell and the thickness of these junctions, MAMs also exhibit heterogeneity in the length of the membranes that run in close proximity to one another. Stoica *et al* (2014) illustrated changes of this nature from alterations to the levels of VAPB or PTPIP51 (Stoica et al., 2014). As it stands, the BiFC technique is unable to detect these kinds of structural changes in the contact sites due to resolution limits of confocal microscopy. It is possible that using the Venus reporter plasmids with a super-resolution imaging technique such as structured illumination microscopy (SIM) may allow for combined detection of membrane contact changes in both length and thickness. However, this would depend on the extent of the change as SIM only doubles the resolution limit to around 120 nm in the lateral plane (Gustafsson et al.,

2008). If split photoactivatable fluorescent proteins (fluorophores that can be switched from a "dark" to a "bright" state by a certain wavelength of light) become available in the future, this technique could then be applied to a super-resolution imaging technique such as photoactivated localisation microscopy (PALM) which localises objects to around 20 nm lateral resolution, giving much more accurate measurements of changes to the MAMs (Betzig et al., 2006).

6.3 The BiFC technique and neurodegeneration

Throughout this thesis, a large body of evidence has been presented highlighting the link between organelle contact sites and neurodegeneration. Here, we have applied the BiFC technique specifically in neurodegenerative disease research as illustrated by the example of ALS8 associated VAPB-P56S. Although previously published studies stated that ER-mitochondria contacts increased in response to an over-expression of both wild-type VAPB and mutant VAPB-P56S, in our study BiFC puncta number only increased from the presence of VAPB-P56S (De Vos et al., 2012; Stoica et al., 2014). This data could suggest that VAPB regulates ER-mitochondria associations beyond the detection range of the BiFC reporter proteins and that mutant VAPB-P56S may possess some unique properties that causes it to exert an influence over tight contact sites < 10 nm specifically. Further investigation into the mechanism of VAPB-P56S regulation over contact sites and the exact functional significance of these tight junctions may have important connotations for ALS pathogenesis.

As discussed in the introduction to this thesis, defects in lipid metabolism are a common pathogenic mechanism observed in a variety of neurodegenerative disorders. In ALS specifically, a reduction in phospholipids and sphingolipids is detected in animal models of the disease in both the symptomatic and pre-symptomatic stages (Henriques et al.). If indeed tight ER-mitochondria junctions are functionally related to lipid transport, the BiFC technique could be utilised to investigate whether there is a correlation between the number of tight organelle contact sites and the onset of lipid metabolic defects. Furthermore, as these reporter

proteins are genetically encoded, a feasible future investigation could involve the generation of transgenic animal models constitutively expressing the BiFC reporter proteins. This could allow us to track the structure and dynamics of these contact sites throughout development and deduce at what stage of disease progression an alteration in the number of BiFC puncta is detected. In skeletal muscle tissue from mouse models of ALS, mitochondrial abnormalities and oxidative damage are detected even while the animals are asymptomatic [As reviewed by (Zhou et al.). Combining *in vivo* experiments such as these alongside the BiFC technique might further support the hypothesis that perturbations in organelle membrane contact sites are an early pathogenic mechanism underlying many of the molecular defects observed in neurodegeneration. If this is the case, organelle membrane contact sites may be an attractive therapeutic target in the future.

6.4 VAP proteins may be processed within different sub-cellular compartments

Finally, some preliminary work was presented on the biochemical purification of MAM proteins from rat liver and brain tissue. By using the sub-cellular organelle fractionation technique, our data suggests that the proteolytic cleavage of VAPA and VAPB seems to be confined to specific sub-cellular compartments and that the processing of VAPA and VAPB may predominantly take place in different sub-cellular locations. Although preliminary, it highlights the strength of purifying MAM fractions as previously, this cleavage event had only been examined on a whole tissue level (Gkogkas et al., 2008). Future work in this area could confirm these differences in VAP protein processing and could be used to test for any changes in VAP cleavage events in our VAPB-P56S and VAPB knock-out mutant rat models of which preliminary studies have already been carried out. Several studies have shown that under certain conditions, proteins can re-distribute between sub-cellular fractions for example, when autophagy is induced ATG5 and ATG14 localise to the MAM fraction (Hamasaki et al., 2013). While this may not be reflected in quantifications of total protein levels, sub-cellular organelle experiments could identify these changes. Future experiments could correlate any changes in the distributions of MAM-

associated proteins with the presence of the ALS8 point mutation that may indicate important mechanisms in the neurodegenerative process. In addition, the BiFC technique could be applied to primary cell cultures from the aforementioned rat models to observe any difference in the number of tight organelle contact sites.

In summary, the use of split fluorescent probes is an effective method of labelling organelle contact sites in both fixed and living cells. The publication of two independent studies over the course of this thesis also using split fluorescent probes to label MAMs is a testament to the strength of this technique (Cieri et al., 2018; Yang et al., 2018). By using this method, we were able to replicate changes in the MAMs in agreement with higher resolution EM studies while also conducting studies into ER-mitochondria contact dynamics in living cells. Future modifications to this technique will expand its range of applications, making the BiFC technique a diverse and efficient tool in the field of organelle membrane contact sites.

References

.

Akerboom, J., Carreras Calderon, N., Tian, L., Wabnig, S., Prigge, M., Tolo, J., Gordus, A., Orger, M. B., Severi, K. E., Macklin, J. J., Patel, R., Pulver, S. R., Wardill, T. J., Fischer, E., Schuler, C., Chen, T. W., Sarkisyan, K. S., Marvin, J. S., Bargmann, C. I., Kim, D. S., Kugler, S., Lagnado, L., Hegemann, P., Gottschalk, A., Schreiter, E. R. & Looger, L. L. (2013). Genetically encoded calcium indicators for multi-color neural activity imaging and combination with optogenetics. *Front Mol Neurosci,* **6**, 2.

Al-Saif, A., Al-Mohanna, F. & Bohlega, S. (2011). A mutation in sigma-1 receptor causes juvenile amyotrophic lateral sclerosis. *Ann Neurol,* **70**, 913-9.

Alford, S. C., Ding, Y., Simmen, T. & Campbell, R. E. (2012). Dimerization-dependent green and yellow fluorescent proteins. *ACS Synth Biol,* **1**, 569-75.

Alpy, F., Rousseau, A., Schwab, Y., Legueux, F., Stoll, I., Wendling, C., Spiegelhalter, C., Kessler, P., Mathelin, C., Rio, M. C., Levine, T. P. & Tomasetto, C. (2013). STARD3 or STARD3NL and VAP form a novel molecular tether between late endosomes and the ER. *J Cell Sci,* **126**, 5500-12.

Alva, V. & Lupas, A. N. (2016). The TULIP superfamily of eukaryotic lipid-binding proteins as a mediator of lipid sensing and transport. *Biochim Biophys Acta,* **1861**, 913-923.

Amarilio, R., Ramachandran, S., Sabanay, H. & Lev, S. (2005). Differential regulation of endoplasmic reticulum structure through VAP-Nir protein interaction. *J Biol Chem,* **280**, 5934-44.

Area-Gomez, E., de Groof, A. J., Boldogh, I., Bird, T. D., Gibson, G. E., Koehler, C. M., Yu, W. H., Duff, K. E., Yaffe, M. P., Pon, L. A. & Schon, E. A. (2009). Presenilins are enriched in endoplasmic reticulum membranes associated with mitochondria. *Am J Pathol,* **175**, 1810-6.

Area-Gomez, E., Del Carmen Lara Castillo, M., Tambini, M. D., Guardia-Laguarta, C., de Groof, A. J., Madra, M., Ikenouchi, J., Umeda, M., Bird, T. D., Sturley, S. L. & Schon, E. A. (2012). Upregulated function of mitochondria-associated ER membranes in Alzheimer disease. *EMBO J,* **31**, 4106-23.

Armbruster, B. N., Li, X., Pausch, M. H., Herlitze, S. & Roth, B. L. (2007). Evolving the lock to fit the key to create a family of G protein-coupled receptors potently activated by an inert ligand. *Proc Natl Acad Sci U S A,* **104**, 5163-8.

Atkin, J. D., Farg, M. A., Turner, B. J., Tomas, D., Lysaght, J. A., Nunan, J., Rembach, A., Nagley, P., Beart, P. M., Cheema, S. S. & Horne, M. K. (2006). Induction of the unfolded protein response in familial amyotrophic lateral sclerosis and association of protein-disulfide isomerase with superoxide dismutase 1. *J Biol Chem,* **281**, 30152-65.

Atkin, J. D., Farg, M. A., Walker, A. K., McLean, C., Tomas, D. & Horne, M. K. (2008). Endoplasmic reticulum stress and induction of the unfolded protein response in human sporadic amyotrophic lateral sclerosis. *Neurobiol Dis,* **30**, 400-7.

Atsumi, T. (1981). The ultrastructure of intramuscular nerves in amyotrophic lateral sclerosis. *Acta Neuropathol,* **55**, 193-8.

Axe, E. L., Walker, S. A., Manifava, M., Chandra, P., Roderick, H. L., Habermann, A., Griffiths, G. & Ktistakis, N. T. (2008). Autophagosome formation from membrane compartments enriched in phosphatidylinositol 3-phosphate and dynamically connected to the endoplasmic reticulum. *J Cell Biol,* **182**, 685-701.

Bedford, L., Paine, S., Sheppard, P. W., Mayer, R. J. & Roelofs, J. (2010). Assembly, structure, and function of the 26S proteasome. *Trends Cell Biol,* **20**, 391-401.

Bendotti, C., Marino, M., Cheroni, C., Fontana, E., Crippa, V., Poletti, A. & De Biasi, S. (2012). Dysfunction of constitutive and inducible ubiquitin-proteasome system in amyotrophic lateral sclerosis: implication for protein aggregation and immune response. *Prog Neurobiol,* **97**, 101-26.

Bernard-Marissal, N., Medard, J. J., Azzedine, H. & Chrast, R. (2015). Dysfunction in endoplasmic reticulum-mitochondria crosstalk underlies SIGMAR1 loss of function mediated motor neuron degeneration. *Brain,* **138**, 875-90.

Betzig, E., Patterson, G. H., Sougrat, R., Lindwasser, O. W., Olenych, S., Bonifacino, J. S., Davidson, M. W., Lippincott-Schwartz, J. & Hess, H. F. (2006). Imaging intracellular fluorescent proteins at nanometer resolution. *Science,* **313**, 1642-5.

Bezprozvanny, I. & Mattson, M. P. (2008). Neuronal calcium mishandling and the pathogenesis of Alzheimer's disease. *Trends Neurosci,* **31**, 454-63.

Blass, J. P. (2000). The mitochondrial spiral. An adequate cause of dementia in the Alzheimer's syndrome. *Ann N Y Acad Sci,* **924**, 170-83.

Blond-Elguindi, S., Fourie, A. M., Sambrook, J. F. & Gething, M. J. (1993). Peptide-dependent stimulation of the ATPase activity of the molecular chaperone BiP is the result of conversion of oligomers to active monomers. *J Biol Chem,* **268**, 12730-5.

Borthwick, G. M., Taylor, R. W., Walls, T. J., Tonska, K., Taylor, G. A., Shaw, P. J., Ince, P. G. & Turnbull, D. M. (2006). Motor neuron disease in a patient with a mitochondrial tRNAIle mutation. *Ann Neurol,* **59**, 570-4.

Bottino, D., Mogilner, A., Roberts, T., Stewart, M. & Oster, G. (2002). How nematode sperm crawl. *J Cell Sci,* **115**, 367-84.

Bozner, P., Grishko, V., LeDoux, S. P., Wilson, G. L., Chyan, Y. C. & Pappolla, M. A. (1997). The amyloid beta protein induces oxidative damage of mitochondrial DNA. *J Neuropathol Exp Neurol,* **56**, 1356-62.

Bravo, R., Vicencio, J. M., Parra, V., Troncoso, R., Munoz, J. P., Bui, M., Quiroga, C., Rodriguez, A. E., Verdejo, H. E., Ferreira, J., Iglewski, M., Chiong, M., Simmen, T., Zorzano, A., Hill, J. A., Rothermel, B. A., Szabadkai, G. & Lavandero, S. (2011). Increased ER-mitochondrial coupling promotes mitochondrial respiration and bioenergetics during early phases of ER stress. *J Cell Sci,* **124**, 2143-52.

Brown, T. A., Tkachuk, A. N., Shtengel, G., Kopek, B. G., Bogenhagen, D. F., Hess, H. F. & Clayton, D. A. (2011). Superresolution fluorescence imaging of mitochondrial nucleoids reveals their spatial range, limits, and membrane interaction. *Mol Cell Biol,* **31**, 4994-5010.

Burkhard, P., Stetefeld, J. & Strelkov, S. V. (2001). Coiled coils: a highly versatile protein folding motif. *Trends Cell Biol,* **11**, 82-8.

Byrne, D. J., Harmon, M. J., Simpson, J. C., Blackstone, C. & O'Sullivan, N. C. (2017). Roles for the VCP co-factors Npl4 and Ufd1 in neuronal function in Drosophila melanogaster. *J Genet Genomics*.

Calfon, M., Zeng, H., Urano, F., Till, J. H., Hubbard, S. R., Harding, H. P., Clark, S. G. & Ron, D. (2002). IRE1 couples endoplasmic reticulum load to secretory capacity by processing the XBP-1 mRNA. *Nature,* **415**, 92-6.

Cali, T., Ottolini, D., Negro, A. & Brini, M. (2012). alpha-Synuclein controls mitochondrial calcium homeostasis by enhancing endoplasmic reticulum-mitochondria interactions. *J Biol Chem,* **287**, 17914-29.

Cali, T., Ottolini, D., Negro, A. & Brini, M. (2013). Enhanced parkin levels favor ER-mitochondria crosstalk and guarantee Ca(2+) transfer to sustain cell bioenergetics. *Biochim Biophys Acta,* **1832**, 495-508.

Cashman, N. R., Durham, H. D., Blusztajn, J. K., Oda, K., Tabira, T., Shaw, I. T., Dahrouge, S. & Antel, J. P. (1992). Neuroblastoma x spinal cord (NSC) hybrid cell lines resemble developing motor neurons. *Dev Dyn,* **194**, 209-21.

Celardo, I., Costa, A. C., Lehmann, S., Jones, C., Wood, N., Mencacci, N. E., Mallucci, G. R., Loh, S. H. & Martins, L. M. (2016). Mitofusin-mediated ER stress triggers neurodegeneration in pink1/parkin models of Parkinson's disease. *Cell Death Dis,* **7**, e2271.

Chai, A., Withers, J., Koh, Y. H., Parry, K., Bao, H., Zhang, B., Budnik, V. & Pennetta, G. (2008). hVAPB, the causative gene of a heterogeneous group of motor neuron diseases in humans, is functionally interchangeable with its Drosophila homologue DVAP-33A at the neuromuscular junction. *Hum Mol Genet,* **17**, 266-80.

Chami, M., Oules, B., Szabadkai, G., Tacine, R., Rizzuto, R. & Paterlini-Brechot, P. (2008). Role of SERCA1 truncated isoform in the proapoptotic calcium transfer from ER to mitochondria during ER stress. *Mol Cell,* **32**, 641-51.

Chan, S. L., Mayne, M., Holden, C. P., Geiger, J. D. & Mattson, M. P. (2000). Presenilin-1 mutations increase levels of ryanodine receptors and calcium release in PC12 cells and cortical neurons. *J Biol Chem,* **275**, 18195-200.

Chen, H., Detmer, S. A., Ewald, A. J., Griffin, E. E., Fraser, S. E. & Chan, D. C. (2003). Mitofusins Mfn1 and Mfn2 coordinately regulate mitochondrial fusion and are essential for embryonic development. *J Cell Biol,* **160**, 189-200.

Chen, H. J., Anagnostou, G., Chai, A., Withers, J., Morris, A., Adhikaree, J., Pennetta, G. & de Belleroche, J. S. (2010). Characterization of the properties of a novel mutation in VAPB in familial amyotrophic lateral sclerosis. *J Biol Chem,* **285**, 40266-81.

Chen, T. W., Wardill, T. J., Sun, Y., Pulver, S. R., Renninger, S. L., Baohan, A., Schreiter, E. R., Kerr, R. A., Orger, M. B., Jayaraman, V., Looger, L. L., Svoboda, K. & Kim, D. S. (2013). Ultrasensitive fluorescent proteins for imaging neuronal activity. *Nature,* **499**, 295-300.

Chen, Y. Z., Bennett, C. L., Huynh, H. M., Blair, I. P., Puls, I., Irobi, J., Dierick, I., Abel, A., Kennerson, M. L., Rabin, B. A., Nicholson, G. A., Auer-Grumbach, M., Wagner, K., De Jonghe, P., Griffin, J. W., Fischbeck, K. H., Timmerman, V., Cornblath, D. R. & Chance, P. F. (2004). DNA/RNA helicase gene mutations in a form of juvenile amyotrophic lateral sclerosis (ALS4). *Am J Hum Genet,* **74**, 1128-35.

Cheung, K. H., Mei, L., Mak, D. O., Hayashi, I., Iwatsubo, T., Kang, D. E. & Foskett, J. K. (2010). Gain-of-function enhancement of IP3 receptor modal gating by familial Alzheimer's disease-linked presenilin mutants in human cells and mouse neurons. *Sci Signal,* **3**, ra22.

Choubey, V., Cagalinec, M., Liiv, J., Safiulina, D., Hickey, M. A., Kuum, M., Liiv, M., Anwar, T., Eskelinen, E. L. & Kaasik, A. (2014). BECN1 is involved in the initiation of mitophagy: it facilitates PARK2 translocation to mitochondria. *Autophagy,* **10**, 1105-19.

Cieri, D., Vicario, M., Giacomello, M., Vallese, F., Filadi, R., Wagner, T., Pozzan, T., Pizzo, P., Scorrano, L., Brini, M. & Cali, T. (2018). SPLICS: a split green fluorescent protein-based contact site sensor for narrow and wide heterotypic organelle juxtaposition. *Cell Death Differ,* **25**, 1131-1145.

Colombo, M. I., Beron, W. & Stahl, P. D. (1997). Calmodulin regulates endosome fusion. *J Biol Chem,* **272**, 7707-12.

Comi, G. P., Bordoni, A., Salani, S., Franceschina, L., Sciacco, M., Prelle, A., Fortunato, F., Zeviani, M., Napoli, L., Bresolin, N., Moggio, M., Ausenda, C. D., Taanman, J. W. & Scarlato, G. (1998). Cytochrome c oxidase subunit I microdeletion in a patient with motor neuron disease. *Ann Neurol,* **43**, 110-6.

Conner, S. D. & Schmid, S. L. (2003). Regulated portals of entry into the cell. *Nature,* **422**, 37-44.

Corbett, E. F., Oikawa, K., Francois, P., Tessier, D. C., Kay, C., Bergeron, J. J., Thomas, D. Y., Krause, K. H. & Michalak, M. (1999). Ca2+ regulation of interactions between endoplasmic reticulum chaperones. *J Biol Chem,* **274**, 6203-11.

Cosson, P., Marchetti, A., Ravazzola, M. & Orci, L. (2012). Mitofusin-2 independent juxtaposition of endoplasmic reticulum and mitochondria: an ultrastructural study. *PLoS One,* **7**, e46293.

Costello, J. L., Castro, I. G., Hacker, C., Schrader, T. A., Metz, J., Zeuschner, D., Azadi, A. S., Godinho, L. F., Costina, V., Findeisen, P., Manner, A., Islinger, M. & Schrader, M. (2017). ACBD5 and VAPB mediate membrane associations between peroxisomes and the ER. *J Cell Biol,* **216**, 331-342.

Csordas, A. (2006). Mitochondrial transfer between eukaryotic animal cells and its physiologic role. *Rejuvenation Res,* **9**, 450-4.

Csordas, G., Renken, C., Varnai, P., Walter, L., Weaver, D., Buttle, K. F., Balla, T., Mannella, C. A. & Hajnoczky, G. (2006). Structural and functional features and significance of the physical linkage between ER and mitochondria. *J Cell Biol,* **174**, 915-21.

Csordas, G., Varnai, P., Golenar, T., Roy, S., Purkins, G., Schneider, T. G., Balla, T. & Hajnoczky, G. (2010). Imaging interorganelle contacts and local calcium dynamics at the ER-mitochondrial interface. *Mol Cell,* **39**, 121-32.

Cui, Z., Vance, J. E., Chen, M. H., Voelker, D. R. & Vance, D. E. (1993). Cloning and expression of a novel phosphatidylethanolamine N-methyltransferase. A specific biochemical and cytological marker for a unique membrane fraction in rat liver. *J Biol Chem,* **268**, 16655-63.

D'Angelo, G., Polishchuk, E., Di Tullio, G., Santoro, M., Di Campli, A., Godi, A., West, G., Bielawski, J., Chuang, C. C., van der Spoel, A. C., Platt, F. M., Hannun, Y. A., Polishchuk, R., Mattjus, P. & De Matteis, M. A. (2007). Glycosphingolipid synthesis requires FAPP2 transfer of glucosylceramide. *Nature,* **449**, 62-7.

Day, K. J., Staehelin, L. A. & Glick, B. S. (2013). A three-stage model of Golgi structure and function. *Histochem Cell Biol,* **140**, 239-49.

de Brito, O. M. & Scorrano, L. (2008). Mitofusin 2 tethers endoplasmic reticulum to mitochondria. *Nature,* **456**, 605-10.

De Stefani, D., Raffaello, A., Teardo, E., Szabo, I. & Rizzuto, R. (2011). A forty-kilodalton protein of the inner membrane is the mitochondrial calcium uniporter. *Nature,* **476**, 336-40.

De Vos, K. J., Morotz, G. M., Stoica, R., Tudor, E. L., Lau, K. F., Ackerley, S., Warley, A., Shaw, C. E. & Miller, C. C. (2012). VAPB interacts with the mitochondrial protein PTPIP51 to regulate calcium homeostasis. *Hum Mol Genet,* **21**, 1299-311.

Deidda, I., Galizzi, G., Passantino, R., Cascio, C., Russo, D., Colletti, T., La Bella, V. & Guarneri, P. (2014). Expression of vesicle-associated membrane-protein-associated protein B cleavage products in peripheral blood leukocytes and cerebrospinal fluid of patients with sporadic amyotrophic lateral sclerosis. *Eur J Neurol,* **21**, 478-85.

Deng, H. X., Chen, W., Hong, S. T., Boycott, K. M., Gorrie, G. H., Siddique, N., Yang, Y., Fecto, F., Shi, Y., Zhai, H., Jiang, H., Hirano, M., Rampersaud, E., Jansen, G. H., Donkervoort, S., Bigio, E. H., Brooks, B. R., Ajroud, K., Sufit, R. L., Haines, J. L., Mugnaini, E., Pericak-Vance, M. A. & Siddique, T. (2011). Mutations in UBQLN2 cause dominant X-linked juvenile and adult-onset ALS and ALS/dementia. *Nature,* **477**, 211-5.

Dexter, D. T., Carter, C. J., Wells, F. R., Javoy-Agid, F., Agid, Y., Lees, A., Jenner, P. & Marsden, C. D. (1989). Basal lipid peroxidation in substantia nigra is increased in Parkinson's disease. *J Neurochem,* **52**, 381-9.

Dickey, A. S. & Strack, S. (2011). PKA/AKAP1 and PP2A/Bbeta2 regulate neuronal morphogenesis via Drp1 phosphorylation and mitochondrial bioenergetics. *J Neurosci,* **31**, 15716-26.

Dong, R., Saheki, Y., Swarup, S., Lucast, L., Harper, J. W. & De Camilli, P. (2016). Endosome-ER Contacts Control Actin Nucleation and Retromer Function through VAP-Dependent Regulation of PI4P. *Cell,* **166**, 408-423.

Du, X., Kumar, J., Ferguson, C., Schulz, T. A., Ong, Y. S., Hong, W., Prinz, W. A., Parton, R. G., Brown, A. J. & Yang, H. (2011). A role for oxysterol-binding protein-related protein 5 in endosomal cholesterol trafficking. *J Cell Biol,* **192**, 121-35.

Eden, E. R., White, I. J., Tsapara, A. & Futter, C. E. (2010). Membrane contacts between endosomes and ER provide sites for PTP1B-epidermal growth factor receptor interaction. *Nat Cell Biol,* **12**, 267-72.

Ekstrand, M. I., Terzioglu, M., Galter, D., Zhu, S., Hofstetter, C., Lindqvist, E., Thams, S., Bergstrand, A., Hansson, F. S., Trifunovic, A., Hoffer, B., Cullheim, S., Mohammed, A. H., Olson, L. & Larsson, N. G. (2007). Progressive parkinsonism in mice with respiratory-chain-deficient dopamine neurons. *Proc Natl Acad Sci U S A,* **104**, 1325-30.

English, A. R. & Voeltz, G. K. (2013). Endoplasmic reticulum structure and interconnections with other organelles. *Cold Spring Harb Perspect Biol,* **5**, a013227.

Fasana, E., Fossati, M., Ruggiano, A., Brambillasca, S., Hoogenraad, C. C., Navone, F., Francolini, M. & Borgese, N. (2010). A VAPB mutant linked to amyotrophic lateral sclerosis generates a novel form of organized smooth endoplasmic reticulum. *FASEB J,* **24**, 1419-30.

Filadi, R., Greotti, E., Turacchio, G., Luini, A., Pozzan, T. & Pizzo, P. (2015). Mitofusin 2 ablation increases endoplasmic reticulum-mitochondria coupling. *Proc Natl Acad Sci U S A,* **112**, E2174-81.

Filadi, R., Greotti, E., Turacchio, G., Luini, A., Pozzan, T. & Pizzo, P. (2016). Presenilin 2 Modulates Endoplasmic Reticulum-Mitochondria Coupling by Tuning the Antagonistic Effect of Mitofusin 2. *Cell Rep,* **15**, 2226-38.

Filippov, V., Song, M. A., Zhang, K., Vinters, H. V., Tung, S., Kirsch, W. M., Yang, J. & Duerksen-Hughes, P. J. (2012). Increased ceramide in brains with Alzheimer's and other neurodegenerative diseases. *J Alzheimers Dis,* **29**, 537-47.

Frank, S., Gaume, B., Bergmann-Leitner, E. S., Leitner, W. W., Robert, E. G., Catez, F., Smith, C. L. & Youle, R. J. (2001). The role of dynamin-related protein 1, a mediator of mitochondrial fission, in apoptosis. *Dev Cell,* **1**, 515-25.

Friedman, J. R., Dibenedetto, J. R., West, M., Rowland, A. A. & Voeltz, G. K. (2013). Endoplasmic reticulum-endosome contact increases as endosomes traffic and mature. *Mol Biol Cell,* **24**, 1030-40.

Friedman, J. R., Lackner, L. L., West, M., DiBenedetto, J. R., Nunnari, J. & Voeltz, G. K. (2011). ER tubules mark sites of mitochondrial division. *Science,* **334**, 358-62.

Friedman, J. R., Webster, B. M., Mastronarde, D. N., Verhey, K. J. & Voeltz, G. K. (2010). ER sliding dynamics and ER-mitochondrial contacts occur on acetylated microtubules. *J Cell Biol,* **190**, 363-75.

Fujimoto, M., Hayashi, T. & Su, T. P. (2012). The role of cholesterol in the association of endoplasmic reticulum membranes with mitochondria. *Biochem Biophys Res Commun,* **417**, 635-9.

Garrido, N., Griparic, L., Jokitalo, E., Wartiovaara, J., van der Bliek, A. M. & Spelbrink, J. N. (2003). Composition and dynamics of human mitochondrial nucleoids. *Mol Biol Cell,* **14**, 1583-96.

Gautier, C. A., Erpapazoglou, Z., Mouton-Liger, F., Muriel, M. P., Cormier, F., Bigou, S., Duffaure, S., Girard, M., Foret, B., Iannielli, A., Broccoli, V., Dalle, C., Bohl, D., Michel, P. P., Corvol, J. C., Brice, A. & Corti, O. (2016). The endoplasmic reticulum-mitochondria interface is perturbed in PARK2 knockout mice and patients with PARK2 mutations. *Hum Mol Genet,* **25**, 2972-2984.

Gelmetti, V., De Rosa, P., Torosantucci, L., Marini, E. S., Romagnoli, A., Di Rienzo, M., Arena, G., Vignone, D., Fimia, G. M. & Valente, E. M. (2017). PINK1 and BECN1 relocalize at mitochondria-associated membranes during mitophagy and promote ER-mitochondria tethering and autophagosome formation. *Autophagy,* **13**, 654-669.

Geng, J., Nair, U., Yasumura-Yorimitsu, K. & Klionsky, D. J. (2010). Post-Golgi Sec proteins are required for autophagy in Saccharomyces cerevisiae. *Mol Biol Cell,* **21**, 2257-69.

Giacomello, M. & Pellegrini, L. (2016). The coming of age of the mitochondria-ER contact: a matter of thickness. *Cell Death Differ,* **23**, 1417-27.

Giorgio, V., von Stockum, S., Antoniel, M., Fabbro, A., Fogolari, F., Forte, M., Glick, G. D., Petronilli, V., Zoratti, M., Szabo, I., Lippe, G. & Bernardi, P. (2013). Dimers of mitochondrial ATP synthase form the permeability transition pore. *Proc Natl Acad Sci U S A,* **110**, 5887-92.

Gkogkas, C., Middleton, S., Kremer, A. M., Wardrope, C., Hannah, M., Gillingwater, T. H. & Skehel, P. (2008). VAPB interacts with and modulates the activity of ATF6. *Hum Mol Genet,* **17**, 1517-26.

Gkogkas, C., Wardrope, C., Hannah, M. & Skehel, P. (2011). The ALS8-associated mutant VAPB(P56S) is resistant to proteolysis in neurons. *J Neurochem,* **117**, 286-94.

Glater, E. E., Megeath, L. J., Stowers, R. S. & Schwarz, T. L. (2006). Axonal transport of mitochondria requires milton to recruit kinesin heavy chain and is light chain independent. *J Cell Biol,* **173**, 545-57.

Gluzman, Y. (1981). SV40-transformed simian cells support the replication of early SV40 mutants. *Cell,* **23**, 175-82.

Goate, A., Chartier-Harlin, M. C., Mullan, M., Brown, J., Crawford, F., Fidani, L., Giuffra, L., Haynes, A., Irving, N., James, L. & et al. (1991). Segregation of a missense mutation in the amyloid precursor protein gene with familial Alzheimer's disease. *Nature,* **349**, 704-6.

Goedert, M. & Spillantini, M. G. (2006). A century of Alzheimer's disease. *Science,* **314**, 777-81.

Goetz, J. G., Genty, H., St-Pierre, P., Dang, T., Joshi, B., Sauve, R., Vogl, W. & Nabi, I. R. (2007). Reversible interactions between smooth domains of the endoplasmic reticulum and mitochondria are regulated by physiological cytosolic Ca2+ levels. *J Cell Sci,* **120**, 3553-64.

Gomez-Suaga, P., Paillusson, S., Stoica, R., Noble, W., Hanger, D. P. & Miller, C. C. J. (2017). The ER-Mitochondria Tethering Complex VAPB-PTPIP51 Regulates Autophagy. *Curr Biol,* **27**, 371-385.

Gonatas, N. K., Stieber, A., Mourelatos, Z., Chen, Y., Gonatas, J. O., Appel, S. H., Hays, A. P., Hickey, W. F. & Hauw, J. J. (1992). Fragmentation of the Golgi apparatus of motor neurons in amyotrophic lateral sclerosis. *Am J Pathol,* **140**, 731-7.

Gosavi, N., Lee, H. J., Lee, J. S., Patel, S. & Lee, S. J. (2002). Golgi fragmentation occurs in the cells with prefibrillar alpha-synuclein aggregates and precedes the formation of fibrillar inclusion. *J Biol Chem,* **277**, 48984-92.

Graham, F. L., Smiley, J., Russell, W. C. & Nairn, R. (1977). Characteristics of a human cell line transformed by DNA from human adenovirus type 5. *J Gen Virol,* **36**, 59-74.

Grosskreutz, J., Van Den Bosch, L. & Keller, B. U. (2010). Calcium dysregulation in amyotrophic lateral sclerosis. *Cell Calcium,* **47**, 165-74.

Gustafsson, M. G., Shao, L., Carlton, P. M., Wang, C. J., Golubovskaya, I. N., Cande, W. Z., Agard, D. A. & Sedat, J. W. (2008). Three-dimensional resolution doubling in wide-field fluorescence microscopy by structured illumination. *Biophys J,* **94**, 4957-70.

Hailey, D. W., Rambold, A. S., Satpute-Krishnan, P., Mitra, K., Sougrat, R., Kim, P. K. & Lippincott-Schwartz, J. (2010). Mitochondria supply membranes for autophagosome biogenesis during starvation. *Cell,* **141**, 656-67.

Haj, F. G., Verveer, P. J., Squire, A., Neel, B. G. & Bastiaens, P. I. (2002). Imaging sites of receptor dephosphorylation by PTP1B on the surface of the endoplasmic reticulum. *Science,* **295**, 1708-11.

Hamasaki, M., Furuta, N., Matsuda, A., Nezu, A., Yamamoto, A., Fujita, N., Oomori, H., Noda, T., Haraguchi, T., Hiraoka, Y., Amano, A. & Yoshimori, T. (2013). Autophagosomes form at ER-mitochondria contact sites. *Nature,* **495**, 389-93.

Han, C., Jin, L., Mei, Y. & Wu, M. (2013a). Endoplasmic reticulum stress inhibits cell cycle progression via induction of p27 in melanoma cells. *Cell Signal,* **25**, 144-9.

Han, S. M., El Oussini, H., Scekic-Zahirovic, J., Vibbert, J., Cottee, P., Prasain, J. K., Bellen, H. J., Dupuis, L. & Miller, M. A. (2013b). VAPB/ALS8 MSP ligands regulate striated muscle energy metabolism critical for adult survival in caenorhabditis elegans. *PLoS Genet,* **9**, e1003738.

Han, S. M., Tsuda, H., Yang, Y., Vibbert, J., Cottee, P., Lee, S. J., Winek, J., Haueter, C., Bellen, H. J. & Miller, M. A. (2012). Secreted VAPB/ALS8 major sperm protein domains modulate mitochondrial localization and morphology via growth cone guidance receptors. *Dev Cell,* **22**, 348-62.

Hara, T., Nakamura, K., Matsui, M., Yamamoto, A., Nakahara, Y., Suzuki-Migishima, R., Yokoyama, M., Mishima, K., Saito, I., Okano, H. & Mizushima, N. (2006). Suppression of basal autophagy in neural cells causes neurodegenerative disease in mice. *Nature,* **441**, 885-9.

Harding, H. P., Novoa, I., Zhang, Y., Zeng, H., Wek, R., Schapira, M. & Ron, D. (2000a). Regulated translation initiation controls stress-induced gene expression in mammalian cells. *Mol Cell,* **6**, 1099-108.

Harding, H. P., Zhang, Y., Bertolotti, A., Zeng, H. & Ron, D. (2000b). Perk is essential for translational regulation and cell survival during the unfolded protein response. *Mol Cell,* **5**, 897-904.

Harding, H. P., Zhang, Y. & Ron, D. (1999). Protein translation and folding are coupled by an endoplasmic-reticulum-resident kinase. *Nature,* **397**, 271-4.

Hardy, J. A. & Higgins, G. A. (1992). Alzheimer's disease: the amyloid cascade hypothesis. *Science,* **256**, 184-5.

Harmon, M., Larkman, P., Hardingham, G., Jackson, M. & Skehel, P. (2017). A Bi-fluorescence complementation system to detect associations between the Endoplasmic reticulum and mitochondria. *Sci Rep,* **7**, 17467.

Haughey, N. J., Bandaru, V. V., Bae, M. & Mattson, M. P. (2010). Roles for dysfunctional sphingolipid metabolism in Alzheimer's disease neuropathogenesis. *Biochim Biophys Acta,* **1801**, 878-86.

Hayashi, T. & Fujimoto, M. (2010). Detergent-resistant microdomains determine the localization of sigma-1 receptors to the endoplasmic reticulum-mitochondria junction. *Mol Pharmacol,* **77**, 517-28.

Hayashi, T., Rizzuto, R., Hajnoczky, G. & Su, T. P. (2009). MAM: more than just a housekeeper. *Trends Cell Biol,* **19**, 81-8.

Hayashi, T. & Su, T. P. (2007). Sigma-1 receptor chaperones at the ER-mitochondrion interface regulate Ca(2+) signaling and cell survival. *Cell,* **131**, 596-610.

Hayashi-Nishino, M., Fujita, N., Noda, T., Yamaguchi, A., Yoshimori, T. & Yamamoto, A. (2009). A subdomain of the endoplasmic reticulum forms a cradle for autophagosome formation. *Nat Cell Biol,* **11**, 1433-7.

Hayrapetyan, V., Rybalchenko, V., Rybalchenko, N. & Koulen, P. (2008). The N-terminus of presenilin-2 increases single channel activity of brain ryanodine receptors through direct protein-protein interaction. *Cell Calcium,* **44**, 507-18.

Haze, K., Yoshida, H., Yanagi, H., Yura, T. & Mori, K. (1999). Mammalian transcription factor ATF6 is synthesized as a transmembrane protein and activated by proteolysis in response to endoplasmic reticulum stress. *Mol Biol Cell,* **10**, 3787-99.

Heilemann, M. (2010). Fluorescence microscopy beyond the diffraction limit. *J Biotechnol,* **149**, 243-51.

Henne, W. M., Liou, J. & Emr, S. D. (2015). Molecular mechanisms of inter-organelle ER-PM contact sites. *Curr Opin Cell Biol,* **35**, 123-30.

Henriques, A., Croixmarie, V., Priestman, D. A., Rosenbohm, A., Dirrig-Grosch, S., D'Ambra, E., Huebecker, M., Hussain, G., Boursier-Neyret, C., Echaniz-Laguna, A., Ludolph, A. C., Platt, F. M., Walther, B., Spedding, M., Loeffler, J. P. & Gonzalez De Aguilar, J. L. (2015). Amyotrophic lateral sclerosis and denervation alter sphingolipids and up-regulate glucosylceramide synthase. *Hum Mol Genet,* **24**, 7390-405.

Hirabayashi, Y., Kwon, S. K., Paek, H., Pernice, W. M., Paul, M. A., Lee, J., Erfani, P., Raczkowski, A., Petrey, D. S., Pon, L. A. & Polleux, F. (2017). ER-mitochondria tethering by PDZD8 regulates Ca(2+) dynamics in mammalian neurons. *Science,* **358**, 623-630.

Hirsch, E. C., Hunot, S., Faucheux, B., Agid, Y., Mizuno, Y., Mochizuki, H., Tatton, W. G., Tatton, N. & Olanow, W. C. (1999). Dopaminergic neurons degenerate by apoptosis in Parkinson's disease. *Mov Disord,* **14**, 383-5.

Hoepfner, D., Schildknegt, D., Braakman, I., Philippsen, P. & Tabak, H. F. (2005). Contribution of the endoplasmic reticulum to peroxisome formation. *Cell,* **122**, 85-95.

Hopper, R. K., Carroll, S., Aponte, A. M., Johnson, D. T., French, S., Shen, R. F., Witzmann, F. A., Harris, R. A. & Balaban, R. S. (2006). Mitochondrial matrix phosphoproteome: effect of extra mitochondrial calcium. *Biochemistry,* **45**, 2524-36.

Hosokawa, N., Hara, T., Kaizuka, T., Kishi, C., Takamura, A., Miura, Y., Iemura, S., Natsume, T., Takehana, K., Yamada, N., Guan, J. L., Oshiro, N. & Mizushima, N. (2009). Nutrient-dependent mTORC1 association with the ULK1-Atg13-FIP200 complex required for autophagy. *Mol Biol Cell,* **20**, 1981-91.

Hsu, L. J., Sagara, Y., Arroyo, A., Rockenstein, E., Sisk, A., Mallory, M., Wong, J., Takenouchi, T., Hashimoto, M. & Masliah, E. (2000). alpha-synuclein promotes mitochondrial deficit and oxidative stress. *Am J Pathol,* **157**, 401-10.

Ilieva, E. V., Ayala, V., Jove, M., Dalfo, E., Cacabelos, D., Povedano, M., Bellmunt, M. J., Ferrer, I., Pamplona, R. & Portero-Otin, M. (2007). Oxidative and endoplasmic reticulum stress interplay in sporadic amyotrophic lateral sclerosis. *Brain,* **130**, 3111-23.

Imamura, K., Sahara, N., Kanaan, N. M., Tsukita, K., Kondo, T., Kutoku, Y., Ohsawa, Y., Sunada, Y., Kawakami, K., Hotta, A., Yawata, S., Watanabe, D., Hasegawa, M., Trojanowski, J. Q., Lee, V. M., Suhara, T., Higuchi, M. & Inoue, H. (2016). Calcium dysregulation contributes to neurodegeneration in FTLD patient iPSC-derived neurons. *Sci Rep,* **6**, 34904.

Ingerman, E., Perkins, E. M., Marino, M., Mears, J. A., McCaffery, J. M., Hinshaw, J. E. & Nunnari, J. (2005). Dnm1 forms spirals that are structurally tailored to fit mitochondria. *J Cell Biol,* **170**, 1021-7.

Ishihara, T., Ban-Ishihara, R., Maeda, M., Matsunaga, Y., Ichimura, A., Kyogoku, S., Aoki, H., Katada, S., Nakada, K., Nomura, M., Mizushima, N., Mihara, K. & Ishihara, N. (2015). Dynamics of mitochondrial DNA nucleoids regulated by mitochondrial fission is essential for maintenance of homogeneously active mitochondria during neonatal heart development. *Mol Cell Biol,* **35**, 211-23.

Issop, L., Fan, J., Lee, S., Rone, M. B., Basu, K., Mui, J. & Papadopoulos, V. (2015). Mitochondria-associated membrane formation in hormone-stimulated Leydig cell steroidogenesis: role of ATAD3. *Endocrinology,* **156**, 334-45.

Itakura, E., Kishi, C., Inoue, K. & Mizushima, N. (2008). Beclin 1 forms two distinct phosphatidylinositol 3-kinase complexes with mammalian Atg14 and UVRAG. *Mol Biol Cell,* **19**, 5360-72.

Itoh, K., Tamura, Y., Iijima, M. & Sesaki, H. (2013). Effects of Fcj1-Mos1 and mitochondrial division on aggregation of mitochondrial DNA nucleoids and organelle morphology. *Mol Biol Cell,* **24**, 1842-51.

Iwasawa, R., Mahul-Mellier, A. L., Datler, C., Pazarentzos, E. & Grimm, S. (2011). Fis1 and Bap31 bridge the mitochondria-ER interface to establish a platform for apoptosis induction. *EMBO J,* **30**, 556-68.

Iwatsubo, T., Odaka, A., Suzuki, N., Mizusawa, H., Nukina, N. & Ihara, Y. (1994). Visualization of A beta 42(43) and A beta 40 in senile plaques with end-specific A beta monoclonals: evidence that an initially deposited species is A beta 42(43). *Neuron,* **13**, 45-53.

Jastroch, M., Divakaruni, A. S., Mookerjee, S., Treberg, J. R. & Brand, M. D. (2010). Mitochondrial proton and electron leaks. *Essays Biochem,* **47**, 53-67.

Johannsen, P., Velander, G., Mai, J., Thorling, E. B. & Dupont, E. (1991). Glutathione peroxidase in early and advanced Parkinson's disease. *J Neurol Neurosurg Psychiatry,* **54**, 679-82.

Johnson, J. O., Mandrioli, J., Benatar, M., Abramzon, Y., Van Deerlin, V. M., Trojanowski, J. Q., Gibbs, J. R., Brunetti, M., Gronka, S., Wuu, J., Ding, J., McCluskey, L., Martinez-Lage, M., Falcone, D., Hernandez, D. G., Arepalli, S., Chong, S., Schymick, J. C., Rothstein, J., Landi, F., Wang, Y. D., Calvo, A., Mora, G., Sabatelli, M., Monsurro, M. R., Battistini, S., Salvi, F., Spataro, R., Sola, P., Borghero, G., Consortium, I., Galassi, G., Scholz, S. W., Taylor, J. P., Restagno, G., Chio, A. & Traynor, B. J. (2010). Exome sequencing reveals VCP mutations as a cause of familial ALS. *Neuron,* **68**, 857-64.

Johri, A. & Beal, M. F. (2012). Mitochondrial dysfunction in neurodegenerative diseases. *J Pharmacol Exp Ther,* **342**, 619-30.

Kaiser, S. E., Brickner, J. H., Reilein, A. R., Fenn, T. D., Walter, P. & Brunger, A. T. (2005). Structural basis of FFAT motif-mediated ER targeting. *Structure,* **13**, 1035-45.

Kamiyama, D., Sekine, S., Barsi-Rhyne, B., Hu, J., Chen, B., Gilbert, L. A., Ishikawa, H., Leonetti, M. D., Marshall, W. F., Weissman, J. S. & Huang, B. (2016). Versatile protein tagging in cells with split fluorescent protein. *Nat Commun,* **7**, 11046.

Kamp, F., Exner, N., Lutz, A. K., Wender, N., Hegermann, J., Brunner, B., Nuscher, B., Bartels, T., Giese, A., Beyer, K., Eimer, S., Winklhofer, K. F. & Haass, C. (2010). Inhibition of mitochondrial fusion by alpha-synuclein is rescued by PINK1, Parkin and DJ-1. *EMBO J,* **29**, 3571-89.

Kanekura, K., Nishimoto, I., Aiso, S. & Matsuoka, M. (2006). Characterization of amyotrophic lateral sclerosis-linked P56S mutation of vesicle-associated membrane protein-associated protein B (VAPB/ALS8). *J Biol Chem,* **281**, 30223-33.

Kang, J., Lemaire, H. G., Unterbeck, A., Salbaum, J. M., Masters, C. L., Grzeschik, K. H., Multhaup, G., Beyreuther, K. & Muller-Hill, B. (1987). The precursor of Alzheimer's disease amyloid A4 protein resembles a cell-surface receptor. *Nature,* **325**, 733-6.

Kato, S. (2008). Amyotrophic lateral sclerosis models and human neuropathology: similarities and differences. *Acta Neuropathol,* **115**, 97-114.

Kawano, M., Kumagai, K., Nishijima, M. & Hanada, K. (2006). Efficient trafficking of ceramide from the endoplasmic reticulum to the Golgi apparatus requires a VAMP-associated protein-interacting FFAT motif of CERT. *J Biol Chem,* **281**, 30279-88.

Kennedy, B. E., Charman, M. & Karten, B. (2012). Niemann-Pick Type C2 protein contributes to the transport of endosomal cholesterol to mitochondria without interacting with NPC1. *J Lipid Res,* **53**, 2632-42.

Kero, J., Ahmed, K., Wettschureck, N., Tunaru, S., Wintermantel, T., Greiner, E., Schutz, G. & Offermanns, S. (2007). Thyrocyte-specific Gq/G11 deficiency impairs thyroid function and prevents goiter development. *J Clin Invest,* **117**, 2399-407.

Kerppola, T. K. (2006). Design and implementation of bimolecular fluorescence complementation (BiFC) assays for the visualization of protein interactions in living cells. *Nat Protoc,* **1**, 1278-86.

Kerr, J. F., Wyllie, A. H. & Currie, A. R. (1972). Apoptosis: a basic biological phenomenon with wide-ranging implications in tissue kinetics. *Br J Cancer,* **26**, 239-57.

Kholmukhamedov, A., Schwartz, J. M. & Lemasters, J. J. (2013). Isolated mitochondria infusion mitigates ischemia-reperfusion injury of the liver in rats: mitotracker probes and mitochondrial membrane potential. *Shock,* **39**, 543.

Kikuchi, H., Almer, G., Yamashita, S., Guegan, C., Nagai, M., Xu, Z., Sosunov, A. A., McKhann, G. M., 2nd & Przedborski, S. (2006). Spinal cord endoplasmic reticulum stress associated with a microsomal accumulation of mutant superoxide dismutase-1 in an ALS model. *Proc Natl Acad Sci U S A,* **103**, 6025-30.

Kim, S., Leal, S. S., Ben Halevy, D., Gomes, C. M. & Lev, S. (2010). Structural requirements for VAP-B oligomerization and their implication in amyotrophic lateral sclerosis-associated VAP-B(P56S) neurotoxicity. *J Biol Chem,* **285**, 13839-49.

Klionsky, D. J., Cregg, J. M., Dunn, W. A., Jr., Emr, S. D., Sakai, Y., Sandoval, I. V., Sibirny, A., Subramani, S., Thumm, M., Veenhuis, M. & Ohsumi, Y. (2003). A unified nomenclature for yeast autophagy-related genes. *Dev Cell,* **5**, 539-45.

Kogot-Levin, A. & Saada, A. (2014). Ceramide and the mitochondrial respiratory chain. *Biochimie,* **100**, 88-94.

Kornmann, B., Currie, E., Collins, S. R., Schuldiner, M., Nunnari, J., Weissman, J. S. & Walter, P. (2009). An ER-mitochondria tethering complex revealed by a synthetic biology screen. *Science,* **325**, 477-81.

Kornmann, B., Osman, C. & Walter, P. (2011). The conserved GTPase Gem1 regulates endoplasmic reticulum-mitochondria connections. *Proc Natl Acad Sci U S A,* **108**, 14151-6.

Koyano, F., Okatsu, K., Kosako, H., Tamura, Y., Go, E., Kimura, M., Kimura, Y., Tsuchiya, H., Yoshihara, H., Hirokawa, T., Endo, T., Fon, E. A., Trempe, J. F., Saeki, Y., Tanaka, K. & Matsuda, N. (2014). Ubiquitin is phosphorylated by PINK1 to activate parkin. *Nature,* **510**, 162-6.

Kuijpers, M., van Dis, V., Haasdijk, E. D., Harterink, M., Vocking, K., Post, J. A., Scheper, W., Hoogenraad, C. C. & Jaarsma, D. (2013a). Amyotrophic lateral sclerosis (ALS)-associated VAPB-P56S inclusions represent an ER quality control compartment. *Acta Neuropathol Commun,* **1**, 24.

Kuijpers, M., Yu, K. L., Teuling, E., Akhmanova, A., Jaarsma, D. & Hoogenraad, C. C. (2013b). The ALS8 protein VAPB interacts with the ER-Golgi recycling protein YIF1A and regulates membrane delivery into dendrites. *EMBO J,* **32**, 2056-72.

Lai, K. O., Ip, F. C., Cheung, J., Fu, A. K. & Ip, N. Y. (2001). Expression of Eph receptors in skeletal muscle and their localization at the neuromuscular junction. *Mol Cell Neurosci,* **17**, 1034-47.

Langou, K., Moumen, A., Pellegrino, C., Aebischer, J., Medina, I., Aebischer, P. & Raoul, C. (2010). AAV-mediated expression of wild-type and ALS-linked mutant VAPB selectively triggers death of motoneurons through a Ca2+-dependent ER-associated pathway. *J Neurochem,* **114**, 795-809.

Larsson, N. G., Wang, J., Wilhelmsson, H., Oldfors, A., Rustin, P., Lewandoski, M., Barsh, G. S. & Clayton, D. A. (1998). Mitochondrial transcription factor A is necessary for mtDNA maintenance and embryogenesis in mice. *Nat Genet,* **18**, 231-6.

Leal, N. S., Schreiner, B., Pinho, C. M., Filadi, R., Wiehager, B., Karlstrom, H., Pizzo, P. & Ankarcrona, M. (2016). Mitofusin-2 knockdown increases ER-mitochondria contact and decreases amyloid beta-peptide production. *J Cell Mol Med,* **20**, 1686-95.

Lee, A. H., Iwakoshi, N. N. & Glimcher, L. H. (2003). XBP-1 regulates a subset of endoplasmic reticulum resident chaperone genes in the unfolded protein response. *Mol Cell Biol,* **23**, 7448-59.

Lee, K. W., Im, J. Y., Song, J. S., Lee, S. H., Lee, H. J., Ha, H. Y., Koh, J. Y., Gwag, B. J., Yang, S. D., Paik, S. G. & Han, P. L. (2006). Progressive neuronal loss and behavioral impairments of transgenic C57BL/6 inbred mice expressing the carboxy terminus of amyloid precursor protein. *Neurobiol Dis,* **22**, 10-24.

Lee, S., Lee, K. S., Huh, S., Liu, S., Lee, D. Y., Hong, S. H., Yu, K. & Lu, B. (2016). Polo Kinase Phosphorylates Miro to Control ER-Mitochondria Contact Sites and Mitochondrial Ca(2+) Homeostasis in Neural Stem Cell Development. *Dev Cell,* **37**, 174-189.

Leigh, P. N., Anderton, B. H., Dodson, A., Gallo, J. M., Swash, M. & Power, D. M. (1988). Ubiquitin deposits in anterior horn cells in motor neurone disease. *Neurosci Lett,* **93**, 197-203.

Lev, S., Ben Halevy, D., Peretti, D. & Dahan, N. (2008). The VAP protein family: from cellular functions to motor neuron disease. *Trends Cell Biol,* **18**, 282-90.

Levine, B. & Kroemer, G. (2008). Autophagy in the pathogenesis of disease. *Cell,* **132**, 27-42.

Lewis, R. S. (2007). The molecular choreography of a store-operated calcium channel. *Nature,* **446**, 284-7.

Lewis, S. C., Uchiyama, L. F. & Nunnari, J. (2016). ER-mitochondria contacts couple mtDNA synthesis with mitochondrial division in human cells. *Science,* **353**, aaf5549.

Lim, M. L., Minamikawa, T. & Nagley, P. (2001). The protonophore CCCP induces mitochondrial permeability transition without cytochrome c release in human osteosarcoma cells. *FEBS Lett,* **503**, 69-74.

Lim, Y., Cho, I. T., Schoel, L. J., Cho, G. & Golden, J. A. (2015). Hereditary spastic paraplegia-linked REEP1 modulates endoplasmic reticulum/mitochondria contacts. *Ann Neurol,* **78**, 679-96.

Litvak, V., Dahan, N., Ramachandran, S., Sabanay, H. & Lev, S. (2005). Maintenance of the diacylglycerol level in the Golgi apparatus by the Nir2 protein is critical for Golgi secretory function. *Nat Cell Biol,* **7**, 225-34.

Loewen, C. J., Roy, A. & Levine, T. P. (2003). A conserved ER targeting motif in three families of lipid binding proteins and in Opi1p binds VAP. *EMBO J,* **22**, 2025-35.

Lopez-Sanjurjo, C. I., Tovey, S. C., Prole, D. L. & Taylor, C. W. (2013). Lysosomes shape Ins(1,4,5)P3-evoked Ca2+ signals by selectively sequestering Ca2+ released from the endoplasmic reticulum. *J Cell Sci,* **126**, 289-300.

Lustbader, J. W., Cirilli, M., Lin, C., Xu, H. W., Takuma, K., Wang, N., Caspersen, C., Chen, X., Pollak, S., Chaney, M., Trinchese, F., Liu, S., Gunn-Moore, F., Lue, L. F., Walker, D. G., Kuppusamy, P., Zewier, Z. L., Arancio, O., Stern, D., Yan, S. S. & Wu, H. (2004). ABAD directly links Abeta to mitochondrial toxicity in Alzheimer's disease. *Science,* **304**, 448-52.

Lynes, E. M., Bui, M., Yap, M. C., Benson, M. D., Schneider, B., Ellgaard, L., Berthiaume, L. G. & Simmen, T. (2012). Palmitoylated TMX and calnexin target to the mitochondria-associated membrane. *EMBO J,* **31**, 457-70.

Maiuri, M. C., Zalckvar, E., Kimchi, A. & Kroemer, G. (2007). Self-eating and self-killing: crosstalk between autophagy and apoptosis. *Nat Rev Mol Cell Biol,* **8**, 741-52.

Manczak, M., Anekonda, T. S., Henson, E., Park, B. S., Quinn, J. & Reddy, P. H. (2006). Mitochondria are a direct site of A beta accumulation in Alzheimer's disease neurons: implications for free radical generation and oxidative damage in disease progression. *Hum Mol Genet,* **15**, 1437-49.

Mannan, A. U., Krawen, P., Sauter, S. M., Boehm, J., Chronowska, A., Paulus, W., Neesen, J. & Engel, W. (2006). ZFYVE27 (SPG33), a novel spastin-binding protein, is mutated in hereditary spastic paraplegia. *Am J Hum Genet,* **79**, 351-7.

Mannella, C. A., Pfeiffer, D. R., Bradshaw, P. C., Moraru, II, Slepchenko, B., Loew, L. M., Hsieh, C. E., Buttle, K. & Marko, M. (2001). Topology of the mitochondrial inner membrane: dynamics and bioenergetic implications. *IUBMB Life,* **52**, 93-100.

Mapstone, M., Cheema, A. K., Fiandaca, M. S., Zhong, X., Mhyre, T. R., MacArthur, L. H., Hall, W. J., Fisher, S. G., Peterson, D. R., Haley, J. M., Nazar, M. D., Rich, S. A., Berlau, D. J., Peltz, C. B., Tan, M. T., Kawas, C. H. & Federoff, H. J. (2014). Plasma phospholipids identify antecedent memory impairment in older adults. *Nat Med,* **20**, 415-8.

Martin, L. J., Pan, Y., Price, A. C., Sterling, W., Copeland, N. G., Jenkins, N. A., Price, D. L. & Lee, M. K. (2006). Parkinson's disease alpha-synuclein transgenic mice develop neuronal mitochondrial degeneration and cell death. *J Neurosci,* **26**, 41-50.

Maruyama, H., Morino, H., Ito, H., Izumi, Y., Kato, H., Watanabe, Y., Kinoshita, Y., Kamada, M., Nodera, H., Suzuki, H., Komure, O., Matsuura, S., Kobatake, K., Morimoto, N., Abe, K., Suzuki, N., Aoki, M., Kawata, A., Hirai, T., Kato, T., Ogasawara, K., Hirano, A., Takumi, T.,

Kusaka, H., Hagiwara, K., Kaji, R. & Kawakami, H. (2010). Mutations of optineurin in amyotrophic lateral sclerosis. *Nature,* **465**, 223-6.
Matern, H., Yang, X., Andrulis, E., Sternglanz, R., Trepte, H. H. & Gallwitz, D. (2000). A novel Golgi membrane protein is part of a GTPase-binding protein complex involved in vesicle targeting. *EMBO J,* **19**, 4485-92.
Matsunaga, K., Morita, E., Saitoh, T., Akira, S., Ktistakis, N. T., Izumi, T., Noda, T. & Yoshimori, T. (2010). Autophagy requires endoplasmic reticulum targeting of the PI3-kinase complex via Atg14L. *J Cell Biol,* **190**, 511-21.
McMaster, C. R. (2001). Lipid metabolism and vesicle trafficking: more than just greasing the transport machinery. *Biochem Cell Biol,* **79**, 681-92.
Meek, S., Mashimo, T. & Burdon, T. (2017). From engineering to editing the rat genome. *Mamm Genome,* **28**, 302-314.
Menzies, F. M., Cookson, M. R., Taylor, R. W., Turnbull, D. M., Chrzanowska-Lightowlers, Z. M., Dong, L., Figlewicz, D. A. & Shaw, P. J. (2002). Mitochondrial dysfunction in a cell culture model of familial amyotrophic lateral sclerosis. *Brain,* **125**, 1522-33.
Mesmin, B., Bigay, J., Moser von Filseck, J., Lacas-Gervais, S., Drin, G. & Antonny, B. (2013). A four-step cycle driven by PI(4)P hydrolysis directs sterol/PI(4)P exchange by the ER-Golgi tether OSBP. *Cell,* **155**, 830-43.
Miller, M. A., Ruest, P. J., Kosinski, M., Hanks, S. K. & Greenstein, D. (2003). An Eph receptor sperm-sensing control mechanism for oocyte meiotic maturation in Caenorhabditis elegans. *Genes Dev,* **17**, 187-200.
Mizushima, N. (2005). The pleiotropic role of autophagy: from protein metabolism to bactericide. *Cell Death Differ,* **12 Suppl 2**, 1535-41.
Mizushima, N., Yamamoto, A., Hatano, M., Kobayashi, Y., Kabeya, Y., Suzuki, K., Tokuhisa, T., Ohsumi, Y. & Yoshimori, T. (2001). Dissection of autophagosome formation using Apg5-deficient mouse embryonic stem cells. *J Cell Biol,* **152**, 657-68.
Mizushima, N., Yoshimori, T. & Ohsumi, Y. (2011). The role of Atg proteins in autophagosome formation. *Annu Rev Cell Dev Biol,* **27**, 107-32.
Morotz, G. M., De Vos, K. J., Vagnoni, A., Ackerley, S., Shaw, C. E. & Miller, C. C. (2012). Amyotrophic lateral sclerosis-associated mutant VAPBP56S perturbs calcium homeostasis to disrupt axonal transport of mitochondria. *Hum Mol Genet,* **21**, 1979-88.
Motulsky, H. J. & Brown, R. E. (2006). Detecting outliers when fitting data with nonlinear regression - a new method based on robust nonlinear regression and the false discovery rate. *BMC Bioinformatics,* **7**, 123.
Moumen, A., Virard, I. & Raoul, C. (2011). Accumulation of wildtype and ALS-linked mutated VAPB impairs activity of the proteasome. *PLoS One,* **6**, e26066.
Mourelatos, Z., Gonatas, N. K., Stieber, A., Gurney, M. E. & Dal Canto, M. C. (1996). The Golgi apparatus of spinal cord motor neurons in transgenic mice expressing mutant Cu,Zn superoxide dismutase becomes fragmented in early, preclinical stages of the disease. *Proc Natl Acad Sci U S A,* **93**, 5472-7.
Mukherjee, S. & Maxfield, F. R. (2004). Lipid and cholesterol trafficking in NPC. *Biochim Biophys Acta,* **1685**, 28-37.
Munoz, J. P., Ivanova, S., Sanchez-Wandelmer, J., Martinez-Cristobal, P., Noguera, E., Sancho, A., Diaz-Ramos, A., Hernandez-Alvarez, M. I., Sebastian, D., Mauvezin, C., Palacin, M. & Zorzano, A. (2013). Mfn2 modulates the UPR and mitochondrial function via repression of PERK. *EMBO J,* **32**, 2348-61.
Murley, A., Lackner, L. L., Osman, C., West, M., Voeltz, G. K., Walter, P. & Nunnari, J. (2013). ER-associated mitochondrial division links the distribution of mitochondria and mitochondrial DNA in yeast. *Elife,* **2**, e00422.
Nagai, T., Ibata, K., Park, E. S., Kubota, M., Mikoshiba, K. & Miyawaki, A. (2002). A variant of yellow fluorescent protein with fast and efficient maturation for cell-biological applications. *Nat Biotechnol,* **20**, 87-90.
Nagai, T., Sawano, A., Park, E. S. & Miyawaki, A. (2001). Circularly permuted green fluorescent proteins engineered to sense Ca2+. *Proc Natl Acad Sci U S A,* **98**, 3197-202.

Nakamichi, S., Yamanaka, K., Suzuki, M., Watanabe, T. & Kagiwada, S. (2011). Human VAPA and the yeast VAP Scs2p with an altered proline distribution can phenocopy amyotrophic lateral sclerosis-associated VAPB(P56S). *Biochem Biophys Res Commun,* **404**, 605-9.

Nakamura, K., Nemani, V. M., Azarbal, F., Skibinski, G., Levy, J. M., Egami, K., Munishkina, L., Zhang, J., Gardner, B., Wakabayashi, J., Sesaki, H., Cheng, Y., Finkbeiner, S., Nussbaum, R. L., Masliah, E. & Edwards, R. H. (2011). Direct membrane association drives mitochondrial fission by the Parkinson disease-associated protein alpha-synuclein. *J Biol Chem,* **286**, 20710-26.

Navone, F., Genevini, P. & Borgese, N. (2015). Autophagy and Neurodegeneration: Insights from a Cultured Cell Model of ALS. *Cells,* **4**, 354-86.

Neumann, M., Sampathu, D. M., Kwong, L. K., Truax, A. C., Micsenyi, M. C., Chou, T. T., Bruce, J., Schuck, T., Grossman, M., Clark, C. M., McCluskey, L. F., Miller, B. L., Masliah, E., Mackenzie, I. R., Feldman, H., Feiden, W., Kretzschmar, H. A., Trojanowski, J. Q. & Lee, V. M. (2006). Ubiquitinated TDP-43 in frontotemporal lobar degeneration and amyotrophic lateral sclerosis. *Science,* **314**, 130-3.

Ng, F. W., Nguyen, M., Kwan, T., Branton, P. E., Nicholson, D. W., Cromlish, J. A. & Shore, G. C. (1997). p28 Bap31, a Bcl-2/Bcl-XL- and procaspase-8-associated protein in the endoplasmic reticulum. *J Cell Biol,* **139**, 327-38.

Ngoh, G. A., Papanicolaou, K. N. & Walsh, K. (2012). Loss of mitofusin 2 promotes endoplasmic reticulum stress. *J Biol Chem,* **287**, 20321-32.

Nicholls, D. G. & Budd, S. L. (2000). Mitochondria and neuronal survival. *Physiol Rev,* **80**, 315-60.

Nicholson-Fish, J. C., Smillie, K. J. & Cousin, M. A. (2016). Monitoring activity-dependent bulk endocytosis with the genetically-encoded reporter VAMP4-pHluorin. *J Neurosci Methods,* **266**, 1-10.

Nicotera, P. & Orrenius, S. (1998). The role of calcium in apoptosis. *Cell Calcium,* **23**, 173-80.

Nishimura, A. L., Mitne-Neto, M., Silva, H. C., Richieri-Costa, A., Middleton, S., Cascio, D., Kok, F., Oliveira, J. R., Gillingwater, T., Webb, J., Skehel, P. & Zatz, M. (2004). A mutation in the vesicle-trafficking protein VAPB causes late-onset spinal muscular atrophy and amyotrophic lateral sclerosis. *Am J Hum Genet,* **75**, 822-31.

Nishimura, Y., Hayashi, M., Inada, H. & Tanaka, T. (1999). Molecular cloning and characterization of mammalian homologues of vesicle-associated membrane protein-associated (VAMP-associated) proteins. *Biochem Biophys Res Commun,* **254**, 21-6.

Nitsch, R. M., Blusztajn, J. K., Pittas, A. G., Slack, B. E., Growdon, J. H. & Wurtman, R. J. (1992). Evidence for a membrane defect in Alzheimer disease brain. *Proc Natl Acad Sci U S A,* **89**, 1671-5.

Obara, K., Noda, T., Niimi, K. & Ohsumi, Y. (2008). Transport of phosphatidylinositol 3-phosphate into the vacuole via autophagic membranes in Saccharomyces cerevisiae. *Genes Cells,* **13**, 537-47.

Oslowski, C. M. & Urano, F. (2011). Measuring ER stress and the unfolded protein response using mammalian tissue culture system. *Methods Enzymol,* **490**, 71-92.

Paillusson, S., Stoica, R., Gomez-Suaga, P., Lau, D. H. W., Mueller, S., Miller, T. & Miller, C. C. J. (2016). There's Something Wrong with my MAM; the ER-Mitochondria Axis and Neurodegenerative Diseases. *Trends Neurosci,* **39**, 146-157.

Palecek, J., Lips, M. B. & Keller, B. U. (1999). Calcium dynamics and buffering in motoneurones of the mouse spinal cord. *J Physiol,* **520 Pt 2**, 485-502.

Papiani, G., Ruggiano, A., Fossati, M., Raimondi, A., Bertoni, G., Francolini, M., Benfante, R., Navone, F. & Borgese, N. (2012). Restructured endoplasmic reticulum generated by mutant amyotrophic lateral sclerosis-linked VAPB is cleared by the proteasome. *J Cell Sci,* **125**, 3601-11.

Pappolla, M. A., Chyan, Y. J., Omar, R. A., Hsiao, K., Perry, G., Smith, M. A. & Bozner, P. (1998). Evidence of oxidative stress and in vivo neurotoxicity of beta-amyloid in a transgenic mouse model of Alzheimer's disease: a chronic oxidative paradigm for testing antioxidant therapies in vivo. *Am J Pathol,* **152**, 871-7.

Pennetta, G., Hiesinger, P. R., Fabian-Fine, R., Meinertzhagen, I. A. & Bellen, H. J. (2002). Drosophila VAP-33A directs bouton formation at neuromuscular junctions in a dosage-dependent manner. *Neuron,* **35**, 291-306.

Pera, M., Larrea, D., Guardia-Laguarta, C., Montesinos, J., Velasco, K. R., Agrawal, R. R., Xu, Y., Chan, R. B., Di Paolo, G., Mehler, M. F., Perumal, G. S., Macaluso, F. P., Freyberg, Z. Z., Acin-Perez, R., Enriquez, J. A., Schon, E. A. & Area-Gomez, E. (2017). Increased localization of APP-C99 in mitochondria-associated ER membranes causes mitochondrial dysfunction in Alzheimer disease. *EMBO J*.

Peretti, D., Dahan, N., Shimoni, E., Hirschberg, K. & Lev, S. (2008). Coordinated lipid transfer between the endoplasmic reticulum and the Golgi complex requires the VAP proteins and is essential for Golgi-mediated transport. *Mol Biol Cell,* **19**, 3871-84.

Phillips, M. J. & Voeltz, G. K. (2016). Structure and function of ER membrane contact sites with other organelles. *Nat Rev Mol Cell Biol,* **17**, 69-82.

Pich, S., Bach, D., Briones, P., Liesa, M., Camps, M., Testar, X., Palacin, M. & Zorzano, A. (2005). The Charcot-Marie-Tooth type 2A gene product, Mfn2, up-regulates fuel oxidation through expression of OXPHOS system. *Hum Mol Genet,* **14**, 1405-15.

Pilling, A. D., Horiuchi, D., Lively, C. M. & Saxton, W. M. (2006). Kinesin-1 and Dynein are the primary motors for fast transport of mitochondria in Drosophila motor axons. *Mol Biol Cell,* **17**, 2057-68.

Polymeropoulos, M. H., Lavedan, C., Leroy, E., Ide, S. E., Dehejia, A., Dutra, A., Pike, B., Root, H., Rubenstein, J., Boyer, R., Stenroos, E. S., Chandrasekharappa, S., Athanassiadou, A., Papapetropoulos, T., Johnson, W. G., Lazzarini, A. M., Duvoisin, R. C., Di Iorio, G., Golbe, L. I. & Nussbaum, R. L. (1997). Mutation in the alpha-synuclein gene identified in families with Parkinson's disease. *Science,* **276**, 2045-7.

Powell, K. S. & Latterich, M. (2000). The making and breaking of the endoplasmic reticulum. *Traffic,* **1**, 689-94.

Prasad, M. R., Lovell, M. A., Yatin, M., Dhillon, H. & Markesbery, W. R. (1998). Regional membrane phospholipid alterations in Alzheimer's disease. *Neurochem Res,* **23**, 81-8.

Prause, J., Goswami, A., Katona, I., Roos, A., Schnizler, M., Bushuven, E., Dreier, A., Buchkremer, S., Johann, S., Beyer, C., Deschauer, M., Troost, D. & Weis, J. (2013). Altered localization, abnormal modification and loss of function of Sigma receptor-1 in amyotrophic lateral sclerosis. *Hum Mol Genet,* **22**, 1581-600.

Prosser, D. C., Tran, D., Gougeon, P. Y., Verly, C. & Ngsee, J. K. (2008). FFAT rescues VAPA-mediated inhibition of ER-to-Golgi transport and VAPB-mediated ER aggregation. *J Cell Sci,* **121**, 3052-61.

Pryor, P. R., Mullock, B. M., Bright, N. A., Gray, S. R. & Luzio, J. P. (2000). The role of intraorganellar Ca(2+) in late endosome-lysosome heterotypic fusion and in the reformation of lysosomes from hybrid organelles. *J Cell Biol,* **149**, 1053-62.

Qin, H., Wang, W. & Song, J. (2013). ALS-causing P56S mutation and splicing variation on the hVAPB MSP domain transform its beta-sandwich fold into lipid-interacting helical conformations. *Biochem Biophys Res Commun,* **431**, 398-403.

Radford, H., Moreno, J. A., Verity, N., Halliday, M. & Mallucci, G. R. (2015). PERK inhibition prevents tau-mediated neurodegeneration in a mouse model of frontotemporal dementia. *Acta Neuropathol,* **130**, 633-42.

Raiborg, C., Wenzel, E. M., Pedersen, N. M., Olsvik, H., Schink, K. O., Schultz, S. W., Vietri, M., Nisi, V., Bucci, C., Brech, A., Johansen, T. & Stenmark, H. (2015a). Repeated ER-endosome contacts promote endosome translocation and neurite outgrowth. *Nature,* **520**, 234-8.

Raiborg, C., Wenzel, E. M. & Stenmark, H. (2015b). ER-endosome contact sites: molecular compositions and functions. *EMBO J,* **34**, 1848-58.

Rapizzi, E., Pinton, P., Szabadkai, G., Wieckowski, M. R., Vandecasteele, G., Baird, G., Tuft, R. A., Fogarty, K. E. & Rizzuto, R. (2002). Recombinant expression of the voltage-dependent anion channel enhances the transfer of Ca2+ microdomains to mitochondria. *J Cell Biol,* **159**, 613-24.

Ratnaparkhi, A., Lawless, G. M., Schweizer, F. E., Golshani, P. & Jackson, G. R. (2008). A Drosophila model of ALS: human ALS-associated mutation in VAP33A suggests a dominant negative mechanism. *PLoS One,* **3**, e2334.

Ravikumar, B., Vacher, C., Berger, Z., Davies, J. E., Luo, S., Oroz, L. G., Scaravilli, F., Easton, D. F., Duden, R., O'Kane, C. J. & Rubinsztein, D. C. (2004). Inhibition of mTOR induces autophagy and reduces toxicity of polyglutamine expansions in fly and mouse models of Huntington disease. *Nat Genet,* **36**, 585-95.

Raychaudhuri, S. & Prinz, W. A. (2008). Nonvesicular phospholipid transfer between peroxisomes and the endoplasmic reticulum. *Proc Natl Acad Sci U S A,* **105**, 15785-90.

Reddy, P. H., McWeeney, S., Park, B. S., Manczak, M., Gutala, R. V., Partovi, D., Jung, Y., Yau, V., Searles, R., Mori, M. & Quinn, J. (2004). Gene expression profiles of transcripts in amyloid precursor protein transgenic mice: up-regulation of mitochondrial metabolism and apoptotic genes is an early cellular change in Alzheimer's disease. *Hum Mol Genet,* **13**, 1225-40.

Remy, I., Galarneau, A. & Michnick, S. W. (2002). Detection and visualization of protein interactions with protein fragment complementation assays. *Methods Mol Biol,* **185**, 447-59.

Renton, A. E., Majounie, E., Waite, A., Simon-Sanchez, J., Rollinson, S., Gibbs, J. R., Schymick, J. C., Laaksovirta, H., van Swieten, J. C., Myllykangas, L., Kalimo, H., Paetau, A., Abramzon, Y., Remes, A. M., Kaganovich, A., Scholz, S. W., Duckworth, J., Ding, J., Harmer, D. W., Hernandez, D. G., Johnson, J. O., Mok, K., Ryten, M., Trabzuni, D., Guerreiro, R. J., Orrell, R. W., Neal, J., Murray, A., Pearson, J., Jansen, I. E., Sondervan, D., Seelaar, H., Blake, D., Young, K., Halliwell, N., Callister, J. B., Toulson, G., Richardson, A., Gerhard, A., Snowden, J., Mann, D., Neary, D., Nalls, M. A., Peuralinna, T., Jansson, L., Isoviita, V. M., Kaivorinne, A. L., Holtta-Vuori, M., Ikonen, E., Sulkava, R., Benatar, M., Wuu, J., Chio, A., Restagno, G., Borghero, G., Sabatelli, M., Consortium, I., Heckerman, D., Rogaeva, E., Zinman, L., Rothstein, J. D., Sendtner, M., Drepper, C., Eichler, E. E., Alkan, C., Abdullaev, Z., Pack, S. D., Dutra, A., Pak, E., Hardy, J., Singleton, A., Williams, N. M., Heutink, P., Pickering-Brown, S., Morris, H. R., Tienari, P. J. & Traynor, B. J. (2011). A hexanucleotide repeat expansion in C9ORF72 is the cause of chromosome 9p21-linked ALS-FTD. *Neuron,* **72**, 257-68.

Rizzardini, M., Lupi, M., Mangolini, A., Babetto, E., Ubezio, P. & Cantoni, L. (2006). Neurodegeneration induced by complex I inhibition in a cellular model of familial amyotrophic lateral sclerosis. *Brain Res Bull,* **69**, 465-74.

Rizzuto, R., De Stefani, D., Raffaello, A. & Mammucari, C. (2012). Mitochondria as sensors and regulators of calcium signalling. *Nat Rev Mol Cell Biol,* **13**, 566-78.

Rizzuto, R., Pinton, P., Carrington, W., Fay, F. S., Fogarty, K. E., Lifshitz, L. M., Tuft, R. A. & Pozzan, T. (1998). Close contacts with the endoplasmic reticulum as determinants of mitochondrial Ca2+ responses. *Science,* **280**, 1763-6.

Robberecht, W. & Philips, T. (2013). The changing scene of amyotrophic lateral sclerosis. *Nat Rev Neurosci,* **14**, 248-64.

Rocha, N., Kuijl, C., van der Kant, R., Janssen, L., Houben, D., Janssen, H., Zwart, W. & Neefjes, J. (2009). Cholesterol sensor ORP1L contacts the ER protein VAP to control Rab7-RILP-p150 Glued and late endosome positioning. *J Cell Biol,* **185**, 1209-25.

Rogaev, E. I., Sherrington, R., Rogaeva, E. A., Levesque, G., Ikeda, M., Liang, Y., Chi, H., Lin, C., Holman, K., Tsuda, T. & et al. (1995). Familial Alzheimer's disease in kindreds with missense mutations in a gene on chromosome 1 related to the Alzheimer's disease type 3 gene. *Nature,* **376**, 775-8.

Rogers, T. B., Inesi, G., Wade, R. & Lederer, W. J. (1995). Use of thapsigargin to study Ca2+ homeostasis in cardiac cells. *Biosci Rep,* **15**, 341-9.

Rogov, V., Dotsch, V., Johansen, T. & Kirkin, V. (2014). Interactions between autophagy receptors and ubiquitin-like proteins form the molecular basis for selective autophagy. *Mol Cell,* **53**, 167-78.

Rosen, D. R., Siddique, T., Patterson, D., Figlewicz, D. A., Sapp, P., Hentati, A., Donaldson, D., Goto, J., O'Regan, J. P., Deng, H. X. & et al. (1993). Mutations in Cu/Zn superoxide dismutase gene are associated with familial amyotrophic lateral sclerosis. *Nature,* **362**, 59-62.

Ross, C. A. & Poirier, M. A. (2004). Protein aggregation and neurodegenerative disease. *Nat Med,* **10 Suppl**, S10-7.

Rowland, A. A., Chitwood, P. J., Phillips, M. J. & Voeltz, G. K. (2014). ER contact sites define the position and timing of endosome fission. *Cell,* **159**, 1027-1041.

Rowland, A. A. & Voeltz, G. K. (2012). Endoplasmic reticulum-mitochondria contacts: function of the junction. *Nat Rev Mol Cell Biol,* **13**, 607-25.

Rusinol, A. E., Cui, Z., Chen, M. H. & Vance, J. E. (1994). A unique mitochondria-associated membrane fraction from rat liver has a high capacity for lipid synthesis and contains pre-Golgi secretory proteins including nascent lipoproteins. *J Biol Chem,* **269**, 27494-502.

Russ, W. P. & Engelman, D. M. (2000). The GxxxG motif: a framework for transmembrane helix-helix association. *J Mol Biol,* **296**, 911-9.

Rutter, G. A. & Rizzuto, R. (2000). Regulation of mitochondrial metabolism by ER Ca2+ release: an intimate connection. *Trends Biochem Sci,* **25**, 215-21.

Sanhueza, M., Zechini, L., Gillespie, T. & Pennetta, G. (2014). Gain-of-function mutations in the ALS8 causative gene VAPB have detrimental effects on neurons and muscles. *Biol Open,* **3**, 59-71.

Saotome, M., Safiulina, D., Szabadkai, G., Das, S., Fransson, A., Aspenstrom, P., Rizzuto, R. & Hajnoczky, G. (2008). Bidirectional Ca2+-dependent control of mitochondrial dynamics by the Miro GTPase. *Proc Natl Acad Sci U S A,* **105**, 20728-33.

Sasaki, S. (2011). Autophagy in spinal cord motor neurons in sporadic amyotrophic lateral sclerosis. *J Neuropathol Exp Neurol,* **70**, 349-59.

Scarffe, L. A., Stevens, D. A., Dawson, V. L. & Dawson, T. M. (2014). Parkin and PINK1: much more than mitophagy. *Trends Neurosci,* **37**, 315-24.

Schauder, C. M., Wu, X., Saheki, Y., Narayanaswamy, P., Torta, F., Wenk, M. R., De Camilli, P. & Reinisch, K. M. (2014). Structure of a lipid-bound extended synaptotagmin indicates a role in lipid transfer. *Nature,* **510**, 552-5.

Schindelin, J., Arganda-Carreras, I., Frise, E., Kaynig, V., Longair, M., Pietzsch, T., Preibisch, S., Rueden, C., Saalfeld, S., Schmid, B., Tinevez, J. Y., White, D. J., Hartenstein, V., Eliceiri, K., Tomancak, P. & Cardona, A. (2012). Fiji: an open-source platform for biological-image analysis. *Nat Methods,* **9**, 676-82.

Schneider, C. A., Rasband, W. S. & Eliceiri, K. W. (2012). NIH Image to ImageJ: 25 years of image analysis. *Nat Methods,* **9**, 671-5.

Scorrano, L. (2013). Keeping mitochondria in shape: a matter of life and death. *Eur J Clin Invest,* **43**, 886-93.

Scorrano, L., Oakes, S. A., Opferman, J. T., Cheng, E. H., Sorcinelli, M. D., Pozzan, T. & Korsmeyer, S. J. (2003). BAX and BAK regulation of endoplasmic reticulum Ca2+: a control point for apoptosis. *Science,* **300**, 135-9.

Shavali, S., Brown-Borg, H. M., Ebadi, M. & Porter, J. (2008). Mitochondrial localization of alpha-synuclein protein in alpha-synuclein overexpressing cells. *Neurosci Lett,* **439**, 125-8.

Shen, J., Chen, X., Hendershot, L. & Prywes, R. (2002). ER stress regulation of ATF6 localization by dissociation of BiP/GRP78 binding and unmasking of Golgi localization signals. *Dev Cell,* **3**, 99-111.

Sherrington, R., Rogaev, E. I., Liang, Y., Rogaeva, E. A., Levesque, G., Ikeda, M., Chi, H., Lin, C., Li, G., Holman, K., Tsuda, T., Mar, L., Foncin, J. F., Bruni, A. C., Montesi, M. P., Sorbi, S., Rainero, I., Pinessi, L., Nee, L., Chumakov, I., Pollen, D., Brookes, A., Sanseau, P., Polinsky, R. J., Wasco, W., Da Silva, H. A., Haines, J. L., Perkicak-Vance, M. A., Tanzi, R. E., Roses, A. D., Fraser, P. E., Rommens, J. M. & St George-Hyslop, P. H. (1995). Cloning of a gene bearing missense mutations in early-onset familial Alzheimer's disease. *Nature,* **375**, 754-60.

Shi, J., Lua, S., Tong, J. S. & Song, J. (2010). Elimination of the native structure and solubility of the hVAPB MSP domain by the Pro56Ser mutation that causes amyotrophic lateral sclerosis. *Biochemistry,* **49**, 3887-97.

Shiao, Y. J., Lupo, G. & Vance, J. E. (1995). Evidence that phosphatidylserine is imported into mitochondria via a mitochondria-associated membrane and that the majority of mitochondrial phosphatidylethanolamine is derived from decarboxylation of phosphatidylserine. *J Biol Chem,* **270**, 11190-8.

Shimura, H., Hattori, N., Kubo, S., Mizuno, Y., Asakawa, S., Minoshima, S., Shimizu, N., Iwai, K., Chiba, T., Tanaka, K. & Suzuki, T. (2000). Familial Parkinson disease gene product, parkin, is a ubiquitin-protein ligase. *Nat Genet,* **25**, 302-5.

Shuai, J. & Parker, I. (2005). Optical single-channel recording by imaging Ca2+ flux through individual ion channels: theoretical considerations and limits to resolution. *Cell Calcium,* **37**, 283-99.

Simmen, T., Aslan, J. E., Blagoveshchenskaya, A. D., Thomas, L., Wan, L., Xiang, Y., Feliciangeli, S. F., Hung, C. H., Crump, C. M. & Thomas, G. (2005). PACS-2 controls endoplasmic reticulum-mitochondria communication and Bid-mediated apoptosis. *EMBO J,* **24**, 717-29.

Skehel, P. A., Fabian-Fine, R. & Kandel, E. R. (2000). Mouse VAP33 is associated with the endoplasmic reticulum and microtubules. *Proc Natl Acad Sci U S A,* **97**, 1101-6.

Skehel, P. A., Martin, K. C., Kandel, E. R. & Bartsch, D. (1995). A VAMP-binding protein from Aplysia required for neurotransmitter release. *Science,* **269**, 1580-3.

Smith, M. A., Sayre, L. M., Monnier, V. M. & Perry, G. (1995). Radical AGEing in Alzheimer's disease. *Trends Neurosci,* **18**, 172-6.

Sollner, T., Whiteheart, S. W., Brunner, M., Erdjument-Bromage, H., Geromanos, S., Tempst, P. & Rothman, J. E. (1993). SNAP receptors implicated in vesicle targeting and fusion. *Nature,* **362**, 318-24.

Sood, A., Jeyaraju, D. V., Prudent, J., Caron, A., Lemieux, P., McBride, H. M., Laplante, M., Toth, K. & Pellegrini, L. (2014). A Mitofusin-2-dependent inactivating cleavage of Opa1 links changes in mitochondria cristae and ER contacts in the postprandial liver. *Proc Natl Acad Sci U S A,* **111**, 16017-22.

Soussan, L., Burakov, D., Daniels, M. P., Toister-Achituv, M., Porat, A., Yarden, Y. & Elazar, Z. (1999). ERG30, a VAP-33-related protein, functions in protein transport mediated by COPI vesicles. *J Cell Biol,* **146**, 301-11.

Spillantini, M. G., Schmidt, M. L., Lee, V. M., Trojanowski, J. Q., Jakes, R. & Goedert, M. (1997). Alpha-synuclein in Lewy bodies. *Nature,* **388**, 839-40.

Sreedharan, J., Blair, I. P., Tripathi, V. B., Hu, X., Vance, C., Rogelj, B., Ackerley, S., Durnall, J. C., Williams, K. L., Buratti, E., Baralle, F., de Belleroche, J., Mitchell, J. D., Leigh, P. N., Al-Chalabi, A., Miller, C. C., Nicholson, G. & Shaw, C. E. (2008). TDP-43 mutations in familial and sporadic amyotrophic lateral sclerosis. *Science,* **319**, 1668-72.

Stanley, P. (2011). Golgi glycosylation. *Cold Spring Harb Perspect Biol,* **3**.

Stefan, C. J., Manford, A. G., Baird, D., Yamada-Hanff, J., Mao, Y. & Emr, S. D. (2011). Osh proteins regulate phosphoinositide metabolism at ER-plasma membrane contact sites. *Cell,* **144**, 389-401.

Stefani, M. & Liguri, G. (2009). Cholesterol in Alzheimer's disease: unresolved questions. *Curr Alzheimer Res,* **6**, 15-29.

Stevens, F. J. & Argon, Y. (1999). Protein folding in the ER. *Semin Cell Dev Biol,* **10**, 443-54.

Stewart, M., King, K. L. & Roberts, T. M. (1994). The motile major sperm protein (MSP) of Ascaris suum forms filaments constructed from two helical subfilaments. *J Mol Biol,* **243**, 60-71.

Stieber, A., Mourelatos, Z. & Gonatas, N. K. (1996). In Alzheimer's disease the Golgi apparatus of a population of neurons without neurofibrillary tangles is fragmented and atrophic. *Am J Pathol,* **148**, 415-26.

Stoica, R., De Vos, K. J., Paillusson, S., Mueller, S., Sancho, R. M., Lau, K. F., Vizcay-Barrena, G., Lin, W. L., Xu, Y. F., Lewis, J., Dickson, D. W., Petrucelli, L., Mitchell, J. C., Shaw, C. E. & Miller, C. C. (2014). ER-mitochondria associations are regulated by the VAPB-PTPIP51 interaction and are disrupted by ALS/FTD-associated TDP-43. *Nat Commun,* **5**, 3996.

Stolz, A., Hilt, W., Buchberger, A. & Wolf, D. H. (2011). Cdc48: a power machine in protein degradation. *Trends Biochem Sci,* **36**, 515-23.

Stone, S. J., Levin, M. C., Zhou, P., Han, J., Walther, T. C. & Farese, R. V., Jr. (2009). The endoplasmic reticulum enzyme DGAT2 is found in mitochondria-associated membranes and has a mitochondrial targeting signal that promotes its association with mitochondria. *J Biol Chem,* **284**, 5352-61.

Stone, S. J. & Vance, J. E. (2000). Phosphatidylserine synthase-1 and -2 are localized to mitochondria-associated membranes. *J Biol Chem,* **275**, 34534-40.

Su, B., Wang, X., Bonda, D., Perry, G., Smith, M. & Zhu, X. (2010). Abnormal mitochondrial dynamics--a novel therapeutic target for Alzheimer's disease? *Mol Neurobiol,* **41**, 87-96.

Suda, Y. & Nakano, A. (2012). The yeast Golgi apparatus. *Traffic,* **13**, 505-10.

Suzuki, H., Kanekura, K., Levine, T. P., Kohno, K., Olkkonen, V. M., Aiso, S. & Matsuoka, M. (2009). ALS-linked P56S-VAPB, an aggregated loss-of-function mutant of VAPB, predisposes motor neurons to ER stress-related death by inducing aggregation of co-expressed wild-type VAPB. *J Neurochem,* **108**, 973-985.

Szabadkai, G., Bianchi, K., Varnai, P., De Stefani, D., Wieckowski, M. R., Cavagna, D., Nagy, A. I., Balla, T. & Rizzuto, R. (2006). Chaperone-mediated coupling of endoplasmic reticulum and mitochondrial Ca2+ channels. *J Cell Biol,* **175**, 901-11.

Tallini, Y. N., Ohkura, M., Choi, B. R., Ji, G., Imoto, K., Doran, R., Lee, J., Plan, P., Wilson, J., Xin, H. B., Sanbe, A., Gulick, J., Mathai, J., Robbins, J., Salama, G., Nakai, J. & Kotlikoff, M. I. (2006). Imaging cellular signals in the heart in vivo: Cardiac expression of the high-signal Ca2+ indicator GCaMP2. *Proc Natl Acad Sci U S A,* **103**, 4753-8.

Tashiro, Y., Urushitani, M., Inoue, H., Koike, M., Uchiyama, Y., Komatsu, M., Tanaka, K., Yamazaki, M., Abe, M., Misawa, H., Sakimura, K., Ito, H. & Takahashi, R. (2012). Motor neuron-specific disruption of proteasomes, but not autophagy, replicates amyotrophic lateral sclerosis. *J Biol Chem,* **287**, 42984-94.

Tasseva, G., Bai, H. D., Davidescu, M., Haromy, A., Michelakis, E. & Vance, J. E. (2013). Phosphatidylethanolamine deficiency in Mammalian mitochondria impairs oxidative phosphorylation and alters mitochondrial morphology. *J Biol Chem,* **288**, 4158-73.

Teese, M. G. & Langosch, D. (2015). Role of GxxxG Motifs in Transmembrane Domain Interactions. *Biochemistry,* **54**, 5125-35.

Terasaki, M., Slater, N. T., Fein, A., Schmidek, A. & Reese, T. S. (1994). Continuous network of endoplasmic reticulum in cerebellar Purkinje neurons. *Proc Natl Acad Sci U S A,* **91**, 7510-4.

Terry, R. D., Masliah, E., Salmon, D. P., Butters, N., DeTeresa, R., Hill, R., Hansen, L. A. & Katzman, R. (1991). Physical basis of cognitive alterations in Alzheimer's disease: synapse loss is the major correlate of cognitive impairment. *Ann Neurol,* **30**, 572-80.

Teuling, E., Ahmed, S., Haasdijk, E., Demmers, J., Steinmetz, M. O., Akhmanova, A., Jaarsma, D. & Hoogenraad, C. C. (2007). Motor neuron disease-associated mutant vesicle-associated membrane protein-associated protein (VAP) B recruits wild-type VAPs into endoplasmic reticulum-derived tubular aggregates. *J Neurosci,* **27**, 9801-15.

Tokutake, Y., Yamada, K., Ohata, M., Obayashi, Y., Tsuchiya, M. & Yonekura, S. (2015). ALS-Linked P56S-VAPB Mutation Impairs the Formation of Multinuclear Myotube in C2C12 Cells. *Int J Mol Sci,* **16**, 18628-41.

Tooze, S. A. & Yoshimori, T. (2010). The origin of the autophagosomal membrane. *Nat Cell Biol,* **12**, 831-5.

Tsuda, H., Han, S. M., Yang, Y., Tong, C., Lin, Y. Q., Mohan, K., Haueter, C., Zoghbi, A., Harati, Y., Kwan, J., Miller, M. A. & Bellen, H. J. (2008). The amyotrophic lateral sclerosis 8 protein VAPB is cleaved, secreted, and acts as a ligand for Eph receptors. *Cell,* **133**, 963-77.

Tubbs, E., Theurey, P., Vial, G., Bendridi, N., Bravard, A., Chauvin, M. A., Ji-Cao, J., Zoulim, F., Bartosch, B., Ovize, M., Vidal, H. & Rieusset, J. (2014). Mitochondria-associated endoplasmic reticulum membrane (MAM) integrity is required for insulin signaling and is implicated in hepatic insulin resistance. *Diabetes,* **63**, 3279-94.

Urano, F., Bertolotti, A. & Ron, D. (2000a). IRE1 and efferent signaling from the endoplasmic reticulum. *J Cell Sci,* **113 Pt 21**, 3697-702.

Urano, F., Wang, X., Bertolotti, A., Zhang, Y., Chung, P., Harding, H. P. & Ron, D. (2000b). Coupling of stress in the ER to activation of JNK protein kinases by transmembrane protein kinase IRE1. *Science,* **287**, 664-6.

Usenovic, M., Niroomand, S., Drolet, R. E., Yao, L., Gaspar, R. C., Hatcher, N. G., Schachter, J., Renger, J. J. & Parmentier-Batteur, S. (2015). Internalized Tau Oligomers Cause Neurodegeneration by Inducing Accumulation of Pathogenic Tau in Human Neurons Derived from Induced Pluripotent Stem Cells. *J Neurosci,* **35**, 14234-50.

Valente, E. M., Abou-Sleiman, P. M., Caputo, V., Muqit, M. M., Harvey, K., Gispert, S., Ali, Z., Del Turco, D., Bentivoglio, A. R., Healy, D. G., Albanese, A., Nussbaum, R., Gonzalez-Maldonado, R., Deller, T., Salvi, S., Cortelli, P., Gilks, W. P., Latchman, D. S., Harvey, R. J., Dallapiccola, B., Auburger, G. & Wood, N. W. (2004). Hereditary early-onset Parkinson's disease caused by mutations in PINK1. *Science,* **304**, 1158-60.

van Blitterswijk, M., van Es, M. A., Koppers, M., van Rheenen, W., Medic, J., Schelhaas, H. J., van der Kooi, A. J., de Visser, M., Veldink, J. H. & van den Berg, L. H. (2012). VAPB and C9orf72 mutations in 1 familial amyotrophic lateral sclerosis patient. *Neurobiol Aging,* **33**, 2950 e1-4.

Van Den Bosch, L., Vandenberghe, W., Klaassen, H., Van Houtte, E. & Robberecht, W. (2000). Ca(2+)-permeable AMPA receptors and selective vulnerability of motor neurons. *J Neurol Sci,* **180**, 29-34.

van der Kant, R. & Neefjes, J. (2014). Small regulators, major consequences - Ca(2)(+) and cholesterol at the endosome-ER interface. *J Cell Sci,* **127**, 929-38.

van der Vaart, A., Griffith, J. & Reggiori, F. (2010). Exit from the Golgi is required for the expansion of the autophagosomal phagophore in yeast Saccharomyces cerevisiae. *Mol Biol Cell,* **21**, 2270-84.

van Vliet, A. R., Giordano, F., Gerlo, S., Segura, I., Van Eygen, S., Molenberghs, G., Rocha, S., Houcine, A., Derua, R., Verfaillie, T., Vangindertael, J., De Keersmaecker, H., Waelkens, E., Tavernier, J., Hofkens, J., Annaert, W., Carmeliet, P., Samali, A., Mizuno, H. & Agostinis, P. (2017). The ER Stress Sensor PERK Coordinates ER-Plasma Membrane Contact Site Formation through Interaction with Filamin-A and F-Actin Remodeling. *Mol Cell,* **65**, 885-899 e6.

van Vliet, A. R., Verfaillie, T. & Agostinis, P. (2014). New functions of mitochondria associated membranes in cellular signaling. *Biochim Biophys Acta,* **1843**, 2253-62.

van Welsem, M. E., Hogenhuis, J. A., Meininger, V., Metsaars, W. P., Hauw, J. J. & Seilhean, D. (2002). The relationship between Bunina bodies, skein-like inclusions and neuronal loss in amyotrophic lateral sclerosis. *Acta Neuropathol,* **103**, 583-9.

Vance, C., Rogelj, B., Hortobagyi, T., De Vos, K. J., Nishimura, A. L., Sreedharan, J., Hu, X., Smith, B., Ruddy, D., Wright, P., Ganesalingam, J., Williams, K. L., Tripathi, V., Al-Saraj, S., Al-Chalabi, A., Leigh, P. N., Blair, I. P., Nicholson, G., de Belleroche, J., Gallo, J. M., Miller, C. C. & Shaw, C. E. (2009). Mutations in FUS, an RNA processing protein, cause familial amyotrophic lateral sclerosis type 6. *Science,* **323**, 1208-1211.

Vance, J. E. (1990). Phospholipid synthesis in a membrane fraction associated with mitochondria. *J. Biol. Chem.,* **265**, 7248-7256.

Vance, J. E. (2014). MAM (mitochondria-associated membranes) in mammalian cells: lipids and beyond. *Biochim Biophys Acta,* **1841**, 595-609.

Vanselow, B. K. & Keller, B. U. (2000). Calcium dynamics and buffering in oculomotor neurones from mouse that are particularly resistant during amyotrophic lateral sclerosis (ALS)-related motoneurone disease. *J Physiol,* **525 Pt 2**, 433-45.

Verfaillie, T., Rubio, N., Garg, A. D., Bultynck, G., Rizzuto, R., Decuypere, J. P., Piette, J., Linehan, C., Gupta, S., Samali, A. & Agostinis, P. (2012). PERK is required at the ER-mitochondrial contact sites to convey apoptosis after ROS-based ER stress. *Cell Death Differ,* **19**, 1880-91.

Voelker, D. R. (2005). Bridging gaps in phospholipid transport. *Trends Biochem Sci,* **30**, 396-404.

Voeltz, G. K., Rolls, M. M. & Rapoport, T. A. (2002). Structural organization of the endoplasmic reticulum. *EMBO Rep,* **3**, 944-50.

Walter, P. & Ron, D. (2011). The unfolded protein response: from stress pathway to homeostatic regulation. *Science,* **334**, 1081-6.

Wanders, R. J. & Poll-The, B. T. (2017). "Role of peroxisomes in human lipid metabolism and its importance for neurological development". *Neurosci Lett,* **637**, 11-17.

Wang, H. J., Guay, G., Pogan, L., Sauve, R. & Nabi, I. R. (2000). Calcium regulates the association between mitochondria and a smooth subdomain of the endoplasmic reticulum. *J Cell Biol,* **150**, 1489-98.

Wang, P. T., Garcin, P. O., Fu, M., Masoudi, M., St-Pierre, P., Pante, N. & Nabi, I. R. (2015). Distinct mechanisms controlling rough and smooth endoplasmic reticulum contacts with mitochondria. *J Cell Sci,* **128**, 2759-65.

Wang, X., Su, B., Fujioka, H. & Zhu, X. (2008). Dynamin-like protein 1 reduction underlies mitochondrial morphology and distribution abnormalities in fibroblasts from sporadic Alzheimer's disease patients. *Am J Pathol,* **173**, 470-82.

Wang, X. Z., Harding, H. P., Zhang, Y., Jolicoeur, E. M., Kuroda, M. & Ron, D. (1998). Cloning of mammalian Ire1 reveals diversity in the ER stress responses. *EMBO J,* **17**, 5708-17.

Wei, Y., Pattingre, S., Sinha, S., Bassik, M. & Levine, B. (2008). JNK1-mediated phosphorylation of Bcl-2 regulates starvation-induced autophagy. *Mol Cell,* **30**, 678-88.

Wieckowski, M. R., Giorgi, C., Lebiedzinska, M., Duszynski, J. & Pinton, P. (2009). Isolation of mitochondria-associated membranes and mitochondria from animal tissues and cells. *Nat Protoc,* **4**, 1582-90.

Wiedemann, F. R., Winkler, K., Kuznetsov, A. V., Bartels, C., Vielhaber, S., Feistner, H. & Kunz, W. S. (1998). Impairment of mitochondrial function in skeletal muscle of patients with amyotrophic lateral sclerosis. *J Neurol Sci,* **156**, 65-72.

Wolfe, M. S., Xia, W., Ostaszewski, B. L., Diehl, T. S., Kimberly, W. T. & Selkoe, D. J. (1999). Two transmembrane aspartates in presenilin-1 required for presenilin endoproteolysis and gamma-secretase activity. *Nature,* **398**, 513-7.

Wong, Y. C. & Holzbaur, E. L. (2014). Optineurin is an autophagy receptor for damaged mitochondria in parkin-mediated mitophagy that is disrupted by an ALS-linked mutation. *Proc Natl Acad Sci U S A,* **111**, E4439-48.

Wozniak, M. J., Bola, B., Brownhill, K., Yang, Y. C., Levakova, V. & Allan, V. J. (2009). Role of kinesin-1 and cytoplasmic dynein in endoplasmic reticulum movement in VERO cells. *J Cell Sci,* **122**, 1979-89.

Wu, M. M., Buchanan, J., Luik, R. M. & Lewis, R. S. (2006). Ca2+ store depletion causes STIM1 to accumulate in ER regions closely associated with the plasma membrane. *J Cell Biol,* **174**, 803-13.

Wu, M. M., Covington, E. D. & Lewis, R. S. (2014). Single-molecule analysis of diffusion and trapping of STIM1 and Orai1 at endoplasmic reticulum-plasma membrane junctions. *Mol Biol Cell,* **25**, 3672-85.

Xie, Z. & Klionsky, D. J. (2007). Autophagosome formation: core machinery and adaptations. *Nat Cell Biol,* **9**, 1102-9.

Yamanaka, K., Sasagawa, Y. & Ogura, T. (2012). Recent advances in p97/VCP/Cdc48 cellular functions. *Biochim Biophys Acta,* **1823**, 130-7.

Yang, Y., Hentati, A., Deng, H. X., Dabbagh, O., Sasaki, T., Hirano, M., Hung, W. Y., Ouahchi, K., Yan, J., Azim, A. C., Cole, N., Gascon, G., Yagmour, A., Ben-Hamida, M., Pericak-Vance, M., Hentati, F. & Siddique, T. (2001). The gene encoding alsin, a protein with three guanine-nucleotide exchange factor domains, is mutated in a form of recessive amyotrophic lateral sclerosis. *Nat Genet,* **29**, 160-5.

Yang, Z., Zhao, X., Xu, J., Shang, W. & Tong, C. (2018). A novel fluorescent reporter detects plastic remodeling of mitochondria-ER contact sites. *J Cell Sci,* **131**.

Ye, J., Rawson, R. B., Komuro, R., Chen, X., Dave, U. P., Prywes, R., Brown, M. S. & Goldstein, J. L. (2000). ER stress induces cleavage of membrane-bound ATF6 by the same proteases that process SREBPs. *Mol Cell,* **6**, 1355-64.

Yi, M., Weaver, D. & Hajnoczky, G. (2004). Control of mitochondrial motility and distribution by the calcium signal: a homeostatic circuit. *J Cell Biol,* **167**, 661-72.

Yoshii, S. R., Kishi, C., Ishihara, N. & Mizushima, N. (2011). Parkin mediates proteasome-dependent protein degradation and rupture of the outer mitochondrial membrane. *J Biol Chem,* **286**, 19630-40.

Youle, R. J. & van der Bliek, A. M. (2012). Mitochondrial fission, fusion, and stress. *Science,* **337**, 1062-5.

Young, A. R., Chan, E. Y., Hu, X. W., Kochl, R., Crawshaw, S. G., High, S., Hailey, D. W., Lippincott-Schwartz, J. & Tooze, S. A. (2006). Starvation and ULK1-dependent cycling of mammalian Atg9 between the TGN and endosomes. *J Cell Sci,* **119**, 3888-900.

Young, M. J., Humble, M. M., DeBalsi, K. L., Sun, K. Y. & Copeland, W. C. (2015). POLG2 disease variants: analyses reveal a dominant negative heterodimer, altered mitochondrial localization and impaired respiratory capacity. *Hum Mol Genet,* **24**, 5184-97.

Zampese, E., Fasolato, C., Kipanyula, M. J., Bortolozzi, M., Pozzan, T. & Pizzo, P. (2011). Presenilin 2 modulates endoplasmic reticulum (ER)-mitochondria interactions and Ca2+ cross-talk. *Proc Natl Acad Sci U S A,* **108**, 2777-82.

Zborowski, J., Dygas, A. & Wojtczak, L. (1983). Phosphatidylserine decarboxylase is located on the external side of the inner mitochondrial membrane. *FEBS Lett,* **157**, 179-82.

Zhao, Y. G., Liu, N., Miao, G., Chen, Y., Zhao, H. & Zhang, H. (2018). The ER Contact Proteins VAPA/B Interact with Multiple Autophagy Proteins to Modulate Autophagosome Biogenesis. *Curr Biol,* **28**, 1234-1245 e4.

Zhou, J., Li, A., Li, X. & Yi, J. (2019). Dysregulated mitochondrial Ca(2+) and ROS signaling in skeletal muscle of ALS mouse model. *Arch Biochem Biophys,* **663**, 249-258.

Zito, K., Parnas, D., Fetter, R. D., Isacoff, E. Y. & Goodman, C. S. (1999). Watching a synapse grow: noninvasive confocal imaging of synaptic growth in Drosophila. *Neuron,* **22**, 719-29.

Ziviani, E., Tao, R. N. & Whitworth, A. J. (2010). Drosophila parkin requires PINK1 for mitochondrial translocation and ubiquitinates mitofusin. *Proc Natl Acad Sci U S A,* **107**, 5018-23.

Appendix 1
Video Files

The following four video files can be found on the enclosed USB sticks:

Video 4.1: COS-7 cells transfected with V1-ER/V2-mito reporter plamids and stained with MitoTracker CMXRos imaged live for 10 min.

Video 4.2: NSC34 cells expressing Gq-coupled DREADD receptors show an increase in Cyto-GCaMP fluorescence upon the addition of CNO

Video 4.3: The number of BiFC puncta does not significantly change in response to rapid elevations of cytoplasmic Ca^{2+} concentrations mediated by CNO activation of Gq-coupled DREADD receptors

Video 4.4: Live-cell video of COS-7 cells transfected with V1-ER/V2-Mito and POLG2-DsRed2 with the mitochondria labelled in MitoTracker Deep Red FM

Appendix 2
Publication list

Peer-reviewed journals

Harmon, M., Larkman, P., Hardingham, G., Jackon, M. & Skehel, P. 2017. A Bi-fluorescence complementation system to detect associations between the Endoplasmic reticulum and mitochondria. *Sci Rep,* 7, 17467.

Abstract publications

Harmon, M., Jackson, M. & Skehel, P. 2016. An optical method for detecting endoplasmic reticulum and mitochondrial-associated membranes. Theme 3 In Vitro Experimental Models, *Amyotrophic Lateral Sclerosis and Frontotemporal Degeneration*, 17:sup1, 118-134.

SCIENTIFIC REPORTS

OPEN

A Bi-fluorescence complementation system to detect associations between the Endoplasmic reticulum and mitochondria

Received: 6 September 2017
Accepted: 22 November 2017
Published online: 12 December 2017

Mark Harmon[1], Philip Larkman[1], Giles Hardingham[2], Mandy Jackson[1] & Paul Skehel[1]

Close contacts between the endoplasmic reticulum membrane and the mitochondrial outer membrane facilitate efficient transfer of lipids between the organelles and coordinate Ca^{2+} signalling and stress responses. Changes to this coupling is associated with a number of metabolic disorders and neurodegenerative diseases including Alzheimer's, Parkinson's and motor neuron disease. The distance between the two membranes at regions of close apposition is below the resolution of conventional light microscopy, which makes analysis of these interactions challenging. Here we describe a new bifluorescence complementation (BiFC) method that labels a subset of ER-mitochondrial associations in fixed and living cells. The total number of ER-mitochondria associations detected by this approach increases in response to tunicamycin-induced ER stress, serum deprivation or reduced levels of mitofusin 2 (MFN2). This method will facilitate the analysis of dynamic interactions between the ER and mitochondrial membranes.

Regions of close association between the outer membrane of mitochondria (OMM) and the endoplasmic reticulum (ER) were originally identified by ultrastructure analysis[1,2], and subsequently shown to represent specialised structures that facilitate coordinated Ca^{2+} transfer and signalling between the two organelles[3]. These regions of the ER membrane have been biochemically purified as Mitochondrial Associated Membranes, or "MAMs", and shown to be enriched for a range of proteins including enzymes responsible for lipid synthesis[4] and transfer between the two membrane systems[5–7]. mtDNA synthesis and mitochondrial division appear to be co-ordinated at sites of close apposition with the ER[8,9], as is the formation of the autophagosome[10]. More recently the properties of ER-mitochondrial junctions have been implicated in a number of pathologies. Metabolic activities associated with MAMs are increased in Alzheimer's Disease[11,12] and transgenic mice expressing P301L tau appear to have more ER membrane associated with mitochondria[13]. In familial Parkinson's loss of DJ-1 reduces ER-mitochondria associations and disrupts mitochondrial Ca^{2+} homeostasis[14] and α-synuclein has been localized to MAMs[15,16]. An interaction between the ER protein VAPB and mitochondrial PTPIP51/Rmdn3 influences the coupling of Ca^{2+} levels in these organelles by a mechanism that is sensitive to TDP-43 activity[17] thus linking ER-mitochondrial interactions to both spontaneous and familial forms of Amyotrophic Lateral Sclerosis[18–20]. In addition the metabolic homeostasis signalling through ER-mitochondrial contacts is suggested to have a central role in metabolic diseases[21,22].

Close appositions between the ER and OMM measured in fixed cells using electron microscopy vary in distance between 5–30 nm and the extent of mitochondrial area covered by the ER depends on cell type and metabolic activity[3,23]. Membrane associations have been detected and quantified by co-localisation analysis of fluorescent signals targeted to the separate membranes[24], but this has a limited spatial resolution of 150–200 nm and cannot, therefore, distinguish between ER/OMM contacts of differing distance. Alternative methods to detect and quantify ER mitochondrial associations have been successfully developed based on proximity ligation in fixed cells[25], luciferase complementation and dimerization-dependent fluorescent protein (ddFP) approaches in living cells[26,27]. Here we report a Bimolecular Fluorescence Complementation BiFC system[28] in which two

[1]Centre for Integrative Physiology, Euan MacDonald Centre for Motor Neurone Disease Research, The University of Edinburgh, Edinburgh EH8 9XD, UK. [2]UK Dementia Research Institute at the University of Edinburgh, Edinburgh Medical School, Edinburgh EH8 9XD, UK. Correspondence and requests for materials should be addressed to P.S. (email: paul.skehel@ed.ac.uk)

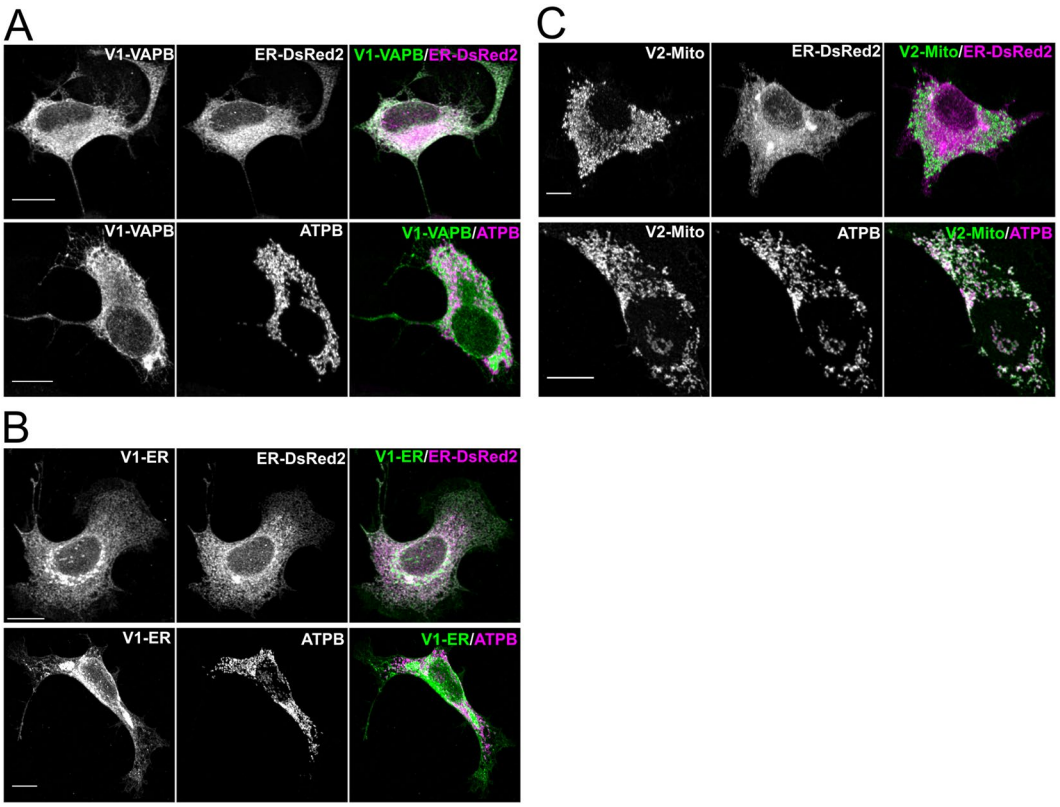

Figure 1. The complementing YFP Venus fusion proteins are correctly targeted to the ER and mitochondria. NSC 34 cells transiently expressing V1-VAPB (**A**), V1-ER (**B**), or V2-Mito (**C**), were analysed by immunocytochemistry using an anti-GFP antibody that recognises both fragments of YFP. The endoplasmic reticulum was identifed by co-expression of ER-DsRed2 (Clontech), and mitochondria were labelled immunolcytochemically for ATPB. The extent of colocalisation of Venus fusion proteins with the orgamelle markers was analysed by Pearon's Correlation Coefficient (PCC) (Table 1). Values indicate mean PCC ± SEM; n = 3 independent experiments (9–10 cells total). Antibody details Table 3. Scale bars, 10 μm.

complementing fragments of a fluorescent protein are expressed on the ER or mitochondria. When the membranes of these organelles are in very close apposition the two complementing fragments of the fluorescent protein can associate and reconstitute a functional fluorescent protein. The BiFC signal is only generated when the OMM and the cytoplasmic face of the ER are in close apposition. Therefore, this method provides structural information at a higher resolution than co-localisation and with a lower background than ddFP. As with ddFP this method may readily be applied to follow the dynamics and distribution of membrane juxtapositions within living cells in real time. Furthermore, as the complementing fragments can only produce fluorescence when directly interacting and are not fluorescent individually, the quantification of organelle contacts with BiFC is potentially less sensitive to changes in the local protein concentrations protein concentrations than ddFP methods.

Results

To generate a BiFC reporter for the close apposition of the ER and OMM the two complementing fragments of the split YFP Venus protein were targeted separately to the ER and OMM. In principle a functional YFP will only be generated at regions where the two membranes are sufficiently close for the direct interaction of the two complementing Venus fragments. The N-terminal fragment Venus1[28] was targeted to the cytoplasmic face of the ER membrane by fusion to either the full length or the C-terminal 25 amino acids of the mouse VAPB protein, creating V1-VAPB and V1-ER respectively. The C-terminal fragment Venus 2 was targeted to the outer mitochondrial membrane by fusion to the first 34 amino acids of TOMM20, to generate V2-Mito[29]. Limiting the size of the targeting sequences ensures that only the closest associations of the membranes will be detected. The sub-cellular localisation of these fusion proteins in the cell line NSC34 was determined by immunocytochemical analysis using a polyclonal anti-serum against GFP that recognises both N- and C-terminal fragments of the Venus protein (Fig. 1). The immunofluorescent signal from V1-VAPB co-localized with the co-expressed ER marker ER-DsRed2 (Clontech), but not with the mitochondrial protein ATPB (Fig. 1A and Table 1). Similarly, V1-ER also co-localized with the ER marker, but not with the mitochondrial protein ATPB (Fig. 1B and Table 1). In contrast, V2-Mito co-localized with ATPB but not with co-expressed ER-DsRed2 (Fig. 1C, Table 1). Co-expression of either V1-VAPB or V1-ER with V2-Mito in NSC34 cells produced readily detectable BiFC signals (Fig. 2). V1-VAPB/V2-Mito produced a fluorescence pattern surrounding almost all mitochondria, similar to that reported by dimerization-dependent fluorescent proteins targeted to the ER and OMM[27]. Co-expression

V1-VAPB/ER-DsRed2	0.876 ± 0.009
V1-VAPB/ATPB	0.035 ± 0.010
V1-ER/ER-DsRed2	0.870 ± 0.017
V1-ER/ATPB	0.070 ± 0.020
V2-Mito/ER-DsRed2	0.050 ± 0.011
V2-Mito/ATPB	0.910 ± 0.008

Table 1. Fluorescent signal co-localisation quantified by Pearson's Correlation Coefficient (PCC).

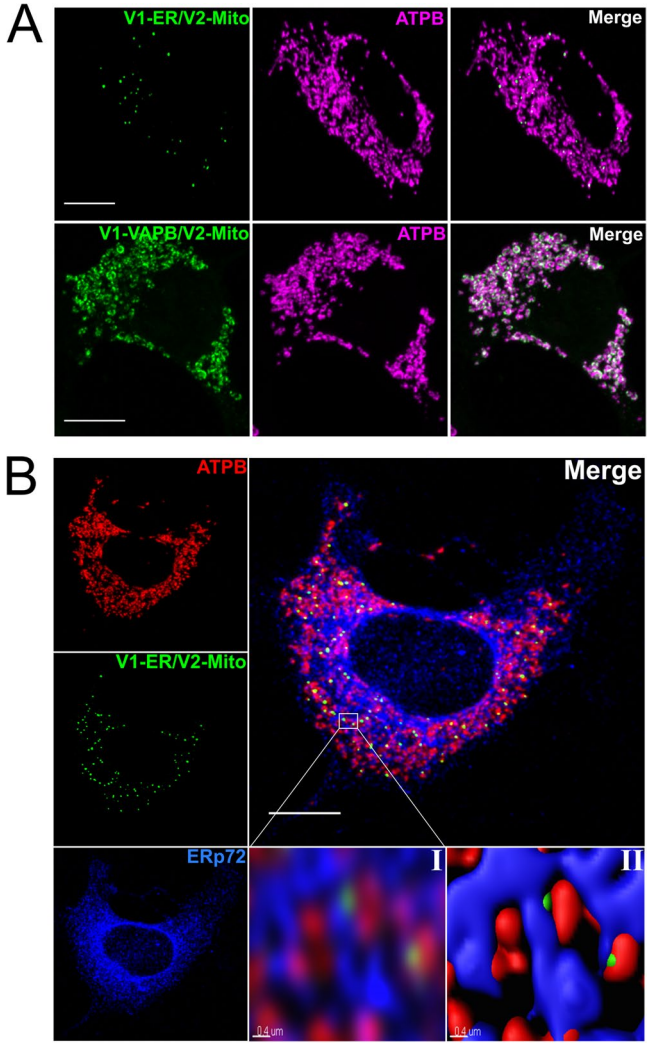

Figure 2. ER-targetted Venus 1 fusion proteins generate BiFC signals when co-expressed with mitochonrial Venus 2. V1-ER and V1-VAPB were co-expressed with V2-Mito in NSC34 cells (**A**). The resulting BiFC signal was associated with mitochondria as indicated by ATPB expression. The two Venus 1 fusion proteins differ in length by 218 aa, and produce distinct subcellular BiFC paterns. Triple labelling of the ER (Erp72, *blue*) and mitochondria (ATPB, *red*) demonstrate that the V1-ER/V2-Mito BiFC lables descete puncta at junctions between the ER and mitochodria (**B**). Higher magnification of boxed region (B.I), processed and rendered in 3D by Imaris image analysis software (**B.II**). Scale bar 10 μm, or 0.4 μm in panels B.I and B.II.

of the shorter V1-fusion protein, V1-ER with V2-Mito generated a distinct fluorescent signal with discrete puncta of fluorescence associated with a subset of mitochondria (Fig. 2). These signals appear to lie exclusively at areas of close apposition of the ER and mitochondria as revealed by immunolabelling for ERp72 and ATPB respectively (Fig. 2). Expression of either V1-VAPB, V1-ER or V2-Mito individually produced no YFP signal (Fig. S1). Co-expression of V1-ER with V2-Mito over 48 hrs produced no gross changes to ER or mitochondria morphology in NSC34, COS7 or HEK293 cells (Fig. S2). The V1-ER with V2-Mito BiFC was further characterised in the remainder of the study.

It would be anticipated that if the presence of V1-ER and V2-Mito was inducing ER-mitochondria associations as an artefact, then increasing the expression levels of V1-ER and V2-Mito would distort ER morphology and lead to an increase in the number or size of BiFC signals, but this was not the case (Fig. S3). Transfection with increasing amounts of V1-ER and V2-Mito expression plasmid DNA lead to an increase in the number of fluorescent cells but the average number of fluorescent signals in any transfected cell was unaltered (Fig. S3). Therefore, the presence of V1-ER and V2-Mito seems not to directly induce the formation of membrane associations, but labels existing sites of close apposition between the ER and OMMs.

The ER comes in close apposition to other organelles including the Golgi apparatus and endosomes[30–33]. However the BiFC puncta generated by V1-ER and V2-Mito appear selective for the ER and OMM, with very few signals associated with the Golgi apparatus, the nucleus or EEA1-positive endosomes (Fig. 3, Table 2). Details of the antibodies used are shown in Table 3.

Many of the BiFC signals were at the limit of resolution for conventional confocal microscopy. In order to gain a more accurate measurement super resolution STED microscopy was done on NSC34 cells transiently expressing V1-ER and V2-Mito (Fig. 4). The pattern of signals was heterogeneous, with areas of association detected in a single optical section ranging in length between 100–700 nm. This super resolution microscopic analysis indicated that puncta are discrete single structures, the number of which may be quantified by conventional confocal microscopy.

ER stress has been shown to increase the amount of ER-mitochondria membrane association[34]. To test if the BiFC system was sensitive to this dynamic change an ER stress was induced in NSC34 cells co-expressing V1-ER and V2-Mito by incubating with 2 or 10 μg/ml tunicamycin for 6 hours. A robust ER stress response was induced at both drug concentrations as indicated by splicing of XBP1 mRNA[35] (Fig. 5). The highest tunicamycin level induced a two-fold increase in the average number of punctate fluorescent signals per cell and an increase of similar magnitude in the size of this fluorescent signal as a percentage of the total mitochondrial volume, consistent with an increase in membrane associations (Fig. 5(Ai&ii)). Previous studies have used co-localisation analysis of fluorescent signals separately targeted to the ER and mitochondria as a measure of association between the membranes of the two organelles. To compare such co-localisation analysis with the BiFC method, ER stress was induced in parallel cultures and analysed by co-localisation of ER-targeted DsRed2 and the mitochondrial protein ATPB. In this case, co-localisation detected a similar increase in ER – mitochondria associations as that reported by the BiFC. These results are consistent with previous observations (Fig. 5C)[34].

Serum deprivation has also been shown to increase the number of tight associations (<16 nm) between the ER and OMM[36]. 24 hrs following removal of serum, a significant increase in the number of fluorescent puncta was detected in NSC34 cells co-expressing V1-ER and V2-Mito (Fig. 6). However, in this case, co-localisation analysis of fluorescence from separately labelled ER and mitochondria did not detect a significant change as quantified by two different methods of analysis (Fig. 6). This illustrates that this BiFC method can detect changes in ER-OMM associations that may be undetected by simple co-localization analysis.

The role of Mitofusin-2 (MFN2) in maintaining ER/mitochondria associations has been controversial. Initial reports that reduced levels or absence of MFN2 resulted in less ER-mitochondrial contacts led to the suggestion that the protein acts as a tether between the two membranes[37]. However, more recent analysis of cells from *mfn2* (−/−) animals detected an increased level of ER-mitochondrial juxtapostion and Ca^{2+} coupling between the organelles[38,39]. Changes in mitochondrial shape may interfere with fluorescence-based co-localization reporter systems[37] but the exact role of MFN2 in maintaining ER-mitochondria contacts remains controversial[40–42]. To further test the utility of the BiFC system, MFN2 levels were reduced in NSC34 cells using siRNA knockdown. An 80% reduction in MFN2 resulted in a significant increase in the number of fluorescent puncta detected by V1-ER/V2-Mito BiFC (Fig. 7). This suggests that the ER-OMM associations detected here by BiFC are not dependent on MFN2.

These results indicate that the BiFC system presented can report changes in ER-mitochondrial associations under three different conditions, and that in some instances it is more sensitive than previous fluorescence co-localization approaches.

Discussion

A BiFC reporter system for close associations between the ER and mitochondria has been produced by targeting the two complementing fragments of the split Venus fluorescent protein to the cytoplasmic faces of the ER and the outer membrane of mitochondria. Tethering the complementing YFP Venus fragments with fusion proteins of different size generated distinct fluorescent signals, indicating that associations of different distance may be reported by a BiFC system. BiFC, therefore, may be used to distinguish between membrane associations of varying distance, which are thought to have specific functional roles[36,43]. The closest contacts as detected by the V1-ER/V2-Mito combination formed on a subset of mitochondria and were heterogeneous in size ranging from 100–700 nm in length. Csordas *et al.*[44], artificially forced the close association of ER and OMM by expressing a fluorescent fusion protein containing both an ER targeting sequence and a mitochondrial targeting sequence. In that case, the fusion protein had 84 amino acids in addition to the fluorescent protein, and resulted in an association between the ER and OMM with a distance of approximately 6 nm between the two membranes[36]. The combination of the V1-ER and V2-Mito fusion proteins adds a total of 85 additional amino acids to the Venus protein, suggesting that the contact sites reported by the V1-ER/V2-Mito combination are of similar dimensions to those previously reported[36]. Assuming the extra-membrane residues to be in a fully extended conformation would give an upper estimate of the largest gap compatible with fluorescent protein formation of approximately 10 nm. Therefore the distance between the ER and mitochondrial membranes detected by this BiFC combination is most likely in the range of 6 to 10 nm.

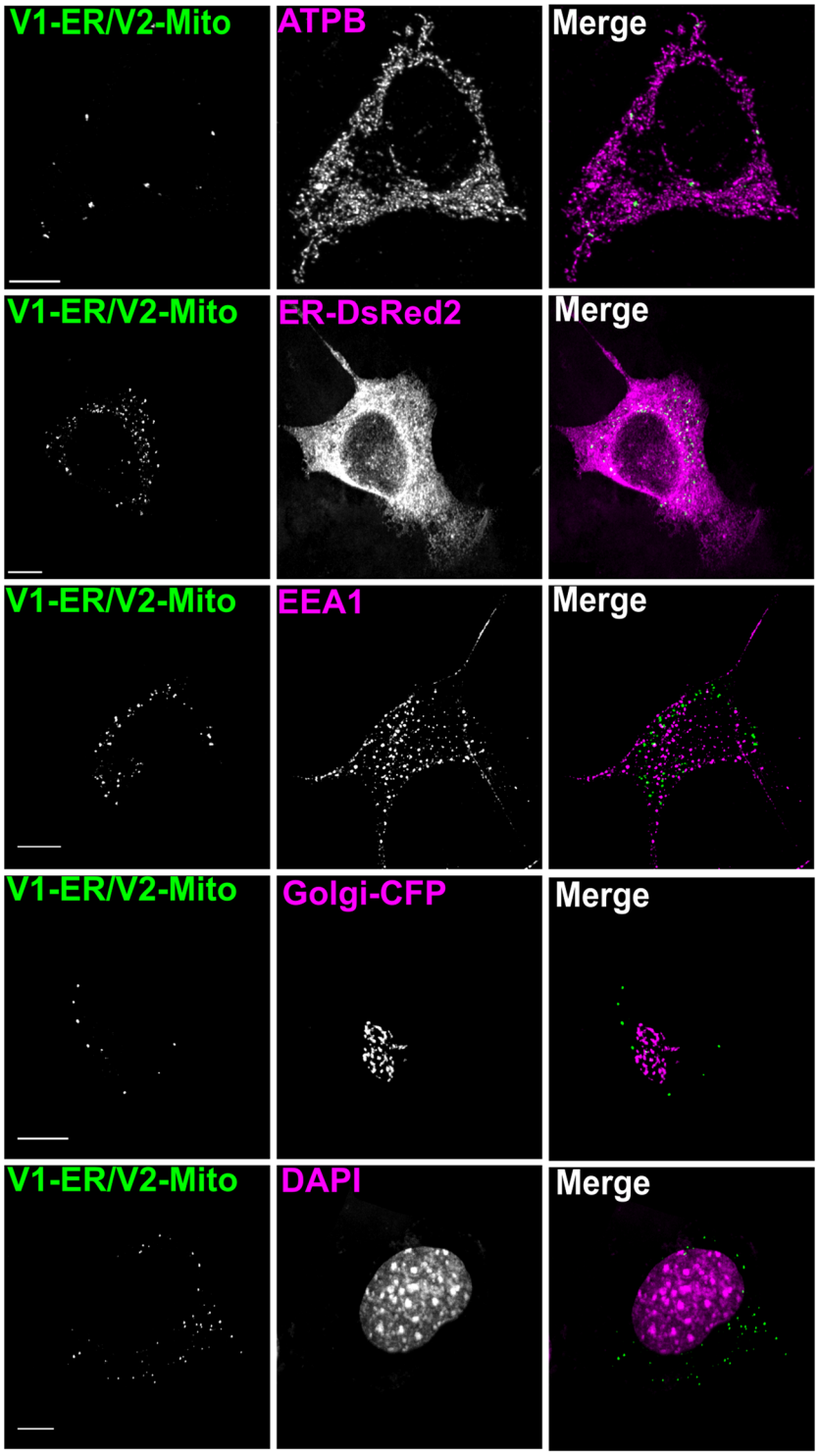

Figure 3. Quantification of V1-ER/V2-Mito BiFC signal overlapping with organelle markers. The number of BiFC puncta in NSC 34 cells expressing V1-ER/V2-Mito was quantified using a maximum intensity threshold in Imaris image analysis software **(A)**. The co-localisation channels were then built between the YFP channel and fluorescent organelle markers. The ER and Golgi were labeled by co-expression of ER-DsRed2 and Golgi-ECFP respectively (Clontech), early endosomes and mitochondria were immunolabeled for EEA1 or ATPB, and the nucleus was labeled with DAPI. anti-ATPB (mitochondria), ER-DsRed (ER), anti-EEA1 (Endosomes), Golgi-CFP (Golgi), DAPI (Nucleus). Using the same intensity threshold value, the number of BiFC puncta that had a point of colocalisation with the fluorescent organelle signal were quantified. n = 3 independent experiments (10–15 cells total). Scale bars, 10 μm. Values indicate the mean number of colocalised BiFC puncta over three independent experiments ± SEM (Table 2, Antibody details Table 3).

ATPB (mitochondria)	97.07 ± 1.34
ER-DsRed2 (ER)	99.07 ± 0.27
EEA1 (Endosomes)	10.74 ± 2.36
Golgi-CFP (Golgi)	8.95 ± 3.47
DAPI (Nucleus)	6.81 ± 0.57

Table 2. % of BiFC puncta overlapping with fluorescent organelle marker.

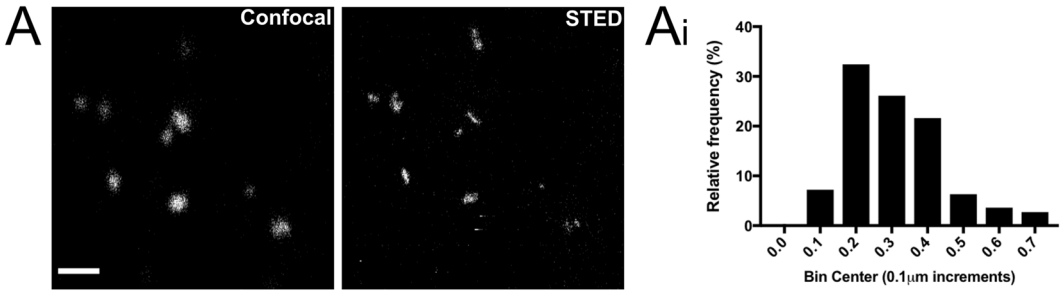

Figure 4. Super-resolution imaging of fluorescent BiFC puncta in NSC34 cells. Representative confocal image versus STED super-resolution image of the same region of an NSC34 cell transiently expressing the V1-ER and V2-Mito reporters (**A**). Scale bar, 1 μm. Pixel size = 0.2 μm. Frequency distribution graph illustrating the relative distribution of BiFC punctum size as measured by the straight line tool in ImageJ across the widest point of an individual fluorescent punctum (**B**). n = 111 BiFC puncta (7 cells total, mean value = 0.31 μm).

Large receptor proteins and complexes such as the IP_3R and ribosomes may impose limits on the close association of the ER and OMM. Giacomello and Pellegrini have proposed that different gaps between the membranes reflect functionally distinct domains participating in Ca^{2+} signalling, lipid biosynthesis and transfer, and autophagocytosis[43]. The predicted 6–10 nm gap identified here would be consistent with sites of lipid transfer mediated by members of the tubular lipid-binding (TULIP) superfamily of membrane proteins, forming a 9 nm long channel that may mediate lipid transfer between organelles (reviewed[45]). Increased associations between ER cisternae and mitochondria are made following induction of the Unfolded Protein Response[46]. Since ribosomes are localised to ER cisternae the observation that BiFC puncta numbers increase following tunicamycin treatment suggests that V1-ER and V2-Mito can interact at ER cisternae despite the restrictions imposed by ribosome size.

When tight contacts between the ER and OMM are induced artificially, gross changes in organelle morphology can occur over time[44]. In contrast, the pattern of the V1-ER/V2-Mito BiFC signal is generally stable over time with no gross changes in ER or mitochondrial morphology seen in transient or stably transfected cells. Therefore the association of the separate halves of the Venus protein appears insufficient to disrupt the normal pattern of ER-mitochondria associations. The BiFC system complements existing methods to detect organelle associations. Electron microscopy has the highest resolution however localising specific proteins to particular regions of apposition requires correlative electron and fluorescent microscopy or immune gold labelling, both of which are technically very challenging and must be done on fixed material. Fluorescent proximity ligation assays are more readily quantified and can detect specific proteins at regions of contact (25). Again, however, this method is used on fixed samples. Fluorescent protein- based methods have the significant advantage that they can be readily detected in living cells or tissues. An example of BiFC in living cells in shown in Supplementary video S4. Co-localization of distinct fluorescent proteins localised on separate membranes has a limited resolution and cannot distinguish between contacts less than approximately 150 nm. Dimerization dependent Fluorescent proteins (ddFPs) and BiFC have improved detection limits as they both depend on the direct association of polypeptides targeted to separate membranes. In both cases the proximity of membrane associations that can be detected depends on the size of the targeting and linker sequences of the respective fusion proteins. One potential advantage of a BiFC approach over ddFPs is a reduced background as the complementing halves of the YFP show no fluorescence. The resulting improvement of signal to noise would allow the detection of weaker transient signals.

The average number of BiFC puncta increases in response to homeostatic stress and reduction in MFN2 levels. This seems incompatible with the proposal that MFN2 is required to maintain close ER-mitochondria associations. However, it is possible that the V1-ER/V2-Mito BiFC as configured may detect MFN2-independent contacts induced following a mitochondrial stress resulting from a reduction of MFN2 levels. Alternatively, MFN2 may not be directly responsible for maintaining ER-mitochondria associations as suggested. The magnitude of the increase in V1-ER/V2-Mito signal following MFN2 knock-down here is similar to that seen for ER-mitochondria fluorescence co-localisation in studies using *mfn2*$^{-/-}$ mice[38].

All mitochondria appear to come into contact with the ER, as indicated by the V1-VAPB/V2-Mito BiFC signal (Fig. 2A) and previously using dimerization-dependent fluorescent proteins[27]. However, not all mitochondria have an ER association detectable by V1-ER/V2-Mito. Ultrastructure analysis of mouse liver indicated that 25% of mitochondria have close ER associations and it is suggested that this heterogeneity is a cell type specific characteristic and changes in response to the physiological environment[23]. The mitochondria identified as interacting

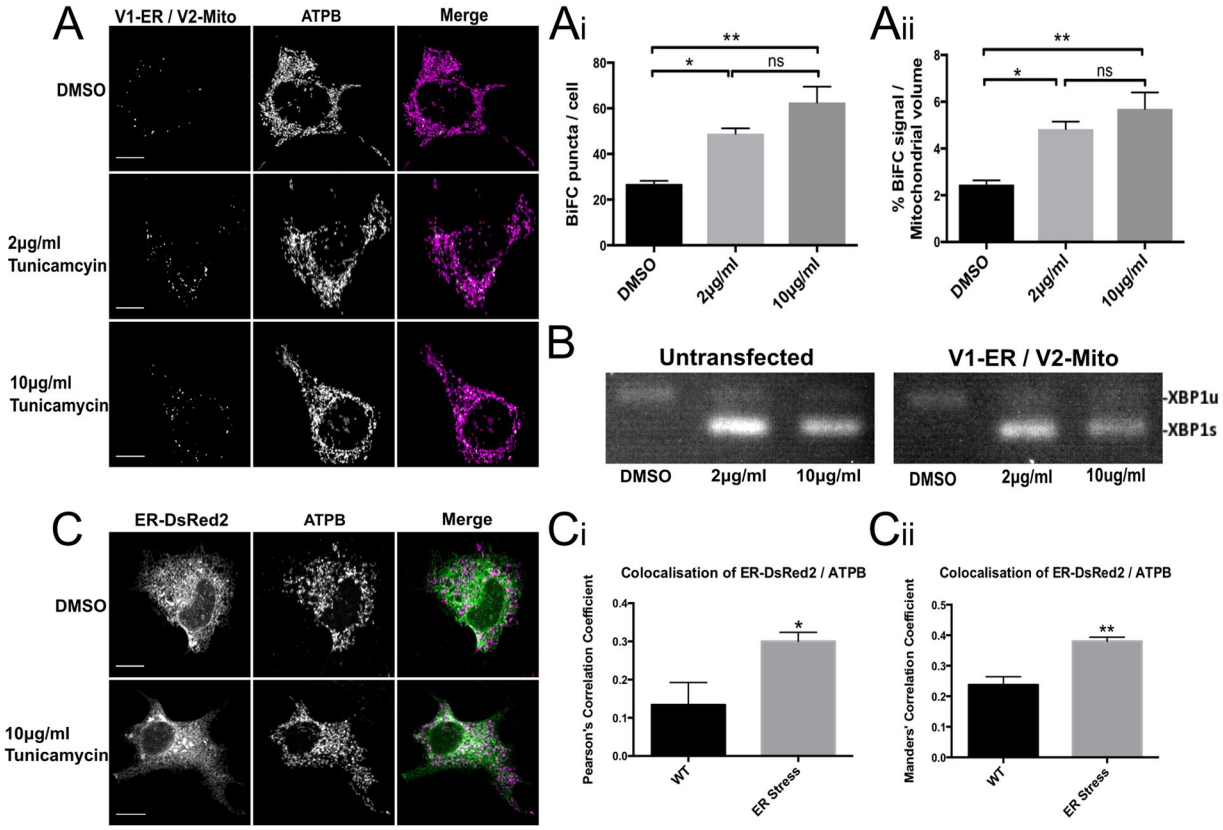

Figure 5. ER Stress significantly increases the number of ER-mitochondria contacts in NSC34 cells. NSC34 cells expressing V1-ER/V2-Mito were treated with 2 μg/ml or 10 μg/ml tunicamycin to induce an ER stress (**A**). ER stress significantly increases the mean number of BiFC puncta per cell in and (**A(i)**) significantly increases the total volume of BiFC signal as a percentage of total mitochondrial volume (**A(ii)**). n = 3 independent experiments (32–34 cells total). Values indicate mean values of three independent experiments. Error bars indicate SEM. Statistical significance was measured using one-way ANOVA followed by Holm-Sidak's multiple comparison test, ns (non-significant) $P > 0.05$, *$P < 0.05$, **$P < 0.01$. ER stress was confirmed by detection of spliced XBP1 mRNA. Expression of the Venus reporter plasmids alone did not induce an ER stress (**B**). For comparison, in parallel NSC34 cultures the ER and mitochondria were labeled by co-expression of ER-DsRed2 (Green) and anti-ATPB (Magenta) respectively (**C**). A significant increase in the co-localisation of ER-DsRed and ATPB signals was detected following ER stress induced with 10 μg/ml tunicamycin as quantified by both Pearsons' Correlation Coefficient (**C(i)**) and Manders' Correlation Coefficient (**C(ii)**). n = 4 independent experiments (26 cells total). Statistical significance was measured using unpaired two-tailed t-test. *$P < 0.05$, **$P < 0.01$. Error bars indicate SEM.

Name	Company	Class	Host	Antigen	Catalogue number	Dilution
Anti-ATPB	Abcam	Monoclonal	Mouse	Whole heart mitochondria (human)	ab14730	1:250 (IF)
Anti-MFN2	Abcam	Monoclonal	Mouse	a.a. 661–758 of MFN2	ab56889	1:5000 (WB)
Anti-GFP	Life Technologies	Polyclonal	Rabbit	GFP isolated from *Aequorea victoria*	A6455	1:400 (IF)
Anti-ERp72 (PDI)	Enzo Life Sciences	Polyclonal	Rabbit	a.a. 623–638 of ERp72	ADI-SPS-720	1:100 (IF)
Anti- α-Tubulin	EMD Millipore	Monoclonal	Mouse	a.a. 426–450 of α-Tubulin	05–829	1:50,000 (WB)
Anti-EEA1	Cell Signaling Technology	Polyclonal	Rabbit	Synthetic peptide corresponding to residues surrounding Gly14 of human EEA1	2411 S	1:100 (IF)

Table 3. Source and concentrations of the primary antibodies used in the study.

with the ER by this BiFC system might therefore have distinct morphologies, respiratory rates and/or, distinct Ca^{2+} signalling activities.

Subtle changes in distances between ER and mitochondrial membranes are not measurable by co-localization of fluorescence as they may fall bellow the resolution limit of conventional optical microscopy. Notably, induction of an Unfolded Protein Response produced changes in ER mitochondria associations that were detectable by both

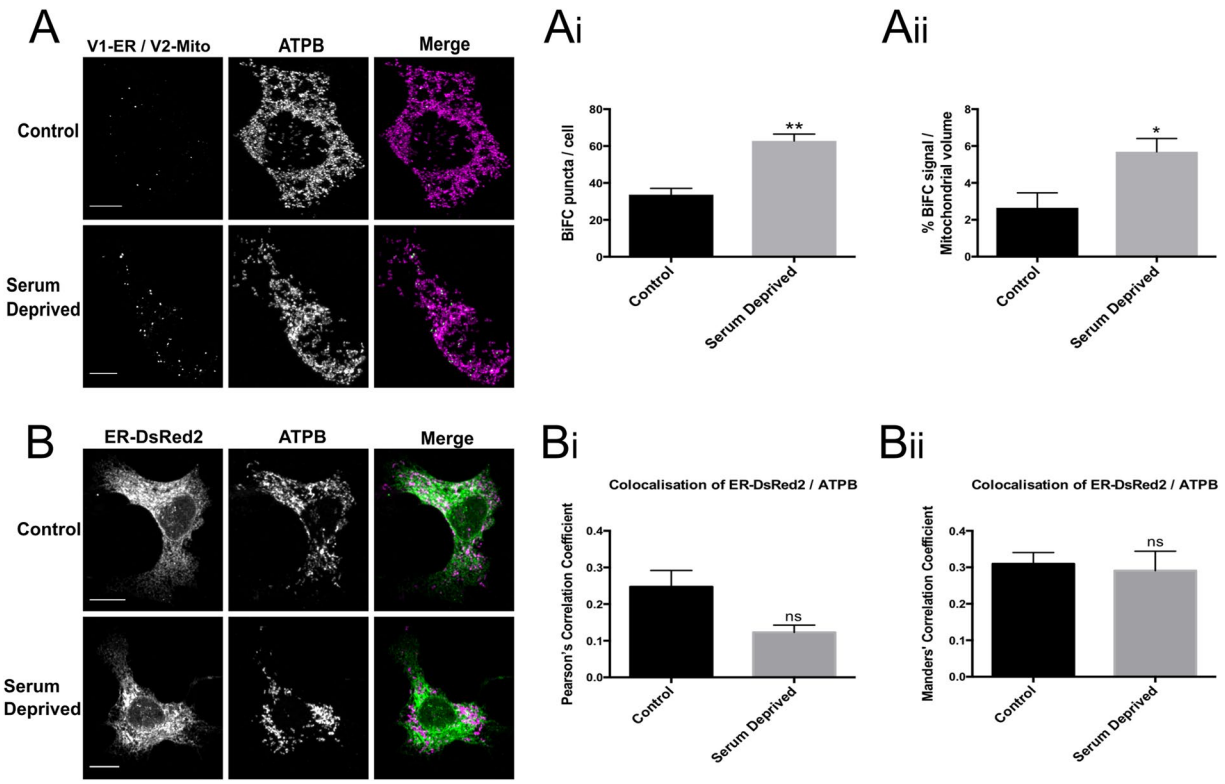

Figure 6. Serum deprivation significantly increases the number of ER-mitochondria contacts in NSC34 cells. NSC34 cells transiently expressing V1-ER/V2-Mito were grown in 10% FBS (control) or 0% FBS (serum deprived) for 24 h post transfection **(A)**. Serum deprivation significantly increases the mean number of BiFC puncta per cell (**A(i)**) and the total volume of BiFC signal as a percentage of total mitochondrial volume (**A(ii)**). n = 3 independent experiments (36–37 cells total). Statistical significance was measured using unpaired two-tailed t-test, *P < 0.05, **P < 0.01. Values indicate mean value of three independent experiments. Error bars indicate SEM. Co-localisation of ER and mitochondrial fluorescence does not detect a significant change in ER/mitochondrial contact **(B)**. In parallel NSC34 cultures the ER and mitochondria were labeled by co-expression of ER-DsRed2 (Green) and anti-ATPB (Magenta) respectively. No significant change in the co-localisation of ER and mitochondria was detected as measured by either Pearson's Correlation Coefficient (PCC) (**B(i)**), or Mander's Correlation Coefficient (MCC) (**B(ii)**). n = 3 independent experiments (19 cells total); ns (non-significant) P > 0.05. Error bars indicate SEM. Scale bars, 10 μm.

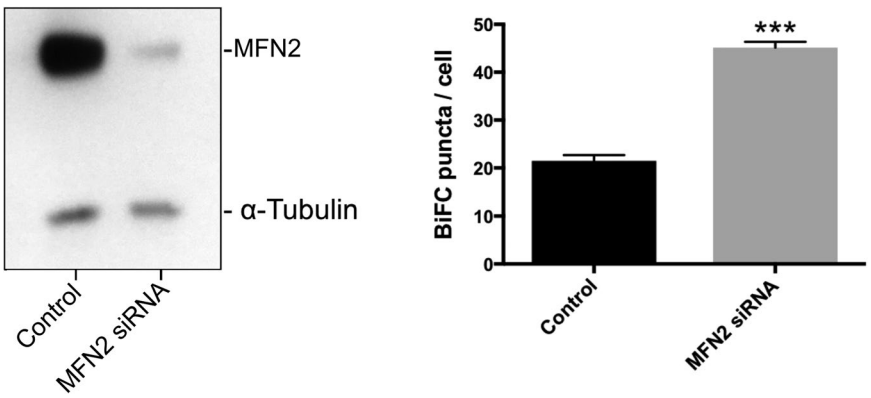

Figure 7. Mitofusin-2 (MFN2) levels influence the number of V1-ER/V2-Mito BiFC signals. siRNA was used to induced a knock-down of MFN2 to less than 20% of normal levels in NSC34 cells stably expressing V1-ER/V2-Mito (**A(i)**). This was associated with an increase the mean number of BiFC puncta per cell (**A(ii)**). n = 3 independent experiments (30–32 cells total). Values indicate the mean values from three independent experiments. Error bars represent SEM. Statistical significance was determined using unpaired two-tailed t-test, ***P < 0.01.

the V1-ER/V2-Mito BiFC and fluorescence co-localisation. In contrast, serum removal only produced a significant change in V1-ER/V2-Mito BiFC puncta number, and not fluorescence co-localisation. BiFC, therefore, may represent a more sensitive *in vivo* technique that also avoids the technically challenging ultrastructure analysis using electron microscopy on fixed samples.

The increase in BiFC puncta following tunicamycin treatment is consistent with studies showing increases in ER mitochondrial contacts in the early phases of ER stress[24]. It may also be the case that the associations detected by BiFC are related to sites of mitochondrial fusion and biogenesis[34], and the signal is somewhat reminiscent of Miro1 labelling in COS-7 cells[47]. However, it has been suggested that mitochondria biogenesis is independent of UPR stress activity from the ER[48]. Further studies are required to determine if these mitochondria contacted via these BiFC puncta have particular properties relating to biogenesis, Ca^{2+} signalling or respiratory activity.

Materials and Methods

Plasmids and primers. V1-VAPB has been described previously[49]. V1-ER was derived from V1-VAPB by a deletion PCR mutagenesis using the primers gggtcctccggaatgggcctgagcgcccggctgct and cattccggaggacccaccacctccagagc generating a Venus 1–C terminal fusion with the C-terminal 25 amino acids from mouse VAPB, GLSARLLALVVLFFIVGVIIGKIAL.

V2-Mito contains the first 34 amino acids of human TOMM20, fused to the terminus of Venus(2). The coding sequence for MVGRNSAIAAGVCGALFIGYCIYFDRKRRSDPN was generated from the human TOMM20 cDNA by a PCR using oligonucleotide primers cggcggccgctccggaccatggtgggccggaacagcgcc and atctagattaatcgattgcagacccgatgccgctgc, The PCR product was digested and ligated into the NotI and ClaI restrictions sites of pcDNA3.1 Venus(2)-zip. (Generous gift of S.W.Michnick), to create Mito-V2 fusion gene.

Primers used for RT-PCT across slice junction of mouse XBP1 mRNA: ccaaggggaatgaagtgagg and aagggaggctg gtaaggaac.

Cell culture and transfection. NSC34[50], COS-7[51], and HEK-293[52] cells were maintained at 37 °C and 5% CO_2 in Dulbecco's modified high glucose Eagle's medium supplemented with 10% fetal bovine serum and 1% antibiotic-antimycotic (Thermo Fisher Scientific). For imaging, cells were plated on glass coverslips coated with poly-L-lysine (50 μg/ml) and bovine plasma fibronectin (10 μg/ml) (Life Technologies). Plasmid transfections were done using Lipofectamine 2000 (Invitrogen) in Opti-MEM media (Thermo Fisher Scientific). Cells were imaged or harvested 48 h post-transfection. V1-ER and V2-Mito reporter plasmids were transfected at a 1:1 ratio at a total DNA of concentration of 1 μg per well of a 12 well dish (except where otherwise indicated). MFN2 siRNA (Dharmacon) transfection was performed with lipofectamine RNAiMAX at an siRNA concentration of 50 nM for 48 h.

Stably transfected NSC34 cells co-expressing V1-ER and V2-Mito were selected on 400 μg/ml zeocin (InvivoGen).

ER stress was induced with tunicamycin (Calbiochem) at 2 μg/ml or 10 μg/ml for 6 h, with an equivalent volume of DMSO as vehicle only control.

Immunoblot analysis. Cell proteins were extracted in RIPA buffer (1.0% NP40, 0.1% SDS (w/v), 150 mM NaCl, 0.5% (w/v) Sodium deoxycholate, 50 mM Tris pH 8.0, Complete protease inhibitors (Roche)), and quantified by BCA protein assay (Thermo Scientific). Samples in SDS sample buffer (80 mM Tris HCl pH6.9, 2%(w/v) SDS, 100 mM DTT, 10% (v/v) glycerol, were heated at 80 °C for 15 min, prior to separation on NuPAGE 4–12% Bis-Tris Gel (Invitrogen) in MES SDS running buffer (Invitrogen). Proteins were then transferred to PVDF Immobilon P (EMD Millipore) in NuPAGE transfer buffer contain 10% (v/v) methanol. Non-specific protein binding sights on the membranes were blocked by incubating for at least 60 mins in PBS containing 5% (w/v) non-fat dry milk and 0.1% (v/v) Tween-20. Primary antibodies were used in blocking solution at indicated concentrations overnight at 4 °C, following which membranes were washed at room temperature 3 times for 5 min in PBS containing 0.1% (v/v) Tween-20. Bound antibody was detected using horseradish peroxidase-conjugated secondary antibodies at 1:5,000 dilution (Jackson ImmunoResearch) followed by ECL detection (Amersham GE Life Sciences) using X-ray film (FUJIFILM). Band intensities were quantified by densitometric analysis using ImageJ.

Immunocytochemistry. Cells were fixed in 4% (w/v) paraformaldehyde in phosphate buffered saline (PBS) for 15 min at room temperature, except for anti-ERp72 where methanol at −20 °C was used for 5 min. After washing with PBS, cells were permeabilised with 0.4% (v/v) Triton X-100 for 10 min at room temperature. Cells were then incubated in a blocking solution consisting of PBS, 0.2% fish gelatin and 0.02% saponin (PGAS), at 4 °C overnight. Primary and secondary antibodies were diluted in PGAS. Primary antibodies were incubated at room temperature for 30–60 min. Following each incubation cells were washed 3 times with PGAS and an additional final 3 washes were carried out using PBS before coverslips were mounted using Vectashield with DAPI (Vector Laboratories, Inc. Burlingame, CA 94010) or ProLong Diamond Antifade mountant (Thermo Fisher Scientific).

Secondary antibodies used were from Jackson ImmunoResearch. Horseradish-peroxidase conjugated goat anti-rabbit (111-035-003), donkey anti-mouse Cy2 (715-225-150), Cy3 and Cy5-coupled goat anti-mouse (115-165-146, 115-175-156), Cy3 and Cy5-coupled donkey anti-Rabbit (711-175-152, 711-175-152).

RNA extraction and PCR. Total RNA was extracted from NSC34 cells using the RNeasy mini kit (Qiagen) as per manufacturers instructions. cDNA was generated using the Omniscript reverse transcription kit (Qiagen) followed by PCR amplification using Taq DNA polymerase (Qiagen). PCR products were visualised on a 3.5% (w/v) TAE agarose gel stained with SyberSafe (Invirogen).

Confocal Microscopy. Confocal images were acquired using a Nikon A1R microscope. For the quantification and colocalisation analysis experiments, z-stack images were taken with a pixel size of 60×60 nm^2 and z-step size of 150 nm using a 60X (Plan ApoVC NA 1.4 oil) objective. Excitation laser wavelengths were for YFP (Venus) 488 nm, Cy3 and DsRed 561 nm, CFP and DAPI 401.5 nm and Cy5 641 nm. For comparison of the relative levels of protein expression shown in SFig. 2, single plane images were acquired with a 20X objective lens (Plan Apo NA 0.75) with excitation laser wavelengths set at 401.5 nm (DAPI) and 561 nm (Cy3) by keeping the same laser power, detector gain and acquisition parameters. Microscope control and image acquisition were done using the NIS-Elements-v4.13 software.

Live-Cell Imaging. NSC34 cells were plated on poly-D-lysine/fibronectin coated 35 mm glass-bottomed petri dishes (14 mm microwell diameter, glass thickness No. 1.5) (MatTEK). Mitochondria were labeled with 25 nM MitoTracker CMXRos (Invitrogen) for 30 min in pre-warmed DMEM, followed by three five minute washes with DMEM. Two channel, single plane imaging of live-cells was performed in a heated chamber at 37 °C with 5% CO_2 (Okolab) using a 60X objective lens (Plan ApoVC NA 1.4 oil) at an acquisition rate of 0.25 fps.

CW-gSTED microscopy. Continuous wave gated stimulated emission depletion (CW-gSTED) microscopy was done using a Leica SP5 confocal laser scanning microscope equipped with a 592 nm depletion laser and 100×1.4 NA HCX PL Apo oil immersion objective lens. YFP was excited using a white light laser tuned to 514 nm with an 80 MHz pulse rate. STED was achieved by concurrent 592 nm depletion aligned to the excitation laser. 524–580 nm emission was isolated by an acousto-optical beamsplitter and detected with a Leica HyD hybrid detector gated to detect 0.5–8 ns following each excitation pulse. Single slice images were acquired with a 0.02 µm pixel size to achieve Nyquist sampling.

Image analysis. Deconvolution of confocal images was performed using Huygens Essential (Huygens Software 4.5.1p3) before subsequent analysis. Colocalisation analyses were done on 3D, deconvolved images and quantified using ImarisColoc (Imaris v8.2.1, Bitplane Inc, software available at http://bitplane.com). Quantification of BiFC puncta was automated using the 3D volume rendering function of Imaris followed by the 'total number of disconnected components' measurement. For quantification of the signal overlap between fluorescent puncta and organelle markers (Fig. 3) first the number of BiFC puncta in a cell was quantified on Imaris with the 'Spots' function using the maximum intensity value as a threshold. Using this same threshold intensity value, a colocalisation channel was built between the BiFC and organelle marker channel. Finally, the number of spots in the colocalisation channel was quantified in the same manner and expressed as a percentage of total BiFC puncta. Analysis of images acquired by STED microscopy was carried out using the "straight line" tool in ImageJ. A straight line was drawn manually across the point of widest distance of each individual fluorescent puncta and the length of the line calculated in µm.

All image analysis and quantification of images acquired with confocal microscopy were performed on deconvolved images without any additional processing. Brightness and contrast settings were adjusted in ImageJ for presentation purposes only.

Statistical analysis. All experiments were repeated at least three times for statistical analysis. Statistical analysis was carried out using Prism version 6.0 h (GraphPad). Unless otherwise stated, statistical significance was measured using unpaired two-tailed t-test or one-way ANOVA followed by Holm-Sidak's multiple comparison test; $^*P < 0.05$, $^{**}P < 0.01$, $^{***}P < 0.001$.

References

1. Morre, D. J., Merritt, W. D. & Lembi, C. A. Connections between mitochondria and endoplasmic reticulum in rat liver and onion stem. *Protoplasma* **73**, 43–49 (1971).
2. Franke, W. W. & Kartenbeck, J. Outer mitochondrial membrane continuous with endoplasmic reticulum. *Protoplasm.* **73**, 35–41 (1971).
3. Rizzuto, R. *et al.* Close contacts with the endoplasmic reticulum as determinants of mitochondrial Ca2+ responses. *Science* **280**, 1763–1766, https://doi.org/10.1126/science.280.5370.1763 (1998).
4. Vance, J. E. Phospholipid synthesis in a membrane fraction associated with mitochondria. *Journal of Biological Chemistry* **265**, 7248–7256 (1990).
5. Flis, V. V. & Daum, G. Lipid transport between the endoplasmic reticulum and mitochondria. *Cold Spring Harb Perspect Biol.* **5** (2013).
6. Vance, J. E. MAM (mitochondria-associated membranes) in mammalian cells: lipids and beyond. *Biochim Biophys Acta* **1841**, 595–609 (2014).
7. Poston, C. N., Krishnan, S. C. & Bazemore-Walker, C. R. In-depth proteomic analysis of mammalian mitochondria-associated membranes (MAM). *J Proteomics* **79**, 219–230 (2013).
8. Lewis, S. C., Uchiyama, L. F. & Nunnari, J. ER-mitochondria contacts couple mtDNA synthesis with mitochondrial division in human cells. *Science* **353**, 261 (2016).
9. Friedman, J. R. *et al.* ER tubules mark sites of mitochondrial division. *Science* **334**, 358–362 (2011).
10. Hamasaki, M. *et al.* Autophagosomes form at ER-mitochondria contact sites. *Nature* **495**, 389–393 (2013).
11. Area-Gomez, E. *et al.* Upregulated function of mitochondria-associated ER membranes in Alzheimer disease. *Embo J.* **31**, 4106–4123 (2012).
12. Schon, E. A. & Area-Gomez, E. Mitochondria-associated ER membranes in Alzheimer disease. *Mol Cell Neurosci.* **55**, 26–36 (2013).
13. Perreault, S., Bousquet, O., Lauzon, M., Paiement, J. & Leclerc, N. Increased association between rough endoplasmic reticulum membranes and mitochondria in transgenic mice that express P301L tau. *J Neuropathol Exp Neurol.* **68**, 503–514 (2009).
14. Ottolini, D., Cali, T., Negro, A. & Brini, M. The Parkinson disease-related protein DJ-1 counteracts mitochondrial impairment induced by the tumour suppressor protein p53 by enhancing endoplasmic reticulum-mitochondria tethering. *Hum Mol Genet.* **22**, 2152–2168 (2013).
15. Guardia-Laguarta, C. *et al.* alpha-Synuclein is localized to mitochondria-associated ER membranes. *J Neurosci.* **34**, 249–259 (2014).
16. Rodriguez-Arribas, M. *et al.* Mitochondria-Associated Membranes (MAMs): Overview and Its Role in Parkinson's Disease. *Mol Neurobiol.* **54**, 2687 (2017).

17. Stoica, R. *et al*. ER-mitochondria associations are regulated by the VAPB-PTPIP51 interaction and are disrupted by ALS/FTD-associated TDP-43. *Nat Commun.* **5**, 3996 (2014).
18. Nishimura, A. L. *et al*. A mutation in the vesicle-trafficking protein VAPB causes late-onset spinal muscular atrophy and amyotrophic lateral sclerosis. *Am J Hum Genet.* **75**, 822–831 (2004).
19. De Vos, K. J. *et al*. VAPB interacts with the mitochondrial protein PTPIP51 to regulate calcium homeostasis. *Hum Mol Genet.* **21**, 1299–311 (2012).
20. Erpapazoglou, Z., Mouton-Liger, F. & Corti, O. From dysfunctional endoplasmic reticulum-mitochondria coupling to neurodegeneration. *Neurochem Int.* **109**, 171–183 (2017).
21. Thoudam, T., Jeon, J. H., Ha, C. M. & Lee, I. K. Role of Mitochondria-Associated Endoplasmic Reticulum Membrane in Inflammation-Mediated Metabolic Diseases. *Mediators Inflamm.* **2016**, 1851420 (2016).
22. Tubbs, E. & Rieusset, J. Metabolic signaling functions of ER-mitochondria contact sites: role in metabolic diseases. *J Mol Endocrinol.* **58**, 87–106 (2017).
23. Sood, A. *et al*. A Mitofusin-2-dependent inactivating cleavage of Opa1 links changes in mitochondria cristae and ER contacts in the postprandial liver. *Proc. Natl. Acad. Sci. USA* **111**, 16017–16022 (2104).
24. Bravo, R. *et al*. Increased ER-mitochondrial coupling promotes mitochondrial respiration and bioenergetics during early phases of ER stress. *J. Cell Sci.* **124**, 2143–2152 (2011).
25. Tubbs, E. *et al*. Mitochondria-Associated Endoplasmic Reticulum Membrane (MAM) Integrity Is Required for Insulin Signaling and Is Implicated in Hepatic Insulin Resistance. *Diabetes* **63**, 3279 (2014).
26. Lim, Y., Cho, I. T., Schoel, L. J., Cho, G. & Golden, J. A. Hereditary spastic paraplegia-linked REEP1 modulates endoplasmic reticulum/mitochondria contacts. *Ann. Neurol.* **78**, 679–696 (2015).
27. Alford, S. C., Ding, Y., Simmen, T. & Campbell, R. E. Dimerization-dependent green and yellow fluorescent proteins. *ACS Synth. Biol.* **1**, 569–575 (2012).
28. Remy, I., Galarneau, A. & Michnick, S. W. Detection and visualization of protein interactions with protein fragment complementation assays. *Methods Mol. Biol.* **185**, 447–459 (2002).
29. Kanaji, S., Iwahashi, J., Kida, Y., Sakaguchi, M. & Mihara, K. Characterization of the signal that directs Tom20 to the mitochondrial outer membrane. *J. Cell Biol.* **151**, 277–288 (2000).
30. Raiborg, C. *et al*. Repeated ER-endosome contacts promote endosome translocation and neurite outgrowth. *Nature* **520**, 234–238 (2015).
31. Dong, R. *et al*. Endosome-ER Contacts Control Actin Nucleation and Retromer Function through VAP-Dependent Regulation of PI4P. *Cell* **166**, 408–423 (2016).
32. Uchiyama, Y. The membrane association among the rough-and smooth-surfaced endoplasmic reticulum and Golgi apparatus in rat hepatocytes at certain circadian stages. *Tohoku J. Exp. Med.* **136**, 299–302 (1982).
33. Levine, T. & Rabouille, C. Endoplasmic reticulum: one continuous network compartmentalized by extrinsic cues. *Curr. Opin. Cell Biol.* **17**, 362–368 (2005).
34. Bravo, R. *et al*. Endoplasmic reticulum: ER stress regulates mitochondrial bioenergetics. *Int. J. Biochem. Cell Biol.* **44**, 16–20 (2011).
35. Yoshida, H., Matsui, T., Yamamoto, A., Okada, T. & Mori, K. XBP1 mRNA Is Induced by ATF6 and Spliced by IRE1 in Response to ER Stress to Produce a Highly Active Transcription Factor. *Cell* **107**, 881–891 (2001).
36. Csordas, G. *et al*. Structural and functional features and significance of the physical linkage between ER and mitochondria. *J. Cell Biol.* **174**, 915–921 (2006).
37. de Brito, O. M. & Scorrano, L. Mitofusin 2 tethers endoplasmic reticulum to mitochondria. *Nature* **456**, 605–610 (2008).
38. Cosson, P., Marchetti, A., Ravazzola, M. & Orci, L. Mitofusin-2 independent juxtaposition of endoplasmic reticulum and mitochondria: an ultrastructural study. *PLoS ONE* **7**, e46293 (2012).
39. Filadi, R. *et al*. Mitofusin 2 ablation increases endoplasmic reticulum-mitochondria coupling. *Proc. Natl. Acad. Sci. USA* **112**, E2174–2181 (2015).
40. Leal, N. S. *et al*. Mitofusin-2 knockdown increases ER-mitochondria contact and decreases amyloid beta-peptide production. *J. Cell Mol. Med.* **20**, 1686–1695 (2016).
41. Naon, D. *et al*. Critical reappraisal confirms that Mitofusin 2 is an endoplasmic reticulum-mitochondria tether. *Proc. Natl. Acad. Sci. USA* **113**, 11249–11254 (2016).
42. Filadi, R. *et al*. On the role of Mitofusin 2 in endoplasmic reticulum-mitochondria tethering. *Proc. Natl. Acad. Sci. USA* **114**, E2266–E2267 (2016).
43. Giacomello, M. & Pellegrini, L. The coming of age of the mitochondria-ER contact: a matter of thickness. *Cell Death Differ.* **23**, 1417–1427 (2016).
44. Csordas, G. *et al*. Imaging interorganelle contacts and local calcium dynamics at the ER-mitochondrial interface. *Mol. Cell* **39**, 121–132 (2010).
45. Alva, V. & Lupas, A. N. The TULIP superfamily of eukaryotic lipid-binding proteins as a mediator of lipid sensing and transport. *Biochim Biophys Acta* **1861**, 913–923 (2016).
46. Simmen, T., Lynes, E. M., Gesson, K. & Thomas, G. Oxidative protein folding in the endoplasmic reticulum: tight links to the mitochondria-associated membrane (MAM). *Biochim. Biophys. Acta* **1798**, 1465–1473 (2010).
47. Kornmann, B., Osman, C. & Walter, P. The conserved GTPase Gem1 regulates endoplasmic reticulum-mitochondria connections. *Proc. Natl. Acad. Sci. USA* **108**, 14151–14156 (2011).
48. Mesbah Moosavi, Z. S. & Hood, D. A. The Unfolded Protein Response in Relation to Mitochondrial Biogenesis in Skeletal Muscle Cells. *Am. J. Physiol. Cell Physiol.* **312**, C583–C594 (2017).
49. Gkogkas, C. *et al*. VAPB interacts with and modulates the activity of ATF6. *Hum. Mol. Genet.* **11**, 1517–26 (2008).
50. Cashman, N. R. *et al*. Neuroblastoma x spinal cord (NSC) hybrid cell lines resemble developing motor neurons. *Dev. Dyn.* **194**, 209–221 (1992).
51. Gluzman, Y. SV40-transformed simian cells support the replication of early SV40 mutants. *Cell* **23**, 175–182 (1981).
52. Graham, F. L., Smiley, J., Russell, W. C. & Nairn, R. Characteristics of a human cell line transformed by DNA from human adenovirus type 5. *J. Gen. Virol.* **36**, 59–74 (1977).

Acknowledgements

We gratefully acknowledge the expertise and infrastructure offered by the MRC-funded Edinburgh Super-Resolution Imaging Consortium, Heriot Watt University, and the IMPACT facility in the Hugh Robson Building Edinburgh University. The Wellcome Trust for funding.

Author Contributions

M.H. Data Curation, Formal Analysis, Investigation, Methodology, Original Visualization, Writing and Reviewing. P.L. Supervision, Writing and Reviewing. G.H. Supervision, Writing and Reviewing. M.J. Supervision, Resources, Conceptualization, Writing and Reviewing. P.S. Conceptualization, Investigation, Methodology, Resources, Funding Acquisition, Supervision, Original Writing.

Additional Information

Supplementary information accompanies this paper at https://doi.org/10.1038/s41598-017-17278-1.

Competing Interests: The authors declare that they have no competing interests.

Publisher's note: Springer Nature remains neutral with regard to jurisdictional claims in published maps and institutional affiliations.